TECHNISCHE UNIVERSITÄT MÜNCHEN

TUM School of Natural Sciences

Biosensor-based monitoring of TNF antagonists and anti-drug antibodies in inflammatory bowel disease

Melina Katharina Grasmeier

Vollständiger Abdruck der von der TUM School of Natural Sciences der Technischen Universität München zur Erlangung des akademischen Grades einer

Doktorin der Naturwissenschaften (Dr. rer. nat.)

genehmigten Dissertation.

Vorsitz:	Prof. Dr. Matthias Feige
Prüfende der Dissertation:	1. Prof. Dr. Martin Elsner
	2. Prof. Dr. Peter B. Luppa
	3. Prof. Dr. Philip Tinnefeld

Die Dissertation wurde am 19.12.2023 bei der Technischen Universität München eingereicht und durch die TUM School of Natural Sciences am 21.09.2024 angenommen.

Teile der vorliegenden Arbeit wurden bereits veröffentlicht unter:

Grasmeier MK, Weber S, Treiber M, Thaler MA and Luppa PB. Surface plasmon resonance assays for the therapeutic drug monitoring of infliximab indicate clinical relevance of anti-infliximab antibody binding properties. *Clin Chem Lab Med.* 2023;61(7):1255–1265.

Grasmeier MK, Langmann AF, Langmann P, Treiber M, Thaler MA and Luppa PB. Dynamics of serum concentrations of antibodies to infliximab: A new approach for predicting secondary loss of response in inflammatory bowel diseases. *Therap Adv Gastroenterol.* 2021;14:17562848211037849.

Die vorliegende Arbeit wurde am Institut für Klinische Chemie und Pathobiochemie am Klinikum rechts der Isar in der Arbeitsgruppe für Biosensorik im Zeitraum von Juli 2019 bis Januar 2023 angefertigt.

It is not the mountain we conquer, but ourselves.

Sir Edmund Hillary (1919–2008)

Danksagung

Mein ganz besonderer Dank gilt **Herrn Professor Peter Luppa** für die ausgezeichnete Betreuung dieses Projekts. Sein Vertrauen in meine Arbeit hat es mir ermöglicht, meine Ideen zu entfalten, mein Projekt selbstständig zu lenken und an meinen Aufgaben zu wachsen. Auf seine Unterstützung konnte ich allzeit zählen und seine Tür stand immer offen, wenn ich seinen Rat benötigte.

Herrn Professor Martin Elsner danke ich für die Ko-Betreuung meiner Doktorarbeit. Unsere Diskussionen waren wertvoll für mein fachliches Vorankommen und haben meine Arbeit durch einen neuen Blickwinkel auf meine Ergebnisse bereichert.

Herrn Professor Peter Langmann danke ich herzlich für die Überlassung von Patientenseren aus seiner Praxis. Sein herausragender Einsatz für seine Patient*innen hat es erst möglich gemacht, so spannende Daten zu generieren. Außerdem möchte ich **Dr. Anna Langmann** danken, die unschätzbare Arbeit beim Probenmanagement geleistet hat. Ihre Unterstützung bei den Experimenten zur IFXmon-Studie war sehr wertvoll.

Die Kolleg*innen der Biosensor-Arbeitsgruppe haben meine Arbeit maßgeblich beeinflusst und unterstützt. **Dr. Susanne Weber** hatte stets ein offenes Ohr und war allzeit verfügbar für fachliche Diskussionen und Korrekturen. **Christine Grubmüller** danke ich herzlich für die tatkräftige und unterhaltsame Unterstützung bei meinen Experimenten. **Priv.-Doz. Dr. Markus Thaler** war eine große Hilfe bei der statistischen Auswertung und den Korrekturen für unsere Publikationen. Außerdem möchte ich mich bei **Jasmin Arnold**, **Dr. Stefanie Mak**, **Jennifer Mittermaier**, **Janine Potreck** und **Dr. Ruoyu Sun** bedanken. Sie haben sowohl die Arbeit im Labor als auch geteilte Momente außerhalb des Labors zu einer Bereicherung für mich gemacht. Nicht zuletzt gilt mein Dank allen Student*innen, die Teilstrecken dieser Arbeit engagiert und hochmotiviert begleitet haben.

Auch den anderen Kolleg*innen des Instituts für Klinische Chemie möchte ich meinen Dank aussprechen. Von der Warennannahme über die IT-Abteilung und Routinediagnostik bis hin zum Sekretariat konnte ich jederzeit auf tatkräftige Unterstützung und Hilfe bei allen Fragen zählen. Auch **Dr. Matthias Treiber** aus der Inneren Medizin II danke ich für seine Hilfe bei klinischen Fragen.

Ohne den Rückhalt meiner Freunde und Familie wäre diese Arbeit undenkbar gewesen. Sie haben die Funkstille in anstrengenden Zeiten geduldig ertragen, mich in den richtigen Momenten abgelenkt und haben immer an mich geglaubt. Lieber **Michael**, danke, dass du während des Abenteuers Doktorarbeit mein Fels in der Brandung warst. Du hast dich mitgefreut und mitgeärgert, immer das Richtige gekocht und mich immerzu motiviert. Danke für alles – ohne dich hätte ich es nicht bis hierhin geschafft. **Mama**, **Papa** und **Janine** – ihr habt mich zu dem Menschen gemacht, der ich heute bin. Danke für eure bedingungslose Unterstützung und Liebe. Diese Arbeit ist für euch.

Zusammenfassung

Tumor-Nekrose-Faktor(TNF)-Antagonisten, eine Klasse therapeutischer Proteine, haben die Behandlung chronisch-entzündlicher Darmerkrankungen (CED), wie Morbus Crohn und Colitis ulcerosa, maßgeblich verbessert. Das pro-inflammatorische Zytokin TNF ist ein Hauptakteur der gastrointestinalen Entzündungsprozesse bei CED. Die pharmakologische Blockierung von TNF mittels TNF-Antagonisten bei CED hat sich als sehr wirksam und teilweise sicherer im Vergleich zur Therapie mit traditionellen *small molecule*-Medikamenten erwiesen. Der chimäre therapeutische Antikörper Infliximab (IFX) erhielt als erster TNF-Antagonist die Arzneimittelzulassung und ist noch heute weit verbreitet im Einsatz. Allerdings entwickeln bis zu 65 % der mit IFX behandelten Patienten Anti-Drug-Antikörper. Anti-Drug-Antikörper treten bei parenteraler Applikation von Biologika auf. Sie können die Medikamentenwirkung beeinträchtigen und zu einer beschleunigten Eliminierung des Wirkstoffs aus dem Blutkreislauf beitragen, was zu Therapieversagen führen kann.

Die Messung der Serumspiegel von Biologika und der zugehörigen Anti-Drug-Antikörper wird als therapeutisches Drug Monitoring (TDM) bezeichnet und ist ein Werkzeug zur Optimierung der Wirksamkeit und Sicherheit biologischer Therapien. Jedoch beeinträchtigen analytische Herausforderungen und die fehlende Harmonisierung der verfügbaren Methoden die Aussagekraft aktueller TDM-Assays. Diese Problematik erschwert auch die Etablierung evidenzbasierter Strategien für das Management von Anti-Drug-Antikörpern. Während die meisten Assays zur Bestimmung von Anti-Drug-Antikörpern rein (semi-) quantitative Ergebnisse liefern, spielt möglicherweise auch die Qualität der individuellen Anti-Drug-Antikörper eine Rolle für die therapeutische Entscheidungsfindung. Zur qualitativen Analyse von Anti-Drug-Antikörpern sind aktuell jedoch nur wenige Studien publiziert.

Ziele dieser Dissertation waren die Entwicklung Oberflächenplasmonenresonanz(SPR)-spektroskopiebasierter Biosensor-Assays für das TDM von IFX als exemplarischen TNF-Antagonisten und die Bewertung der Eignung von SPR-Biosensoren für routinemäßiges TDM. Mittels SPR können Analyten sowohl quantifiziert als auch hinsichtlich ihrer Bindungseigenschaften charakterisiert werden. In der vorliegenden Arbeit wurde daher auch untersucht, ob Kenntnisse über die Stabilität von Anti-Infliximab-Antikörper(ADA):IFX-Komplexen von Bedeutung für die Steuerung der IFX-Therapie sein könnten. Unter Verwendung eines Biacore X100 SPR-Systems wurden zwei Biosensor-Assays entwickelt: “IFXmon” zur Quantifizierung von IFX und “ADAmon” zur Quantifizierung und Charakterisierung von ADA. IFXmon und ADAmon wurden anschließend zur Analyse von Seren IFX-behandelter CED-Patienten eingesetzt. Die Biosensor-Daten wurden mit Ergebnissen der Analyse derselben Seren mittels *In Vitro Diagnostic Regulation*-konformer Enzymimmunoassays (ELISA) verglichen.

Die Methodenvalidierung zeigte, dass IFXmon akzeptable Biosensorstabilität, analytische Sensitivität, Präzision und Richtigkeit aufwies. Die Analyse von 84 Serumproben mittels IFXmon und ELISA ergab, dass die Methoden in hohem Maße übereinstimmten. Während IFXmon verdünntes Serum als Probenmaterial verwendete, wurde für den ADAmon-Assay eine präanalytische Affinitätsreinigung unter Einsatz magnetischer *Beads* entwickelt. Dieser zusätzliche Schritt war notwendig, um eine IFX-tolerante ADA-Quantifizierung zu ermöglichen, das heißt auch in Anwesenheit typischer IFX-Serumkonzentrationen. Insgesamt erzielte ADAmon vergleichbare Leistungsparameter wie der ELISA in Bezug auf Biosensorstabilität, analytische Sensitivität, Präzision und Richtigkeit. Die Resultate der ADA-Quantifizierung mittels ADAmon und ELISA in Patientenseren unterschieden sich jedoch deutlich und korrelierten nicht miteinander. Dies lässt darauf schließen, dass ADAmon und ELISA möglicherweise unterschiedliche, potenziell von der ADA-Qualität abhängige ADA-Populationen erfassen.

Um die ADA:IFX-Bindungsstabilität einzelner Patienten zu untersuchen, wurde der Dissoziationquotient "DissR" eingeführt. DissR ist ein simpler Index, welcher ein Maß für die Dissoziationsgeschwindigkeit von ADA:Wirkstoff-Komplexen darstellt. Nach der erfolgreichen Validierung seiner Robustheit wurde DissR retrospektiv für ADAmon-positive Patienten berechnet. Diese Studie stellt die bisher umfangreichste Arbeit zur Untersuchung der ADA:IFX-Bindungsstabilität dar. Hierbei konnte gezeigt werden, dass eine hohe ADA:IFX-Bindungsstabilität signifikant mit zukünftigem Therapieversagen und nicht detektierbaren IFX-Spiegeln korrelierte, was auf einen prognostischen Wert der ADA:IFX-Bindungsstabilität hindeutet. Die Assay-Prinzipien von IFXmon und ADAmon, insbesondere auch DissR, wurden mit minimalen Anpassungen erfolgreich auf Adalimumab als einen weiteren weit verbreiteten TNF-Antagonisten übertragen. Dies lässt darauf schließen, dass die hierin entwickelten Biosensormethoden schnell adaptiert werden können.

Zusammenfassend legen die vorgestellten Ergebnisse nahe, dass SPR-basierte Biosensor-Assays den erforderlichen bioanalytischen Anforderungen für die routinemäßige TDM-Analytik genügen. Insbesondere die Beurteilung der ADA-Bindungsstabilität könnte eine frühzeitigere therapeutische Entscheidungsfindung bei der Behandlung von CED ermöglichen. Diese Dissertation untermauert die praktische und wirtschaftliche Eignung von SPR für die labormedizinische Analytik und hebt ihr Potenzial für das proaktive TDM im Rahmen der personalisierten Medizin hervor.

Summary

Tumor necrosis factor (TNF) antagonists, a class of therapeutic proteins, have significantly improved the treatment of inflammatory bowel diseases (IBD), such as Crohn's disease and ulcerative colitis. The pro-inflammatory cytokine TNF is a key player in IBD-related intestinal inflammation. Pharmacological blockade of TNF using TNF antagonists in IBD has been shown to be very effective and in some cases safer compared with application of traditional small-molecule drugs. The chimeric therapeutic antibody infliximab (IFX) was the first TNF antagonist to receive drug approval and remains widely prescribed. Yet, up to 65 % of IFX-treated patients develop anti-drug antibodies. Anti-drug antibodies can emerge with parenteral application of biologics. They can neutralize drug function and enhance its clearance from the blood stream, which may lead to treatment failure.

Measuring serum levels of biologic drug and corresponding anti-drug antibodies, termed therapeutic drug monitoring (TDM), is an essential tool to optimize effectiveness and safety of biologic therapies. However, current TDM assays suffer from the analytic complexity of anti-drug antibody assessment and poor harmonization of available assays. This hampers the establishment of evidence-based consensus strategies for anti-drug antibody management. In addition to the mainly (semi-)quantitative data provided by state of the art TDM assays, qualitative data on patient-individual anti-drug antibodies may be of importance for therapeutic decision-making. Though, the research literature regarding qualitative analysis of anti-drug antibodies is very limited.

The aim of this dissertation was to develop surface plasmon resonance (SPR) spectroscopy-based biosensor assays for the TDM of the exemplary TNF antagonist IFX and to evaluate the feasibility of SPR biosensors for routine TDM. With SPR, analytes can both be quantified and characterized regarding their binding properties. Thus, it was additionally investigated whether knowledge about the binding stability of anti-infliximab antibody(ADA):IFX complexes adds diagnostic value in IFX therapy management. Using a Biacore X100 SPR instrument, two biosensor assays were developed: "IFXmon" for the quantification of IFX and "ADAmon" for the quantification and characterization of ADA. Both IFXmon and ADAmon were compared to *in vitro* diagnostics-approved enzyme-linked immunosorbent assays (ELISA) by analysis of sera from IFX-treated IBD patients.

Method validation showed that IFXmon comprised acceptable biosensor stability, analytic sensitivity, precision and accuracy. Analysis of 84 patient sera by IFXmon and ELISA demonstrated method interchangeability. While IFXmon utilized diluted serum as sample material, a pre-analytic affinity purification protocol with magnetic beads was developed for the ADAmon assay. This additional step was necessary to allow IFX-tolerant ADA quantification, that is, even in the presence of typical IFX serum concentrations. Overall, ADAmon achieved similar performance parameters as ELISA with respect to biosensor stability, analytic sensitivity, precision and accuracy. However, the results of

ADA quantification by ADAmon and ELISA in patient sera differed substantially and did not correlate. This suggests that ADAmon and ELISA assess different, potentially ADA quality-dependent ADA populations.

In order to characterize patient-individual ADA:IFX binding stabilities, the dissociation ratio "DissR" was introduced. DissR is an easily accessible index that describes the dissociation velocity of ADA:drug complexes. After successful validation of its robustness, DissR was retrospectively calculated for ADAmon-positive patients in the so far largest study to analyze ADA:IFX binding stability. It was shown that high ADA:IFX binding stability was significantly correlated with the development of therapy failure and undetectable IFX concentrations in the future, suggesting a prognostic value of ADA:IFX binding properties. The assay principles of IFXmon and ADAmon, in particular also DissR, were successfully transferred with minimal adaptations to adalimumab as another widely used TNF antagonist. This implies that the established assays can be rapidly adapted.

In conclusion, the presented findings suggest that SPR-based biosensor assays suffice the bioanalytic requirements for routine TDM. Particularly the assessment of ADA binding stability may enable earlier therapeutic decision-making in IBD treatment. This dissertation substantiates the practical and economic suitability of SPR for laboratory medical analysis and highlights its potential for proactive TDM in the context of personalized medicine.

Contents

Abbreviations

A	**ACG**	American College of Gastroenterology
	ADA	anti-infliximab antibodies
	ADA488	Alexa 488-labeled ADA calibrator
	ADAmon	developed SPR spectroscopy-based biosensor assay for ADA quantification and characterization
	ADAmon-EpiM	developed SPR spectroscopy-based biosensor assay for ADA epitope mapping
	ADM	adalimumab
	ADMmon	developed SPR spectroscopy-based biosensor assay for ADM quantification
	AGA	American Gastroenterological Association
	AIEC	adherent and invasive *Escherichia coli*
	anti-ADMmon	developed SPR spectroscopy-based biosensor assay for anti-ADM quantification and characterization
	APS	ammonium persulfate
	ATG16L1	autophagy-related protein 16 like protein 1
	AU	arbitrary units
	AUC	area under the curve
B	**bromophenol blue**	3',3",5',5"-tetrabromophenol sulfone phthalein
	BSA	bovine serum albumin
C	**CD**	Crohn's disease
	CHAPS	3-dimethyl[3-(3α,7α,12α-trihydroxy-5β-cholan-24-amido)propyl]azaniumyl-propane-1-sulfonate
	CI	confidence interval
	cIAP	cellular inhibitor of apoptosis protein
	CLIA	chemiluminescence immunoassay
	CRP	C-reactive protein
	CS	corticosteroids
	CV	coefficient of variation
D	**DissR**	dissociation ratio

	dkαgt	donkey anti-goat IgG
	DQ	direct ADA quantification in diluted serum
E	***E. coli***	*Escherichia coli*
	ECCO	European Crohn's and Colitis Organization
	ECLIA	electrochemiluminescence immunoassay
	EDC	1-ethyl-3-(3-dimethylaminopropyl)-carbodiimide
	EDTA	ethylenediaminetetraacetic acid
	ELISA	enzyme-linked immunosorbent assay
	EMA	European Medicines Agency
F	**FC**	fecal calprotectin
	Fc	flow cell
	FcRn	neonatal Fc receptor
	FDA	Food and Drug Administration
	FL	fluorescently-labeled
	FPLC	fast protein liquid chromatography
G	**GESA**	Gastroenterological Society of Australia
	GuHCl	guanidinium chloride
H	**HLA**	human leukocyte antigen
	HMSA	homogeneous mobility shift assay
	HRP	horseradish peroxidase
	hSA	human serum albumin
	hTf	human transferrin
I	**IBD**	inflammatory bowel disease
	IBSEN	inflammatory bowel disease in South-Eastern Norway
	IdeS	immunoglubulin-degrading enzyme from *Streptococcus pyogenes*
	IFN	interferon
	IFX	infliximab
	IFXmon	developed SPR spectroscopy-based biosensor assay for IFX quantification
	IgG	immunoglobulin G
	IL	interleukin

	IMAC	immobilized metal ion affinity chromatography
	IMID	immune-mediated inflammatory diseases
	IPTG	isopropyl-β-D-1-thiogalactopyranoside
	IRGM	immunity-related GTPase M
	IVD	*in vitro* diagnostics
J	**JAK**	Janus kinase
L	**LB**	lysogeny broth
	LOB	limit of blank
	LOD	limit of detection
	LOQ	limit of quantification
	LOR	secondary loss of response
	LUBAC	linear ubiquitin chain assembly complex
M	**mAb**	monoclonal antibody
	MAPK	mitogen-activated kinase
	MLKL	mixed lineage kinase domain-like protein
	msαhu	mouse anti-human IgG
	MW	molecular weight
	MWCO	molecular weight cut-off
N	**NFκB**	nuclear factor κB
	NHS	N-hydroxysuccinimide
	NOD2	nucleotide-binding oligomerization domain-containing protein 2
P	**PA**	pre-analytic acidification
	PAGE	polyacrylamide gel electrophoresis
	PBS	phosphate-buffered saline
	PBSC	PBS with casein
	PEG	polyethylene glycol
	PQ	ADA quantification after pulldown from diluted serum
	PVDF	polyvinylidene difluoride
R	**RA**	rheumatoid arthritis
	RIA	radioimmunoassay
	RIPK1	receptor-interacting serine/threonine kinase 1

	ROC	receiver operating characteristic
	RT	room temperature
	RU	resonance units
S	**SCFA**	short chain fatty acid
	SD	standard deviation
	SDS	sodium dodecyl sulfate
	SEC	size-exclusion chromatography
	SMP	skim milk powder
	SN	serum supernatant
	spECTRUM	intErnational Consortium of Therapeutic dRUg Monitoring
	SPR	surface plasmon resonance
	sTNF	soluble TNF
T	**TACE**	TNF-α converting enzyme
	TAXIT	Trough Concentration Adapted Infliximab Treatment trial
	TBST	Tris-buffered saline wiht Tween 20
	TDM	therapeutic drug monitoring
	TEMED	tetramethylethylenediamine
	TEV	tobacco etch virus
	Th	T helper (cell)
	tmTNF	transmembrane TNF
	TNF	tumor necrosis factor
	TNFR	TNF receptor
	TRADD	TNFR1-associated death domain protein
	TRAF2	TNFR-associated factor 2
	Tris	tris(hydroxymethyl)aminomethane
	TrxA	thioredoxin A
U	**UC**	ulcerative colitis
W	**WB**	western blot
µ	**µgEq/mL**	concentration equivalents

List of Figures

List of Tables

1. Introduction

1.1. Inflammatory bowel disease

Inflammation is a physiological process encompassing both cellular and non-cellular players, with which the organism defends itself against exogenous noxa, clears endogenous tissue damage or reacts to tissue malfunction. Controlled inflammatory reactions aim at restoring host homeostasis by eliminating the pathogens or initiating tissue repair and adaptation[1,2]. A healthy inflammatory response is characterized by a balance between pro-inflammatory processes and processes involved in inflammation resolution. However, a complex interplay between endogenous and exogenous factors can cause this process to derail towards excessive and persisting inflammation, resulting in a pathological failure to establish homeostasis.

The umbrella term immune-mediated inflammatory disease (IMID) describes a heterogeneous group of diseases with overactive and chronic inflammatory activity associated with tissue destruction and organ damage[3,4]. While all IMID share some alterations in common immunologic pathways, their clinical phenotype and tissue localization are defined by disease-specific pathomechanisms[3]. As summarized in a comprehensive review by Schett et al., IMID have classically been categorized by the respectively affected tissues, whereby it is noteworthy that many IMID subtypes involve the outer and inner surfaces of the body, i.e., the gastrointestinal tract, skin, bones or joints. These surfaces exhibit barrier functions and are particularly exposed to external influences, such as pathogens or mechanical stress[4]. This exposure explains their increased need for immunological protection and repair activities, which goes along with increased harm in the case of immunological dysfunction[4]. All IMID are characterized by a progressive course and currently, no causal cures are available for their treatment[3,4]. Conditions belonging to the IMID family encompass rheumatic disorders, connective tissue disorders, neurological autoimmune conditions, like multiple sclerosis, asthma and inflammatory bowel disease (IBD). Since the present project involved a study with IBD patients, the state of the art of regarding IBD epidemiology, pathophysiology and therapy will be summarized in the following subsections.

1.1.1. Epidemiology and economic impact

IBD, majorly represented by the two disorders Crohn's disease (CD) and ulcerative colitis (UC), is characterized by progressive and chronic inflammation of the gastrointestinal tract and unpredictable clinical course[5,6]. Ethnicity, geographic factors and lifestyle play central roles in IBD epidemiology[7]. For IBD, a rising incidence has been observed worldwide in the past decades, with large regional differences[8,9]. While traditionally, IBD was understood as a disease of the western world, the disease has followed the geographical patterns of industrialization: In recent decades, emerging countries – including large-

population countries, such as India and China – have reported increasing cases owed to the adoption of Westernized lifestyle[9,10]. The prevalence of IBD in Europe is about 0.3 %, equivalent to 2.5–3.0 million affected patients[11]. Given its high prevalence, chronic nature and high therapy cost, IBD has become a growing socioeconomic burden in the industrialized world. A systematic review by van Linschoten et al. from 2021 reported a global increase in healthcare cost of IBD, which has been mainly driven by increased use of expensive biologic medication, while inpatient and outpatient cost have remained stable[12]. Furthermore, the authors provided an in-depth evaluation of healthcare cost for prevalent IBD cases in different geographic regions: In Europe, for example, the annual per-patient cost from the last ten years amounted to $ 12,439 and $ 7,224 for CD and UC treatment, respectively[12]. Only about one third of all IBD patients experience a mild disease, whereas aggressive disease courses are often associated with numerous exhaustive treatment cycles[6,13–16].

1.1.2. Diagnostic criteria

The initial diagnosis of IBD is mainly based on patient history and physical examination, together with findings from endoscopy, laboratory parameters, radiologic and histologic results[17]. In this process, endoscopy constitutes the gold standard for definitive diagnosis[18,19]. In order to exclude other pathologies, patients should be examined for gastrointestinal infections, irritable bowel syndrome, chronic granulomatous disease and specific food intolerance to name just some examples for differential diagnoses that need to be excluded[20]. In most cases, the initial diagnosis of IBD is made in adolescence or young adulthood; however, the disease can theoretically arise at any age[20].

1.1.2.1. Clinical manifestation

The symptoms of IBD include abdominal pain, non-bloody or bloody diarrhea, fever, intestinal obstruction, weight loss, fatigue and rectal discharge of blood and mucus (see **Figure 1.1**). However, the patient-individual clinical presentation depends on disease localization and diverges between CD and UC[7]. In this paragraph, the clinical pictures of CD and UC will be summarized in reference to the comprehensive overview article by Daniel Baumgart (2009)[7]. CD patients suffer from transmural mucosal inflammation, which may be located at any part of the gastrointestinal tract between mouth and anus and may present a discontinuous inflammatory pattern, also known as skip lesions (see **Figure 1.2A+B**). Disease progression is episodic and symptoms predominantly include abdominal pain, non-bloody diarrhea and nonspecific abdominal symptoms. In comparison to UC, CD is understood to be associated with more frequent complications, such as penetrating and stricturing disease behavior, and overall higher negative impact on the quality of life[10,20,21]. Approximately 20–25 % of all CD patients develop perianal fistulae[10,22]. UC is characterized by non-transmural, continuous inflammation restricted to the colon and sub-classified into proctitis, left colitis or pancolitis/extensive colitis, de-

pending on disease localization (see **Figure 1.2A+B**). Frequent stools, bloody diarrhea and perianal bleeding are observed more frequently in UC than CD [20,23]. UC-associated complications include severe bleeding, toxic megacolon or epithelial displasia [23].

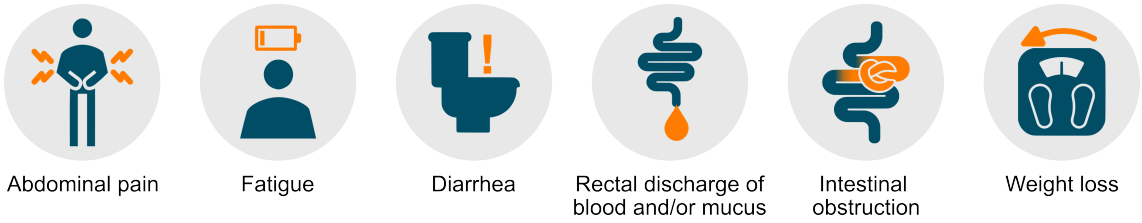

Figure 1.1.: IBD symptoms.

Unfortunately, many IBD patients develop extra-intestinal manifestation that can affect nearly every organ of the body and often further decrease life quality. Reported frequencies vary considerable between studies and have been reported to amount for 6–47 % [24–28]. Cutaneous, ophthalmological and rheumatologic extra-intestinal manifestations are observed most commonly, but the cardiovascular system, lungs and the hepatobiliary system may be affected, as well [28]. Both CD and UC are linked to an increased risk for gastrointestinal neoplasms [29,30].

In approximately 25 % of both CD and UC patients, the disease progresses to an extensive, complicated condition [10]. Major surgery as a consequence of disease progression or complications at diagnosis is required in 5–10 % of UC and 10–30 % of CD patients within the first five years after diagnosis [10]. In a follow-up evaluation of the inflammatory bowel disease in South-Eastern Norway (IBSEN) study, a large, population-based inception cohort, it was found that 10 years after IBD diagnosis, 18.8 % of patients received disability pension [31]. This rate equaled to a 2.0-fold and 1.8-fold relative risk for CD and UC patients, respectively, as compared to background population [31]. A similar study from Hungary found an overall disability pension rate of 32.3 % in IBD patients [32].

1.1.2.2. Tools for diagnosis and disease monitoring

Currently, no causal cure is available for IBD and both disease course and treatment response are poorly predictable [6]. Additionally, IBD symptoms often occur disconnected from active inflammation [33–35]. This means that a patient may temporarily feel well while inflammatory foci in the gastrointestinal tract flare up, which at worst can lead to irreversible damage. In order to achieve sustainable remission, objective indicators of inflammation are not only utilized to diagnose but also to monitor IBD disease activity, including endoscopic and histologic examinations, radiologic imaging techniques and laboratory parameters [6,36]. Modern treatment options have enabled a paradigm shift in IBD treatment targets from damage control towards mucosal healing and deep remission [37–40]. Within these new strategies, early resolution of inflammation plays a crucial role, underlining the significance of effective disease monitoring tools [6,39,40].

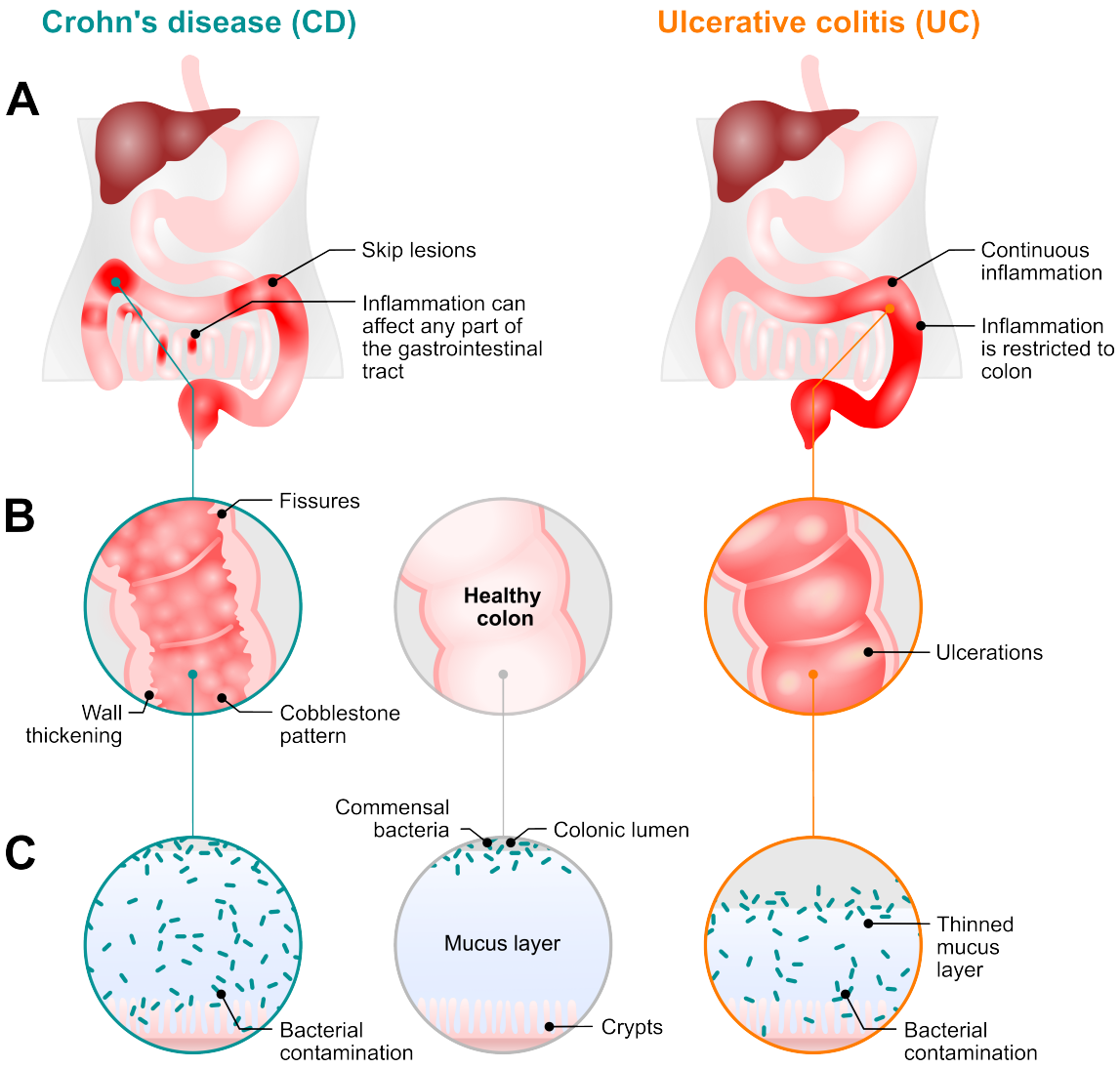

Figure 1.2.: Gastrointestinal manifestation of CD and UC. (**A**) Macroscopic inflammatory pattern. (**B**) Endoscopic characteristics of CD and UC. (**C**) Mucosal structure deficits in IBD.

For diagnosis, colonoscopic evaluation of the mucosa with intubation of the terminal ileum is the gold standard method [6,41]. Common scoring systems to classify disease severity are the simple endoscopic score for CD and the Mayo endoscopic subscore for UC [19,42,43]. These systems are frequently applied in both standard patient care and in clinical studies. The simple endoscopic score assesses ulcers, percentage of ulcerated surface, affected surface and narrowings [42]. The Mayo score differentiates between normal mucosa, mild, moderate and severe UC and assigns a score between 0 and 3, respectively [43].

To estimate disease extension, areas with macroscopically active disease and healthy mucosa are biopsied for subsequent histologic analysis. Nevertheless, endoscopy does not permit to examine the entire bowel. This gap can be filled by non-invasive, cross-sectional imaging techniques, which are therefore less stressful for patients [6]. The importance of additional imaging has been demonstrated for example by Samuel et al [44]. In this study, 53.7 % of CD patients with inconspicuous ileo-colonoscopy had active disease in the small

bowel, which was detected by additional computer tomography enterography [44]. In magnetic resonance enterography and computer tomography enterography, the patients are instructed to drink large volumes of neutral contrast liquid in order to distend the intestines and visualize possible macroscopic abnormalities and complications, e.g., strictures, ulcers, inflammation and fistulae [6,41]. Magnetic resonance enterography is considered the best method to detect perianal disease [41]. Since disease monitoring via cross-sectional imaging techniques is required throughout the patients' lifetime after diagnosis, the cumulative radiation exposure of computer tomography enterography has to be considered. Ultrasonography is another suitable imaging method and capable, e.g., to differentiate inflammation from fibrotic intestinal wall thickening, but has a relatively high inter-observer variability [17,41].

Owed to their non-specific nature and inability to differentiate between CD and UC, laboratory parameters are utilized rather for disease monitoring than initial diagnosis [41]. C-reactive protein (CRP) is the most sensitive serum marker for inflammation, which is secreted by the liver in response to inflammation-related tissue injury, but also in response to other influences, such as smoking, overweight and particular drugs [41,45]. The CRP signaling pathway is initiated by macrophages and potent enough to generate a 500–1000-fold increase in CRP serum concentration within hours [46]. The relatively short half-life of 19 hours makes CRP an attractive biomarker for inflammation [41,45]. Nevertheless, up to 30 % of endoscopy-confirmed CD cases with active inflammation are tested CRP-negative [47]. Another biomarker with higher specificity for intestinal tissue is fecal calprotectin (FC). Calprotectin in stool is stable for approximately one week and originates from the degranulation of neutrophils recruited to the intestinal mucosa, where calprotectin exerts antimicrobial functions [41,48,49]. FC is capable to distinguish between active and quiescent disease, whereby levels exceeding 250 µg/g are considered indicative of active inflammation [41,50]. In addition to CRP and FC analysis, anemia, thrombocytosis, hypoalbuminemia and vitamin deficiencies may be detected in the laboratory as a consequence from chronic inflammation and malabsorption [41].

1.1.3. Pathogenesis

Although the exact causes for IBD remain subject to research, it is undoubted that IBD pathogenesis is multifactorial [10,17,51]. IBD is a complex disease, in which genetic susceptibility and environmental variables cause an imbalance of the immune–microbiome axis [52,53]. This imbalance manifests as loss of tolerance for the host commensal microbiota, a dysbalanced microbibiota ecosystem and barrier malfunction of the intestinal mucosa (see **Figure 1.2C**) [53].

1.1.3.1. Genetic susceptibility

Genetic studies suggest that IBD is a polygenic disease and more than 250 genetic loci are known to be associated with IBD susceptibility [54]. 80–90 % of these loci are in noncoding sequences and are therefore linked to epigenetic, microRNA-related and noncoding RNA-related processes [55]. Studies have demonstrated that the genetic component is stronger in the etiology of CD compared to UC [56,57]. In identical twins, 58 % concordance for CD has been reported [58]. As reviewed by Graham et al., IBD-related susceptibility genes are involved in gut-microbe interaction and thereby exert functions in microbe sensing, intestinal barrier integrity, adaptive immunity, cell stress pathways, inflammation, fibrosis and cytokine networks, whereby single susceptibility genes may be involved in multiple functions [53,59]. Susceptibility gene variants, such as for *nucleotide-binding oligomerization domain-containing protein 2* (*NOD2*), vary across geographic regions and ethnicity [60]. However, the previously mentioned twin studies prove that IBD cannot be fully explained by genetic predisposition [56,57]. Some exemplary genes and the impact of their IBD-related variants are highlighted in the following.

NOD2 was the first identified IBD suceptibility gene. IBD-related polymorphisms of *NOD2*, whose product NOD2 functions as an intracellular sensor of bacterial cell wall components, result in an unproductive antibacterial response, which leads to inadequate inflammation [53,61,62]. Other susceptibility genes, such as *immunity-related GTPase M* (*IRGM*) and *autophagy-related protein 16 like protein 1* (*ATG16L1*), are involved in autophagy as part of the cellular stress response [53,63–65]. In CD patients, the $ATG16L1^{T300A}$ polymorphism is associated with compromised antibacterial autophagy and resulting excess endoplasmatic reticulum stress in Paneth cells, an intestinal cell type that resides in the small bowel crypts and secretes antimicrobial and immune system-modulating molecules [66,67]. This contributes to a malfunctional epithelial barrier [68]. In addition, genome-wide association studies have identified the genes encoding interleukin (IL)-23R and -12B to be linked to IBD pathogenesis [69–71]. Both genes are involved in the differentiation and expansion of type 17 T helper (Th) cells that initiate pro-inflammatory responses, e.g., by secretion of IL-17A [52]. IL-17A activates various cellular targets, such as epithelium, macrophages and neutrophils, which leads to the secretion of tumor necrosis factor (TNF), IL-1B, chemokines and metaloproteases [72–74]. Elevated IL-17A levels and an increase in Th17 cells have been observed in IBD patients' intestinal mucosa and lamina propria [75–77].

1.1.3.2. Microbiome

The human bowel is colonized by four major phyla of commensal bacteria, namely *Bacteroidetes*, *Firmicutes*, *Actinobacteria*, and *Proteobacteria*, that comprise thousands of individual species and live in symbiosis with the host [78]. The human microbiome comprises impressive inter-individual variability and its composition depends on genetics, acquired microbiome at birth, medication, diet and other environmental factors [79]. A highly so-

phisticated relationship exists between the gut microbiota, intestinal cells and the immune system [52].

Microbiome studies have shown that IBD is associated with a decrease in the diversity of the commensal microbiota, particularly within the *Firmicutes* phyla [80–82]. Another study reported that the microbiome in IBD was less stable as compared to healthy individuals [83]. The healthy colon epithelium is continuously covered by two layers of mucus: The outer layer is of loose constitution and allows for bacterial colonization, while the dense inner layer is usually sterile [84]. In IBD, especially CD, a characteristic increase in bacterial colonization of the inner mucus layer is observed [85]. An adherent and invasive *Escherichia coli* (AIEC) phenotype has been identified as a relatively new pathogenic group with higher abundance in IBD patients [86,87]. AIEC mainly reside in the ileal mucosa, where they stimulate inflammation, invade epithelial cells and infect macrophages [79,88].

In a healthy host, the microbiome produces a diverse set of metabolites, such as short chain fatty acids (SCFA), tryptophan derivatives and secondary bile acids [89]. SCFA, mainly encompassing acetate, propionate and butyrate, are produced from commensal bacteria in the gut from accessible dietary carbohydrates passing the bowel [89,90]. They modulate protective intestinal immune responses and execute anti-inflammatory functions [91,92]. Studies have shown that fecal SCFA is reduced in IBD patients [93–95]. In IBD, tryptophan metabolites and secondary bile acids have been observed to be decreased, as well [96,97]. Commensal bacteria can convert tryptophan into indol-containing molecules, while primary bile acids are converted into secondary bile acids [96,97]. Both products possess anti-inflammatory functions [96,97]. The bacterial product indoleacrylic acid also stimulates mucus production and thereby contributes to a healthy intestinal flora [98]. Overall, the disturbance of microbial metabolism in IBD impairs the barrier function of the intestinal mucosa.

1.1.3.3. Immunologic dysfunction

Immunological dysregulation is involved in the initiation and perpetuation of IBD. As the innate and adaptive immune systems are intimately connected with the intestinal mucosa and directly exposed to environmental influences, IBD-specific immunologic dysfunctions can only be understood in a mutual context. Research into IBD-related pathoimmunologic processes has been focusing for a long time on the adaptive immune system, in particular on the T cell response within the lamina propria [58]. In CD, excess Th1 and Th17 responses trigger a vicious cycle of inflammation via secretion of pro-inflammatory cytokines, such as IL-17, interferon (IFN)-γ and TNF [55,99]. UC has been understood to be mediated by an atypical dominance of the Th2 pathway, which results in the secretion of IL-5, IL-13 and the activation of B cells and natural killer T cells [55,100]. However, more recent research findings cast doubt on this strict separation [101]. Furthermore, the activity of regulatory T cells, which suppress excessive immune responses against the commensal microbiota, is reduced in IBD [102,103].

More recently, also innate immunologic dysfunction in IBD has been subject to investigations[85]. Innate immunity processes involved in IBD particularly concern the intestinal barrier function[85]. Cell types involved therein and contributing to IBD pathogenesis encompass intestinal epithelial cells, i.e., enterocytes, Paneth cells, goblet cells, M cells and neuroendocrine cells, and immune cells, i.e., macrophages, dendritic cells and neutrophils[85]. Epithelial cell dysfunctions contribute to a leaky barrier that allows closer contact between the epithelium and luminal antigens or microbes and triggers inflammation[58,104]. A mouse model of mucin production deficiency, for example, developed an IBD phenotype[105]. As previously mentioned, Paneth cell defects causing inefficient antibacterial responses and reduced defensin secretion are linked to CD[53,61,62]. In addition, CD patients have been observed to exhibit impaired macrophage activity and dendritic cell trafficking that cause insufficient antigen sampling and inappropriate inflammatory reactions[41,55,106]. In conclusion, alterations in the complex cross-talk between epithelial barrier, innate and adaptive immunity contribute to the immunopathogenesis of IBD and the perpetuation of inflammation towards chronicity.

1.1.3.4. Environmental influences

Multiple environmental influences have been reported to contribute to IBD etiology. Geographical gradients in IBD prevalence from north to south, west to east and urban to rural regions have been well-known for decades[78]. However, lifestyle rather than geographical influences explain this observation, since the incidence rates in traditionally less affected Hispanic and Asian population have been rising recently[107]. A westernized diet high in saturated fat and sugar is linked to increased risk to develop IBD, while a high-fiber diet is protective[108]. Furthermore, the effect of smoking on the risk for IBD has been studied extensively[109]. Controversially, heavy smoking is inversely correlated with UC risk and relapse rate, while positively correlated with CD risk[27,110,111]. Intake of drugs known to perturb the gut microbiome, e.g., aspirin, non-steroidal anti-inflammatory drugs and contraceptives, has also been found to increase the risk for IBD development[55,112]. Exposure to pathogens can also increase the individual risk for IBD, such as infectious gastroenteritis[113]. Recent studies have reported that air pollution may contribute to IBD pathogenesis.

1.1.4. Therapy options

Both in the therapeutic armamentarium and treatment perspectives for IBD, paradigms have shifted within the past 20 years: Standard treatment largely relied on relatively low specific immunosuppressants and anti-inflammatory drugs that were borrowed from other clinical disciplines[3]. Today, targeted biologic and small molecule drugs are available that have not only transformed the drug landscape but also treatment perspectives: Long-term disability is no longer the norm for IBD patients and more ambitious treatment goals, including mucosal healing, can be achieved[3,39,40]. Therapeutic strategies are

established depending on disease subtype, location and severity [20]. By repetitive assessment of patient-individual therapy responsiveness, beginning sub-clinical relapse may be recognized early and therapeutic interventions and decisions can be rationalized [6]. Standard IBD treatment begins with well-tolerated drugs and may be escalated towards more aggressive immunosuppression, as shown by the treatment algorithm scheme in **Figure 1.3** [20].

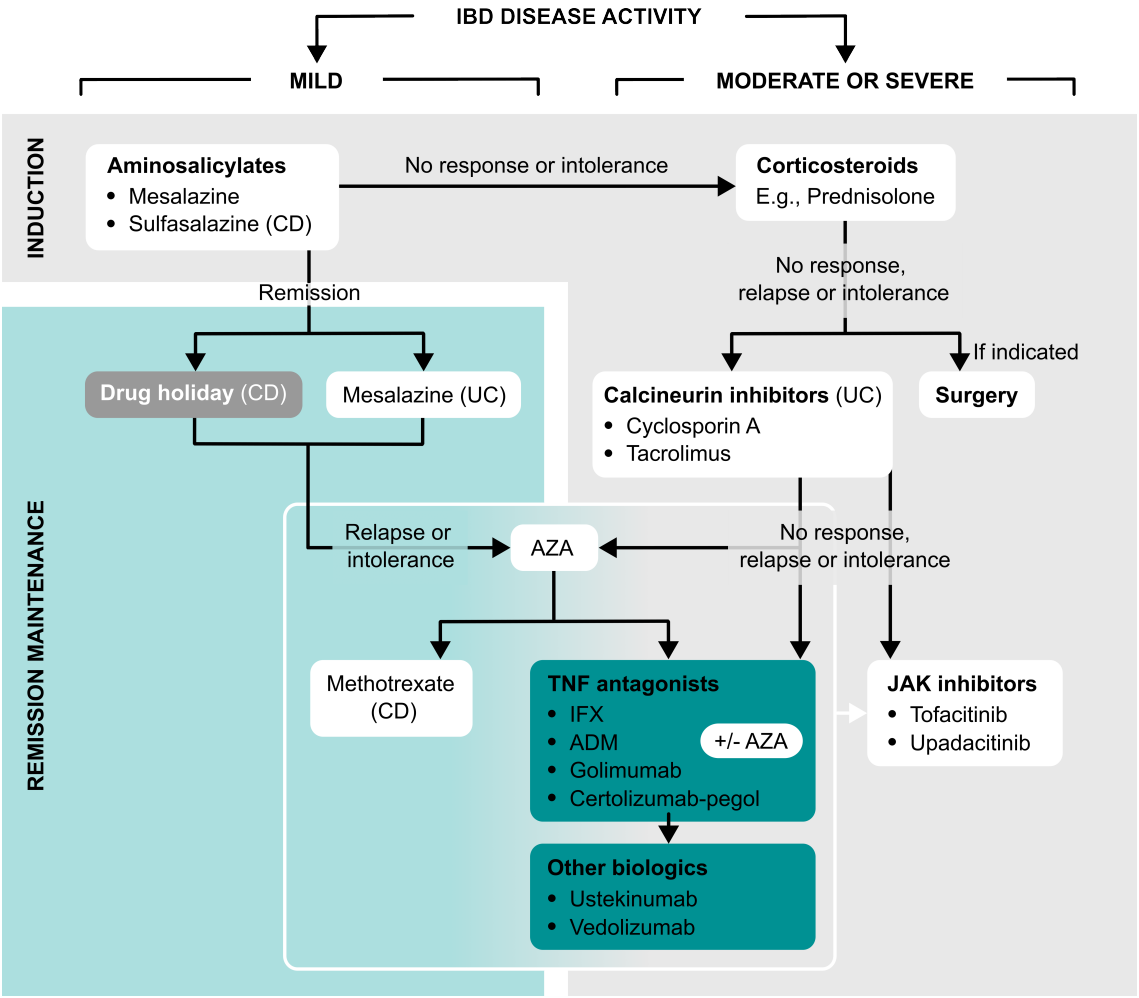

Figure 1.3.: IBD therapy algorithm. Different therapeutic tools are applied for remission induction therapy (gray area) as compared to remission maintenance (blue area) and in the treatment of mild disease (left) as compared to moderate or severe disease (right). Particular drugs, including azathioprine (AZA), methotrexate and biologics may be chosen for both remission induction in severe disease as well as for maintenance of remission. Prior to immunosuppressive therapy escalation, surgery should be considered, if indicated. Janus kinase (JAK) inhibitors are indicated for moderate or severe disease after other therapies have failed [114]. Selective usage of drugs in either CD or UC is denoted. Figure adapted from [20].

Traditionally, mild or moderate IBD therapy is initiated with aminosalicylates, e.g., mesalazine or sulfasalazine, which have been used in IBD treatment for more than 80 years [115]. The mechanism of action of aminosalicylates is not fully understood, but likely acts on the prostaglandin metabolism and exerts anti-inflammatory and antibacterial effects [115,116]. In moderate to severe IBD and in the case of aminosalicylate failure, corticosteroids (CS),

such as prednisone, may be applied [20]. As agonists of the glucocorticosteroid receptor, they suppress the immune system and reduce inflammation [117]. However, CS have only been proven efficient in the induction of remission, but not in remission maintenance [115]. Immunomodulatory agents like azathioprine, 6-mercaptopurine, methotrexate or calcineurin inhibitors (cyclosporine A and tacrolimus) are applied in further therapy escalation, whereby azathioprine and mesalazine are suitable for remission maintenance [20]. All drugs mentioned in this paragraph belong to the traditional therapeutic armamentarium for IBD treatment and are associated with relatively high risk for adverse effects due to their unspecific action [3].

In the case of CS resistance, frequent recurrences under immunomodulator-based maintenance therapy or adverse effects, a therapy with newer biologic drugs or targeted small molecules can be induced and maintained [115,118]. These therapeutics have been developed based on the accumulated knowledge about IBD pathogenesis to specifically interfere in pro-inflammatory cytokine networks and immunologic processes. IBD with its complex and overlapping cytokine networks has been an ideal model disease for showcasing of the potency of rational drug development for targeted therapies [3,119]. As such, therapeutic proteins – mostly, antibodies – directed against TNF, IL-12/23 signaling and integrins have been approved within the past three decades [115,118,119]. TNF antagonists will be discussed in detail in **section 1.2**. Nevertheless, it should be mentioned at this point that recent evidence suggests a therapeutic benefit for the first-line use of TNF antagonists [120–123].

IL-12 and IL-23 play a crucial role in IBD-related mucosal inflammation and are involved in the differentiation of Th1 cells and activation of Th17 cells, which results in their secretion of pro-inflammatory cytokines including IL-6, IFN-γ, TNF, IL-17, among others [115,124]. Ustekinumab is a human monoclonal antibody (mAb) directed against the p40 subunit common to both IL-12 and IL-23 and thereby prevents these molecules from binding to their receptors on T cells [125]. A drug class more specifically targeting immunologic dysfunction in the gut are integrin antagonists. Integrins are membrane-bound glycoprotein receptors on leukocytes that are involved in tissue-specific homing [126]. Gut-selective leukocytes express the $\alpha 4\beta 7$ integrin, which specifically interacts with the intestinal mucosal addressin cell adhesion molecule(MAdCAM)-1 [127]. $\alpha 4\beta 7$+ intestinal leukocyte infiltration into the intestinal mucosa is enhanced in IBD and associated with mucosal leukocyte accumulation and enhanced leukocyte-mediated intestinal inflammation [115,118]. Vedolizumab is a human anti-$\alpha 4\beta 7$ integrin antibody and efficiently prevents this gut-specific leukocyte homing and its pathology in IBD patients [128–130].

In addition to modern biopharmaceuticals, novel small molecules inhibiting tyrosine kinases of the JAK family have been developed. JAK inhibitors, e.g. tofacitinib, interrupt multiple converging pro-inflammatory intracellular signaling cascades with good specificity and impressive effectiveness [114,131,132]. Another advantage of these drugs is that they can be administered orally, which facilitates therapy compliance [3]. It must not be neglected

that also surgery, i.e. intestinal resection, ostomy, and restorative procedures to reconnect the intestine and fistula surgery, presents a therapeutic measure to address uncontrollable inflammation or complications[20,115]. Beside the so far discussed therapy options, pain management, nutritional support and psychological support can improve the life quality of affected patients[115].

1.2. TNF antagonists in IBD therapy

Even though no causal cure is available for IBD, TNF represents a key molecular interface in the overlapping processes of innate and adaptive immunity involved in IMID pathogenesis[133,134]. Its potential as a therapeutic target has been exploited by TNF antagonists, the first biopharmaceutical drug class to be successfully used in IBD treatment.

1.2.1. History of TNF antagonists

The history of TNF antagonists is best described by the history of infliximab (IFX), the first-in-class TNF antagonist (see **Figure 1.4**). Its approval by the Food and Drug Administration (FDA) 1998 represented the fruitful convergence of two initially independent research paths, which both began in 1975: The first publication of hybridoma-based mAb production by Köhler and Milstein and the first description of a novel cytokine later termed TNF by Carswell et al[133,135].

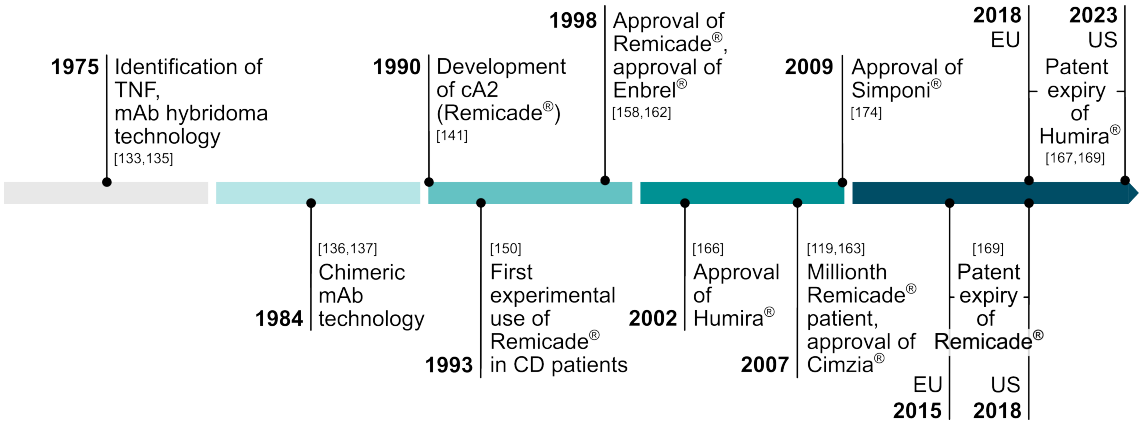

Figure 1.4.: Landmarks in TNF antagonist history. Figure adapted from[119].

1.2.1.1. Immunological and biotechnological research base for IFX development

The groundbreaking potential of the hybridoma technique to engineer therapeutic proteins was quickly recognized and further evolved through the generation of chimeric mAb[136,137]. Chimeric mAb are composed of approximately 75 % human sequence and 25 % murine sequence restricted to the antigen-binding variable domain[138]. TNF obtained its name owed to the finding that the administration of bacterial endotoxin caused tumor regression in mice[133]. This regression could be attributed to the appearance of a tumor-necrotizing

substance in murine serum following exposure[133]. In the 1980s and 1990s, researchers found that several diseases were linked to increased TNF levels. In particular, mortality in sepsis patients was found to be positively correlated with TNF elevation. Furthermore, septic shock in animal models induced by lethal doses of endotoxin or *Escherichia coli* (*E. coli*) could be prevented by immunization against TNF[139,140]. These findings led to the question whether inflammatory conditions could be treated by addressing TNF pharmacologically.

1.2.1.2. Clinical trials

Based on these intriguing findings and questions, Janssen (a Johnson & Johnson daughter) developed cA2, a chimeric mAb directed against TNF, for sepsis therapy[141]. Clinical trials, however, failed to demonstrate its efficacy in sepsis treatment[119,142]. Elevated TNF levels were also found in non-infectious conditions, e.g., in the mucosa and stool of IBD patients and in the synovial fluid of patients affected by rheumatoid arthritis (RA)[143–149]. When in 1993, a therapy-resistant pediatric CD patient in Amsterdam was administered cA2 as compassionate-use medication, she responded immediately to the first infusion[150]. This first positive clinical experience encouraged successful trials that could confirm the long-term effectiveness of regularly repeated infusions in both CD and RA[150–157]. On August 24 of 1998, cA2 renamed to infliximab received FDA approval for its first indication CD, initially for single use and later for repeated administration, and entered the drug market under its trade name Remicade®[119,158]. The next year, approval of Remicade® by the European Medicines Agency (EMA) followed. Over the years, the approval was extended by the additional indications pediatric CD, (pediatric) UC, RA and other rheumatic conditions including ankylosing spondylitis, psoriatic arthritis and plaque psoriasis[158,159].

1.2.1.3. Contribution of IFX to modernizing medicine

In their review article on Melsheimer et al. comprehensively summarize the main lessons from the development and first 20 years of Remicade® usage after approval[119]: First, Remicade® demonstrated that targeted therapies can be successfully utilized for IMID therapy. Second, as the first mAb indicated for long-time treatment in chronic conditions, Remicade® development initiated the efforts to establish adequate dosing strategies for repeated administration of therapeutic mAbs. Third, IFX approval required the establishment of new methods to characterize therapeutic mAbs and to conduct post-marketing safety trials, which later facilitated these processes in similar drugs. Fourth, the research leading to the development of Remicade® and the findings obtained from studies after approval broadened the knowledge on immunologic processes in IMID. Fifth, the remarkable treatment efficacy of IFX and other TNF antagonists has allowed to shift treatment goals from merely halting disease progression towards remission. Treat-to-target approaches combining patient-reported outcomes and objective markers of inflammation have replaced

symptom-based therapy approaches and promise higher success rates[160,161].

1.2.1.4. Currently approved TNF antagonists

Inspired by the groundbreaking success of IFX and in line with recent biotechnological advances, four other originator TNF antagonists and various biosimilars have been developed (see **Figure 1.4** and **Table 1.1**). In the same year as Remicade®, Enbrel® with the active ingredient etanercept obtained FDA approval[162]. Etanercept is probably the most exotic among all TNF antagonists, as it is composed of TNF receptor (TNFR) 2 fused to a human immunoglobulin G (IgG) 1 Fc part. Another TNF antagonist, Cimzia®, contains certolizumab-pegol, a humanized Fab' fragment linked to a polyethylene glycol (PEG) moiety[163–165]. The two human mAb adalimumab (ADM; Humira®) and golimumab (Simponi®) were approved in 2002 and 2009, respectively[166–168]. All TNF antagonists except for Remicade® and Simponi® Aria, which are administered intravenously, are administered subcutaneously. In 2015, Remicade® lost its market exclusiveness, which paved the way for their biosimilar alternatives[169]. 7, 15 and 4 biosimilars of IFX, ADM and etanercept have so far been approved by EMA and FDA. TNF antagonists are not only a clinical, but also commercial success: In 2022, AbbVie achieved 21.6 billion $ of sales with Humira®, which made it the drug with the third-highest worldwide sales, following Pfizer's Comirnaty and Moderna's Spikevax COVID-19 vaccines[170].

1.2.2. Pharmacology of TNF antagonists

The cytokine TNF plays a central role in the IBD-related chronic inflammation of the gastrointestinal tract[152,171,172]. During inflammation, infection and tissue injury, elevated TNF levels can be measured in serum and affected tissues, whereas TNF is undetectable in healthy individuals[119]. As engaged in first-line, rapid immunologic reactions, TNF appears in the bloodstream only within minutes after the initial tissue insult[173]. It is expressed by macrophages, monocytes, neutrophils, T cells, natural killer cells and non-immune cells[119,134]. TNF belongs to the TNF superfamily and is produced as a homotrimeric 26 kDa type II transmembrane protein denoted as tmTNF[174]. tmTNF can be cleaved by the metalloprotease TNF-α converting enzyme (TACE), also known as ADAM17, into a 17 kDa soluble portion, sTNF. sTNF is released into extracellular space to exert its functions via autocrine and paracrine signaling[134,175]. Both tmTNF and sTNF are biologically active[134].

Table 1.1.: Approved TNF antagonists.

	Infliximab (Remicade®) [158,176]	**Etanercept (Enbrel®)** [162,177]	**Adalimumab (Humira®)** [166,178]	**Certolizumab-pegol (Cimzia®)** [164,165]	**Golimumab (Simponi®)** [179,180]
Structure	Chimeric IgG1κ mAb (human constant regions, murine variable regions)	Human fusion protein consisting of dimeric TNFR2 and IgG1 Fc part	Human IgG1κ mAb	Humanized Fab' fragment conjugated to a 40 kDa PEG moiety	Human IgG1κ mAb
Indications*	CD, pCD, UC, pUC, RA, AS, PsA, Ps	RA, JIA, PsA, AS, Ps, SpA	RA, JIA, PsA, AS, CD, UC, Ps, HS, UV, SpA	RA, PsA, SpA, Ps, CD, AS	RA, PsA, AS, UC, JIA
Administration route	intravenous infusion	subcutaneous injection	subcutaneous injection	subcutaneous injection	subcutaneous injection
Approval year	1998	1998	2002	2007	2009
Applicant	Centocor Inc (now Janssen)	Immunex (acquired by Amgen)	AbbVie Inc.	Celltrion (acquired by UCB)	Centocor Inc (now Janssen)
Biosimilars*	Inflectra™, Flixabi®, Remsima®, Zessly®, Avsola®, Ixifi™, Renflexis® [159,181]	Erelzi®, Benepali®, Nepexto®, Eticovo™ [177,181]	Hulio®, Idacio®, Amgevita™, Amsparity™, Halimatoz™, Hefiya®, Hukyndra®, Imraldi®, Libmyris®, Abrilada™, Amjevita™, Cyltezo®, Hadlima™, Hyrimoz™, Yuflyma®, Yusimry™ [178,181]	None [165,181]	None [179,181]

*Indications and biosimilars written in teal or orange are approved by the European Medicines Agency (EMA) or the United States Food and Drug Administration (FDA) only, respectively. AS, ankylosing spondylitis; HS, hidradenitis suppurativa; IgG, immunoglobulin G; JIA, juvenile idiopathic arthritis; pCD, pediatric CD; PEG, polyethylene glycol; Ps, plaque psoriasis; PsA, psoriatic arthritis; pUC, pediatric UC; SpA, spondyloarthritis; TNFR, TNF receptor; UV, uveitis.

1.2.2.1. TNF at the molecular crossroads of cellular fate

The target structures of TNF are the two TNF receptors, TNFR1 and TNFR2[182–185]. TNFR1 is expressed ubiquitously and is activated by both tmTNF and sTNF[185]. TNFR2, however, can only be fully activated by tmTNF and is found on selected cell types only, which among others include certain T cell subtypes, endothelial cells and neurons[186]. Via binding to its receptors, TNF (co-)regulates pleiotropic cellular functions and fates, including inflammation, proliferation, survival and death by apoptosis or necroptosis, also known as inflammatory cell death[134,185]. Some of these processes are opposed to each other, which is due to the fact that the cellular interpretation of TNF signaling strongly depends on the respective cellular context and environment[185]. TNFR1, but not TNFR2 contains a death domain, which means that only TNFR1 can directly stimulate cell death[185,187].

The main molecular effector pathways initiated by TNF-TNFR binding are depicted in **Figure 1.5**. The interaction between TNF and TNFR1 leads to recruitment of the adaptor protein TNFR1-associated death domain protein (TRADD) that can initiate the assembly of the signaling complexes I, IIa, IIb and IIc, all of which are involved in distinct downstream signaling pathways (see **Figure 1.5A**)[185,188,189]. Complex I is assembled at the cytoplasmic part of TNFR1 and is composed of TRADD, receptor-interacting serine/threonine kinase 1 (RIPK1), TNFR-associated factor 2 (TRAF2), cellular inhibitor of apoptosis protein (cIAP) 1 or cIAP2, and linear ubiquitin chain assembly complex (LUBAC), as depicted in **Figure 1.5C**[185,188,190–194]. The step-wise ubiquitin-decoration of RIPK1 by LUBAC and cIAPs results in complex I stabilization and the activation of two distinct signaling cascades: The mitogen-activated kinase (MAPK) cascade and the nuclear factor κB (NFκB) cascade, thereby regulating the transcription of genes involved in inflammation, host defense, proliferation and survival[185,192,193,195].

Opposed to complex I, complexes IIa, IIb and IIc are assembled in the cytoplasm upon TNFR1 activation[185,189]. Complexes IIa and IIb activate a caspase-8-depending cascade that leads to apoptosis[189]. Complex IIc activates the mixed lineage kinase domain-like protein (MLKL), which leads to necroptosis[185,196,197]. Necroptosis involves plasma membrane destruction and the release of intracellular components into the extra-cellular matrix, which reinforces inflammation[198]. TNF binding to TNFR2 recruits TRAF2 to the plasma membrane and provokes the assembly of complex I, which activate the MAPK, NFκB or Akt pathways[185,199]. By this means, TNFR2-mediated signaling can trigger pro-inflammatory response or host defense mechanisms against pathogens (see **Figure 1.5B**)[185]. Nevertheless, it is primarily understood to mediate homeostatic, immunomodulatory and regenerative bioactivities, which follow the removal of the insult that caused inflammation in the first place[185].

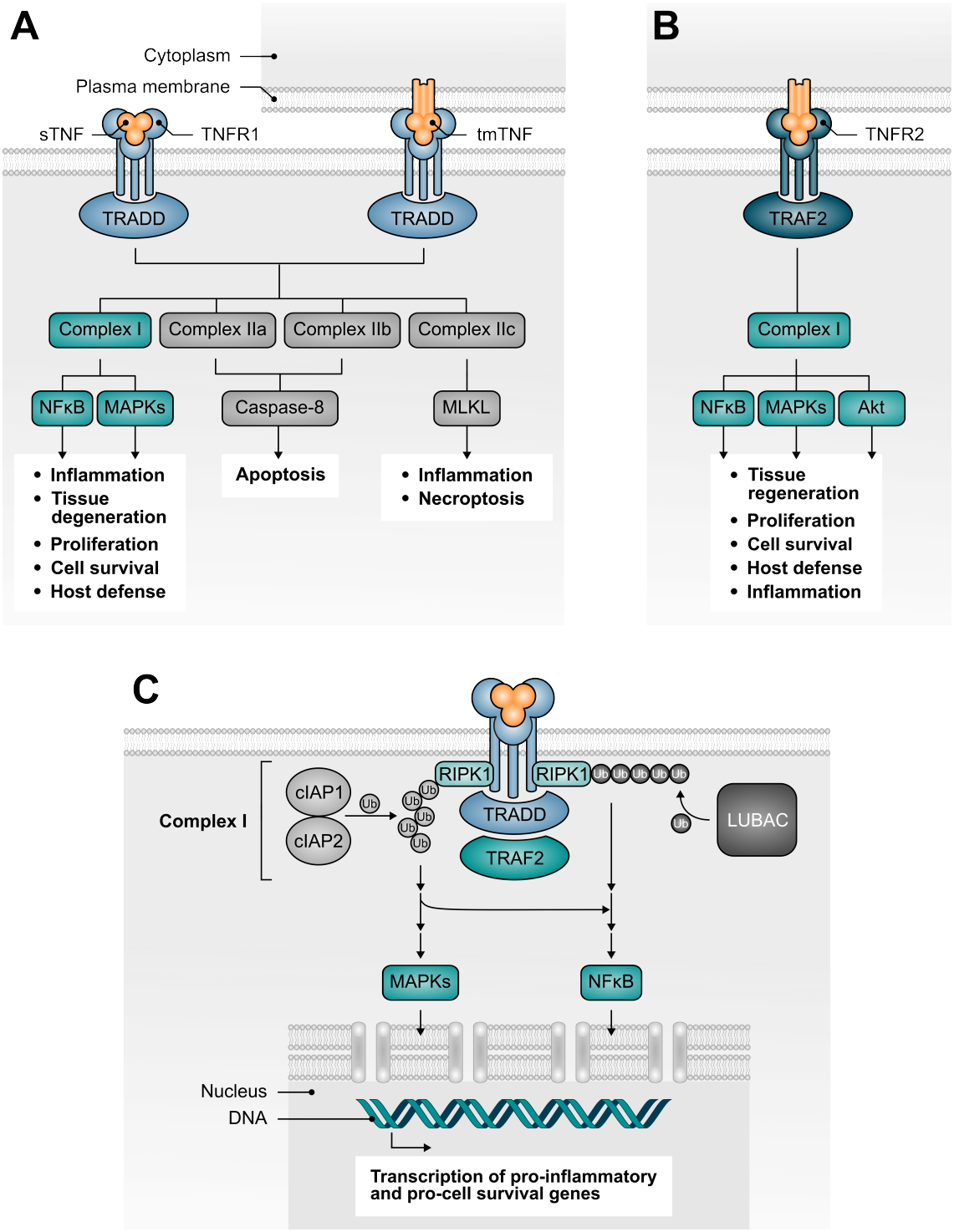

Figure 1.5.: Main signaling pathways and cell fates induced by TNF. (**A**) TNF signaling via TNFR1. (**B**) TNF signaling via TNFR2. (**C**) Molecular details of complex I-dependent signaling downstream of TNFR1. cIAP1/2-dependent ubiquitination of RIPK1 generates K63-linked Ub chains (depicted as light gray Ub), which recruit adaptor proteins for downstream MAPK signaling. LUBAC attaches linear M1-linked Ub chains (dark gray Ub) to RIPK1, which recruit adaptor proteins for further proteins involved in the NFκB pathway. Activation of the canonical NFκB pathway requires an interplay between the protein complexes recruited to both K63-linked and M1-linked Ub chains. Both the MAPK and the NFκB pathway activate the transcription of pro-inflammatory and pro-cell survival genes. Ub, ubiquitin. Figure adapted from [185] and [200].

1.2.2.2. Effects and blockage of TNF in IBD

How is TNF implicated in the specific pathobiochemistry of IBD? The disruption of the intestinal epithelial barrier plays a central role in IBD pathophysiology. Increased levels of intestinal epithelial cell death occur in the gastrointestinal tract of IBD patients [201]. Epithelial cell death by apoptosis and necroptosis, as well as the intrusion of microbial pathogens through the damaged barrier represent pro-inflammatory stimuli that lead to increased TNF expression [200]. As reviewed in **section 1.1.3**, the dysregulation of T cells in the intestinal lamina propria substantially drive IBD-related autoinflammatory processes [58]. TNF antagonists prevent TNF from interacting with TNFR, thereby interrupting the IBD-characteristic, pathologically enhanced TNF signaling. The efficacy of TNF antagonists in IBD relies on distinct pharmacological effects. First, the rapid induction of lamina propria T cell apoptosis, probably through direct or indirect prevention on anti-apoptotic TNFR2 signaling in these cells, and second, the Fc-dependent induction of M2-type wound-healing macrophages [202–208].

It has been confirmed that blockage of TNF significantly reduces epithelial cell death associated with IBD, whereas sole inhibition of TNFR1 downstream signaling, encompassing the cell death pathways, fails to restore homeostasis [202,209–211]. A study reported that the activation of TNFR2 on intestinal T cells caused disease worsening in a colitis model [212]. In line with these findings, a mouse model of T cell-mediated colitis, antagonizing the more TNFR2-specific tmTNF, induced disease remission, while sTNF-selective blocking alone did not [213]. These results also translate to clinical trials: The TNF antagonist etanercept selectively inhibits sTNF, but not tmTNF and has been found to be ineffective in CD patients [202,214]. A recent study with CD-patient derived intestinal organoids revealed that TNF synergizes with IFN-γ to induce non-canonical cell death via JAK/STAT dependent signaling [211]. Altogether, these findings underscore the particular importance of the tmTNF:TNFR2 interaction in the IBD pathomechanism, the redundance of the TNFR1-associated pathways and their complex cross-talk with other cytokines.

TNF antagonists are associated with several adverse effects, including accute infusion reactions, neutropenia, increased risk of microbial infection and malignancies [215]. Nevertheless, TNF antagonists have a better safety profile compared to the traditional therapy with small molecule immunomodulators. On one hand, the high target specificity of TNF antagonists is associated with reduced off-target effects and on the other hand, the therapeutic proteins are cleared via the same pathways as endogeneous proteins, namely proteolysis [216]. Owed to their high molecular weight (MW), which prohibits renal clearance, and neonatal Fc receptor (FcRn)-mediated IgG recycling, mAbs exhibit relatively long half-lives of approximately two weeks [176,178,179,216]. The similar longevity of certolizumab-pegol, which lacks an Fc region, is compensated by increased apparent MW conveyed by PEGylation [165]. Etanercept is the only TNF antagonist with a shorter half-live of approximately 70 h [177].

1.2.3. Immunogenicity

Even though many patients with moderate or severe disease activity respond well to TNF antagonists, more than one third does not meet primary endpoints in clinical trials and another 50 % experience loss of response after successful treatment induction [217–220]. This compromise in treatment efficiency is attributable to a considerable extent to the immunogenicity of biologic drugs: The repeated parenteral administration of therapeutic proteins can elicit a humoral immunogenic response against the drug, which manifests in anti-drug antibodies [221]. Thus, also TNF antagonists exhibit immunogenic potential that affects both drug safety and efficacy [151,221]. Reported rates of immunogenicity vary not only between different drugs, but also between studies with the same drug, whereby this variability is in part attributed to heterogeneity of anti-drug antibody assays and the duration of availability on the market [222]. In IBD patient studies, the highest immunogenicity rates have been observed with IFX and were 0.0–65.3 %, followed by 0.3–38.0 % for ADM, 3.3–25.3 % for certolizumab-pegol and 0.4–2.9 % for golimumab [222].

1.2.3.1. Factors influencing anti-drug antibody emergence

The emergence of anti-drug antibodies is influenced by several drug-related and patient-related factors [223]. Drug-related contributors include structure, dose and co-medication. Genetic predisposition and disease type present important patient-related factors. Regarding drug structure, the immunogenic potential increases with the proportion of non-human sequences. However, also fully human mAb comprise immunogenicity, even though at lower rates than chimeric mAb. Low TNF antagonist serum concentrations are associated with higher immunogenicity, while immunosuppressive co-medication reduces anti-drug antibody emergence [224–226]. Several genetic polymorphisms of the human leukocyte antigen (HLA), are associated with an increased risk to develop anti-TNF antagonist antibodies [227–231]. Furthermore, individual or disease-specific immunologic pathways, such as variability in IL-10 levels, are understood to modulate anti-drug antibody levels [223,232–236].

1.2.3.2. Impact of TNF antagonist immunogenicity

Anti-drug antibodies can reduce drug efficacy by affecting both TNF antagonist pharmacodynamics and pharmacokinetics. Neutralizing anti-drug antibodies bind the drug's TNF-binding region and thereby directly interfere with its mechanism of action [221,237]. Non-neutralizing anti-drug antibodies bind TNF antagonists in a manner that does not inhibit drug function [221,237]. However, non-neutralizing anti-drug antibodies can result in immune complex formation and accelerated drug elimination [237,238]. As the TNF-binding region is characterized by higher "foreignness" and thus higher immunogenicity, the vast majority of anti-drug antibodies is estimated to be neutralizing [237]. Clinically, anti-drug antibodies are associated with shortened response to therapy, lower TNF antagonists serum concentrations and higher risk for infusion reactions [222,239–241]. Infusion

reactions constitute the main adverse reaction associated with biologic immunogenicity and manifest as rash, dizziness, fever, bronchospasms or cardiovascular collapse [242]. The prevalence of infusion reactions in IFX treatment has been reported as 4–15 % [243]. In conclusion, immunogenicity poses the risk for treatment failure, is associated with adverse effects and can thus require the necessity to discontinue the TNF antagonist and switch to alternative medication.

1.2.4. TDM

Therapy failure in TNF antagonist therapy is described by absent or insufficient response to the drug. Primary non-response is defined as the absence of response during the induction of drug [244]. Secondary loss of response (LOR) is understood to be the loss of response to therapy after successful drug induction [244]. Both primary non-response and LOR can occur with or without immunogenicity involvement. As anti-drug antibodies can cause therapy failure, they need to be considered in its management [245,246]. Beside anti-drug antibody status, serum drug concentration is a well-known determinant of therapy success, whereby low drug concentrations are associated with anti-TNF failure [244,245,247]. Thus, therapeutic drug monitoring (TDM) is recommended for TNF antagonists in IBD treatment in order to optimize drug concentrations, identify reasons of therapy failure and rationalize therapeutic decisions [248]. In the present work, TDM refers to assessment of both the biologic drug and anti-drug antibody levels. In routine diagnostics, these parameters are measured in serum.

1.2.4.1. Goals and strategies

Based on anti-drug antibody status and serum drug concentrations, TNF antagonist failure can be classified into different subtypes, each of which requires different therapeutic intervention (see **Figure 1.6**) [246]: Mechanistic or pharmacodynamic failure describes LOR at drug levels within the therapeutic target concentration range. For mechanistic failure, switching out of drug class (i.e., to a biologic outside the TNF antagonist class) is recommended. If anti-drug antibodies are detectable, combination with immunosuppression should be considered. LOR at subtherapeutic drug concentrations is classified as pharmacokinetic failure. In absence of anti-drug antibodies, TNF antagonist dose escalation is recommended, either by increased dosing or shortened dosing intervals. LOR patients with immunogenicity-mediated pharmacokinetic failure benefit more from switching within drug class (i.e., to a different TNF antagonist) and concomitant immunosuppression.

Recent expert consensus statements by Cheifetz et al. and Vande Casteele et al. report the serum concentration targets for maintenance therapy with IFX (5–10 µg/mL), ADM (8–12 µg/mL) and certolizumab-pegol ($\geq$ 20 µg/mL) [220,248]. Recent research has suggested, however, that these goals should be revised or further individualized, since certain disease subtypes or complications (e.g. fistulizing CD) may require higher drug levels to

achieve clinical response[220]. Defining a therapeutic goal for anti-drug antibody serum levels is even more complicated: Due to the lack of a gold standard method for anti-drug antibody quantification and the resulting assay heterogeneity, including differences in calibrators and reported units, anti-drug antibody concentrations cannot be compared between assays[249–252]. Immunogenicity is highly prevalent among TNF antagonists, but low or transient anti-drug antibodies do likely not impair clinical remission. Hence, a mere discrimination between positive and negative immunogenicity status would result in unnecessary drug switches and uneconomic drug use[240,253,254]. Reference ranges for TDM assays are commonly established at the discretion of the individual medical laboratories. Of note, the medical reports available to us indicated therapeutic windows of 3–8 µg/mL for IFX and 5–12 µg/mL for ADM, which are in line with a consensus statement published by Mitrev et al.[255]. Thus, these reference ranges were applied in the present work (see **Figure 1.6**). In spite of the variability among TDM assays and practices, studies with IFX-treated IBD patients have shown that TDM was more cost-efficient as compared to empiric dose optimization and led to better endoscopic outcomes[256–258].

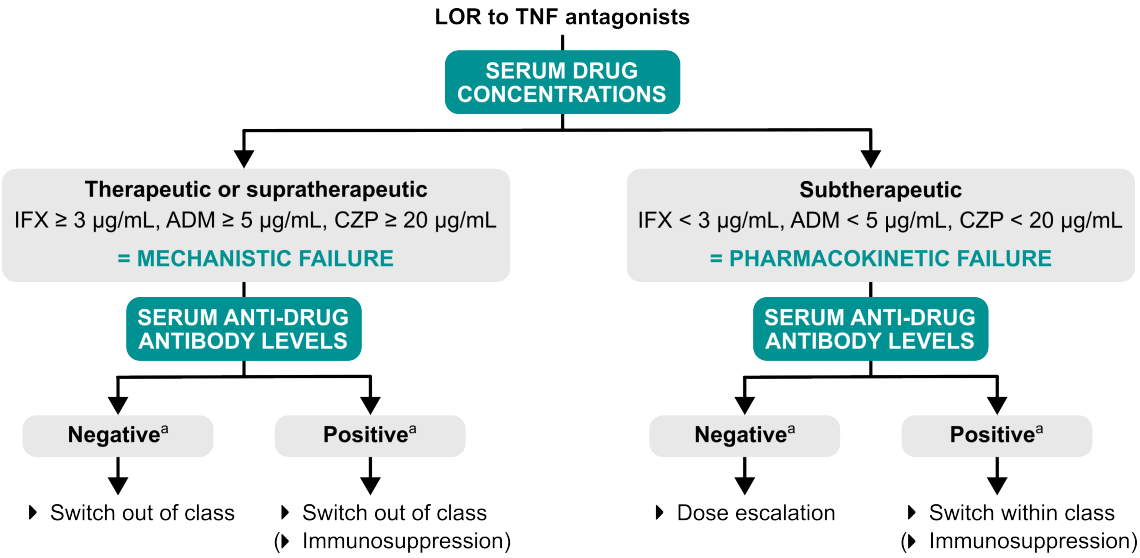

Figure 1.6.: Recommended algorithm for reactive TDM in IBD. [a]Anti-drug antibody-negative or -positive status is replaced by concentration cut-offs in some medical laboratories depending on the particular assay and the availability of relevant data for the assay. CZP, certolizumab-pegol. Figure adapted from[246].

1.2.4.2. Assays

For the TDM of TNF antagonists, different methods have been established[221,259–261]. It has to be kept in mind that serum samples can potentially contain both TNF antagonist and anti-drug antibodies. Regarding TNF antagonist quantification, commonly only the free fraction, which is not bound to TNF, is measured. Anti-drug antibody assays are classified into drug-sensitive and drug-tolerant assays[262]. In drug-sensitive assays, anti-drug antibodies can only be quantified in absence of free (i.e., detectable) TNF antagonist levels, since TNF antagonist interferes with anti-drug antibody quantification[262]. Drug-

tolerance, in contrast, is usually conveyed by a specific pre-analytic sample acidification step (PA) that enables these assays to assess the total anti-drug antibody fraction, i.e., free plus drug-bound anti-drug antibodies[262–266]. Even though drug-tolerant assays for anti-drug antibody quantification are more sensitive, their utility for routine TDM is still under debate[221]. An overview of the different methods is provided in **Figures 1.7 + 1.8**.

Variants of the enzyme-linked immunosorbent assay (ELISA) are most commonly applied in routine TDM for analysis of both drug and anti-drug antibodies (see **Figures 1.7A + 1.8A**)[260]. Antigen capture ELISA formats, for example, are relatively inexpensive[246,260]. However, capture ELISA is prone to non-specific binding and false positive results when analyzing serum[261]. The bridging ELISA format exploits the bivalency of antibody analytes and involves both analyte mAb paratopes in the detection process, therefore reducing non-specific binding[261]. Especially for routine anti-drug antibody measurement, bridging ELISA are frequently applied, which employ TNF antagonists as capture and detection agent. However, many bridging ELISA are drug-sensitive[260,261]. Chemiluminescence immunoassays (CLIA) and electrochemiluminescence immunoassays (ECLIA) utilize analogous immunoassay formats as compared to ELISA, but different detection and readout methods[267–274]. Instead of horseradish peroxidase (HRP)- or alkaline phosphatase-catalyzed color changes, CLIA detection involves the emission of light by luminophores, mostly in the UV or visible spectrum, which is triggered by a chemical reaction[268,269,272–274]. The luminophoric substrates can be directly attached to the detection antibody (e.g., acridinium esters) or added as a substrate (e.g., luminol), which is converted by a suitable enzyme attached to the detection antibody[268]. ECL also relies on luminophore-dependent light emission[271,275]. In ECL, an electrogenerated high-energy electron transfer causes light emission, whereby the luminophore (e.g., ruthenium tris-bipyridine) is attached to the detection antibody[271,275]. ECL and CLIA exhibit higher sensitivity, as bioluminescence detection is associated with lower background signals than color change detection[275]. Regardless on the detection technology, bridging immunoassays are capable of detecting immunoglobulins across all classes, except for bispecific IgG4, which however also contribute to anti-TNF antagonist immunogenicity[276].

Fluid-phase techniques, such as the homogeneous mobility shift assay (HMSA) and radioimmunoassay (RIA), are less drug-sensitive and more sensitive for low-affinity anti-drug antibodies as compared to solid-phase techniques like ELISA and comparable immunoassays[260]. In HMSA, serum samples are incubated with a known, excess amount of fluorescently-labeled (FL) probe (TNF for IFX quantification or drug for anti-drug antibody quantification; see **Figures 1.7B + 1.8B**)[264]. This incubation step results in the formation of complexes between analyte and the FL probe, if analyte is present in the sample. Following incubation, the samples are subjected to size-exclusion chromatography (SEC)-high-performance liquid chromatography coupled with fluorescence detection. During SEC, analyte-bound and free FL probe are separated and the respective peak areas provide information on analyte concentration. As the HMSA procedure for anti-drug anti-

body analysis involves a pre-analytic acidification step, it is drug-tolerant [260,264,271].

In RIA, similar to HMSA, serum samples are incubated with a radioactively labeled probe of defined activity [261,271,277,278]. For drug quantification, complexes of drug, ^{125}I-labeled TNF and an anti-human IgG antibody are separated from free ^{125}I-TNF by centrifugation [277]. Then, radioactivity in the pellet is measured by a gamma counter (see **Figure 1.7C**). For anti-drug antibody quantification, IgG are captured from serum with protein A sepharose beads, which are then incubated with ^{125}I-labeled drug. After separation, bead-bound radioactivity is quantified (see **Figure 1.8C**) [271]. Of note, other RIA setups have been developed as well, which are not explained herein [271]. In spite of superior analytic sensitivity, fluid-phase assays are more labor-intensive as compared to solid-phase assays [260].

In addition to the so far discussed assays, reporter gene assays and cell-based assays have been developed for both drug and anti-drug antibody assessment [260,279,280]. With these methods, only neutralizing anti-drug antibodies are captured [260]. Furthermore, lateral flow assays and biosensor-based techniques have been developed [281–289]. These are, however, not commonly utilized in routine TDM so far. Since the approval of IFX as the first TNF antagonist, methods to analyze drug levels and anti-drug antibodies have improved substantially. Still, no consensus regarding a gold standard method has been established and the available assays notoriously lack harmonization. Therefore, the comparison of both TDM and study data is only meaningful for results obtained with the same tests [246,247,252,262]. Despite the effort already invested in this regard, these obstacles still challenge the generation of robust TDM data and therefore also the development of TDM-based therapeutic algorithms [252,290]. [268] [269]

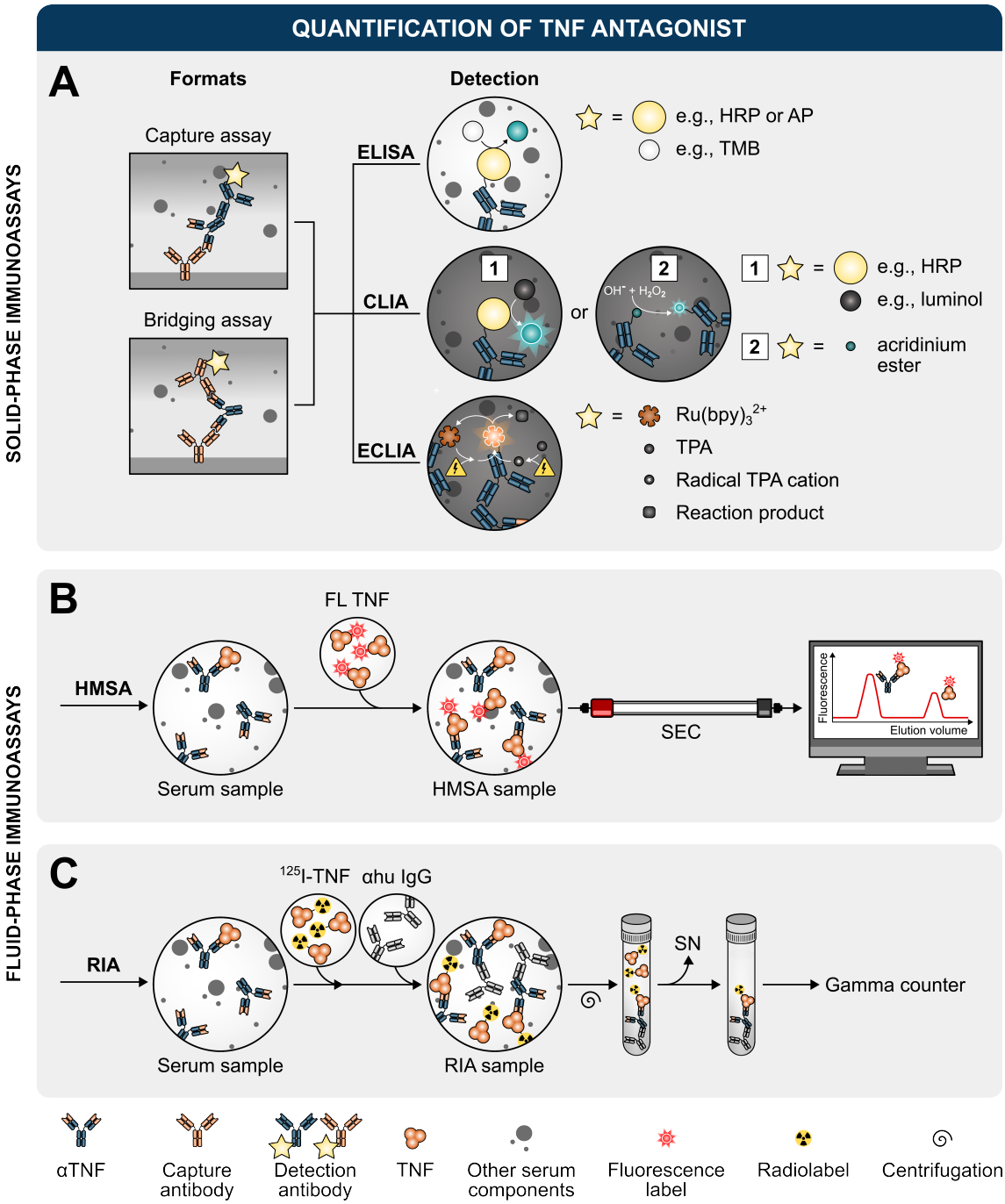

Figure 1.7.: Common assays for TNF antagonist quantification. (**A**) Solid-phase immunoassay formats and detection principles for ELISA, CLIA and ECLIA. (**B**) HMSA principle. (**C**) RIA principle. αhu, anti-human; αTNF, TNF antagonist; AP, alkaline phosphatase; bpy, 2,2'-bipyridine; SN, supernatant; TMB, 3,3',5,5'-tetramethylbenzidine; TPA, tripropylamine.

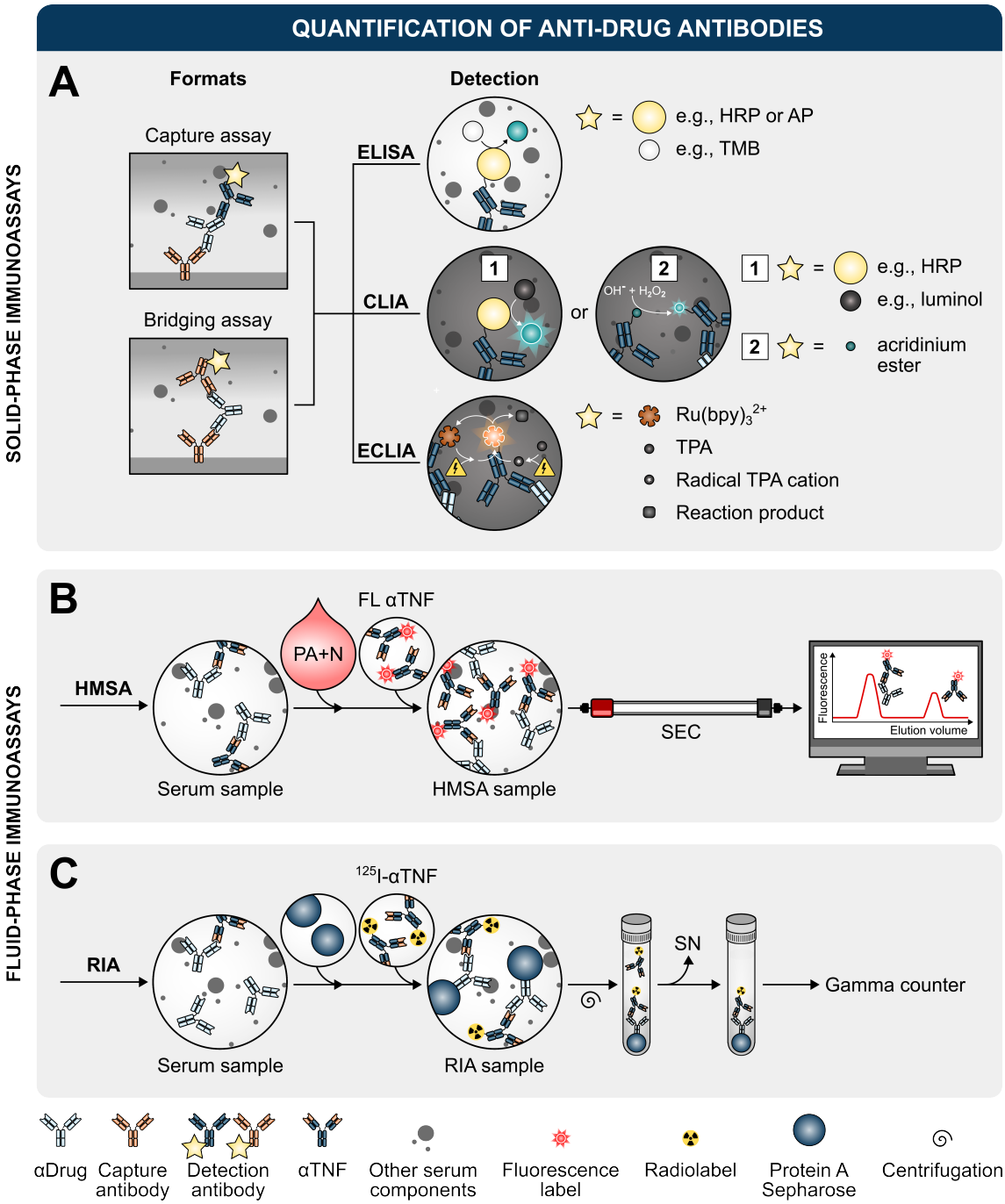

Figure 1.8.: Common assays for anti-drug antibody quantification. (**A**) Solid-phase immunoassay formats and detection principles for ELISA, CLIA and ECLIA. (**B**) HMSA principle. (**C**) RIA principle. αDrug, anti-drug antibody; αTNF, TNF antagonist; AP, alkaline phosphatase; bpy, 2,2'-bipyridine; PA + N, pre-analytic acidification and neutralization; SN, supernatant; TMB, 3,3',5,5'-tetramethylbenzidine; TPA, tripropylamine.

1.3. Surface plasmon resonance (SPR) spectroscopy

Surface plasmon resonance (SPR) revolutionized molecular interaction studies, arising from the convergence of physics, optics and chemistry. SPR exploits optophysical phenomena of photon-electron interactions that occur under defined circumstances at phase boundaries involving thin metal layers [291]. In biosensor setups, SPR can be exploited for the detection and analysis of biological substances. Biosensors combine a biological recognition element with a transducer, converting biological responses into measurable signals [292]. This biological recognition element, typically a biomolecular interactant attached to the metal surface, interacts with its soluble binding partner, which is passed over the sensor surface [292]. The solid phase-attached interactant is defined as ligand, whereas the fluid-phase interactant, which commonly is the interactant to be analyzed, is termed analyte [292]. SPR biosensors assess molecular interactions in a label-free environment and in real-time for manifold biomolecules, such as proteins, DNA, lipids, or small molecules and intra-molecular conformational changes [291,293–300]. Even though commonly used for binding kinetic analyses, SPR is also applied to detect and quantify analytes of interest or investigate binding specificity [301,302].

1.3.1. History of SPR: From Wood's anomalies to modern application

The history of SPR dates back to the early 20th century, when the physicist Robert W. Wood shone polarized light onto a metal-backed diffraction grating and observed anomalous reflection patterns that he could not explain [303]. Over the subsequent decades, Woods' anomalies would remain one of the most intriguing scientific puzzles, engaging contemporary scientists in their quest for a solution [304]. Colleagues from the field, such as Maystre (2012), have claimed that Wood "must be considered as the initiator of plasmonics" [304]. Fano et al. and Ritchie et al. contributed important theoretical work suggesting that Wood's experimental observations were caused by the oscillative excitation of metal surface electrons [305,306]. In 1952, Pines and Bohm coined the term "plasmon" for collective oscillations of electron density in thin metal layers when bombarded with fast electrons and added theoretical models for this phenomenon [307–309].

In 1968, Kretschmann and Otto first published experimental configurations that applied attenuated total reflection for the optical excitation of surface plasmons [310–312]. As summarized by Homola et al., the Kretschmann geometry has evolved to the most commonly employed SPR configuration in biosensor applications [291]. Beside the Kretschmann configuration, diffraction grating-based systems for SPR sensing have been developed [313]. Breakthrough work was accomplished in the 1980s and 1990s with the development of practical SPR-based sensing systems [314–316]. In 1983, Liedberg and Nylander demonstrated the first practical biosensing application of SPR for gas detection [317,318].

Intrigued by the simplicity and sensitivity achieved with the non-optimized instrumentation utilized by Liedberg and Nylander, the Swedish company Pharmacia Biosensor AB

(later renamed Biacore AB) was founded to develop, produce and market SPR instrumentation for the analysis of biomolecular interactions in 1986 [319]. With the BIAcore SPR system, the first commercial SPR instrument was released in 1990 [316,319,320]. The potential of SPR for biomolecular analysis application was recognized. As reviewed by Homola et al., earlier studies on antigen-antibody interactions served to optimize SPR method development [291]. Soon, more complicated interactions were investigated using SPR, including protein-protein interactions, protein-DNA interactions, protein conformational changes or small molecule binding [291].

Over the years, SPR technology has evolved, with advancements in sensor design, instrumentation, and data analysis methods. Miniaturization, automation, and improvements in sensitivity have made SPR a versatile and indispensable tool in various scientific and industrial applications, expanding its utility in fields ranging from medical diagnostics to material science.

1.3.2. SPR theory

The following review of SPR theory is based on the comprehensive publications provided by Homola et al. (1999) and Nguyen et al. (2015) [291,301]. Total internal reflection occurs when light is shone onto the interface to a medium with lower refractive index (e.g., from glass to air) at the so-called critical angle. At this angle, the incident light beam is reflected completely, i.e., at identical intensity and wavelength as the incident beam [321]. SPR spectroscopy exploits optophysical phenomena at the interface between a conductor (usually a metal) and a dielectric (typically air or a non-conductive material).

When polarized light is shone onto metal under the conditions of total internal reflection (e.g., through a glass prism) and at a specific wavelength, photons of the incident light beam couple resonantly with the free metal electrons. As a consequence of this photon-electron interaction, the metal electrons are excited to oscillate. These collective electron oscillations at the metal-dielectric interface are called surface plasmons and propagate parallel to the metal surface. SPR owes its name to the resonance effects causal for this phenomenon.

The oscillations of the negatively charged electrons generate a transversal electromagnetic wave, the evanescent field. The evanescent field penetrates into the medium adjacent to the metal surface. Exemplary penetration depths of the evanescent field for glass-gold-water interfaces are 400 nm for 850 nm light wavelength and 162 nm for 630 nm light wavelength [291]. The ability of the evanescent wave to interact with molecules in close proximity to the metal surface without the need for labels is a key advantage of SPR-based biosensors. The incident light beam energy portion absorbed by the evanescent wave causes a characteristic and measurable intensity dip in the reflected light beam.

The emergence of SPR depends on angle and wavelength of the incident light beam, whereby a constant wavelength is typically utilized. The incident light angle, at which the

photons couple resonantly with the electrons and thereby cause surface plasmon excitation, is called the resonance angle. This angle is highly sensitive to changes in the refractive index of the material adjacent to the metal surface. Consequently, changes in the refractive index in vicinity to the metal surface, for example due to the binding of molecules to the metal surface, alter the resonance condition. By monitoring changes in the resonance condition, for example by measuring the angle of minimum intensity within the reflected light beam, interactions occurring at the metal surface can be detected and monitored. Since the detected changes are proportional to the mass of interactant binding to the sensor surface, the surface concentration of interactant can be quantified.

1.3.3. Principles of SPR biosensing

In SPR biosensors, the Kretschmann configuration is most commonly applied, which utilizes a radiation source and a high-reflective-index glass prism in the attenuated total reflection geometry (see **Figure 1.9**)[291]. The ligand, constituting the biological recognition element, is immobilized onto the metal surface[292]. Some commercially available gold sensor chips comprise carboxy-dextrane, protein A/G or streptavidin adherent to the surface, which facilitates ligand immobilization via common chemical coupling or affinity capturing techniques. The sample solution is pumped over the ligand-modified metal surface through microfluidic flow channels. If inter-molecular interactions occur at the sensor surface, the refractive index adjacent to the sensor surface increases and the resulting SPR changes can be monitored[301].

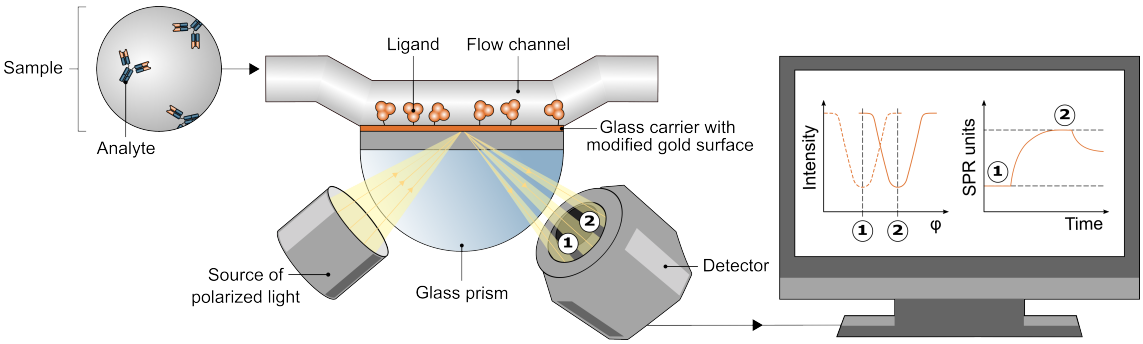

Figure 1.9.: SPR biosensor in Kretschmann configuration. The sensor surface consists of a gold layer, which is located on a glass carrier. The glass carrier is docked onto the glass prism and thereby connected to the optical system. The ligand is attached covalently to the sensor surface. When sample is pumped through the flow cell, an optical detector monitors the SPR angle (φ) shift, which occurs when analyte binds to the ligand. Angle shifts are proportional to the amount of analyte binding and are translated to sensorgrams that depict the interactions in real-time. Adapted from[322].

Depending on the light characteristic to be analyzed, SPR setups can be classified into angular, wavelength- and intensity-modulated systems[323]. Most commonly, angular detection systems are utilized, in which monochromatic light is directed in variable incident angles to the metal surface[323]. The intensity dip angle in the reflected angular spectrum is assessed[324]. In classical SPR, the biomolecular interaction is recorded in real-time as a

sensorgram showing SPR angle variation versus time. Typically, SPR signals are reported as resonance units (RU) proportional to the SPR angle variation. For example, in Biacore systems combined with the broadly utilized CM5 sensor chip, an SPR signal of 1 RU corresponds to a protein surface concentration of approximately 1 pg/mm^2 [325].

The classical application of SPR has been the determination of kinetic parameters for inter-molecular interactions. However, the development of SPR biosensors intended for use in medical diagnostics or analytics has gained interest in the scientific community in recent years [288,302,326–329]. SPR comprises several favorable features that can meet the needs for diagnostic tests, such as high sensitivity, real-time monitoring, label-free detection, quantitative analysis, small sample volume, and the potential for automation, multiplexing and high throughput. These attributes collectively contribute to the rising interest in developing SPR biosensor assays for medical purposes.

1.4. Aims of this thesis

These days, assays for TDM of TNF antagonists mainly address the quantification of drug and anti-drug antibodies. However, the lack of a consensus therapeutic algorithm for and from the TDM of TNF antagonists suggests that the information delivered by state of the art assays may be insufficient. SPR comprises some significant advantages over other methods, such as its label-free nature, the capacity for analyte multiplexing and the potential to simultaneously obtain quantitative and qualitative data on analytes. Thus, the aim of this dissertation was to develop SPR-based biosensor assays for the TDM of TNF antagonists and their corresponding anti-drug antibodies.

Proof-of-concept assays should be established for the exemplary TNF antagonist IFX utilizing a Biacore X100 SPR device. The new biosensor assays should be able to reliably quantify both IFX and anti-infliximab antibodies (ADA) trough concentrations for the respectively expectable analyte concentration ranges in patient serum. In particular, ADA quantification was intended to be drug-tolerant, such that the presence of serum IFX would not interfere with ADA analytics. The protocols for both assays should be as simple and short as possible.

Beside quantification, the SPR measurements should be exploited to gain additional qualitative information about ADA. As the major application purpose of SPR lies in biomolecular interaction analysis, a simple method should be developed to characterize the binding stability of patient-individual ADA. Of note, this method should circumvent standard kinetic analysis, as neither patient ADA nor serum as sample matrix fulfill the requirements for meaningful kinetic analysis. Additionally, a biosensor approach for ADA epitope mapping should be established in order to evaluate the IFX-neutralizing nature of individual patients' ADA.

The developed biosensor assays should be validated in terms of biosensor stability, calibra-

tion, analytic sensitivity, accuracy and precision and - only in the case of ADA quantification - analytic drug tolerance. The performance of the biosensors should then be evaluated by analysis of IBD patient sera. Method comparison with respective diagnostics-approved ELISA should be conducted in order to estimate the suitability of the new SPR biosensor assays for routine diagnostic application. Considering the special features of SPR analytics, the competitiveness of both assay performance and feasibility for the developed biosensor assays compared with other commercially available assay formats was evaluated.

Additionally, it should be studied how the diagnostic value of TDM results, both from the developed SPR biosensors and ELISA, can be increased. Therefore, a small observational study was performed and the data were statistically analyzed in a retrospective fashion. As unique selling point of SPR, ADA binding properties should be in the focus of these evaluations. Last, the transferability of the assay principles to other TNF antagonists should be tested.

2. Materials and methods

2.1. Materials, equipment and software

2.1.1. Supplier companies

Boldface print indicates the supplier company abbreviations, which are utilized in all following sections.

Supplier	**Headquarter**
Abcam plc.	Cambridge, UK
Andreas **Hettich** GmbH & Co. KG	Tuttlingen, DE
B. Braun SE	Melsungen, DE
BANDELIN electronic GmbH & Co. KG	Berlin, DE
Bemis Company, Inc.	Neenah, US
Bio-Rad Laboratoris, Inc.	Hercules, US
BioRender	Toronto, CA
BioTek Instruments, Inc.	Winooski, US
Brand GmbH & Co. KG	Wertheim, DE
Carl **Roth** GmbH + Co. KG	Karlsruhe, DE
Celltrion Healthcare Co., Ltd.	Incheon, KR
Cytiva	Marlborough, US
Eppendorf, SE	Hamburg, DE
GraphPad Software, LLC	San Diego, US
Greiner Bio-One International GmbH	Kremsmünster, AT
GSL Biotech, LLC	Chicago, US
Heathrow Scientific, LLC	Vernon Hills, US
Honeywell International, Inc.	Charlotte, US
HP, Inc.	Palo Alto, US
IKA-Werke GmbH & Co. KG	Staufen, DE
Immundiagnostik AG	Bensheim, DE
INTAS Science Imaging Instruments GmbH	Göttingen, DE
Jackson ImmunoResearch Laboratories, Inc.	West Grove, US
Janssen Biologics B.V.	Leiden, NL

Köttermann GmbH	Uetze, DE
LI-COR Biosciences, Inc.	Lincoln, US
Macherey-Nagel GmbH & Co. KG	Düren, DE
Memmert GmbH & Co. KG	Schwabach, DE
Merck KGaA	Darmstadt, DE
Microsoft Corporation	Redmond, US
Miltenyi Biotec B.V. & Co. KG	Bergisch Gladbach, DE
New **E**ngland **B**iolabs, Inc.	Ipswich, US
Otto Fischar GmbH & Co. KG	Saarbrücken, DE
PerkinElmer, Inc.	Waltham, US
Pfizer, Inc.	New York, US
R-Biopharm AG	Darmstadt, DE
Roche Holding AG	Basel, CH
RStudio PBC	Boston, US
Sarstedt AG & Co. KG	Nümbrecht, DE
Sartorius AG	Göttingen, DE
SCHOTT AG	Mainz, DE
Scientific Industries, Inc.	Bohemia, US
Siemens AG	Munich, DE
Sino Biological, Inc.	Beijing, CN
Takeda, Ltd.	Tokyo, JP
Th. Geyer GmbH & Co. KG	Renningen, DE
Thermo Fisher Scientific, Inc.	Waltham, US
Viatris, Inc.	Canonsburg, US
VWR International, LLC	Radnor, US

2.1.2. Patients and sera

In this thesis, sera from IBD patients under IFX or ADM therapy were used for the validation of the developed SPR biosensor assays. Inclusion criteria were legal age (18 years or older) and confirmed diagnosis of CD or UC. The IFX cohort comprised patients treated with the originator drug Remicade® and with the biosimilars Remsima® (Celltrion) or Inflectra® (Pfizer). ADM patients received the biosimilar Hulio®. In total, 204 sera from 73 different patients collected at two different clinics between May 2015 and August 2022 were included in the present doctoral thesis project:

- Specialized gastroenterologic outpatient clinic:
  Gastroenterologische Gemeinschaftspraxis
  Prof. Dr. Peter Langmann and Dr. Monika Weikert
  (Karlstadt, DE)

- Tertiary care center:
  Clinic and Polyclinic for Internal Medicine II (Gastroenterology)
  Klinikum rechts der Isar der Technischen Universität München
  (Munich, DE)

Within the patients' routine TDM, all included sera were sent to the MVZ Medizinisches Labor Oldenburg GmbH (Oldenburg, DE) for the quantification of TNF antagonist and/or respective anti-drug antibodies (see **sections 2.2.4, 2.3.7 and 2.5.3**). Besides IBD patient material, healthy volunteer sera and leftover sera from IFX- and ADM-naive patients were used as negative controls. Blank serum matrix pools differed for the different developed assays, since they depended on the availability of sera. All aliquots were stored at -80 °C.

The study was approved by the local Ethics Committee (Ethikkommission der Fakultät für Medizin der Technischen Universität München, approval number 289/19 S) and conducted in accordance with the 1964 Helsinki declaration and its later amendments, or comparable ethical standards. Written informed consent was obtained from all patients. No financial compensation was provided. All data from patients and healthy control subjects were pseudonymized and were not shared with external entities. A comprehensive list of enrolled patients, sera, collection sites and TDM analytes is included in the appendix.

2.1.3. Chemically competent *E. coli* cell strains

Cell strain	Genotype	Supplier	Product no.
BL21 (DE3)	F$^-$ *omp*T *hsd*S$_B$ (r_B^-, m_B^-) *gal dcm* (DE3)	Merck	CMC0014
NEB5α	F$^-$ *fhuA2* Δ*(argF-lacZ)U169 phoA glnV44* ϕ*80* Δ*(lacZ)M15 gyrA96 recA1 relA1 endA1 thi-1 hsdR17* (r_K^-, m_K^+)	NEB	C2987I

2.1.4. Cell culture media, supplements and antibiotics

Substance	Purpose	Supplier	Product no.
Agar-agar, Kobe I for microbiology	Lysogeny broth (LB) agar plates	Roth	5210.3
Isopropyl β-D-1-thiogalacto-pyranoside (IPTG), BioScience Grade, ≥ 99 %, dioxane-free	Expression induction	Roth	2316.4
LB Broth (Luria/Miller)	Culture medium	Roth	X968.2
Kanamycin sulfate from *Streptomyces kanamyceticus*, BioReagent, suitable for cell culture	Antibiotic	Merck	K1377-5G

2.1.5. DNA plasmids

Plasmid	Insert	Donator
pET_1b_TrxA_IdeS	IdeS	Ulrich von Pawel-Rammingen (Uppsala, SE)[330,331]

2.1.6. Pharmaceutical products

Drug name	Supplier	PZN
Hulio® (ADM biosimilar)	Viatris	14338725
Human® serum albumin (hSA)	Takeda	11128720
Remicade® (IFX)	Janssen Biologics	10822631

2.1.7. Antibodies

Primary antibodies.

Antibody	Host	Supplier	Product no.
Anti-ADM	Human	Bio-Rad	HCA203
Anti-goat IgG	Donkey	Jackson	705-005-147
Anti-hSA	Mouse	Abcam	ab10241
Anti-human IgG	Mouse	Jackson	209-005-082
Anti-IFX	Human	Bio-Rad	HCA233

Secondary antibodies.

Antibody	Host	Supplier	Product no.
Anti-mouse IgG + HRP	Goat	Jackson	115-035-062

2.1.8. Other proteins and enzymes

Protein	Supplier	Product no.
Blocker casein in PBS	Thermo	37528
Bovine serum albumin (BSA)	Merck	A3059
DNase I	Roche	4536282001
Human TNF	Sino Biological	10602-HNAE
Human transferrin (hTf)	Merck	T3309
Lysozyme	Merck	62971-10G-F
Skim milk powder (SMP)	Merck	70166-500G
Tobacco etch virus (TEV) protease	NEB	P8112S

2.1.9. Kits, reagents and stains

Material	Purpose	Supplier	Product no.
Acrylamide/bisacrylamide solution, 40%, 37.5:1	SDS-PAGE	Bio-Rad	1610148
APEX™ Antibody Labeling Kit Alexa 488	ADA calibrator fluorescence labeling	Thermo	A10468
cOmplete™ Mini EDTA-free Protease Inhibitor Cocktail	Protein expression	Roche	11836170001
IDKmonitor® Adalimumab drug level ELISA	ADM quantification validation	Immundiagnostik	K 9657
IDKmonitor® Adalimumab total ADA ELISA	anti-ADM quantification validation	Immundiagnostik	K 9651
IDKmonitor® Infliximab drug level ELISA	IFX quantification validation	Immundiagnostik	K 9655
IDKmonitor® Infliximab total ADA ELISA	ADA quantification validation	Immundiagnostik	K 9654
Monarch® Plasmid Miniprep Kit	Purification of plasmid DNA	NEB	T1010S
PageRuler™ Prestained Protein Ladder	SDS-PAGE	Thermo	26616
Pierce™ ECL Western Blotting Substrate	WB	Thermo	32109
Quick Start™ Bovine γ-Globulin Standard Set	Protein quantification	Bio-Rad	5000209
Quick Start™ Bovine Serum Albumin Standard Set	Protein quantification	Bio-Rad	5000207
Quick Start™ Bradford 1x Dye Reagent	Protein quantification	Bio-Rad	5000205
ROTI®Blue quick	Gel staining	Roth	4829.2

2.1.10. Beads, columns and resins

Material	Supplier	Product no.
Dynabeads™ M-280 Tosylactivated	Thermo	14204
His-Trap™ High Performance	Cytiva	17524701
Superdex™ 200 Increase 10/300 GL	Cytiva	28990944

2.1.11. Chemicals

Substance	Supplier	Product no.
1-Ethyl-3-(3-dimethyla-minopropyl)-carbodiimide hydrochloride (EDC-HCl), PEPTIPURE®, $\geq 99\,\%$	Roth	2156.1
2-Mercaptoethanol, $\geq 99\,\%$, p.a.	Roth	4227.1
2-Propanol, gradient grade for liquid chromatography LiChrosolv®	Merck	1.01040.2500
3-{Dimethyl[3-(3α,7α,12α-trihydroxy-5β-cholan-24-amido)propyl]azaniumyl}-propane-1-sulfonate (CHAPS)	Thermo	28300
3',3",5',5"-Tetrabromophenol sulfone-phthalein (bromophenol blue), indicator ACS, Reag. Ph. Eur	Merck	8122
Acetic acid, glacial, EMSURE® ACS, ISO, Reag. Ph. Eur, $100\,\%$	Merck	1.00063.1000
Ammonium persulfate (APS) for molecular biology, $\geq 98\,\%$	Merck	A3678-25G
Ammonium sulfate ($(NH_4)_2SO_4$), Suprapur® ACS, $\geq 99.9999\,\%$	Merck	1.01209.0500
Ethanol (EtOH)		
denatured, $\geq 80\,\%$	Otto Fischar	27680
for molecular biology, $\geq 99.8\,\%$	Merck	1.08543.0250
ROTIPURAN®, $\geq 99.8\,\%$, p.a.	Roth	9065.2
Ethanolamine, $\geq 99\,\%$	Merck	15014-1L
Ethylenediaminetetraacetic acid (EDTA), anhydrous, crystalline, BioReagent	Merck	E6758-100G

Formaldehyde solution		
16 %, methanol-free	Thermo	28906
37 %, ACS, contains 10-15 % methanol	Merck	252549-100ML
Glycerol, for analysis EMSURE® ACS, Reag. Ph. Eur	Merck	1.04092.1000
Glycine, for electrophoresis, $\geq 99.7\,\%$	Merck	1.04169.1000
Guanidinium chloride (GuHCl) for biochemistry, $\geq 99.5\,\%$	Roth	0037.1
Hydrochloric acid (HCl), ROTIPURAN® 37 % fuming, p.a., ACS, ISO	Roth	4625.1
Imidazole, $\geq 99\,\%$	Roth	3899.1
Magnesium chloride hexahydrate ($MgCl_2{\cdot}6\ H_2O$), $\geq 99\,\%$, p.a.	Roth	2189.2
Methanol (MeOH), ROTIPURAN® HPLC, $\geq 99.8\,\%$	Roth	P717.1
N-hydroxysuccinimide (NHS) for synthesis, $\geq 99\,\%$	Roth	9670.1
Nickel(II) sulfate hexahydrate ($NiSO_4{\cdot}6\,H_2O$), for analysis EMSURE®	Merck	1.06727.0250
Oxalic acid, puriss. p.a., anhydrous, $\geq 99.0\,\%$	Merck	75688-50G
Potassium chloride (KCl), $\geq 99.5\,\%$, p.a.	Roth	6781.3
Potassium dihydrogen phosphate (KH_2PO_4) for HPLC, $\geq 99.5\,\%$	Honeywell	60230
Potassium thiocyanate (KSCN), ReagentPlus®, $\geq 99.0\,\%$	Merck	P3011-100G
Silver nitrate ($AgNO_3$)		
Crystalline solid: EMSURE® ACS, ISO, Reag. Ph. Eur, $\geq 99.8\,\%$	Merck	1.01512.0025
Solution, 5 %	Roth	N053.1
Sodium acetate (NaOAc) ACS reagent, puriss. p.a., $\geq 99.0\,\%$	Merck	71180
Sodium carbonate (Na_2CO_3), anhydrous, $\geq 99.0\,\%$	Merck	S-2127

Sodium chloride (NaCl) for analysis EMSURE® ACS, ISO, Reag. Ph. Eur, $\geq 99.5\,\%$	Merck	1.06404.5000
Sodium dodecyl sulfate (SDS) pellets for biochemistry, $\geq 99\,\%$	Roth	CN30.1
Sodium hydroxide (NaOH) pellets for analysis EMSURE®, $\geq 99.0\,\%$	Merck	1.06498.1000
Sodium phosphate dibasic dihydrate ($Na_2HPO_4{\cdot}2\,H_2O$), BioUltra, for molcular biology, $\geq$ 99.0 %	Merck	71643-250G
Sodium phosphate monobasic monohydrate ($NaH_2PO_4{\cdot}H_2O$), ACS Reagent, $\geq 98\,\%$	Merck	S9638-250G
Sodium thiosulfate, plant cell culture tested	Merck	S7026-250G
Tetramethylethylenediamine (TEMED)	Bio-Rad	161-0800
Tris(hydroxymethyl)aminomethane (Tris), ACS, Reag. Ph. Eur	Merck	1.08382.1000
Tris-HCl, PUFFERAN®, $\geq 99\,\%$, p.a.	Roth	9090.3
Tween 20	Merck	P1379-500ML
Tween 80	Merck	P1754-25ML
Urea, Ph. Eur, cryst., $\geq 99.5\,\%$	Roth	X999.2
Zwittergent® 3-12 Detergent, $\geq 99\,\%$	Merck	693015

2.1.12. Consumable materials

Material	**Supplier**
Amicon® Ultra-0.5 centrifugal filter units (MWCO: 10 kDa, 30 kDa)	Merck
Biacore-compatible plastic vials, 11 mm	Cytiva
Biacore-compatible, ventilated rubber caps (type 2), for 11 mm plastic vials	Cytiva
Bottle top filters	
LABSOLUTE®, PES, 1000 mL, 0.22 µm pore size	Th. Geyer
Steritop® PES, 1000 mL,	Merck

0.22 µm pore size	
Cellstar® conical bottom tubes (15 mL, 50 mL, 50 mL with support skirt)	Greiner
Cryogenic vials	Heathrow Scientific
Disposable cuvettes	VWR
Disposable syringes, sterile	B. Braun
Inject® Luer Solo, 10 mL	
Omnifix®-F Luer Solo, 1.0 mL	
Original Perfusor® Luer Lock, 50 mL	
D-Tube™ Dialyzer Maxi (MWCO: 6-8 kDa)	Merck
Immobilon®-P PVDF membrane	Merck
Mini Trans-Blot® filter paper	Bio-Rad
Nunc-Immuno™ 96-MicroWell™ plates, PolySorp™, flat bottom	Thermo
Parafilm® M	Bemis
Petri dishes, PS, 90 mm x 14.2 mm, without vents	VWR
pH indicator strips, non-bleeding	
MQuant® (pH 0-14, pH 6.5-10.0)	Merck
pH-Fix (pH 4.0-7.0, pH 4.5-10.0)	Macherey-Nagel
Pipette tips	
10 µL, 5000 µL	Eppendorf
200 µL, 1000 µL	Sarstedt
Combitips advanced® (0.2-10 mL)	Eppendorf
Reaction tubes	
0.2 mL	VWR
1.5 mL, 2.0 mL	Sarstedt
Protein LoBind® (0.5 mL, 5.0 mL)	Eppendorf
Rotilabo® syringe filters, PVDF, sterile, 0.22 µm pore size	Roth
Sensor chip CM5	Cytiva
Serological pipettes, graduated, sterile (10 mL, 25 mL)	Greiner

Vivaspin 20 centrifugal concentrators (MWCO: 10 kDa)	Sartorius

2.1.13. Equipment and accessories

Analytic instruments, chromatography systems and imagers.

Instrument	**Supplier**
AC 120S analytic balance	Sartorius
ÄKTA FPLC system	Cytiva
Frac-900 fraction collector	
P-920 pump system	
UPC-900 monitor for UV, pH and conductivity	
Basic Meter PB-11 pH meter	Sartorius
Biacore X100 system	Cytiva
BN ProSpec® system	Siemens
ELx80™ microplate reader	BioTek
INTAS Advanced Western Blot imager	INTAS
LS-50B luminescence spectrometer	PerkinElmer
NanoDrop™2000 spectrophotometer	Thermo

Centrifuges.

Instrument	**Supplier**
5415R microcentrifuge with rotor F 45-24-11	Eppendorf
MIKRO 200 microcentrifuge with rotor 2427	Hettich
ROTANTA 460 R benchtop centrifuge with rotor 5624	Hettich
ROTINA 420 R benchtop centrifuge with rotor 4784-A	Hettich

Incubators and mixing devices.

Instrument	**Supplier**
CERTOMAT® IS incubation shaker	Sartorius
Hotplate stirrers (COMBIMAG RCH, RCT basic)	IKA
IPP 200 refrigerated incubator	Memmert
MACSmix™ tube rotator	Miltenyi Biotec
MTS 2 microtiter shaker	IKA
Thermomixer comfort	Eppendorf
Vortex-Genie 2 vortex mixer	Scientific Industries

Other equipment.

Instrument	**Supplier**
Accu-jet® pro pipette controller	Brand
DynaMag™-2 magnet	Thermo
Fume hood	Köttermann
Glass vessels	
Beakers (50-500 mL)	VWR
Erlenmeyer flasks (250 mL)	VWR
Erlenmeyer flasks (500 mL)	SCHOTT
Laboratory bottles (250 mL)	VWR
Laboratory bottles (500 mL)	Merck
Laboratory bottles (500 mL, 1000 mL)	SCHOTT
Luminescence spectroscopy cells	PerkinElmer
Mini-PROTEAN Tetra 2-gel vertical electrophoresis system (1.0 mm + 0.75 mm)	Bio-Rad
Officejet 7500A multifunction printer	HP

Pipettes	Eppendorf
Multipette® E3 multidispenser pipette	
Multipette® stream multidispenser pipette	
Reference® mechanical pipette (10 µL)	
Research® mechanical pipettes (20 µL, 100 µL, 200 µL, 1000 µL)	
Research® plus mechanical pipettes (2.5 µL, 10 µL, 1000 µL, 5 mL)	
PowerPac™ HC high-current power supply	Bio-Rad
SONOPULS HD 2070 homogenizer	BANDELIN
Tetra 2-gel blotting module	Bio-Rad

2.1.14. Databases and Software

Resource (version)	**Publisher or developer**
Biacore X100 Control Software (2.0.1)	Cytiva
Biacore X100 Evaluation Software (2.0.1)	Cytiva
BioRender	BioRender https://www.biorender.com
BLAST	National Center for Biotechnology Information (NCBI; Bethesda, US), https://blast.ncbi.nlm.nih.gov/Blast.cgi
ChemoStar	INTAS
Expasy ProtParam tool	Swiss Institute of Bioinformatics (Lausanne, CH), https://web.expasy.org/protparam/
FL WinLab (4.00.03)	PerkinElmer
Gen5 (1.01.9)	BioTek
GenBank®	NCBI (Bethesda, US), https://www.ncbi.nlm.nih.gov/genbank/
GraphPad Prism (8.1.0)	GraphPad

ImageJ (1.53a)	Wayne Rasband, U. S. National Institutes of Health (Bethesda, US)
Image Studio™ Lite (4.0)	LI-COR
Inkscape (1.2.1)	Inkscape Community
Microsoft Office (16.43)	Microsoft
NanoDrop 2000 (1.6.198)	Thermo
R (4.0.3)	R Foundation for Statistical Computing (Vienna, AT)
RStudio (1.3.1093)	RStudio
SnapGene (5.3.2)	GSL Biotech
TeX Live (1.34)	TeX Users Group
Texmaker (4.5)	Pascal Brachet and Joel Amblard
UNICORN (4.00)	Cytiva
UniProt	UniProt Consortium (Marlborough, US), https://www.uniprot.org
Zotero (6.0.13)	Roy Rosenzweig Center for History and New Media, George Mason University (Washington DC, US)

2.2. Quantification of IFX in diluted serum using the SPR biosensor assay IFXmon

For IFX quantification, an SPR biosensor assay was developed. In the following, this assay is denominated "IFXmon" to distinguish it from the other biosensor assays developed within this doctoral project. For SPR analyses, a Biacore X100 instrument (Cytiva) was employed. This system comprises two microfluidic flow cells (Fc) that can be controlled separately or in quasi-parallel fashion by successively directing injections over Fc1 and Fc2. In general, the ligand is immobilized in the active channel Fc2, while in the reference channel Fc1, a protein similar to the ligand is immobilized, which does not interact with the target analyte. This dual surface system enables the subtraction of non-specific binding and is crucial in view of the fact that SPR is a label-free detection method.

2.2.1. Biosensor surface preparation

When preparing the SPR biosensor surface, low ligand densities are targeted for kinetic analyses. On the contrary, for the specific quantification of analytes by SPR, substantially higher ligand densities as compared to kinetic applications are required to maximize analytic sensitivity. Therefore, the sensor chip CM5 (Cytiva) was selected for IFXmon, since it exhibits high capacity for ligand immobilization. The gold surface of the CM5 sensor chip carries a flexible, dense carboxymethyl dextrane matrix, with which protein ligands can be covalently coupled via NHS ester chemistry.

Table 2.1.: Buffers and solutions for biosensor immobilization*.

Solution	Composition		Volume
PBS	2.6 mM	KCl	500 mL
	138 mM	NaCl	
	10 mM	$Na_2HPO_4 \cdot 2\,H_2O$	
	1.8 mM	KH_2PO_4	
	pH	7.6	
NaOH	50 mM	NaOH	125 µL
EDC	400 mM	EDC	122 µL
NHS	100 mM	NHS	122 µL
Ligand solution	10 mM	sodium acetate	175 µL
	75 µg/mL	hTf or TNF	
	pH	4.5	
Ethanolamine	1 M	ethanolamine	270 µL
	pH	8.5	

* All non protein-containing solutions and buffers were filtrated (0.22 µm), including sodium acetate buffer before the addition of ligand.
PBS, phosphate-buffered saline.

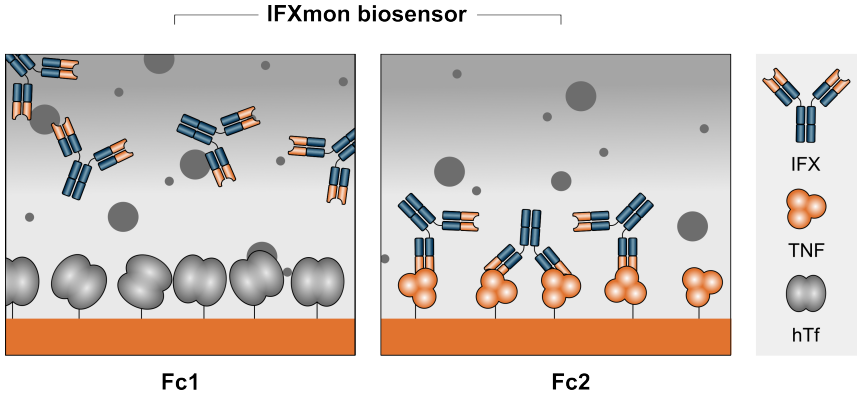

Figure 2.1.: IFXmon biosensor Fcs. Adapted from [322].

For IFXmon surface preparation, the two Fcs were immobilized separately. hTf was immobilized on Fc1 in a first cycle and TNF on Fc2 in a second cycle (see **Figure 2.1**). Prior to immobilization, the Biacore X100 was primed three times on phosphate-buffered saline (PBS) running buffer to equilibrate the system. All buffers and solutions required for biosensor immobilization are enlisted in **Table 2.1**. The procedure was carried out employing the immobilization wizard with fixed ligand target level (5000 RU) at 25 °C and a flow rate of 10 µL/min. Samples for immobilization were prepared in Biacore-compatible reaction vessels with rubber caps. The wizard program controlled the immobilization reaction in five sequential steps (see **Figure 2.2**):

1. Analysis of ligand adsorption response:
   Ligand solution was injected over the unreactive chip surface for approximately 120 s. The herein recorded signal increase caused by ligand adsorption and different refractive indices of running buffer and ligand solution is evaluated automatically. If the signal increase is too abrupt, to flat, or if response is too high from the beginning, the run is aborted. This test ensures that the response of ligand injection is actually within the instrument's detection range. This step was finalized by a 60 s injection of NaOH for removal of adsorbed ligand.

2. Activation of CM5 matrix with the EDC/NHS mix:
   EDC and NHS were mixed automatically in a 1:1 ratio to achieve final concentrations of 200 mM EDC and 50 mM NHS and injected over the chip surface for 420 s. During this injection, EDC and NHS react with carboxy moieties of the carboxymethyl dextrane layer by formation of NHS esters.

3. Covalent attachment of ligand:
   Ligand was cumulatively attached to the activated surface by feedback-controlled pulses of ligand injection. After each injection, the ligand binding response relative to the EDC/NHS signal baseline is evaluated automatically and the duration of the next pulse is adjusted accordingly. The acidic buffer below the ligand's isoelectric point generates a net positive protein charge. Thus, the actual cross-linking reaction is

facilitated by the electrostatic interaction between ligand and the negatively charged carboxymethyl dextrane. Primary amines, i.e., lysine residues and N-termini, react with the NHS esters on the activated chip surface by formation of stable peptide bonds.

4. Ligand cross-linking with EDC/NHS:
   In order to increase ligand stability, a mix of 200 mM EDC and 50 mM NHS was injected for 30 s.

5. Surface deactivation with ethanolamine:
   Unreacted NHS esters were deactivated by a 420 s injection of ethanolamine.

Importantly, the thawing of EDC and NHS aliquots as well as the preparation of ligand solutions were performed only about 2 min before the respective immobilization cycle start. This was considered necessary due to the limited stability of reactants (especially EDC) and to limit the time of acidic exposure for the ligands.

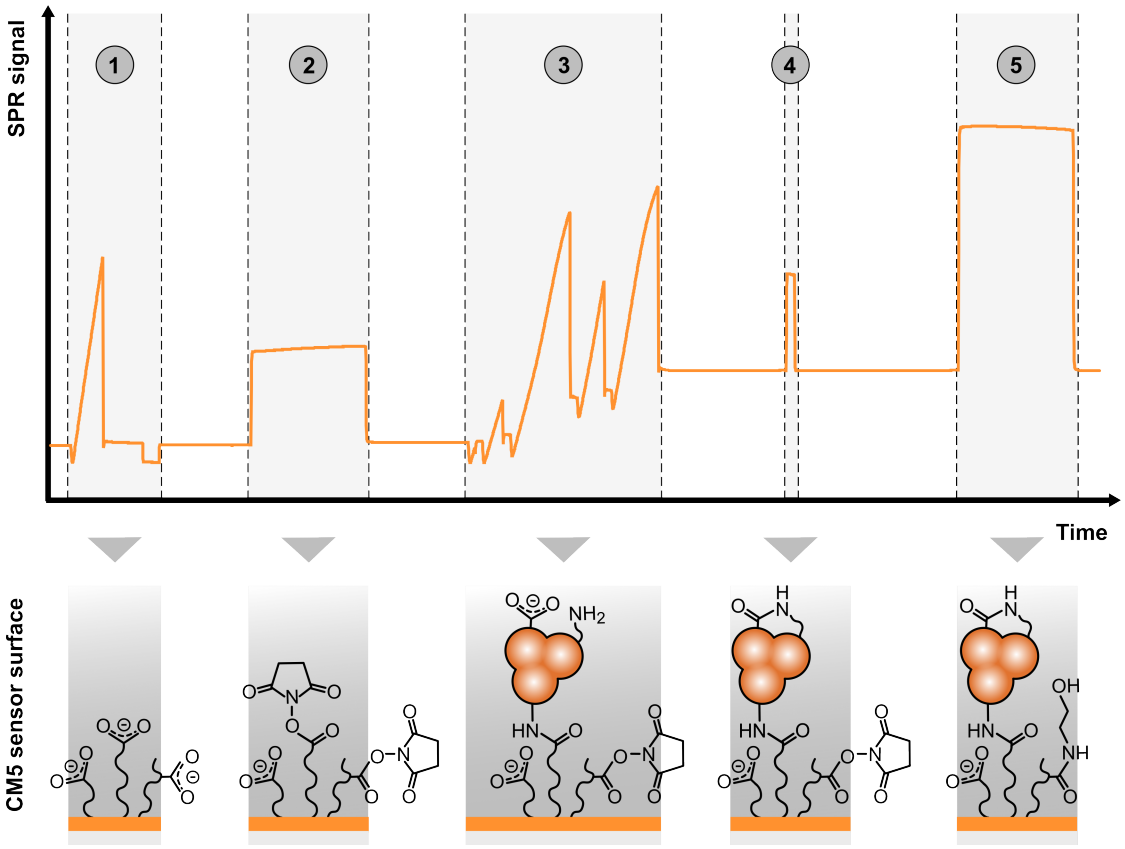

Figure 2.2.: Ligand immobilization via amine coupling. The top panel shows an exemplary SPR sensorgram obtained with the described immobilization protocol for TNF immobilization. Below each immobilization step in the sensorgram, the respective modifications at the sensor surface are depicted schematically. Step 1 shows the analysis of ligand adsorption response, during which the carboxymethylated dextrane matrix (shown as wavy lines with carboxy groups) does not react. In step 2, the carboxy groups are activated by injection of the EDC/NHS mix, which results in formation of amine-reactive NHS esters. Step 3 shows the covalent attachment of ligand through formation of peptide bonds. The sensorgram illustrates the feedback-controlled injection wizard pulses approaching the target ligand level. In step 4, a second EDC/NHS injection causes cross-linking of carboxy groups with neighboring terminal amines within (and between) the ligands: Multimeric complexes can thereby be cross-linked between monomers and ligand denaturation may possibly be hampered through enhanced conformation stability. Step 5 serves to deactivate unreacted NHS esters with ethanolamine.

2.2.2. Biosensor surface stability assessment

The effect of additional cross-linking during immobilization on the complex stability of TNF trimers at the CM5 sensor chip surface was investigated. For this means, the SPR method described by Poiesi *et al.* (1993) was adapted[332]. This method allows for calculation of the TNF monomer dissociation rate k_d based on the following equations:

$$\frac{dR}{dt} = k_d R t \tag{2.1}$$

$$\ln\frac{R(t_1)}{R(t_n)} = k_d(t_n - t_1) \tag{2.2}$$

R is the SPR signal response and t is the time, at which R is measured. Equation 2.1 gives the association of the SPR dissociation sensorgram with time. Its linearized form, equation 2.2, demonstrates that constant k_d represents the slope of the linear relationship between $(t_n - t_1)$ and $\frac{R(t_1)}{R(t_n)}$.

The experiments were performed with an adapted version of the IFXmon biosensor surface (see **section 2.2.1**). On Fc1, TNF instead of hTf was immobilized, without additional cross-linking by EDC/NHS. On Fc2, TNF was immobilized following the standard procedure including the cross-linking step. Immediately after the immobilization procedure, a manual run program with a three-hour wait command was started to monitor surface dissociation in PBS running buffer at 25 °C and 10 µL/min flow rate. 16 report points were distributed within the time interval between 500 s and 1100 s after immobilization. t_n and the respectively recorded absolute SPR response R_n at each report point were utilized to calculate the dissociation constant. The time shift between the independent immobilization cycles for Fc1 and Fc2 immobilization was taken into account for the calculations.

In order to investigate the effect of TNF cross-linking on its capacity to interact with IFX, IFX spiked in PBS was injected over the two surfaces. IFX binding was enhanced by injection of 50 µg/mL mouse anti-human IgG (msαhu) in PBS. All analyses were performed at 25 °C and a flow rate of 10 µL/min PBS running buffer.

2.2.3. IFXmon analytic runs

2.2.3.1. Pre-analytic sample preparation and calibration

All buffers and solutions required for IFX quantification via the IFXmon biosensor are enlisted in **Table 2.2**. After preparation of the IFXmon biosensor surface, the sensor chip and Biacore X100 system were primed on PBS with casein (PBSC), the running buffer for analytic runs. This was achieved by priming three times with PBSC first and leaving the system on standby flow overnight or for at least 2 h. IFX quantification was performed at 25 °C with a flow rate of 10 µL/min and all injections were directed quasi-simultaneously into both Fc1 and Fc2.

Table 2.2.: Buffers and solutions for IFXmon analytic runs.

Buffer	**Composition**	
PBSC	0.25 %	casein in PBS
IFXmon regeneration	10 mM	glycine
solution 1	10 mM	EDTA
	0.1 %	CHAPS
	0.1 %	Tween 20
	0.1 %	Tween 80
	0.1 %	Zwittergent®
	pH	1.5
IFXmon regeneration	30 mM	glycine
solution 2	30 mM	ethanolamine
	150 mM	KSCN
	600 mM	$MgCl_2$
	600 mM	GuHCl
	300 mM	urea
	pH	9.0
Washing solution	20 %	2-propanol
	40 mM	NaOH

All solutions were filtrated (0.22 µm).

Prior to analysis, serum samples were centrifuged (16100 x g, 30 min, room temperature (RT)) for removal of possible aggregates and the supernatants were diluted in a 1:50 ratio with PBSC. All IFX concentrations indicated in this thesis, however, refer to undiluted serum. Analytic cycles generally consisted of three phases: First, the sample was injected for 300 s and dissociation of specific and non-specific binders was monitored for 300 s. Second, IFX signals were enhanced by a 300 s injection of msαhu followed by 300 s of dissociation monitoring. Third, the sensor surface was regenerated by exploiting different chemical properties to ensure complete removal of sample from the ligands: IFXmon regeneration solution 1 (acidic, detergents, chelating) was injected for 25 s , followed by a 12 s injection of IFXmon regeneration solution 2 (basic, high ion strength). After each injection of serum samples, the sample loop was flushed with washing solution. In total, one IFXmon analytic cycle required 29 min.

For IFX quantification, a seven-point calibration curve was recorded in each run (0, 0.5, 1.0, 3.0, 5.0, 15.0, 125 µg/mL). Calibrator concentrations were selected to cover sub-therapeutic, therapeutic and supratherapeutic IFX concentrations. The calibrators were prepared by spiking Remicade® into a pool from 71 negative control sera (blank serum matrix), which was diluted 1:50 in PBSC. SPR signals of the calibrators were fit with a hyperbolic function modeling total binding saturation. In the beginning, the middle and

at the end of each run, a 7.0 µg/mL Remicade® standard in PBSC was injected in order to assess the functionality of the IFXmon biosensor surface.

2.2.3.2. Signal referencing

Only the binding responses of msαhu enhancer antibody were considered for IFX quantification (see **Figure 2.3**). For evaluation, enhancer antibody binding responses were double-referenced: In a first referencing step, the response measured on the hTf surface (Fc1) was subtracted from the binding signal in the TNF-immobilized Fc (Fc2). Additionally, blank serum matrix was repeatedly measured throughout the entire run. The referenced signal of the last blank measured before the respective calibrator or sample was subtracted from the referenced sample binding signal in a second referencing step. This double-referencing procedure ensured correction for non-specific binding as well as for the slight drift of both specific and unspecific binding that was observed throughout the lifespan of the sensor chip surface. The double-referenced SPR signals of calibrators and samples were then utilized for the interpolation of IFX concentrations.

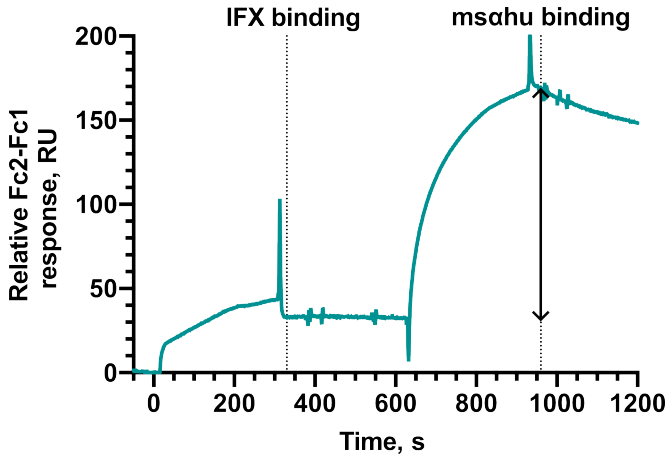

Figure 2.3.: Exemplary IFXmon sensorgram. Adapted from[322].

2.2.4. Commercial IFX quantification assay

The ELISA kit IDKmonitor® Infliximab drug level ELISA (Immundiagnostik), which was employed at the MVZ Oldenburg for routine TDM, was utilized to validate the developed IFXmon biosensor. The assay principle is a sandwich ELISA (microtiter plates are pre-coated with anti-IFX capture antibody) for the quantification of free serum IFX. Immundiagnostik reports the limit of quantification (LOQ) as 0.6 µg/mL IFX.

2.3. Quantification and characterization of ADA in diluted serum using the SPR biosensor assay ADAmon

For IFX quantification, the SPR biosensor assay denominated "ADAmon" was developed analogously to IFXmon. In literature,"ADA" refers to anti-drug antibodies without implication of a certain specificity. However, within the scope of this work, ADA is used as abbreviation for antibodies directed against IFX. This decision is based on the consistent use of this abbreviation in both a method publication based on the present work [322] as well as in all progress reports related with the project "ADAmon" funded by the Stiftung für Pathobiochemie und Molekulare Diagnostik (Bonn, DE).

2.3.1. Biosensor surface preparation

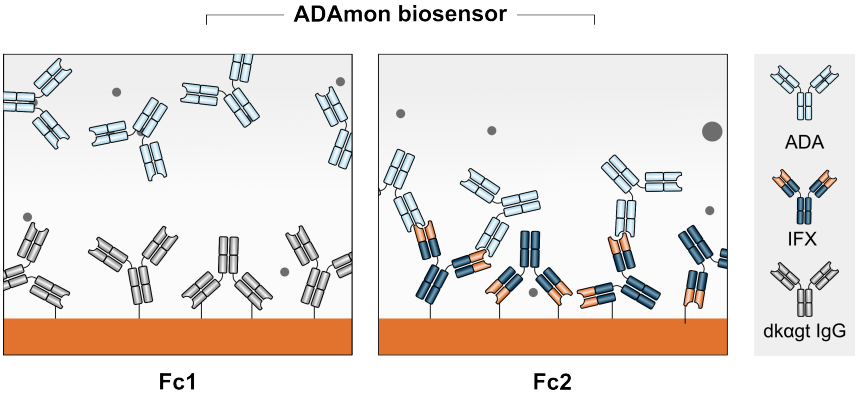

Figure 2.4.: ADAmon biosensor Fcs. dkαgt, donkey anti-goat IgG. Adapted from [322].

The ADAmon biosensor surface was prepared utilizing CM5 sensor chips as described in **section 2.2.1**, except for the following changes (see **Figure 2.4**):

1. The target level value for the immobilization of IFX was set to 4900 RU, since the target level wizard was frequently generating exceeding densities for a target level of 5000 RU.

2. In cycle 1, donkey anti-goat IgG (dkαgt) was immobilized on Fc1 and IFX was immobilized on Fc2 in cycle 2. dkαgt and IFX were diluted in ligand buffer (pH 4.5) at 25 µg/mL and 20 µg/mL, respectively.

2.3.2. Direct quantification of ADA in diluted serum

Prior to PA, patient sera and blank serum matrix were centrifuged for removal of aggregates (16100 x g, 30 min, RT). Calibrator sera were prepared by spiking ADA calibrator (HCA233, Bio-Rad) into blank serum matrix. The method published by Beeg et al. (in the following referred to as "Beeg method") was compared to an in-house developed protocol [288].

2.3.2.1. Beeg method

50 µL of serum were added 950 µL of 100 mM acetic acid, pH 3.0, inverted twice for mixing and the serum dilutions were incubated for 15 min at RT without mixing. For neutralization, 500 µL of 500 mM phosphate buffer, pH 7.4, were added. The samples were mixed by inverting the tube and placed into the autosampler immediately. The Beeg protocol resulted in a final serum dilution of 1:30.

2.3.2.2. In-house method

100 µL of serum were pre-diluted with 550 µL of PBS. For PA, 500 µL 10 mM glycine, pH 1.5, were added, mixed briefly by inverting and incubated at 37 °C at rest. After exactly 5 min, 150 µL 1 M Tris-HCl, pH 8.0 were added for neutralization and after brief mixing, the samples were immediately placed into the autosampler for analysis. The final serum dilution of the in-house protocol was 1:13.

2.3.3. ADA affinity purification from serum employing magnetic IFX beads

2.3.3.1. Preparation of IFX-coupled magnetic beads

Table 2.3.: Dynabeads™ coupling buffers.

Buffer	**Composition**
Buffer B	19 mM $NaH_2PO_4 \cdot H_2O$, 81 mM $Na_2HPO_4 \cdot 2\ H_2O$ pH 7.4
Buffer C	3 M $(NH_4)_2SO_4$ in Buffer B, pH 7.4
Buffer D	0.5 % BSA in PBS, pH 7.4
Buffer E	0.1 % BSA in PBS, pH 7.4

Dynabeads™ M-280 Tosylactivated comprise nucleophile-reactive tosylate groups. Amino and sulfhydryl groups present in protein ligands to be coupled with the beads are nucleophiles and react with the tosylate groups, resulting in the formation of stable amine bonds. This substitution reaction was exploited to covalently attach IFX to the Dynabeads™. IFX-coupled magnetic beads were prepared according to the Dynabeads™ manufacturer's instructions to yield a coupling density of 20 µg IFX per mg beads. All buffers required for bead coupling are enlisted in **Table 2.3**.

Table 2.4.: IFX coupling batch for 20 mg Dynabeads™.

Material	**Volume**
Washed Dynabeads™ *	675 µL
400 µg Remicade®**	x µL
Buffer B	300 µL - x µL
Buffer C	200 µL
Total liquid volume:	500 µL
Buffer D for blocking	1800 µL
Buffer E for washing (2x)	1800 µL
Buffer E for reconstitution	960 µL

* Bead supernatant discarded. ** Varying stock solution concentrations.

Prior to coupling, beads were washed with buffer B. Per standard reaction batch, 20 mg beads were employed. After discarding the bead supernatant, Remicade®, buffer B and buffer C were sequentially added as indicated in **Table 2.4**. The reaction mix was allowed to incubate at 37 ℃ for at least 18 h in an overhead tube rotator. Then, the beads were pelleted on a magnet and the coupling reaction supernatant was either discarded or saved for subsequent determination of coupling efficiency. In order to block non-specific binding sites of the hydrophobic bead material and Remicade® matrix, buffer D was added. Coupled beads were incubated for at least 60 min at 37 ℃ under rotation, before washed twice with buffer E. After final reconstitution in buffer E, coupled beads were stored at 4 ℃ and were stable for at least 2 months after preparation.

2.3.3.2. ADA purification

Table 2.5.: 1X ADA pulldown batch.

Material	**Volume**
IFX-coupled Dynabeads™	200 µL
Serum	100 µL
PBS	550 µL
10 mM glycine, pH 1.5	500 µL
1 M Tris-HCl, pH 8.0	150 µL
Total liquid volume:	1300 µL

Pre-analytic enrichment of ADA from serum, herein referred to as "ADA pulldown" in brief, was performed utilizing IFX-coupled, magnetic Dynabeads™. Blank serum matrix and patient sera were centrifuged prior to spiking and the purification procedure (16100 x g, 30 min, RT) in order to pellet possibly contained aggregates. The standard composition of a 1X ADA pulldown batch is displayed in **Table 2.5**. First, 200 µL of IFX-coupled beads (equivalent to 4 mg beads) were placed on the magnet for 1 min and supernatants were discarded. PBS-diluted serum was immediately added to the beads and the mixture was pre-equilibrated at 37 °C for 10 min under over-head rotation. 10 mM glycine, pH 1.5 was added for PA, mixed by inverting the capped tubes and incubated at 37 °C under over-head rotation. After exactly 5 min, 1 M Tris-HCl, pH 8.0 was added per batch for neutralization and mixed by inverting the capped tubes. The acidic treatement causes ADA to temporarily dissociate from serum IFX, such that ADA re-binds with the excess bead-bound IFX upon neutralization. The neutralized pulldown batches were then incubated for 60 min at 37 °C under over-head rotation.

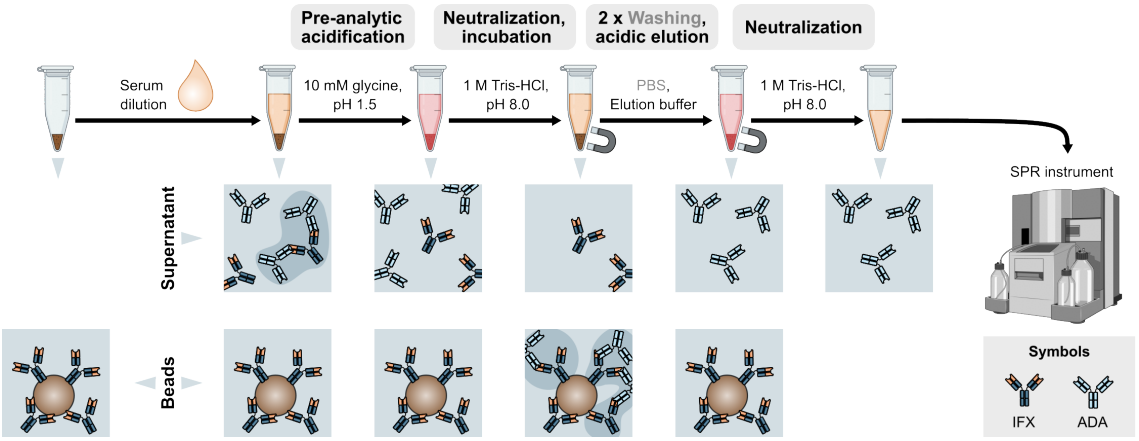

Figure 2.5.: Schematic procedure for pre-analytic ADA purification from serum. Adapted from [322].

All following steps were performed at RT. After incubation, pulldown batches were placed on the magnet for 2 min and supernatants were discarded. For removal of unbound serum components, the beads were resuspended with 1000 µL of PBS (avoiding excessive up- and down-pipetting to minimize bead loss) and the wash supernatant was discarded after magnetic separation. In a second wash step, beads were resuspended thoroughly with 1000 µL of PBS and transferred to a clean 1.5-mL reaction tube. After pelleting the beads on the magnet and discarding the second wash supernatant, ADA were eluted by adding 100 µL of elution buffer (10 mM glycine, 150 mM NaCl, 10 % glycerol, pH 2.0). Of note, up- and down-pipetting and the hereby aspirated suspension volumes shold be minimized, since the glycerol-containing elution buffer causes higher volume losses as compared to the previous steps. Elution batches were incubated for exactly 5 min at rest before magnetic separation. Eluates were transferred to fresh reaction vials containing 8 µL 1 M Tris-HCl, pH 8.0 for immediate pH neutralization. **Figure 2.5** illustrates

the ADA pulldown procedure. The eluates were placed in the magnet and re-transferred to fresh reaction tubes in order to completely remove magnetic beads. For subsequent analysis by the ADAmon SPR biosensor, 90 µL of ADA eluate were mixed with 10 µL of 1 % casein in PBS to achieve a final casein concentration of 0.1 %, matching the ADAmon running buffer.

2.3.4. SDS-polyacrylamide gel electrophoresis-based methods

SDS-polyacrylamide gel electrophoresis (PAGE) was conducted to characterize the protein content of various samples, e.g., ADA pulldown eluates. The gels were subjected to different staining or detection techniques with variable sensitivities.

2.3.4.1. SDS-PAGE

All buffers required for the applied SDS-PAGE protocol are enlisted in **Table 2.6** and gel compositions for different polyacrylamide percentages are indicated in **Table 2.7**. Samples to be analyzed were diluted with MilliQ H_2O, if necessary, and mixed with 5X Laemmli sample buffer (reducing or non-reducing) in a 4:1 ratio. The samples were boiled for 5 min at 95 °C. Handcast, discontinuous gels were placed in Mini-PROTEAN Tetra cells (Bio-Rad) filled with SDS-PAGE running buffer. As a MW standard, PageRuler™ Prestained Protein Ladder (Thermo) was utilized (4 µL for stains, 6 µL for western blot). After loading all samples on the gels, electrophoresis was performed at 120-140 V until the blue stain front left the gel and the desired MW resolution was achieved.

Table 2.6.: Buffers for SDS-PAGE.

Buffer	**Composition**	
5X Laemmli sample buffer	240 mM	Tris-HCl, pH 6.8
	8 %	SDS
	40 %	glycerol
	0.04 %	bromophenol blue
	20 %	2-mercaptoethanol
		or MilliQ H_2O
Separation gel buffer	1.5 M	Tris-HCl, pH 8.8
Stacking gel buffer	0.5 M	Tris-HCl, pH 6.8
SDS-PAGE Running	25 mM	Tris
buffer	192 mM	glycine
	0.1 %	SDS

Table 2.7.: Composition of utilized SDS-polyacrylamide gels.

	Separation gels*			Stacking gel*
Component	**10 %**	**12 %**	**15 %**	**4 %**
Concentrations:				
Tris-HCl		375 mM		125 mM
Acrylamide/ bisacrylamide	10 %	12 %	15 %	4 %
SDS		0.1 %		0.1 %
TEMED		0.1 %		0.1 %
APS		0.1 %		0.1 %
Preparation:				
Ultrapure H_2O	4.75 mL	4.25 mL	3.50 mL	3.0 mL
Separation gel buffer	2.50 mL	2.50 mL	2.50 mL	-
Stacking gel buffer	-	-	-	1.25 mL
40 % acrylamide/ bisacrylamide	2.50 mL	3.00 mL	3.75 mL	0.50 mL
10 % SDS	100 µL	100 µL	100 µL	100 µL
TEMED	10 µL	10 µL	10 µL	5 µL
10 % APS	100 µL	100 µL	100 µL	50 µL

*Indicated amounts refer to the preparation of 2 gels.

If quick visualization of the separated protein bands with limited sensitivity was needed after SDS-PAGE, gels were stained with ROTI®Blue quick solution (Roth) following the manufacturer's recommendations and scanned with a multifunction printer. A sensitivity of 10 ng protein per band is stated for this Coomassie-based stain. However, it was observed that the visualization of bands containing less than 25 ng protein was not feasible using the ROTI®Blue quick stain, at least with respect to the specific applications within this doctoral project. Hence, if higher sensitivity was required, silver staining (**section 2.3.4.2**) or western blotting (WB; **section 2.3.4.3**) was conducted after SDS-PAGE.

2.3.4.2. Silver stain

For purity analysis after SDS-PAGE (**section 2.3.4.1**), the low protein content of ADA pulldown eluates was visualized by silver stain. Silver staining enables the detection of band protein amounts in the low nanogram range[333]. It is important to use thoroughly

cleaned boxes, MilliQ H_2O and work with gloves throughout the protocol, since destaining is not easily possible. All solutions required for the staining protocol are shown in **Table 2.8**.

Table 2.8.: Solutions for silver stain.

Solution	Composition	
Fixation solution 1	30 %	EtOH
	10 %	acetic acid
Fixation solution 2	20 %	EtOH
Sensitizing solution*	0.1 %	sodium thiosulfate
Staining solution*	0.12 %	$AgNO_3$
	0.009 %	formaldehyde
Developing solution*	2.5 %	Na_2CO_3
	0.014 %	formaldehyde
Stopping solution	50 mM	EDTA
	pH	7.5

*Solution was prepared immediately before use.

After SDS-PAGE, gels were briefly rinsed with H_2O. The following incubations and washing steps were all performed at RT while shaking gently, using 20 mL of the respective solution. Primary protein fixation consisted of three sequential steps with fixation solution 1: Two 30 min incubations were followed by a final fixation overnight. Then, gels were incubated twice in fixation solution 2 for 10 min, respectively. After washing twice with H_2O for 10 min, respectively, gels were sensitized for 1 min in sensitizing solution. Two 1 min washing steps with H_2O followed, before staining solution was added to the gels. From this step on, the gel containers were protected from light with help of opaque lids. After 45 min of staining, the gels were washed with H_2O for 2 min and developing solution was poured into the gel contianers. When the desired staining was visible (usually after 30-40 min), the staining reaction was stopped by a 30 min incubation in stopping solution. In the case of high yellowish background or limited staining strength, it is recommendable to replace the relatively unstable sodium thiosulfate reagent. The gels were washed twice with H_2O for 1 min and scanned using a multifunction printer.

2.3.4.3. Western blot

If the presence of specific proteins had to be confirmed in samples, WB was performed employing the Tetra 2-gel blotting module (Bio-Rad) for wet blotting. Required buffers are enlisted in **Table 2.9**. After SDS-PAGE (**section 2.3.4.1**), the gels were pre-equilibrated in transfer buffer for 15 min on a shaker at RT. The Immobilon-P polyvinylidene difluoride (PVDF) membrane (Merck) was activated in MeOH for 1 min and rinsed briefly with transfer buffer, before the wet blot sandwich was assembled in transfer buffer. Of note, the membrane was slightly larger than the gel (approximately 0.5 cm in length and width)

to optimize the transfer. The following components were stacked from cathode to anode side in a gel holder cassette: Fiber pad - filter paper - SDS polyacrylamide gel - PVDF membrane - filter paper - fiber pad. Before closing the cassette, air bubbles were removed by rolling. The cassette, a cooling pack and magnetic stir bar were placed in a cell filled with pre-cooled transfer buffer (4 ℃). The blotting procedure was carried out either for 90 min at 300 mA and RT or overnight at 30 V at 4 ℃ while stirring, which ensures even temperature and ion distribution.

Table 2.9.: Buffers for WB.

Buffer	**Composition**	
Transfer buffer	25 mM	Tris
	19.2 mM	glycine
	0.01 %	SDS
	20 %	MeOH
TBST	15.3 mM	Tris-HCl
	4.7 mM	Tris
	150 mM	NaCl
	0.1 %	Tween 20
	pH	7.6
Blocking buffer	5 %	SMP in TBST
Antibody dilution buffer	0.5 %	SMP in TBST

TBST, Tris-buffered saline with Tween 20.

After the transfer, the fiber pad and filter paper close to the anode were removed from the blotting sandwich and the membrane was trimmed to the dimension of the gel with a scalpel. If more than one primary antibody was to be used on the membrane, the membrane was dissected additionally. Then, the membrane was placed in a plastic box with lid and rinsed briefly with TBS with Tween 20 (TBST). The following membrane incubations and washing steps were all performed under gentle shaking. 20 mL of blocking solution were added and blocking was performed at RT for 1-2 h. After discarding the blocking solution, the membrane was incubated with 15 mL of primary antibody solution at RT for 1-2 h. Employed antibody dilutions are shown in **Table 2.10**. The membrane was washed thrice for 5 min with 20 mL of TBST, respectively. Then, secondary antibody solution was added and allowed to incubate for 1 h at RT, before washed thrice again, as described before.

For development, Pierce™ ECL Western Blotting Substrate (Thermo Fisher) with low pg protein detection sensitivity was utilized. 2 mL of substrate mix were applied per whole membrane and incubated for 5 min at RT. After removal of excess substrate, chemiluminescence was detected with an INTAS Advanced Western Blot imager (INTAS). Please note that blocking and primary antibody incubation were performed overnight at 4 ℃ if pausing the WB protocol was required.

Table 2.10.: Antibody dilutions for WB.

Primary antibodies	
Mouse anti-hSA	1:5000
msαhu	1:2500
Secondary antibodies	
Goat anti-mouse IgG + HRP	1:25000

Antibodies were diluted in antibody dilution buffer.

2.3.5. Fluorometric evaluation of analytic drug tolerance and ADA purification yield

2.3.5.1. Fluorescent labeling of ADA calibrator

ADA calibrator (HCA233, Bio-Rad) was labeled with Alexa Fluor 488 dye using the APEX™ Antibody Labeling Kit Alexa 488 (Thermo Fisher) according to the manufacturer's instructions. This kit provides an IgG-capturing resin in microvolume pipette tips and hence enables the labeling of relatively small antibody amounts.

First, ADA calibrator was concentrated using Amicon® Ultra-0.5 centrifugal filter units with 30 kDa MW cut-off (MWCO; Merck) in order to reach the concentration recommended for the labeling reaction. In total, 50-60 µL antibody stock solution were concentrated in two centrifugation rounds (30 min, RT, 16100 x g) to yield approximately 20 µL of ADA calibrator solution at a concentration of approximately 2 mg/mL. 10 µL of concentrated ADA calibrator solution (equivalent to 20 µg IgG) were applied to the pre-hydrated resin. 20 µL of reconstituted reactive dye were then pushed onto the resin and incubated for 2 h at RT. After washing the resin twice with 50 µL washing buffer, 40 µL of elution buffer were applied to the resin. The eluate was pushed into a fresh reaction vessel and mixed immediately with 10 µL of neutralization buffer. Alexa 488-labeled ADA calibrator (denominated ADA488) solution was stored at 4 °C until analyzed.

2.3.5.2. Fluorometric analysis of ADA purification fractions

Blank serum matrix was spiked with ADA488 only or with both ADA488 and Remicade®. The previously described ADA pulldown protocol (**section 2.3.3**) was then performed to purify ADA488. Throughout the pulldown procedure, ADA488-containing samples were protected from light by wrapping the reaction tubes in aluminum foil. Besides ADA488 eluates, serum supernatants and wash supernatants were additionally saved. In batches without preanalytic acidification, glycine buffer and Tris buffer were replaced with equal volumes of PBS, respectively, to achieve equal dilution.

The ADA488 content of all pulldown fractions was quantified fluorometrically (λ_{ex}: 495 nm, 5 nm slit; λ_{em}: 519 nm, 10 nm slit) utilizing a LS50B luminescence spectrometer (PerkinElmer).

Sample volumes of 150 µL were analyzed. Individual calibration curves were recorded for each fraction matrix in order to ensure accurate ADA488 quantification that takes into account the differential fluorescence quenching and autofluorescence of the different fraction matrices.

2.3.6. ADAmon analytic runs

2.3.6.1. Pre-analytic sample preparation and calibration

Table 2.11.: Buffers and solutions for ADAmon analytic runs.

Buffer	**Composition**	
PBSC	0.1 %	casein in PBS
ADAmon regeneration solution 1	10 mM	glycine
	150 mM	NaCl
	10 %	glycerol
	pH	2.0
ADAmon regeneration solution 2	10 mM	NaOH
Washing solution	20 %	2-propanol
	40 mM	NaOH

All solutions were filtrated (0.22 µm).

All buffers and solutions required for ADA quantification via the ADAmon biosensor are enlisted in **Table 2.11**. Please note the lower casein content of PBSC compared to the IFXmon running buffer, which is owed to the higher sample purity of ADA eluates, which permits less blocking. After ADAmon immobilization, priming on PBSC was performed as described in **section 2.2.3**. Just like the IFXmon assay, ADAmon analytic runs were performed at 25 °C and a flow rate of 10 µL/min, employing Fc1 and Fc2 quasi-simultaneously.

Pre-analytic sample preparation, including ADA purification, is described in detail in **section 2.3.3**. Both nominal and interpolated ADA concentrations stated in this thesis refer to undiluted serum. Please note that ADA calibrator concentrations are given in µg/mL, while interpolated ADA concentrations from patient samples are indicated in µgEq/mL. The unit difference should underline the relativeness of ADA quantification in authentic patient sera. Due to the polyclonality of patient ADA and the high structural similarity to the ligand IFX, no enhancer antibody could be used for ADA quantification. Analytic cycles exhibited one sample injection for 300 s, followed by 300 s of dissociation monitoring (see **Figure 2.6**). Then, the sensor surface was regenerated by two sequential pulses of different regeneration solutions: ADAmon regeneration solution 1 (acidic, physiological NaCl) was injected for 25 s. This solution additionally contained glycerol for ligand

preservation. Then, ADAmon regeneration solution 2 was injected for 12 s (basic). The total duration of one ADAmon analytic cycle amounted to 21 min. After each injection of ADA eluate samples, the sample loop was flushed with washing solution.

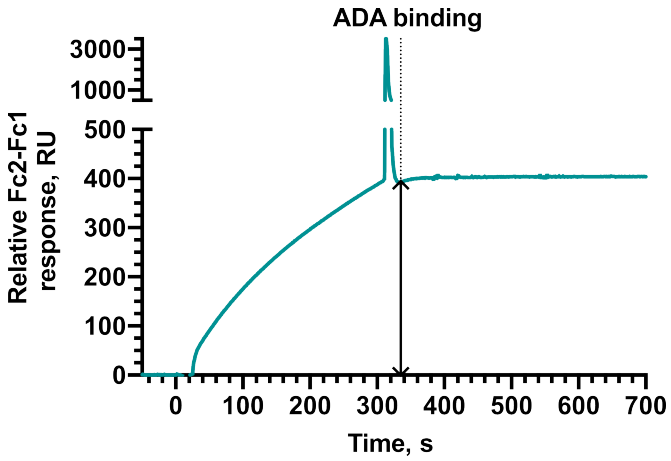

Figure 2.6.: Exemplary ADAmon sensorgram. Adapted from [322].

ADA concentrations were calculated from a six-point calibration curve (0, 0.5, 1.0, 2.0, 5.0, 15 µg/mL), which was included in each analytic run. Calibrator concentrations were selected to cover the expected range of ADA levels after preliminary patient sera screens. The calibrators were prepared by spiking ADA calibrator (HCA233, Bio-Rad) into blank serum matrix pooled from 55 negative control sera and performing the pulldown as described before. A hyperbolic function modeling total binding saturation was utilized as calibration fit. The different calibration with fewer calibration points as compared to the IFXmon assay is owed to economic considerations, as the cost per sample is higher for this assay. For monitoring of ADAmon biosensor ageing, a 2.5 µg/mL ADA calibrator standard in PBSC was injected in the beginning, the middle and at the end of each analytic run.

2.3.6.2. Signal referencing

Due to the overall higher cost and error of ADAmon analyses, only Fc2-Fc1 referencing was applied. With respect to the precision of the ADAmon biosensor, the higher number of sample processing steps inevitably leads to a higher error. Analogously, a higher number of data processing steps would likely introduce additional error. On the other hand, the blank serum matrix analyses that were interspersed over the entire IFXmon analytic run, could not be transferred to the ADAmon biosensor, since each blank serum matrix analysis would require one full pulldown batch, thus unnecessarily inflating assay cost. Furthermore, the higher purity of ADA eluates goes along with lower sensor chip wasteage as compared to the IFXmon assay, which decreases the need for adjustments to surface ageing.

2.3.7. Commercial ADA quantification assay

The ELISA kit IDKmonitor® Infliximab total ADA ELISA (Immundiagnostik), which was employed at the MVZ Oldenburg for routine TDM, was utilized to validate the developed ADAmon biosensor. The assay is constituted as drug-tolerant bridging ELISA for the quantification of total ADA (free and serum IFX-bound): Serum is incubated with HRP-conjugated IFX and biotinylated IFX. Then, conjugate-complexed ADA are captured onto a streptavidin-coated microtiter plate for subsequent detection. Immundiagnostik reports the assay LOQ as 10.0 arbitrary units (AU)/mL.

Similarly to the ADAmon biosensor assay, the IDKmonitor® Infliximab total ADA ELISA protocol incorporated a PA step followed by ADA paratope saturation with excess IFX to facilitate analytic drug tolerance. In brief, serum samples were diluted with acidic assay buffer. Samples were incubated under acidic conditions for 20 min, before a pH-neutralizing tracer/conjugate mix was added. This mixture served the simultaneous capture and detection of ADA in the sample by exploiting its bivalency: Biotinylated tracer IFX immobilized ADA on the streptavidin-coated microtiter plates, while peroxidase-labelled conjugate IFX served to catalyze the chromogenic reaction after addition of the substrate tetramethylbenzidine. ADA quantity was then determined semi-quantitatively by linear extrapolation of sample absorption measured at 450 nm relative to a cut-off control sample.

In order to provide a more meaningful method comparison with ADAmon, the IDKmonitor® Infliximab total ADA ELISA data were referred to the same ADA calibrator as utilized in the ADAmon biosensor assay. For this means, six different dilutions of ADA calibrator in blank serum matrix were analyzed by ELISA and served as calibration curve. This calibration curve was utilized to re-calculate all ADA ELISA data included in this thesis project.

2.3.8. ADA binding stability assessment

Kinetic analysis of ligand:analyte interactions comprise the main application purpose of SPR methodology. The dissociation constant, K_D which equals the quotient of dissociation rate k_d and association rate k_a, is usually used to describe ligand:protein affinity. In SPR, affinity determination is enabled by deriving k_a and k_d from the recorded sensorgram's slopes in the association and dissociation phase, respectively. As schematically depicted in **Figure 2.7**, the signal increase recorded in SPR sensorgrams during sample injection is proportional to both analyte concentration and the association rate k_a (since ligand concentration is constant). This explains, why knowledge of absolute analyte concentration is a crucial prerequisite for standard kinetic analyses.

In patient sera, the determination of absolute ADA concentrations is not possible. Patient ADA are polyclonal and exhibit variable avidities towards IFX. Only a patient-individual, polyclonal ADA calibrator mix in the identical composition (in terms of paratopes, avid-

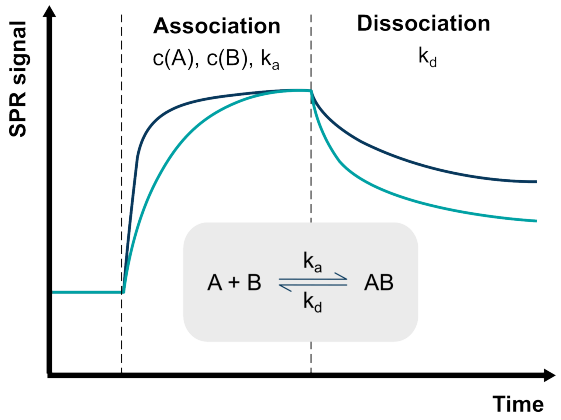

Figure 2.7.: Principle of SPR kinetic analyses. Bidirectional complex formation kinetics are characterized by the association rate k_a and the dissociation rate k_d. In SPR sensorgrams, the slope of the association phase depends on the concentration of educts and on k_a. The recorded slope for complex dissociation solely depends on k_d.

ity, etc.) of the patient's ADA would enable exact quantification. Obviously, patient-individual calibrators are not available. Also, the use of polyclonal calibrators is not feasible, as polyclonal antibodies cannot be harmonized due to the inevitable batch-to-batch variability. For diagnostic purposes, however, it is not necessary to know exact kinetic rates. In fact, a variable that is proportional to ADA binding stability and easily accessible would be ideal for TDM.

The dissociation phase monitored after sample injection, during which the binding decays exponentially, only depends on the dissociation rate k_d. k_d hence constitutes a concentration-independent component of affinity. Therefore, the evaluation of the dissociation phase is a suitable estimator of analyte:ligand complex stability and the dissociation ratio (DissR) was defined as new index to assess ADA binding stability:

$$\text{DissR} = \frac{\text{Diss}_{\text{early}}}{\text{Diss}_{\text{late}}}$$

$\text{Diss}_{\text{early}}$ and $\text{Diss}_{\text{late}}$ are SPR signals early and late in the dissociation phase and are extracted from Fc2 sensorgrams as the binding response at 415 s and 795 s after cycle start, respectively. A DissR value of 1 would indicate maximum avidity, i.e., absent dissociation within the observation time. The more DissR diverges from 1 towards higher values, the lower is the avidity of ADA contained in the sample towards IFX. Fc1 was explicitly not considered for DissR calculation, since the serum-individual unspecific binding behavior of the samples on Fc1 imposed high variance on the slope of the Fc1 binding signals (as opposed to the steady state binding levels used for quantification).

It is important to mention that DissR is not directly proportional to affinity: DissR merely describes the dissociation phase of the ADA:IFX interaction, but contains no information on the association phase. For this reason, the standard terminology of biomolecular interaction analysis (i.e., "kinetics", "affinity", "avidity") must not be used with DissR data. DissR is theoretically applicable to all kinds of anti-drug antibodies that are assessed in

SPR setups comparable to the ADAmon biosensor assay.

2.4. Methods for ADA epitope mapping

ADA epitope mapping was performed by immobilization of IFX F(ab')$_2$ fragments on CM5 sensor chips, resulting in the detection of ADA that likely interfere with IFX function (neutralizing ADA). To generate IFX F(ab')$_2$ fragments, the highly efficient endopeptidase, immunoglubulin-degrading enzyme from *Streptococcus pyogenes* (IdeS), was expressed in *E. coli* and purified via fast protein liquid chromatography (FPLC)[330]. The donated pET_1b_TrxA_IdeS plasmid encodes for IdeS with N-terminal thioredoxin A (TrxA) in order to enhance expression yield[331]. Additionally, a His_6 tag for purification and a TEV protease cleavage site are contained in the linker between TrxA and IdeS, such that untagged IdeS may be obtained after digestion with TEV protease. The fusion protein consists of 445 amino acids (49.4 kDa) and the cleaved IdeS protein counts 313 amino acids (35.2 kDa).

2.4.1. Expression of immunoglubulin-degrading enzyme from *S. pyogenes* (IdeS) in *E. coli*

2.4.1.1. Amplification of pET_1b_TrxA_IdeS plasmid in *E. coli* and sequencing

The composition of all cell culture media is enlisted in **Table 2.12**. LB medium was prepared according to the manufacturer's instructions. For plasmid amplification or expression, chemically competent NEB5α or BL21 (DE3) cells were transformed, respectively, following the same protocol. 50 µL of cell suspension in a 1.5 mL reaction tube were thawed on ice and mixed with 50-70 ng of pET_1b_TrxA_IdeS plasmid (see **section 2.1.5**) by gently flipping the reaction tube. After incubating for 30 min on ice, the cells were heat-shocked for 60 s at 42 °C and immediately allowed to regenerate on ice for 5 min. The cells were diluted with 500 µL of LB medium and incubated for 1.5 h at 37 °C while shaking. 50-100 µL of cell suspension were then plated on LB agar plates containing 40 µg/mL kanamycin for selection. The plates were incubated overnight at 37 °C. Clones were picked with a 10 µL pipette tip, which were then used to inoculate overnight cultures (5 mL or 50 mL of LB medium with 40 µg/mL kanamycin). Glycerol stocks for longterm storage at -80 °C were prepared by mixing 1 mL overnight culture with 0.5 mL sterile glycerol in cryogenic tubes.

In order to obtain sufficient plasmid material for sequencing and storage, 5 mL overnight cultures of NEB5α transformants were cumulatively harvested in 2 mL reaction tubes (16100 x g, 1 min, RT). Plasmid DNA was purified from the cell pellets utilizing the Monarch® Plasmid Miniprep Kit (New England Biolabs) and the DNA concentration was determined with a NanoDrop 2000 spectrophotometer. To control whether the plasmid DNA sequence of picked clones was correct, 2.5 µL of 10 µM sequencing primer

Table 2.12.: *E. coli* culture media.

Medium	Composition	
LB medium	10 g/L	tryptone
(+ kanamycin)	5 g/L	yeast extract
	10 g/L	NaCl
	(40 µg/mL	kanamycin)
	pH	6.8-7.2
LB agar medium	15 g/L	agar-agar
(+ kanamycin)	(40 µg/mL	kanamycin)
		in LB medium

LB (agar) medium was autoclaved for 30 min at 121 °C. For preparation of LB agar medium, kanamycin was added as soon as the medium had cooled to approximately 50 °C and LB agar was poured into petri dishes.

(**Table 2.13**) and 7.5 µL of 50-100 ng/µL plasmid DNA were mixed in a 1.5 mL reaction tube and sent to Eurofins Genomics GmbH (Ebersberg, DE) for Sanger sequencing (LightRun Tube sequencing service). Plasmids with correct sequence were stored at -20 °C.

Table 2.13.: Sequencing primers.

Primer	Binding region	Sequence (5'⟶3')
T7_prom_fw	T7 promotor	GAAATTAATACGACTCACTATAGG
T7_term_rvcom	T7 terminator	GCTAGTTATTGCTCAGCGG

2.4.1.2. Expression of TrxA-IdeS fusion protein

50 mL of LB medium with 40 µg/mL kanamycin were inoculated with BL21 transformants and incubated at 37 °C while shaking overnight. The next morning, 800 mL of LB medium with 30 µg/mL kanamycin were inoculated with 25 mL of overnight culture and allowed to grow at 37 °C while shaking until an OD_{600} of 0.9 was reached. Expression was induced by addition of sterile IPTG at 1 mM final concentration. After 6 h, the cells were harvested (4000 x g, 30 min, RT) and stored at -20 °C until purification of TrxA-IdeS was conducted. Furthermore, 1 mL culture aliquots were collected before induction and at several time points after induction, respectively, to test expression efficiency by SDS-PAGE followed by Coomassie stain. The test expression samples were pelleted by centrifugation (16100 x g, 50 min, RT). Cell pellets were resuspended in 800 µL H_2O and prepared for SDS-PAGE as described in **section 2.3.4.1**.

2.4.1.3. Purification of TrxA-IdeS fusion protein

All buffers required for the purification of TrxA-IdeS fusion protein are listed in **Table 2.14**. For purification of TrxA-IdeS fusion protein from BL21 transformants, its His_6 tag

was exploited (see **Figure 2.8**). Cell pellets from 400 mL BL21 expression culture (see **section 2.4.1.2**) were thawed on ice and resuspended with 5 mL of ice-cold lysis buffer. After transferring the suspension to a 15 mL conical tube, the tube was incubated in ice water for 10 min. Cell lysis was achieved by sonication utilizing a SONOPULS HD 2070 homogenizer (Bandelin), while cooling the suspension in ice water. Three repetitions of 1 min sonication at 70 % power , followed by 1 min of recovery incubation in ice water were conducted. The lysate was centrifuged in 2 mL reaction tubes (10000 x g, 5 min, 4 ℃) to separate the soluble protein fraction from cell debris. The supernatants were collected, pooled and stored on ice. The lysate pellets were resuspended in another 5 mL of lysis buffer and the procedure was repeated once. The two supernatants from both lysis rounds were subjected to final centrifugation (16100 x g, 60 min, 4 ℃) and the supernatants were pooled. 20 µL of lysates and centrifugation supernatants were sampled and diluted with H_2O in a 1:5 ratio for SDS-PAGE from both lysis rounds.

Table 2.14.: Buffers for cell lysis and TrxA-IdeS purification.

Buffer	**Composition**	
Buffer A*	300 mM	NaCl
	50 mM	Tris
	pH	8.0
Buffer B*	50 mM	NaCl
	50 mM	Tris
	500 mM	imidazole
	pH	8.0
Lysis buffer**	150 mM	NaCl
	25 mM	Tris
	1 mM	$MgCl_2$
	1 tablette	protease inhibitor
	1 spatula tip	lysozyme
	10 U/mL	DNase I
	pH	8.0

* filtrated (0.22 µm)

** DNase I was added freshly to ice cold lysis buffer immediately before each lysis round.

For immobilized metal ion affinity chromatography (IMAC)-based purification of TrxA-IdeS, FPLC was performed employing an ÄKTA FPLC system (Cytiva) equipped with His-Trap™ High Performance columns (Cytiva) and a 10 mL Superloop™ (Cytiva). UV absorbance at 280 nm was recorded by a UPC-900 monitor. The inlet tubings of pump A and B were placed in buffer A and B, respectively, and the system was equilibrated to 1 % buffer B. FPLC was performed at a flow rate of 1.0 mL/min. 8.5 mL of lysate supernatant were loaded into the Superloop™ and injected. The flow-through was collected manually

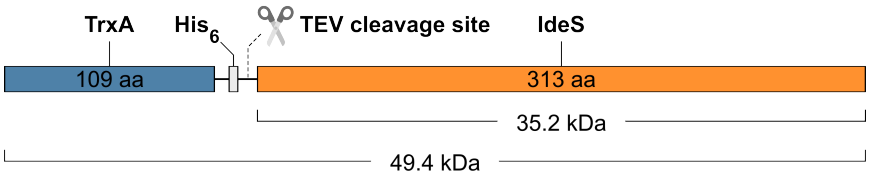

Figure 2.8.: Structure of the TrxA-IdeS fusion protein. The recombinant IdeS differed slightly from the wildtype protein: 28 amino acids (aa) from the from 29 aa N-terminal signal peptide were lacking and one N-terminal glycine as well as a methionine at position 3 were added to the aa sequence.

in 15 mL conical tubes. First, buffer B was increased in a discrete step to 5 %, then to 25 % in a linear fashion, followed by two final steps to 50 % and 100 %, respectively. Prior to each buffer B increase, the UV baseline was allowed to stabilize. Wash and elution fractions for up to 5 % buffer B were collected manually in 15 mL conical tubes. For the linear gradient up to 25 % buffer B, 1 mL fractions were collected automatically using the Frac-900 fraction collector (Cytiva). 20 µL of all fractions were sampled for SDS-PAGE analysis. Except for flow-through (diluted 1:4 with H_2O), all FPLC fractions were used undiluted.

2.4.1.4. TEV protease-mediated cleavage of TrxA-IdeS

After expression and purification of TrxA-IdeS fusion protein, the TrxA and His_6 tags were no longer required. In order to ensure optimal IdeS activity, the tags were removed by TEV protease digestion. FPLC fractions were pooled after SDS-PAGE analysis and concentrated with 10 kDa MWCO Vivaspin 20 centrifugal concentrators (Sartorius) to a volume of 3 mL (5000 x g, 10 min, RT). In order to remove imidazole, the concentrated TrxA-IdeS solution was dialyzed at RT against 350 mL of dialysis buffer (see **Table 2.15**) using 6-8 kDa MWCO D-Tubes™ Dialyzer Maxi (Merck). Then, 150 U of TEV protease (New England Biolabs) were added into the dialyzer tube, the tube was placed in 3 L of fresh dialysis buffer and the digestion reaction was performed for a few hours at RT before continued overnight at 4 °C. IdeS was then purified from the TrxA tag by IMAC-FPLC as described previously, but starting with 100 % buffer A. The digested IdeS does no longer contain a His_6 tag able to bind to the IMAC column resin. Hence, IdeS appears in the flow-through. FPLC fractions were pooled after SDS-PAGE analysis and added 50 % glycerol for longterm storage at -20 °C.

Table 2.15.: Dialysis buffer.

150 mM	NaCl
20 mM	Tris
0.1 %	2-mercaptoethanol
pH	8.0

Dialysis buffer was filtrated (0.22 µm).

2.4.2. Generation of IFX F(ab')$_2$ fragments

IdeS was utilized to digest IFX in order to generate F(ab')$_2$ fragments. As depicted in **Figure 2.9**, IdeS cleaves IgG into one F(ab')$_2$ fragment and two Fc heavy chain fragments. The undesired, smaller IFX heavy chain fragments were subsequently removed by SEC, since they would disturb the immobilization of the epitope mapping biosensor.

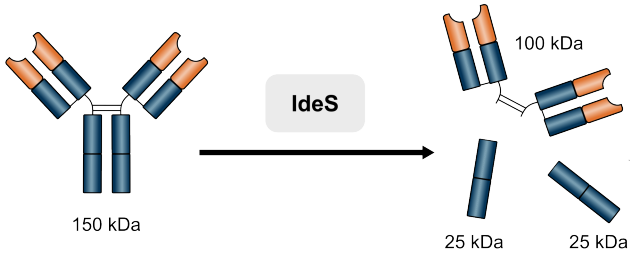

Figure 2.9.: IgG cleavage by IdeS. IdeS catalyzes the cleavage of IgG into one 100 kDa F(ab')$_2$ and two 25 kDa Fc heavy chain fragments.

The IFX digestion batch composition is shown in **Table 2.16**. All components were mixed in a 0.5 mL Protein LoBind reaction vessel and incubated for 2 h at RT. The entire reaction mix was then loaded in a 500 µL sample loop and SEC-FPLC was performed using a Superdex™ 200 Increase 10/300 GL column (Cytiva). The purification was performed at RT and a flow rate of 0.75 mL/min. Dialysis buffer without 2-mercaptoethanol was used as running buffer and 0.5 mL fractions were collected automatically. 20 µL of each fraction were diluted in a 1:8 ratio with H_2O and added non-reducing Laemmli sample buffer for SDS-PAGE. The fractions collected from the higher MW peak were pooled and concentrated to a volume of 600 µL using 30 kDa MWCO Amicon® Ultra-0.5 centrifugal filter units. The concentrated protein solution was finally dialyzed against PBS to remove Tris, whose primary amine group would interfere with the immobilization procedure. First, the F(ab')$_2$ fragments were dialyzed in 500 mL of PBS at RT. Then, the PBS solution was replaced and dialysis was continued overnight at 4 °C. The protein solution was either stored undiluted at 4 °C for up to two weeks or at -20 °C with 10 % glycerol.

Table 2.16.: Reaction batch for the digestion of IFX by IdeS.

Material	**Volume**
700 µg Remicade®*	x µL
8 µg purified IdeS*	y µL
Dialysis buffer	(350-x-y) µL
Total liquid volume:	350 µL

* Varying stock solution concentrations.

2.4.3. Biosensor surface preparation and screening of patient sera

The biosensor surface for ADA epitope mapping ("ADAmon-EpiM") was prepared utilizing CM5 sensor chips. The immobilization protocol was identical with the ADAmon biosensor surface preparation (**section 2.3.1**), except for the following changes:

1. In cycle 2, IFX F(ab')$_2$ was immobilized on Fc2 aiming at a target ligand density of 5000 RU.
2. IFX F(ab')$_2$ ligand solution was prepared as a 20 µg/mL dilution in ligand buffer (pH 4.5).
3. Dkαgt and IFX F(ab')$_2$ were not subjected to additional cross-linking by EDC/NHS.

The analytic procedure and signal referencing for ADA epitope mapping were carried out identically to ADAmon analyses, as described in **section 2.3.6**.

2.5. Quantification of ADM and anti-ADM antibodies in diluted serum using SPR

2.5.1. Biosensor surface preparation

The sensor surface for the ADM quantification assay (denominated "ADMmon") was prepared identically to the IFXmon biosensor surface, as described in **section 2.2.1**.

The biosensor surface for the anti-ADM antibody quantification assay (denominated "anti-ADMmon") was immobilized similarly to the ADAmon biosensor surface (see **section 2.3.1**), with the following changes:

1. In cycle 2, ADM was immobilized on Fc2 (with ligand cross-linking) aiming at a target ligand density of 4900 RU.
2. ADM was diluted in ligand buffer (pH 5.5) at 20 µg/mL.

2.5.2. ADMmon and anti-ADMmon calibration and signal referencing

The analytic procedure and signal referencing for ADMmon were carried out analogously to IFXmon analyses (see **section 2.2.3**). However, the regeneration solutions from the ADAmon biosensor assay (see **Table 2.11**) were employed for biosensor recovery. Furthermore, the therapeutic window of ADM serum trough concentrations differs from IFX. The concentrations of the six ADM calibrators were selected to cover subtherapeutic, therapeutic and overdosed ADM serum concentrations (0, 1.0, 3.0, 10.0, 25.0, 50.0 µg/mL). The ADM standard for monitoring biosensor ageing had a concentration of 10 µg/mL.

Anti-ADMmon analyses followed the methods described for ADAmon analyses (see **section 2.3.6**).

2.5.3. Commercial ADM and anti-ADM quantification assays

Two different commerially available ELISA kits for the quantification of ADM and anti-ADM served as method comparison with the ADMmon and anti-ADMmon biosensor, respectively:

- IDKmonitor® Adalimumab drug level ELISA (Immundiagnostik)
  - sandwich ELISA (plate is pre-coated with anti-ADM capture antibody)
  - quantifies free ADM
  - LOQ: 0.6 µg/mL
- IDKmonitor® Adalimumab total ADA ELISA (Immundiagnostik)
  - bridging ELISA (serum is incubated with HRP-conjugated ADM and biotinylated ADM, conjugate-complexed anti-ADM are captured onto a streptavidin-coated plate)
  - quantifies total anti-ADM (free and serum ADM-bound)
  - LOQ: 10 AU/mL

All assays were executed according to the manufacturers' instructions.

2.6. Statistical analyses

Statistic analyses were performed using GraphPad Prism, Microsoft Excel, R and RStudio. In general, continuous variables were compared with non-parametric statistical tests. Kruskal-Wallis test was selected for comparisons of $n > 2$ groups and Mann-Whitney U test was utilized for pairwise comparisons. For categorical variables, chi-square test was employed if each contingency table cell contained $n \geq 5$ observations; else, Fisher's exact test was performed. In receiver operating characteristic (ROC) analysis, the variable value corresponding to maximum Youden Index was determined as cut-off value indicative of the event of interest and reported together with the area under the curve (AUC). Hazard ratios were calculated with the Cox-proportional hazards method, whereby the likelihood ratio test served to test global significance in univariate analyses. P-values were not corrected for multiple testing and considered significant if < 0.05.

For analytic results below the respective assay LOD, it is unknown which value between zero and LOD is the respective true result. Therefore, if quantitative evaluations were performed with analytic results, data points below LOD had to be transformed to a numeric value first. This was achieved by setting these values to 0.5·LOD.

Method comparison regression between the IDKmonitor infliximab drug level ELISA and IFXmon was performed using the R package "mcr" with an ELISA:IFXmon error ratio

of 1.467. This error ratio was determined by comparing the IFXmon patient serum analysis duplicate variance and the concentration-specific variances indicated in the ELISA manual.

Herein utilized abbreviations of statistical standard parameters include standard deviation (SD), coefficient of variation (CV) and confidence interval (CI).

3. Results

3.1. IFXmon biosensor assay validation

Parts of the presented validation results are also described in Grasmeier et al. (2023) [322].

3.1.1. Sensor stability and regeneration efficacy

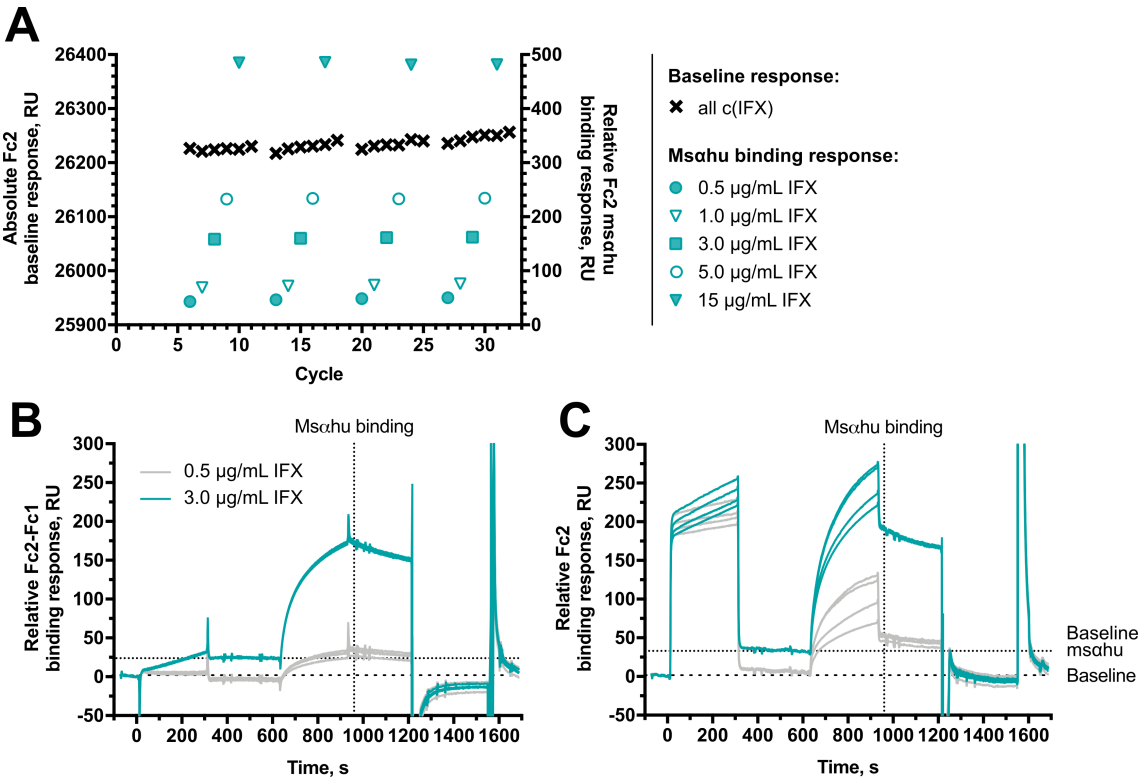

Figure 3.1.: IFXmon regeneration efficacy. IFX calibrators were prepared by spiking blank serum matrix with the indicated concentrations of IFX and diluting the serum as described in **section 2.2.3**. (**A**) Stability analysis of IFXmon for repeated injection of a calibrator series with five different IFX concentrations (n = 4). Absolute baseline response (recorded at the beginning of each cycle) and msαhu binding response relative to the baseline before msαhu injection (see baseline msαhu in (**B**) and (**C**)) are shown for all analytic cycles. (**B**) Fc2-Fc1 sensorgrams for all n = 4 repetitions of the 0.5 µg/mL and 3.0 µg/mL IFX calibrator analyses. (**C**) Fc2 sensorgrams for all n = 4 repetitions of the 0.5 µg/mL and 3.0 µg/mL IFX calibrator analyses. Adapted from [322].

Ideal regeneration conditions for the dissociation of ligand:analyte interactions in SPR analyses enable complete ligand recovery, while at the same time keeping the ligand intact and functional. In chemical terms, this means that the regeneration should be aggressive enough to dissolve the biomolecular interactions (of both specific and unspecific nature). However, the regeneration solution must not harm the ligand to keep it functional for repeated analyte binding. As these requirements are often incompatible with each other, an optimal compromise needs to be found experimentally to obtain the longest possible sensor chip lifetime. Nevertheless, accumulating ligand damage has to be expected with

increasing number of analytic cycles run on a sensor chip.

Regeneration scouting was performed to find the optimal regeneration conditions for the IFXmon biosensor (data not shown). The best results were obtained with sequential injections of two different solutions: An acidic glycine buffer (pH 2.0) with detergents was applied before an alkaline buffer (pH 9.0) with high ion strength. **Figure 3.1A** demonstrates that the chosen regeneration procedure led to a stable baseline and highly reproducible IFX binding responses over a broad IFX concentration range. These results also indicate that non-specific binders contained in the serum matrix were sufficiently removed from the IFXmon surface. If utilized exclusively for patient serum analyses, one IFXmon biosensor chip could be utilized to analyze 60 different patient sera. The indicated sensor capacity included approximately 115 cycles, which were executed in three different runs and contained all calibrators, blanks and standards required to adequately assess sensor quality.

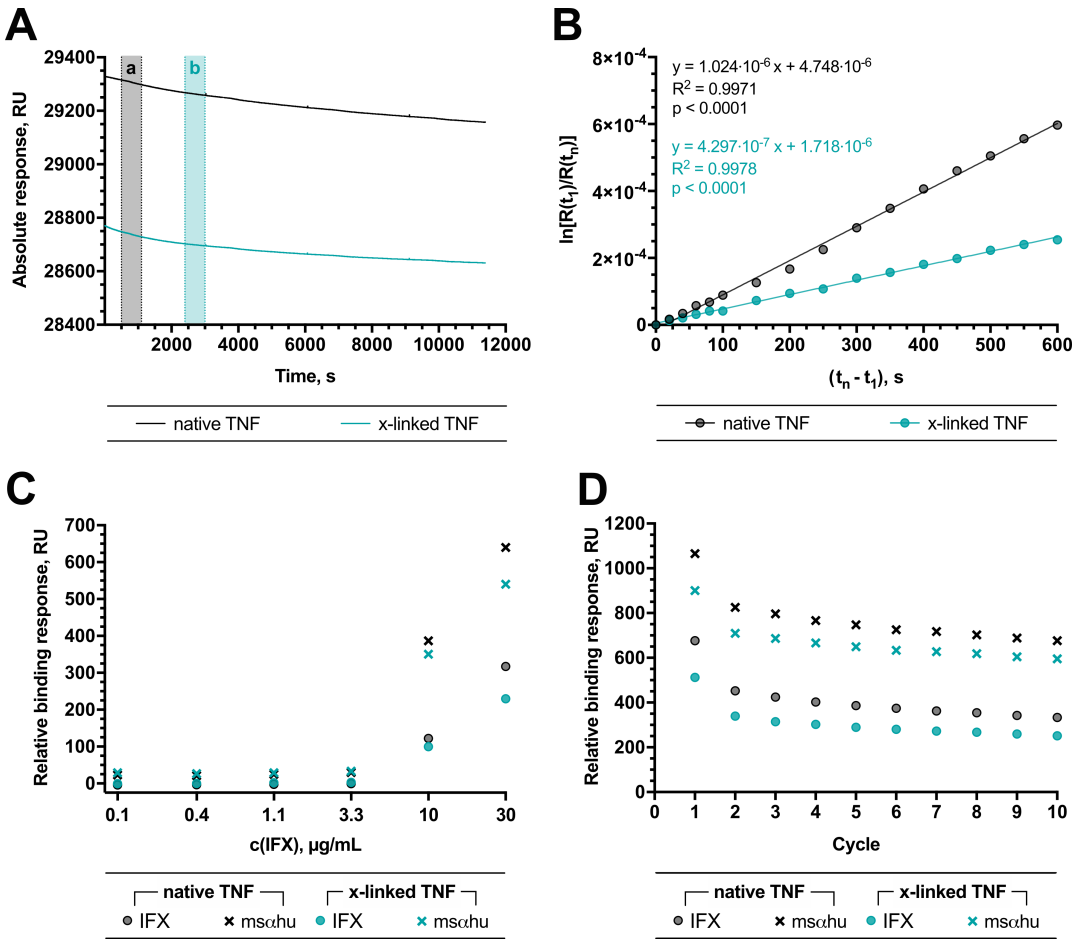

Figure 3.2.: Ligand stability comparison between native and cross-linked TNF. (**A**) Three-hour dissociation monitoring after biosensor preparation. Sensorgrams show absolute SPR signal responses. **a** and **b** highlight the respective time periods within the dissociation monitoring of native and cross-linked TNF, which contained the 16 report points for k_d calculation. (**B**) k_d calculation plot with linear regression for native and cross-linked TNF. (**C**) Comparison of IFX and msαhu binding to native and cross-linked TNF for different IFX concentrations. IFX was spiked in PBS at the indicated concentrations. (**D**) Binding repeatability of 15 µg/mL IFX for sequential injection-regeneration cycles.

TNF immobilization via amine coupling bears the risk that not all monomers of the homotrimer are attached covalently to the sensor surface. This would result in continuous dissociation of TNF monomers from the surface and, consequently, an unstable SPR baseline signal. In order to mitigate complex dissociation after biosensor preparation, the effect of an additional cross-linking step during immobilization was tested (see **section 2.2.1**). For this means, a CM5 sensor chip was immobilized with non-cross-linked TNF on Fc1 and cross-linked TNF on Fc2. Then, TNF dissociation was monitored at the earliest possible timepoint after immobilization (**Figure 3.2A+B**) and the two surfaces were evaluated functionally (**Figure 3.2C+D**). The dissociation rates k_d were determined as 1.024×10^{-6} 1/s (95 % CI: 0.992×10^{-6} – 1.056×10^{-6} 1/s) for native TNF and 4.297×10^{-7} 1/s (95 % CI: 4.181×10^{-7} – 4.412×10^{-7} 1/s) for cross-linked TNF, respectively. The theory of k_d calculation is described in detail in the methods section (see **section 2.2.2**). With native TNF comprising a 2.4-fold higher k_d, these data suggest that the cross-linked TNF surface was significantly more stable. The functional analyses demonstrated that TNF cross-linking did not impair IFX or msαhu binding over an IFX concentration range of two orders of magnitude. The slightly higher binding signals recorded for higher IFX concentrations on the native TNF surface are likely owed to the marginal immobilization level difference (8.2 % higher ligand density on native TNF surface compared to cross-linked TNF surface). Also, IFX binding repeatability was not observed to differ among the two surfaces.

3.1.2. Calibration

For IFXmon calibration, a hyperbolic model was observed to best describe the binding-saturation relationship between IFX concentration and both IFX and msαhu binding responses (see **Figure 3.3A+B**, $R^2 = 1.000$). IFX calibrator concentrations cover both subtherapeutic, therapeutic and also supratherapeutic IFX trough levels. **Figure 3.3C** shows that the repeatability of the calibration curve was excellent, even though considering both intra- and inter-assay replicates. Furthermore, the enhancement by msαhu was analyzed for the different calibrators. Signal enhancement was most effective for low IFX concentrations and became smaller for higher IFX concentrations. The high curvature of the msαhu curve in **Figure 3.3A** indicates that this observation may be owed to binding saturation of the msαhu enhancer antibody.

3.1.3. Limits of blank, detection and quantification

The parameters limit of blank (LOB), limit of detection (LOD) and LOQ characterize the ability of an analytic method to measure low analyte concentrations under consideration of the assay's analytic variability, i.e., its SD. Analytic sensitivity of the IFXmon biosensor assay was determined through analysis of blank serum matrix samples. In nine IFXmon analytic runs performed with five different IFXmon biosensor chips, a total of $n = 43$ blank serum matrix samples were analyzed. Then, IFX concentrations were interpolated from

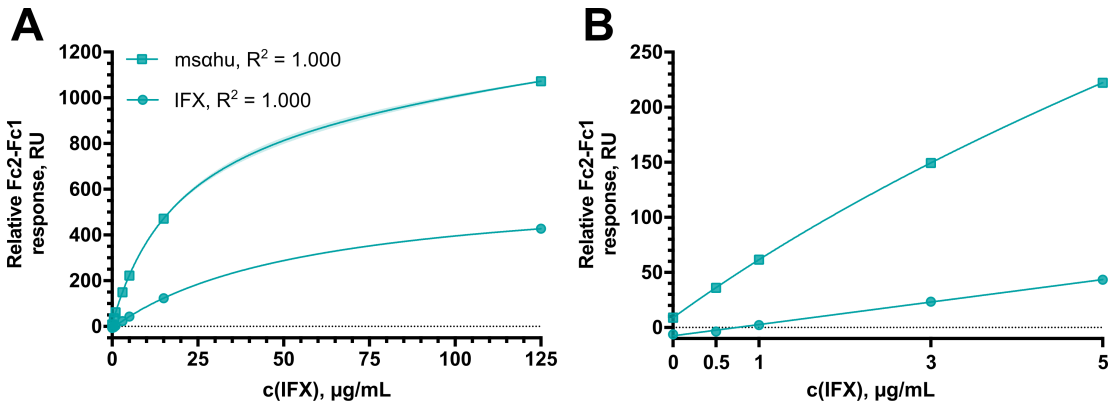

C

c(IFX), µg/mL	IFX binding Mean, RU	IFX binding SD, RU	msαhu binding Mean, RU	msαhu binding SD, RU	Enhancement*
0.0	-6.3	2.4	9.0	4.2	-
0.5	-3.6	1.3	36.0	3.3	10
1.0	2.3	0.8	61.7	2.7	6
3.0	23.5	0.5	149.4	1.6	5
5.0	43.5	0.6	222.2	0.8	4
15	123.6	1.0	471.7	2.1	3
125	427.2	5.2	1072.3	9.4	2

Figure 3.3.: IFXmon calibration curve. (**A**) IFXmon analyses of seven different IFX calibrators (0, 0.5, 1.0, 3.0, 5.0, 15, 125 µg/mL) from n = 4 technical replicates per concentration. Responses of both IFX binding and msαhu binding are shown. Curves were fit with a hyperbolic model. (**B**) Close-up of the low IFX concentration range. (**C**) Summary statistics. *Enhancement factors were calculated with blank-corrected SPR signals to enable consideration of negative SPR signals. Adapted from [322].

the obtained SPR signals with calibration curves recorded within the respective analytic run. The histogram shown in **Figure 3.4A** only includes n = 30 samples, because the interpolation of n = 13 samples resulted in SPR signals that were too low for interpolation. It should be mentioned at this point that each calibration curve contained one blank serum matrix calibrator, which defined the minimum SPR signal within that analytic run, from which an IFX concentration could be interpolated. Biologic sample variability may result in SPR signals below the respective blank calibrator signal. If the negative difference is too large, interpolation fails.

The observed blank serum matrix mean IFX concentration was 0.11 ± 0.13 µg/mL. According to Armbruster et al. (2008), the LOB defines the concentration cut-off, below which 95 % of blank samples can be expected [334]. The formula for the calculation of LOB is given as LOB = $\text{mean}_{\text{blank}}$ + 1.645 SD_{blank}. Accordingly, LOB for the IFXmon biosensor assay is 0.3 µg/mL [334].

Conventional LOD and LOQ determination requires the calculation of LOB from blank sample matrix [334]. LOD is then calculated through additional repeated analysis of analyte close to the expected LOD with the formula LOD = LOB + 1.645 $\text{SD}_{\text{low analyte}}$ [334]. LOQ is determined as the lowest concentration that fulfills the performance criteria (precision,

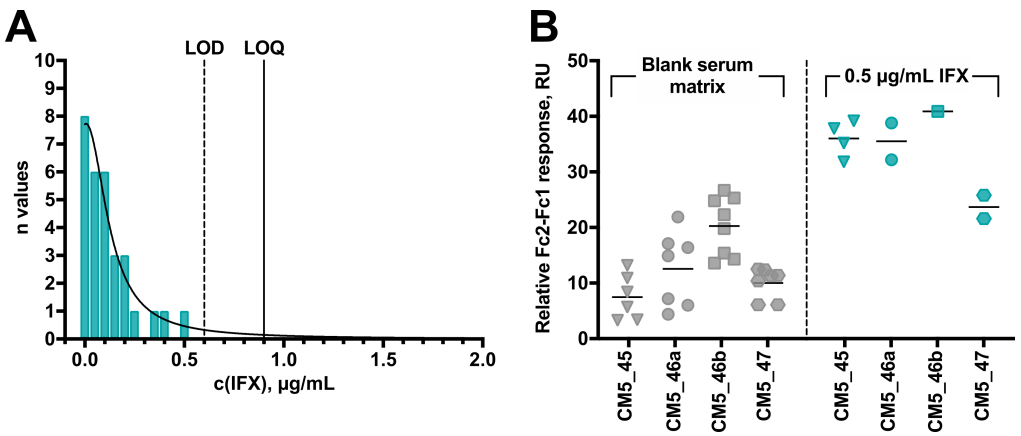

Figure 3.4.: Analytic sensitivity of IFXmon. (**A**) Histogram showing n = 30 IFXmon analyses of blank serum matrix with a Lorentizian fit utilized for the determination of analytic sensitivity. The included data were obtained from nine independent runs and five different sensor chips. (**B**) Comparison of blank serum matrix analyses to analyses of 0.5 µg/mL IFX spiked in blank serum matrix, grouped by sensor chip ID (CM5_45, CM5_46, CM5_47) and run ID (CM5_46a, -b). Adapted from [322].

accuracy, linearity) for reliable quantification [334]. However, LOD and LOQ determination for the IFX biosensor assay deviated from this classical method due to the following reasons: First, the observed mean blank is likely overestimating the true mean blank, since lower blank signals without interpolation results did not contribute to the observed mean. Second, a calibration curve is recorded in each IFXmon run, while the observed SD also considers inter-assay variability. Intra-assay SD, as relevant for IFXmon quantification, is lower than the inter-assay variability and hence, also the LOD and LOQ relevant for IFXmon quantification are lower. Third, the reported statistical method demands a relatively high sample number, as LOQ is detemined in an iterative process, which would translate to a disproportionately high cost and serum consumption for IFXmon validation. Therefore, the statistic method was optimized and the validity of the determined parameters was verified *post hoc* with low-concentration IFX calibrators.

LOD was determined as the 5 % α error of the blank distribution and was 0.6 µg/mL. The frequency distribution was fit with a Lorentizian model. This fit is related to the Gaussian fit, but exhibits more shallow arms. Hence, the Lorentizian curve assigns a higher frequency to extreme values. The calculated LOD is consequently higher (more conservative) than when determined from a Gaussian curve, which should prevent overestimation of analytic sensitivity. None of the n = 30 analyzed blanks was detected above LOD.

The LOQ cut-off was 0.9 µg/mL, calculated as $\text{mean}_{\text{blank}}$ + 6 SD_{blank}, which was also equivalent to the 2.5 % α error of the blank distribution. The statistically determined analytic sensitivity was validated by comparing blank serum matrix samples and 0.5 µg/mL IFX calibrators analyzed within the same run. **Figure 3.4B** demonstrates that within the same run (and even between all runs except for CM5_46b vs. CM5_47), the sub-LOD IFX calibrator signals were clearly higher than serum matrix blanks. In summary,

these results verify the determined LOD and LOQ values. The LOQ of the IDKmonitor Infliximab drug level ELISA was 0.6 µg/mL, and therefore similar to IFXmon.

3.1.4. Accuracy and precision

Accuracy and precision of IFXmon were determined in three different analytic runs performed on three different days with two different IFXmon sensor chips. In each run, three different IFX concentrations were measured in three technical replicates, which served to calculate intra-assay accuracies and precisions (see **Table 3.1**). Precision is hereby given as CV (as the more common estimator) and 100 % - CV in order to provide a value that is more readily comparable to accuracy. In **Table 3.2**, overall accuracy and precision were calculated from all n = 9 available data points. The term "overall" was used instead of "inter-assay" to prevent misleading of the reader, since not only inter-assay but also intra-assay data contributed to the calculations.

Table 3.1.: Intra-assay accuracy and precision of IFXmon.

c(IFX)	Mean interpolated c(IFX) ± SD			CV range,	A range,	P range,
	Run = 1	2	3	%	%	%
1.0	1.07 ± 0.07	0.94 ± 0.01	0.91 ± 0.03	0.6 – 6.1	90.7 – 107.3	93.9 – 99.4
5.0	4.95 ± 0.10	4.32 ± 0.03	4.46 ± 0.02	0.5 – 2.0	86.4 – 98.9	98.0 – 99.5
30	30.9 ± 0.9	29.6 ± 0.3	27.8 ± 0.5	1.2 – 2.8	92.6 – 102.9	97.2 – 98.8

All IFX concentrations are given in µg/mL. Precision is indicated as 100 % - CV. Precision and accuracy were both calculated from n = 3 replicates. A, accuracy; P, precision. Adapted from [322].

Intra-assay accuracy of IFXmon was observed to range from 86.4 – 107.3 % (mean: 96.4 %) recovery of the respectively expected IFX concentrations. Intra-assay precision ranged from 0.5 – 6.1 % (mean: 2.2 %) CV. Overall accuracy ranged from 91.5 – 98.1 % (mean: 95.6 %) recovery and overall precision ranged from 4.9 – 8.8 % (mean: 6.7 %). As expected, intra-assay precision was slightly higher as compared to overall precision. On the contrary, intra-assay accuracy was slightly lower than for the overall data. No concentration dependence of accuracy or precision was observed within the analyzed IFX concentration range.

Table 3.2.: Overall accuracy and precision of IFXmon.

c(IFX)	Interpolated c(IFX)									Mean ± SD	CV,	A,	P,
	Run = 1			2			3				%	%	%
1	1.01	1.14	1.07	0.94	0.93	0.94	0.88	0.91	0.93	0.97 ± 0.09	8.8	97.3	91.2
5	4.84	5.04	4.96	4.35	4.31	4.30	4.48	4.45	4.44	4.57 ± 0.29	6.3	91.5	93.7
30	29.9	31.6	31.1	30.0	29.4	29.4	27.8	28.2	27.3	29.4 ± 1.5	4.9	98.1	95.1

All IFX concentrations are given in µg/mL. Precision is indicated as 100 % - CV.
A, accuracy; P, precision. Adapted from [322].

The lowest analyzed IFX concentration (1 µg/mL) was at the IFXmon LOQ (see **section 3.2.4**) and exhibited overall accuracy and precision of 97.3 % and 8.8 %, respectively. These data suggest high performance reliability of IFXmon at the LOQ and provide evidence that the LOQ was determined conservatively enough. In **Figure 3.5**, accuracy and precision data were utilized to assess assay linearity. Linearity of the IFXmon assay did not significantly differ from the line of identity up to the highest analyzed quality control with highly supratherapeutic IFXmon concentration (30 µg/mL).

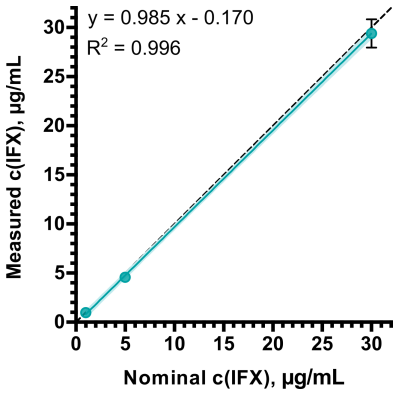

Figure 3.5.: IFXmon assay linearity. Assay linearity for overall accuracy and precision data (see **Table 3.2**) Shown are means of all n = 9 replicate analyses with SD, linear regression (solid teal line), 95 % confidence band (light teal) and line of identity (dashed black line).

To provide a comparison with the *in vitro* diagnostics (IVD)-approved IDKmonitor Infliximab drug level ELISA, a brief summary of the performance characteristics reported by Immundiagnostik is given[335]: Accuracy was determined for seven different IFX concentrations (0.8 – 50.0 µg/mL, measured in unicates) as 94.6 – 113.3 % (mean: 105.4 %) recovery. Inter-assay precision calculated from six different IFX concentrations (2.8 – 20.7 µg/mL) was 5.4 – 12.9 % CV (mean: 8.8 %). Compared with the ELISA, IFXmon performed slightly better with respect to both accuracy and precision.

3.1.5. Patient study and method comparison with ELISA

The developed IFXmon biosensor assay was employed to analyze 84 sera from 15 IBD patients in duplicates (see **Figure 3.6**). The same sera were also analyzed in unicates with the IDKmonitor Infliximab drug level ELISA. Method comparison with the IVD-approved ELISA provides evidence, whether the measurement quality of the IFXmon biosensor can also suffice diagnostic criteria. The patient serum analyses via the IFXmon biosensor assay were co-executed by Anna Felicitas Langmann and a more detailed analysis of the herein presented data is described in her dissertation[336].

The characteristics of the IFXmon patient cohort are listed in **Table 3.3**. The cohort was relatively young and comprised balanced proportions of CD and UC diagnoses. 13.3 % of patients received therapy with the originator IFX Remicade®, while 86.7 % received a biosimilar drug. With 60.0 %, the majority of patients were administered Inflectra® and

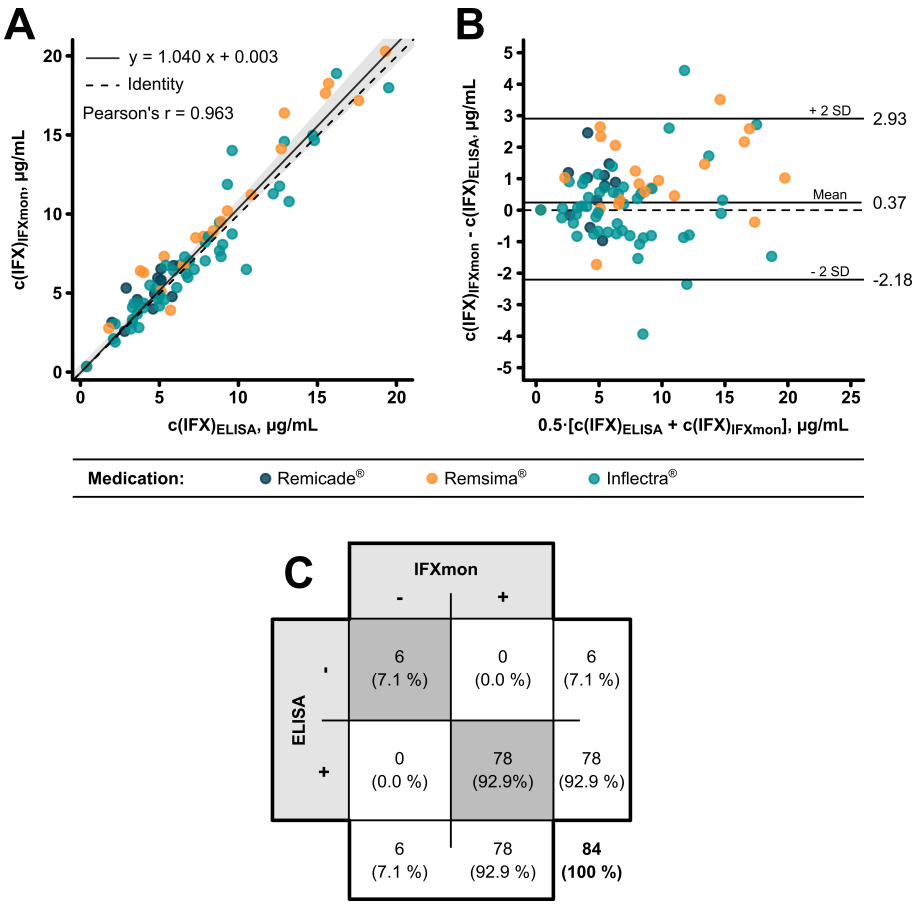

Figure 3.6.: Method comparison of patient serum analyses between IFXmon and ELISA. 84 sera of IFX-treated patients (Remicade®, Remsima® and Inflectra®) were analyzed in unicates by ELISA and in duplicates by IFXmon. (**A**) Passing-Bablok regression (solid black line) with 95 % confidence band (gray area) and identity line (dashed black line). (**B**) Bland-Altman plot with method mean, identity line (dashed black line) and limits of agreement at 95 % confidence. (**C**) IFX detection concordance between IFXmon and ELISA. Adapted from [322].

26.7 % were treated with Remsima®. A median of 6.0 TDM visits per patient in a median frequency of 5.4 weeks indicate a highly proactive IFX monitoring regimen.

Figure 3.6A depicts the Passing-Bablok regression between IFXmon and ELISA analyses. The slope of the regression was 1.040 (95 % CI: 0.961 – 1.113) and the intercept was 0.003 (95 % CI: -0.251 – 0.511). Since the identity line falls within the narrow 95 % confidence band, the data suggest that IFXmon and ELISA are interchangeable. These results also translate to subtherapeutic IFX concentrations (LOQ $\leq$ c(IFX) $\leq$3.0 µg/mL), where precise analytic performance is even more important than for high IFX levels. Slope and intercept of the constricted Passing-Bablok regression were 1.029 (95 % CI: 0.745 – 1.803) and 0.009 (95 % CI: -0.295 – 0.235), respectively, and the higher slope inexactitude is owed to the reduced sample size for this analysis (n = 10). Of the 84 sera, 11, 21 and 52 were obtained from Remicade®-, Remsima®- and Inflectra®-treated patients, respectively. Separate Passing-Bablok regression of data grouped by medication resulted in overlapping 95 % CI of both slope (Remicade®: 0.550 – 2.850, Remsima®: 0.919 – 1.206, Inflectra®:

Table 3.3.: IFXmon patient cohort characteristics.

Characteristic	Summary statistics	
n (%)	15	(100.0)
Sex, n (%)		
Female	7	(46.7)
Male	8	(53.3)
Age, years, median (IQR)*	46	(33 – 55)
Diagnose, n (%)		
CD	9	(60.0)
UC	6	(40.0)
Medication, n (%)		
Remicade®	2	(13.3)
Remsima®	4	(26.7)
Inflectra®	9	(60.0)
Number of TDM visits, median (IQR)	6.0	(4.5 – 6.5)
TDM visit interval, weeks, median (IQR)	5.4	(4.8 – 6.2)

*Patient's age at first included TDM visit. IQR, interquartile range. Adapted from [322].

0.919 – 1.077) and intercept (Remicade®: -7.780 – 3.321, Remsima®: -1.010 – 1.892, Inflectra®: -0.184 – 0.362). Therefore, the quantification of biosimilars and Remicade® did not differ significantly.

Bland-Altman analysis of the sera resulted in a slightly positive method mean (0.37 µg/mL), which indicates that IFXmon analyses resulted in slightly higher IFX concentrations as compared to ELISA (see **Figure 3.6B**). The 95 % limits of agreement, which contain 95 % of all observed differences, were -2.18 µg/mL and 2.93 µg/mL. It was noticeable that IFX concentrations above 10 µg/mL showed larger differences between the two methods. Of note, 90.6 % of sera containing up to 7 µg/mL IFX, which covered subtherapeutic concentrations and the vast majority of the therapeutic window, differed for $\leq$ 1.5 µg/mL. The contingency table in **Figure 3.6C** shows that the IFX detection concordance between IFXmon and ELISA was 100 %, as the same sera (n = 78, 92.9 %) were classified as IFX-positive by the two methods. In conclusion, the presented data indicate high agreement between IFXmon and ELISA analyses.

3.2. ADAmon biosensor assay validation

Parts of the presented validation results are also described in Grasmeier et al. (2023) [322].

3.2.1. Drug-tolerance and efficacy of the ADA pulldown method

3.2.1.1. Direct quantification of ADA in serum

Analytic drug tolerance describes the capacity of a diagnostic test to measure a drug-interacting analyte in the presence of drug [250]. A common method to achieve analytic drug tolerance is subjecting the sample to PA. The direct quantification of ADA in diluted serum (DQ) is the most simple and economic method to quantify ADA in serum. Two different DQ protocols for drug-tolerant ADA quantification were applied within this project: The first method is based on a published protocol ("Beeg method") [288], while the second method was largely modified from the described protocol ("in-house method") and was more similar to the ADA pulldown procedure, which had been established in parallel (see **section 2.3.3**). The two methods differ in final serum dilution, utilized buffers and duration of incubation steps. The general idea of direct PA consists in the temporary dissociation of serum ADA:IFX complexes under acidic conditions. The unbound ADA are then available to form complexes with the highly abundant IFX immobilized on the biosensor, but this re-association requires neutral pH. Accordingly, the addition of neutralizing buffer to acidified serum samples is highly time-critical and must occur as closely as possible to sample injection (see **Figure 3.7A**). Since the Biacore X100 system lacks a function for merged injections beyond immobilization runs, the time points for manual serum acidification and neutralization had to be matched precisely with an active analytic SPR run (see **section 2.3.6**).

The data obtained with the Beeg method generally exhibited higher variability as compared to the in-house method (data not shown). However, the results of the in-house method are also transferable to the Beeg method. **Figure 3.7B+C** compares the DQ and pulldown quantification (PQ) methods with respect to repeatability and discrimination of ADA-negative and ADA-positive sera. Of note, the PQ method also contained a PA step intended to convey drug tolerance. **Figure 3.7B** demonstrates that DQ comprises higher variability for blank serum matrix as compared to PQ. Furthermore, the DQ negative serum data points were only slightly below the 5 µg/mL ADA calibrator, which indicates poor analytic sensitivity. In contrast, PQ negative sera exhibited very small variance and were approximately 300 RU below the 5 µg/mL ADA calibrator, which indicates very good separation. Comparing ADA-negative and ADA-positive IBD patient serum analyses as shown in **Figure 3.7C**, PQ comprised a significant discrimination ($p = 0.0095$), while DQ was not able to discriminate the two groups. Evaluation of the time window for ADA re-association after neutralizing the pre-analytically acidified samples delivered information about why DQ might fail in our setup (**Figure 3.7D**).

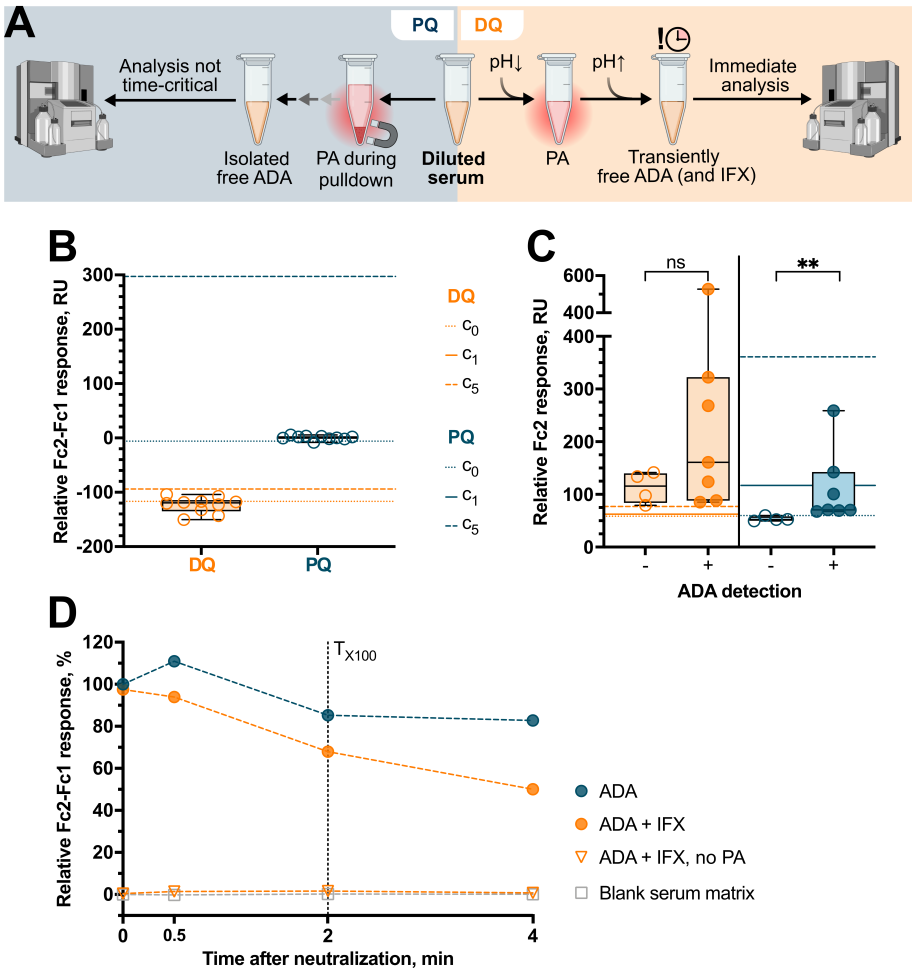

Figure 3.7.: ADA DQ evaluation. (**A**) After neutralizing the pre-analytically acidified samples, DQ samples demand immediate measurement, as ADA quickly re-associate with serum IFX. PQ eluates, on the other hand, no longer contain serum IFX and their analysis is hence not time-critical. (**B**) n = 10 ADA-negative sera were analyzed with DQ and PQ. Dashed lines depict the signals of blank serum matrix spiked with 0 and 5 µg/mL ADA calibrator, which were used as calibrators (c_0, c_5). (**C**) Comparison of SPR signals obtained with DQ and PQ for n = 4 ADA-negative (clear circles) and n = 7 ADA-positive (filled circles) sera. ADA status was determined by ELISA. Dashed lines depict signals of 0, 1 and 5 µg/mL ADA calibrators, respectively (c_0, c_1, c_5). Since DQ exhibited excessive and variable Fc1 signals, only Fc2 signals are shown here. **, p = 0.0095. (**D**) To evaluate if DQ can produce meaningful results with Biacore X100, the velocity of ADA:IFX re-association after neutralization was investigated. IFX beads were incubated with (spiked) blank serum matrix (both ADA and IFX at 30 µg/mL) and pulldown was performed until the PA step. The batch without PA was added PBS instead of 10 mM glycine, pH 1.5. Eluates were neutralized in presence of IFX beads, sampled after the indicated time points and immediately separated from supernatants to assess the remaining amount of free ADA. Created with Bio-Render.

The Biacore X100 instrument automatic injection program comprises a time lag (T_{X100}) of approximately 2 min between sample aspiration and injection. 2 min after sample neutralization, only 67.9 % of ADA remained free for binding to the SPR biosensor in presence of equimolar IFX. The time courses of ADA re-association furthermore clearly demonstrate that PA is necessary to obtain free ADA in the bead supernatant. In summary, T_{X100}, together with high unspecific binding signals, impair reliable DQ in presence of IFX.

3.2.1.2. ADA pulldown characterization

As DQ was found to be incompatible with our Biacore X100 instrument, ADA pulldown was incorporated into the ADAmon assay protocol in order to obtain samples with timely stable free ADA for subsequent quantification (see **section 2.3.3**, **Figure 2.5**). As important performance characteristics of the ADAmon assay, efficacy and drug tolerance of the ADA pulldown procedure had to be evaluated. For this means, ADA488-spiked serum was employed as sample material for ADA pulldown. With the help of the fluorescence label, ADA488 can be detected unequivocally via fluorometry in the different pulldown fractions (serum supernatants (SN), wash supernatants and eluates). Furthermore, ADA488 can be detected regardless of structural integrity, such that the possibly damaging impact of the PA procedure could be investigated.

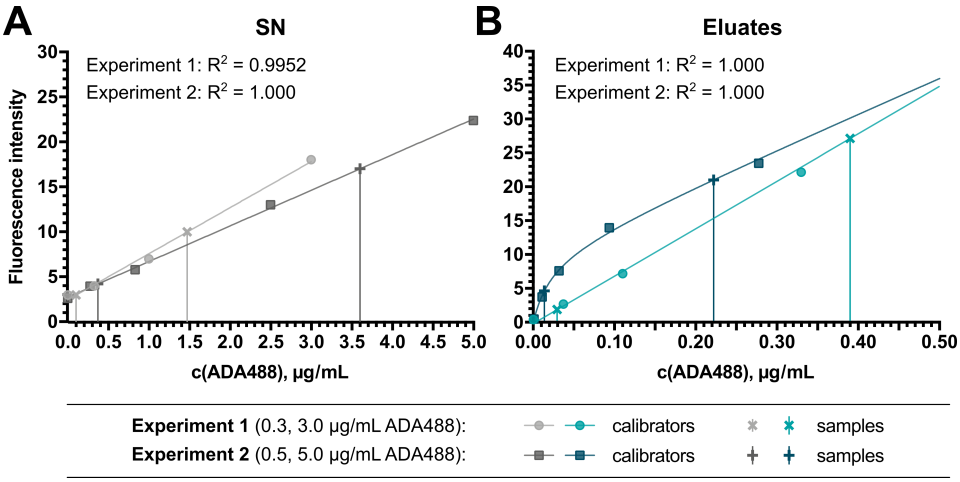

Figure 3.8.: Calibration curves for ADA488 quantification in pulldown SN and eluates. Two pulldown-fluorometry experiments were performed independently on different days: In experiment 1, 0.3 and 3.0 µg/mL ADA488 were spiked in serum, while 0.5 and 5.0 µg/mL ADA488 were analyzed in experiment 2. Maximum SN calibrator was prepared by spiking serum and performing the pulldown procedure up to the 60-min incubation as described previously, but without adding beads. Lower SN calibrators were prepared by serial dilution of the maximum SN calibrator with blank SN matrix (serum, PBS, 10 mM glycine pH 1.5 and 1 M Tris-HCl pH 8.0 mixed in a 1:5.5:5:1.5 ratio). Calibration curves for both SN quantification experiments were fit with linear models. Eluate calibration curves were prepared by spiking different ADA488 concentrations in blank eluate matrix (regeneration solution 3 and 1 M Tris-HCl pH 8.0 mixed in a 1:0.08 ratio). In experiment 1, a linear model was fit, while the data of experiment 2 were better described by a hyperbolic model.

The fraction matrix-specific calibration curves shown in **Figure 3.8** were utilized to quantify ADA488 in the respective pulldown fractions. It is clearly visible that the resolution of low ADA488 concentrations is better in the eluate matrix as compared to the SN matrix, probably due to fluorescence quenching effects of serum components. Consequently, the quantification of low ADA488 concentration in eluates is more reliable. Wash supernatants were also analyzed, but are not shown since ADA488 could not be detected in any wash fraction, likely owed to the high dilution. Coupling efficiency of the magnetic beads with IFX was determined after coupling in n $\geq$ 10 reaction batch SN via nephelometry using a BN ProSpec® system. As no IFX was detectable in any coupling SN (data not shown), coupling efficiency can be expected to be near-complete (limited only by the LOQ of the BN ProSpec® system).

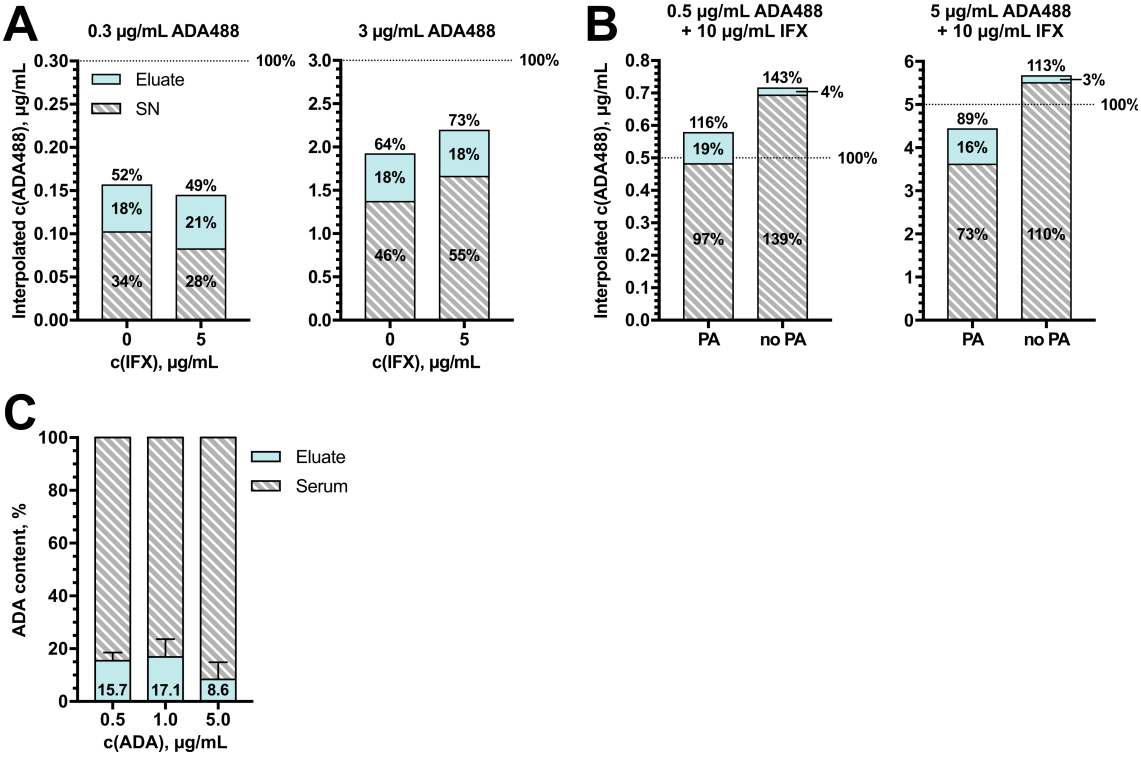

Figure 3.9.: Characterization of ADA pulldown. (A) Effect of serum IFX and ADA488 concentration on ADA488 yield. (B) Effect of PA and ADA488 concentration on ADA488 yield. (C) Validation of fluorometry results by ADAmon. Unlabeled ADA calibrator was spiked in blank serum matrix and analyzed. Data show n = 5 replicates per concentration, recorded on four different analytic runs. In order to determine the ADA content in pulldown eluates, their corresponding ADAmon signals were normalized to the signals of 2.5 µg/mL ADA standards (not subjected to pulldown), which were analyzed within the same run. Adapted from [322].

ADA pulldown yields and the influence of the PA step on pulldown success were characterized in detail. As shown in **Figure 3.9A**, ADA488 yields in eluates ranged from 16–21 %, and were independent of ADA488 concentration. The ADA488 pulldown tolerated the presence of 1.7–17-fold molar excess of IFX without significant reduction in ADA yield. Therefore, the pulldown can be assumed to be drug-tolerant. **Figure 3.9B** demon-

strates that PA is the crucial step during ADA pulldown to achieve drug tolerance. If the pulldown was performed without PA, ADA488 yield was reduced drastically, independent of ADA488 concentration. The less reliable ADA488 quantification in SN fractions and inter-day variability together explain the bar height discrepancies in **Figures 3.9A+B**. **Figures 3.9C** comprises a functional validation of the fluorometry data, as ADAmon can only assess functional ADA. Since the yields calculated from ADAmon data (9–17%) are concordant with ADA488 flurometry analyses, complete paratope functionality of purified ADA can be expected. The yield of the 5 µg/mL sample comprised higher deviation from the fluorescence yield data compared to the other concentrations. As an explanation, it may be possible that the linear extrapolation method utilized for normalization to the 2.5 µg/mL ADA standard is inexact at higher ADA concentrations.

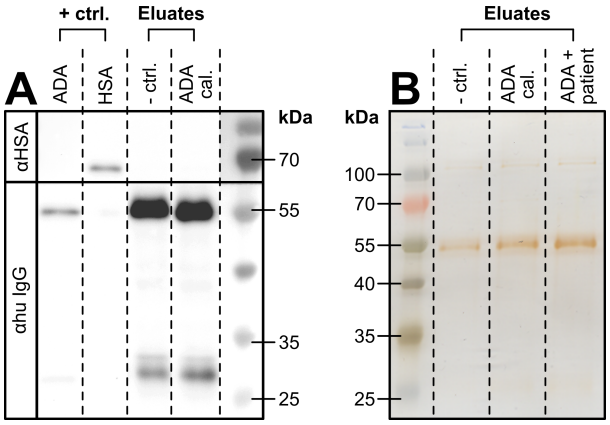

Figure 3.10.: Characterization of ADA pulldown eluate purity. (**A**) Western blot detection of hSA and human IgG in pulldown eluates from blank serum matrix without (- ctrl.) and with 5 µg/mL spiked ADA calibrator (ADA cal.). ADA and hSA positive controls (+ ctrl.) show the respective signals of 10 ng loaded protein. (**B**) Silver stain of ADA pulldown eluates from - ctrl., ADA cal. (1 µg/mL) and an ADA-positive patient serum eluate (as confirmed by ELISA; 85 AU/mL). Ctrl., control; αhSA, anti-hSA; αhu IgG, anti-human IgG.

The purity of ADA pulldown eluates was evaluated by western blot (**Figures 3.10A**) and silver stain (**Figures 3.10B**). hSA as the most abundant serum protein would be expected to contribute to possible impurities and was therefore assessed beside human IgG in western blot. Surprisingly, no hSA but non-ADA IgG were detected in the pulldown eluates, as shown by the strong human IgG bands in blank serum matrix eluates. Furthermore, the IgG signal in the ADA-positive eluate was much higher as expected (maximum approximately 10 ng) for typical ADA yields, when compared to the 10 ng ADA positive control. The silver stain confirmed these findings, showing major signal intensities at approximately 50 kDa, where IgG heavy chains are expected. Additionally, it demonstrated that beside non-ADA IgG (or other proteins with 50 kDa MW), no other relevant impurities were contained in the pulldown eluates. The only other signals were stained slightly above 100 kDa. However, these bands were by far weaker as compared to the IgG signals. The IBD patient serum exhibited the same band pattern as (spiked) blank serum matrix. In conclusion, the presented data demonstrate that the ADA pulldown procedure

is suitable to obtain a sample matrix of significantly reduced complexity as compared to serum.

3.2.2. Sensor stability and regeneration efficacy

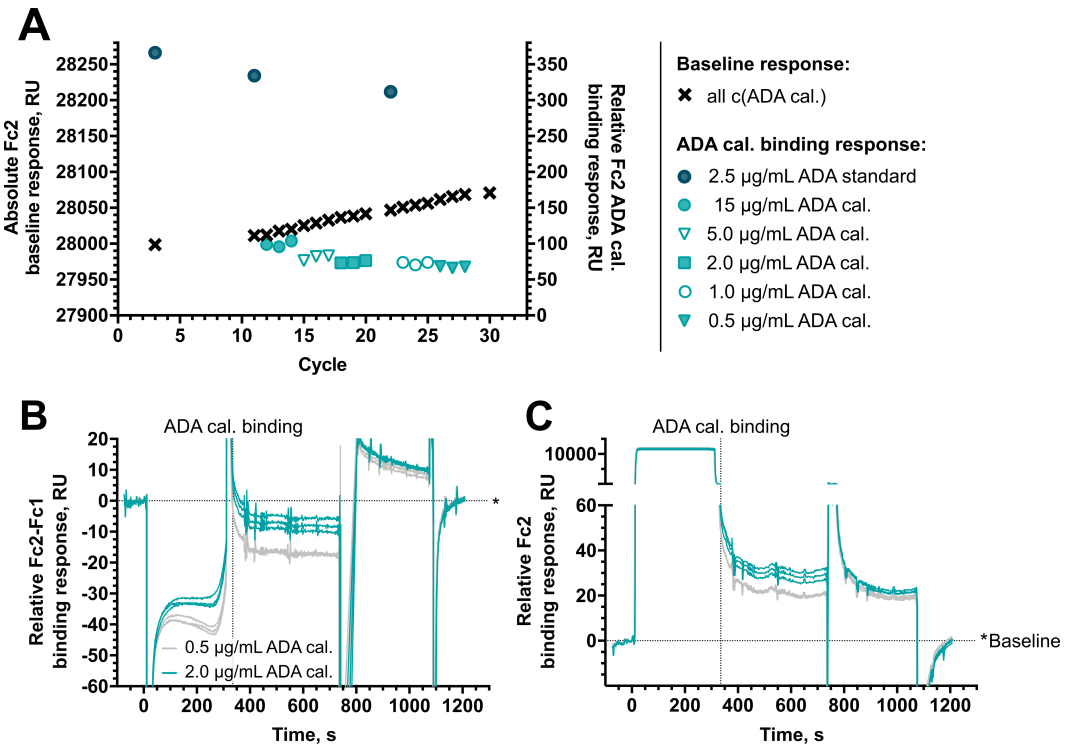

Figure 3.11.: ADAmon regeneration efficacy. ADA calibrator sera were prepared by spiking blank serum matrix with the indicated concentrations of ADA calibrator and diluting the serum as described in **section 2.3.6**. (**A**) Stability analysis of ADAmon for repeated injection of a calibrator series with five different ADA calibrator concentrations (n = 3) and an ADA standard (ADA calibrator spiked in running buffer; n = 4). Absolute baseline response (recorded at the beginning of each cycle) and ADA calibrator binding response relative to baseline are shown for all analytic cycles. (**B**) Fc2-Fc1 sensorgrams for all n = 3 repetitions of the 0.5 µg/mL and 2.0 µg/mL ADA calibrator analyses. (**C**) Fc2 sensorgrams for all n = 3 repetitions of the 0.5 µg/mL and 2.0 µg/mL ADA calibrator analyses. Adapted from [322].

Like for IFXmon (see **section 3.1.1**), regeneration scouting was performed to find the optimal regeneration conditions for ADAmon (data not shown). The best results were obtained with sequential injections of two different solutions: First, acidic glycine buffer (pH 2.0) with glycerol for ligand protection was chosen to dissolve specific protein:protein interactions. Second, a 10 mM NaOH solution was applied to remove adsorbed and aggregated protein. The selected regeneration procedure lead to reproducible ADA binding responses (**Figure 3.11A**). Even though the baseline increased constantly, it did not hamper ADA calibrator binding. Therefore, the regeneration conditions were accepted.

Although the two antibodies immobilized at the ADAmon biosensor surface are relatively robust ligands, the ligand cross-linking step was included in the immobilization procedure

to prolong the sensor chip lifespan. Negative effects of the cross-linking procedure on the analyte-binding capacity of the ADAmon biosensor were ruled out empirically (data not shown). If utilized exclusively for patient serum analyses, one ADAmon biosensor chip could be utilized to analyze 60 different patient sera. The indicated sensor capacity included approximately 180 cycles, which were executed in six different runs and contained all calibrators, blanks and standards required to adequately assess sensor quality.

3.2.3. Calibration

A hyperbolic model described the association between ADA concentration and binding response best (see **Figure 3.12A**, $R^2 = 0.983$). The calibrator concentration range was selected to cover all expectable ADA concentrations in serum. As summarized in **Figure 3.12B**, the calibration curve repeatability was good, even though also considering inter-assay replicates.

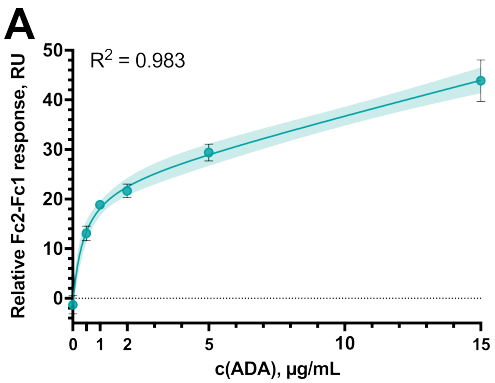

B

	ADA binding	
c(ADA), µg/mL	Mean, RU	SD, RU
0.0	3.5	NA
0.5	13.1	1.5
1.0	18.9	0.8
2.0	21.7	1.4
5.0	29.7	1.7
15	43.9	4.2

Figure 3.12.: ADAmon calibration curve. (**A**) ADAmon analyses of six different ADA calibrators (0, 0.5, 1.0, 2.0, 5.0, 15 µg/mL) from n = 3 technical replicates per concentration, which were recorded in two different analytic runs. The calibration curve was fit with a hyperbolic model. (**B**) Summary statistics. Adapted from [322].

3.2.4. Limits of blank, detection and quantification

Analytic sensitivity of ADAmon was determined with a similar method as previously described for IFXmon (see **section 3.2.4**). In 11 ADAmon analytic runs performed with eight different ADAmon biosensor chips, a total of n = 49 blank serum matrix samples were analyzed. Of note, ADA concentrations determined by ADAmon in patient serum are herein reported as ADA calibrator concentration equivalents, i.e., µgEq/mL.

The histogram shown in **Figure 3.13A** depicts the distribution of interpolated blank serum matrix concentrations. 0.08 ± 0.04 µgEq/mL was the observed mean blank concentration, which defines the LOB of ADAmon as 0.14 µgEq/mL [334].

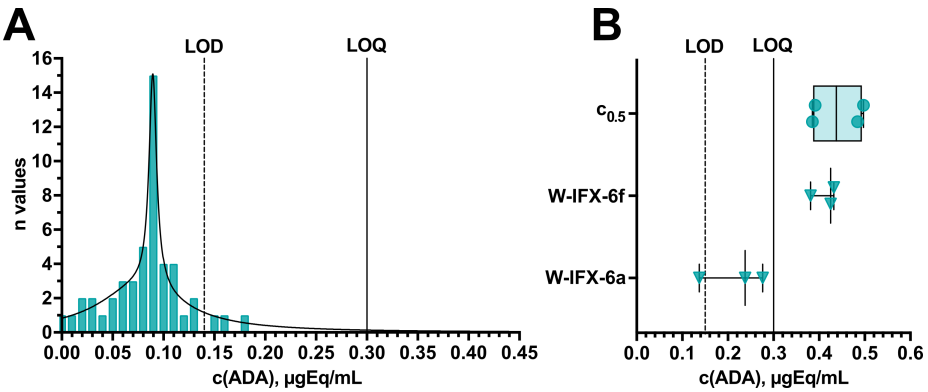

Figure 3.13.: Analytic sensitivity of ADAmon. (**A**) Histogram showing n = 49 ADAmon analyses of blank serum matrix with a sum of two Gaussian fit utilized for the determination of analytic sensitivity. The included data were obtained from 11 independent runs and eight different sensor chips. (**B**) Repeatability of ADAmon analyses of 0.5 µg/mL ADA calibrator in blank serum matrix ($c_{0.5}$, n = 4) and two different patient sera close to the determined LOD and LOQ (W-IFX-6a, n = 3; W-IFX-6f, n = 3). Adapted from [322].

As the ADAmon assay, like IFXmon, was calibrated within each analytic run, the inter-assay variability considered in **Figure 3.13A** leads to a too conservative estimation of LOD and LOQ. Thus, the statistic method was also optimized for ADAmon. The only difference to the optimized IFXmon calculation of LOD and LOQ is that instead of a Lorentizian fit, a sum of two Gaussian fit was selected: Blank data for ADAmon, unlike IFXmon, represented the entire bell-shaped frequency distribution (and not only one half of it). Therefore, all blank data that were too low for interpolation, were assigned to the mean of the distribution, representative of the estimated "true" blank. Consequently, the distribution mean was artificially overrepresented and hence, the sum of two Gaussian fit was a more adequate fit for the data.

LOD was 0.14 µgEq/mL, calculated as the 5 % α error of the blank distribution. n = 3 out of the 49 blank values (6.1 %) were found above LOD, which confirms the exactitude of the chosen distribution model given the sample size. LOQ was calculated as 0.30 µgEq/mL, determined as $\text{mean}_{\text{blank}}$ + 6 SD_{blank}. No blank value was detected above LOQ. LOD and LOQ were validated by analyzing the repeatability of ADA calibrator serum eluates and low-ADA patient serum eluates (see **Figure 3.13B**). Mean (and CV) for patient sera W-IFX-6a, W-IFX-6f and the 0.5 µg/mL ADA calibrator ($c_{0.5}$) were observed to be 0.217 µgEq/mL (33.1 %), 0.413 µgEq/mL (6.5 %) and 0.439 µgEq/mL (13.5 %). The small CV of W-IFX-6f and $c_{0.5}$ confirm that ADAmon comprises acceptable quantitative precision at the determined LOQ.

3.2.5. Accuracy and precision

Accuracy and precision of ADAmon were determined for five different ADA calibrator concentrations in three different analytic runs performed on three different days with two different ADAmon sensor chips. Intra-assay and overall accuracy and precision were

calculated, as previously described for IFXmon (see **section 3.1.4**), and are listed in **Tables 3.4 and 3.5**.

ADAmon intra-assay accuracy and precision ranges were observed to be 84.3 – 128.8 % (mean: 104.4 %) and 71.9 – 96.1 % (84.9 %), respectively. Overall accuracy and precision ranged from 99.9 – 109.6 % (105.3 %) and 73.0 – 88.9 % (83.7 %). Intra-assay performance was therefore minimally higher as compared to overall performance. In **Figure 3.14**, assay linearity is depicted as a plot of overall accuracy and precision data. Up to approximately 2 µg/mL nominal ADA concentration, the narrow 95 % confidence band includes the line of identity. Above 2 µg/mL nominal ADA concentration, the ADA concentration was slightly overestimated. It should be mentioned that only two (1.6 %) of all ADAmon-analyzed patient sera had ADA concentrations higher than 2 µg/mL. Thus, overall assay linearity was deemed acceptable. In summary, these data validate the determined LOD and LOQ for ADAmon.

Table 3.4.: Intra-assay accuracy and precision of ADAmon.

c(ADA)	Mean interpolated c(ADA) ± SD			CV range,	A range,	P range,
	Run = 1	2	3	%	%	%
0.25	0.305 ± 0.051	0.211 ± 0.052	0.322 ± 0.091	16.7 – 28.1	84.3 – 128.8	71.9 – 83.3
0.50	0.514 ± 0.096	0.500 ± 0.039	0.511 ± 0.020	3.9 – 18.7	99.9 – 102.7	81.3 – 96.1
1.0	1.01 ± 0.07	0.94 ± 0.07	1.04 ± 0.23	6.6 – 21.7	94.1 – 104.2	78.3 – 93.4
2.5	2.27 ± 0.05	2.99 ± 0.18	2.86 ± 0.49	2.2 – 17.0	90.9 – 119.6	83.0 – 97.8
5.0	4.92 ± 0.63	5.12 ± 0.73	6.04 ± 0.72	11.9 – 14.3	98.3 – 120.7	85.7 – 88.1

Here, ADA refers to ADA calibrator. All ADA calibrator concentrations are given in µg/mL. Precision is indicated as 100 % - CV. Precision and accuracy were both calculated from n = 3 replicates. A, accuracy; P, precision. Adapted from [322].

Table 3.5.: Overall accuracy and precision of ADAmon.

c(ADA)	Interpolated c(ADA)									Mean ± SD	CV,	A,	P,
	Run = 1			2			3				%	%	%
0.25	0.321	0.346	0.248	0.271	0.178	0.183	0.386	0.258	NA	0.274 ± 0.074	27.0	109.6	73.0
0.50	0.412	0.526	0.603	0.485	0.470	0.544	0.497	0.525	NA	0.508 ± 0.056	11.1	101.6	88.9
1.0	1.09	0.99	0.97	0.87	0.94	1.02	0.88	1.30	0.94	1.00 ± 0.13	13.2	99.9	86.8
2.5	2.21	2.30	2.30	2.85	3.19	2.94	2.41	3.37	2.81	2.71 ± 0.42	15.6	108.3	84.4
5.0	4.22	5.07	5.45	4.29	5.68	5.38	6.67	5.26	6.19	5.36 ± 0.79	14.8	107.1	85.2

Here, ADA refers to ADA calibrator. All ADA calibrator concentrations are given in µg/mL. Precision is indicated as 100 % - CV. A, accuracy; P, precision. Adapted from [322].

For comparison, accuracy and precision of the CE-marked IDKmonitor Infliximab total ADA ELISA are given as reported by Immundiagnostik [337]: Accuracy was determined for four different samples with known ADA concentration as 80.01 – 118.18 % recovery. Inter-assay precision calculated from three different samples with known ADA concentrations (9.49 – 62.15 AU/mL) was 6.1 – 9.2 % CV (mean: 8.0 %). Compared to ELISA inter-assay performance, overall ADAmon trueness was better, while ADAmon precision was slightly lower. ADAmon accuracy and precision were also slightly lower than for IFXmon. This was, however, expected due to the more extensive sample processing during the ADAmon assay.

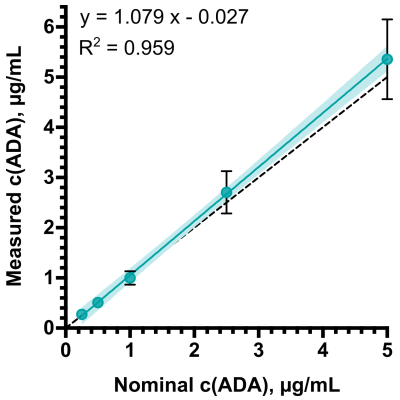

Figure 3.14.: ADAmon assay linearity. Assay linearity for overall accuracy and precision data (see **Table 3.5**) Shown are means of all n = 8 or n = 9 replicate analyses with SD, linear regression (solid teal line), 95 % confidence band (light teal) and line of identity (dashed black line).

3.2.6. DissR validation

Beyond mere ADA quantification, a strategy was established to characterize the binding stability of patient-individual ADA. A graphical explanation how DissR was calculated and exemplary sensorgrams representative of different DissR values are depicted in **Figure 3.15A+B**. Ideally, DissR is independent of ADA concentration and serum matrix effects. However, in practice, DissR may be falsified, e.g., by co-purified impurities in ADA eluates. Therefore, DissR was validated with respect to these confounding factors.

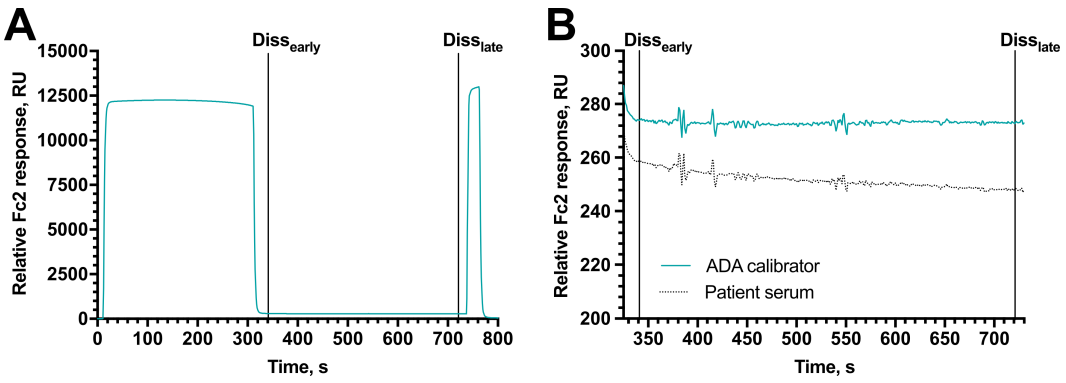

Figure 3.15.: DissR calculation principle. (**A**) Exemplary ADAmon Fc2 sensorgram for ADA pulldown eluates. DissR is the quotient of $\text{Diss}_{\text{early}}$ and $\text{Diss}_{\text{late}}$, which represent binding signals early and late in the ADA dissociation phase. (**B**) Dissociation phase close-up. DissR for the ADA calibrator eluate and patient serum eluate were 1.003 and 1.043, respectively. Adapted from [322].

With respect to concentration independence, a smaller DissR variability for higher ADA concentrations was observed (see **Figure 3.16A**). CV, however, was overall very small (consistently below 1 %), as visible for result group **a** in **Figure 3.16A**. Compared with DissR variability of different ADA-positive sera (**Figure 3.16A**, result group **c**), concentration-dependent variability was negligible. Also, serum matrix-dependent differences in DissR (**Figure 3.16A**, result group **b**) were negligible as compared to the range

of ADA-positive patient sera. Overall, these results confirmed independence of DissR from ADA concentration and absence of significant serum-individual matrix effects on DissR.

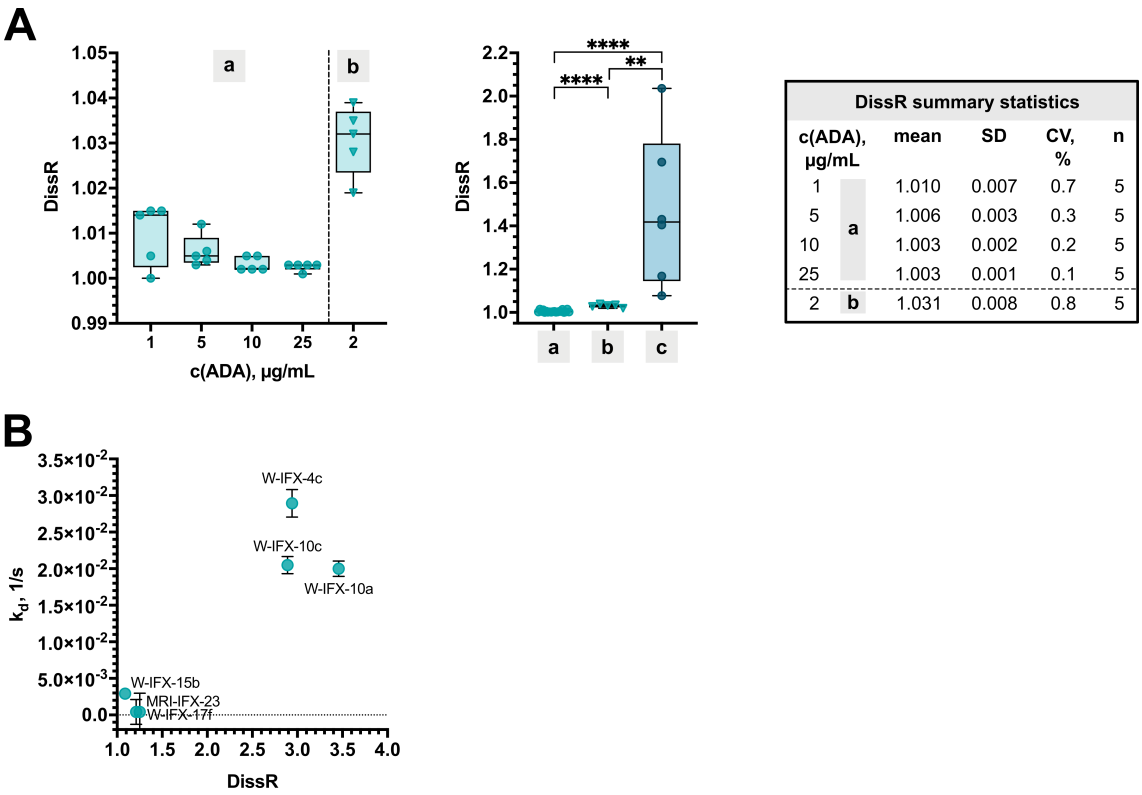

Figure 3.16.: Validation of DissR. (**A**) DissR was calculated for n = 5 technical replicates of variable ADA calibrator concentrations spiked in blank serum matrix (**a**). DissR for n = 5 different healthy control sera spiked with 2.0 µg/mL ADA calibrator (**b**). DissR for n = 6 sera from ADA-positive patients (by ADAmon and ELISA, **c**). ****, $p < 0.0001$; **, $p = 0.0043$. The table summarizes the repeatability for **a** and **b**. (**B**) Comparison of DissR with k_d values for n = 6 patient sera: The three sera with minimum and the three sera with maximum DissR were selected for this analysis. k_d was calculated utilizing the open source online tool Anabel. Adapted from [322].

In the presented work, DissR is favored over classical kinetic analysis due to the reasons given in **section 2.3.8**. Nevertheless, a test calculation was performed to learn about the relationship between DissR and k_d and hence about the comparability of DissR with classical kinetic data in literature. k_d was calculated using the open-source tool Anabel, which however only offers 1:1 binding models (see **Figure 3.16B**). Six exemplary sensorgrams from patient sera were analyzed: Three sera with minimum and three sera with maximum observed DissR values. The sera with minimum DissR clustered at lower k_d compared to the sera with maximum DissR. However, there were discrepancies in trend within the low-DissR and high-DissR clusters. These discrepancies might be attributable to differences in goodness of the individual kinetic model fits. In conclusion, these data can be considered as first hints that k_d correlates with DissR.

3.2.7. Patient study and method comparison with ELISA

3.2.7.1. Harmonization of ELISA data with ADAmon

As described in **section 2.3.7**, ELISA data were re-calculated applying a *post hoc* calibration with the same ADA calibrator used in ADAmon. This procedure generated ELISA data in the same units as ADAmon data and created a meaningful base for quantitative comparison of ELISA and ADAmon data. ELISA analyses of six different ADA calibrator-spiked sera (0, 0.015, 0.050, 0.15, 0.50, 1.5 µg/mL) served as data points to fit the hyperbolic calibration curve shown in **Figure 3.17B** (R^2 = 0.999). Initially, two higher concentrations were additionally analyzed (**Figure 3.17A**). These were excluded from the final calibration curve, since a high-dose Hook effect was observed for ADA calibrator concentrations above 0.5 µg/mL (1027.3 AU/mL). These results confirmed assay performance data provided by Immundiagnostik, which state absence of a high-dose Hook effect below 981 AU/mL[337]. As quality control, a patient serum (MRI-IFX-35c) was re-analyzed by ELISA in addition to the ADA calibrator sera. The difference between first (226.7 AU/mL) and second analysis (257.7 AU/mL) amounted to 13.7 %. Given one freeze-thaw cycle between the measurement repetitions, this difference can be considered acceptable. Furthermore, it suggests that the *post hoc* calibration is valid.

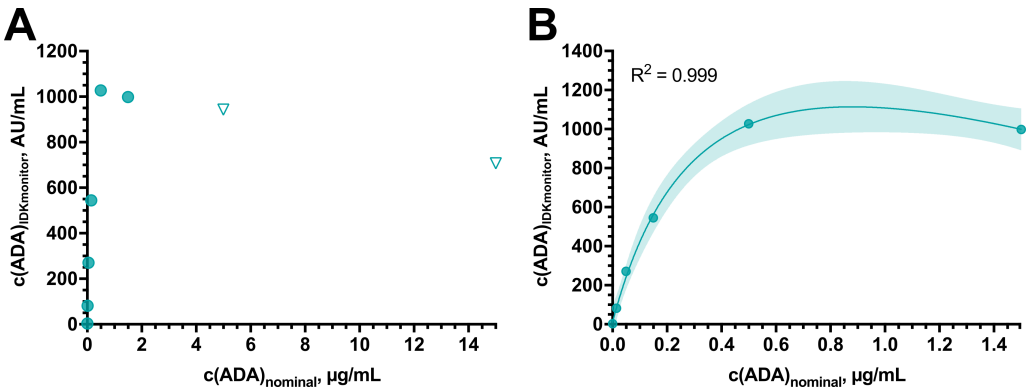

Figure 3.17.: Calibration curve for harmonization of ADAmon and ELISA results. (**A**) Eight different ADA calibrator-spiked sera (0, 0.015, 0.050, 0.15, 0.50, 1.5, 5.0, 15 µg/mL) were analyzed by ELISA. The two calibrators with highest ADA concentrations, which were excluded from the final curve fit, are depicted as clear symbols. (**B**) Calibration curve for re-calculation of ELISA results. The 95 % confidence band of the hyperbolic fit is depicted in light blue. Adapted from[322].

3.2.7.2. Method comparison between ADAmon and ELISA

129 sera from 44 IBD patients were analyzed by ADAmon in unicates (see **Figure 3.18**). The ADAmon patient cohort is characterized in **Table 3.6**. The cohort was relatively young with a higher proportion of male subjects (65.9 %). With 63.6 %, more CD patients than UC patients were represented in the collective. 4.4 % of patients received Remicade®, 8.9 % Remsima®, 20.0 % Inflectra® and for 66.7 % of patients, the administered drug was unknown. The median frequency of TDM visits was 5.5 weeks. For 22.7 % of patients, LOR to IFX therapy was observed.

Table 3.6.: ADAmon patient cohort characteristics.

Characteristic	**Summary statistics**	
n (%)	44	(100.0)
Sex, n (%)		
Female	15	(34.1)
Male	29	(65.9)
Age, years, median (IQR)*	37	(28 – 51)
Diagnose, n (%)		
CD	28	(63.6)
UC	16	(36.4)
Medication, n (%)		
Remicade®	2	(4.4)
Remsima®	4	(8.9)
Inflectra®	9	(20.0)
Unknown	30	(66.7)
Number of TDM visits, median (IQR)	1.0	(1.0 – 5.0)
TDM visit interval, weeks, median (IQR)	5.5	(2.8 – 7.0)
Confirmed LOR, n (%)	10	(22.7)

*Patient's age at first included TDM visit. **Calculated from 20 patients, from whom sera of ≥ 2 TDM visits were available. IQR, interquartile range. Adapted from [322].

Quantitative method comparison between ADAmon and ELISA was performed with n = 127 sera from n = 43 IBD patients. Re-calculated ELISA results (see **section 3.2.7.1**) were included for this and all following quantitative analyses. Applying simple linear regression resulted in poor correlation of ADA concentrations between the two methods (see **Figure 3.18A**; $R^2 = 0.267$, $p < 0.0001$). Of note, despite ELISA results were calibrated with the same ADA calibrator as ADAmon, absolute ADA concentrations exhibited extreme differences. ADA quantities determined by ELISA were consistently lower (by a factor of 3 – 1557; median: 36.5, IQR: 12.5 – 84) as compared to ADAmon results. As shown in **Figure 3.18B** ADA detection concordance between the two methods was relatively good (n = 89, 69.6 %). However, more sera were observed, in which ADA were exclusively detected by ELISA (n = 26, 20.3 %), as compared to sera with exclusive ADAmon-positive status (n = 13, 10.1 %). The respectively applied IFX drug had no influence on ADA quantification by ADAmon, as demonstrated by **Figure 3.19A**. It should be mentioned that only two patients in the ADAmon cohort received the originator preparate Remicade®. The observation that Remicade-treated sera were ADA-negative is attributed to insufficient patient count and not to higher immunogenicity of IFX biosimilars, since the safety (including immunogenicity) of IFX biosimilars has been demonstrated to be indifferent from Remicade® [338].

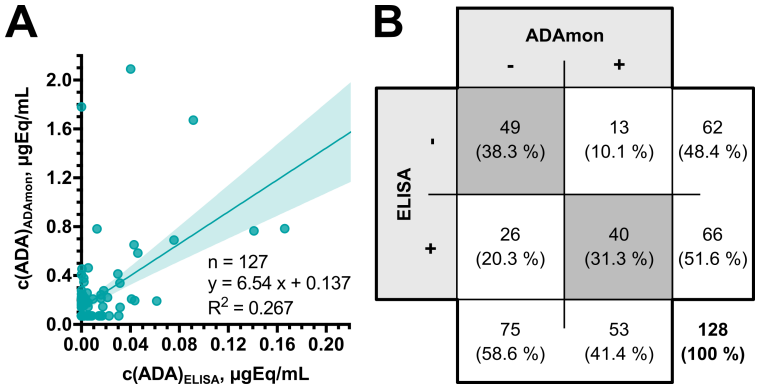

Figure 3.18.: ADA quantification comparison between ADAmon and ELISA. (**A**) Linear method comparison regression with n = 127 ADA quantification results obtained by ADAmon and ELISA from n = 43 patients. 95 % confidence band is depicted as light blue shading. Two sera were excluded (one outlier and one missing ELISA result). (**B**) ADA detection by ADAmon and ELISA in n = 128 sera. One serum was exluded (missing ELISA result). Adapted from [322].

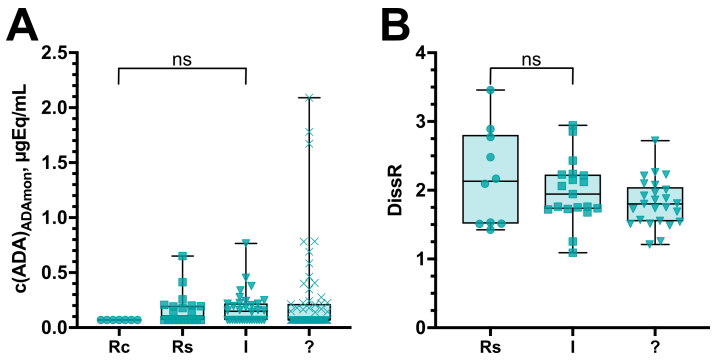

Figure 3.19.: Evaluation of ADAmon analysis depending on applied IFX drug. (**A**) ADA concentrations of individual sera grouped by applied IFX drug. (**B**) DissR of individual sera grouped by applied IFX drug. Rc, Remicade®; Rs, Remsima®; I, Inflectra®; ?, applied drug unknown.

In order to investigate whether analytic drug tolerance does also apply to authentic ADA in patient sera, and not only artificially spiked ADA calibrator sera, the patient data were grouped by subtherapeutic, therapeutic and supratherapeutic IFX concentrations. **Figure 3.20A+B** demonstrates that presence of free serum IFX does not impair the capacity to detect ADA neither for ADAmon nor ELISA. As expected, ADA were detected in least sera with supratherapeutic IFX, since high IFX levels are correlated with reduced IFX immunogenicity [255,339,340].

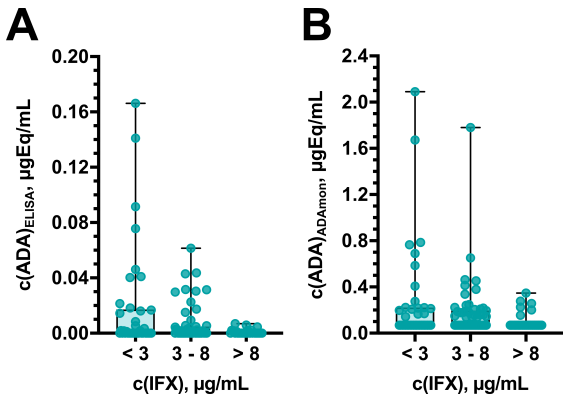

Figure 3.20.: Validation of ADAmon analytic drug tolerance with patient sera. (**A**) ELISA results grouped by IFX concentration determined by ELISA (n = 126). (**B**) ADAmon results grouped by IFX concentration determined by ELISA (n = 125). Three sera were excluded: Two due to missing ELISA results for either IFX or ADA concentration and one serum was an outlier. Adapted from [322].

3.2.7.3. Diagnostic implications of DissR

Median DissR in all ADAmon-positive sera was 1.835, ranging from 1.088 – 3.458. The relationship between ADA quantification and DissR was investigated, as a correlation could represent a hint that (i) ADA quantification is biased by ADA binding stability and/or (ii) the abundance of ADA depends on their binding properties. Answering these hypotheses delivers new information on ADA immunoassay analytics and ADA pathophysiology. The results of this investigation are shown in **Figure 3.21**, grouped by method and DissR.

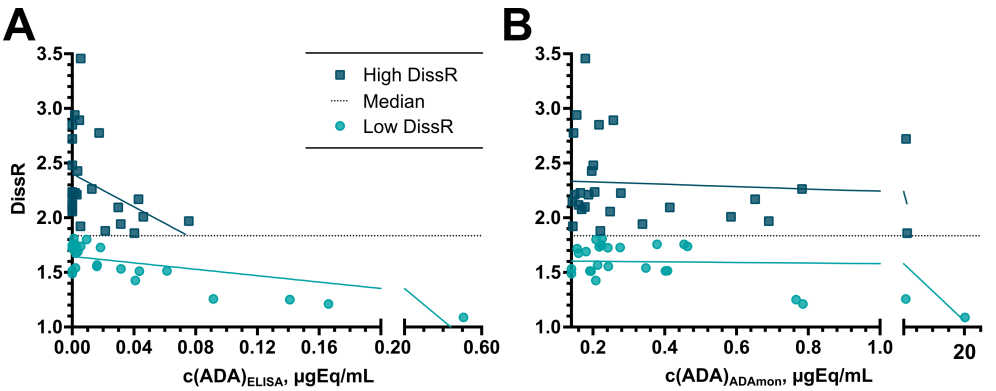

ELISA vs. DissR, linear regression

	n	R^2	p	Line equation
■	27	0.141	0.054	y = -7.545 x + 2.402
●	26	0.581	<0.0001	y = -1.465 x + 1.646

ADAmon vs. DissR, linear regression

	n	R^2	p	Line equation
■	27	0.018	0.503	y = -0.1100 x + 2.351
●	27	0.292	0.004	y = -0.0280 x + 1.608

Figure 3.21.: Regression of ADA concentration with DissR. As DissR can only be determined for ADAmon-positive sera, the presented analysis was restricted to n = 54 sera. (**A**) Regression of ELISA results with DissR (n = 53 due to lacking ELISA result for one serum). (**B**) Regression of ADAmon results with DissR (n = 54). Symbol color and shape indicate low (teal circles) or high DissR (dark blue squares), which are separated by the overall median DissR (1.835). Adapted from [322].

The strongest association was found for ELISA quantification in the low DissR group (see **Figure 3.21A**; $R^2 = 0.581$, $p < 0.0001$), while the corresponding association between ADAmon and DissR was less strong (see **Figure 3.21B**; $R^2 = 0.292$, $p < 0.004$). The linear regression fits for the high DissR group comprised non-significant p values for both methods. Additionally, DissR was compared between positive and negative ADA status, as determined by ELISA (see **Figure 3.22**). Sera, in which ADA were exclusively detected by ADAmon, had a higher median DissR (2.117), as compared to sera, in which ADA were detected by both methods (1.758, $p = 0.052$). These results suggest that in contrast to ADAmon, ELISA is less capable of assessing fast-dissociating ADA.

Especially interesting insights were gained by investigating the temporal evolution of DissR in individual patients (see **Figure 3.23A**), which has never been analyzed before. The median time interval between the ADAmon-positive TDM visits was 14.8 weeks (range: 4.9 – 96.1 weeks). The data demonstrate that DissR - and therefore, ADA binding stability - was very constant over time for most patients. Three patients, however, exhibited a clear change in DissR and interestingly, two of these patients experienced LOR. In general, patients with confirmed LOR tended to have lower DissR and higher ADA concentrations as compared to patients in remission. As therapy outcome was not known for all patients, other prognostic markers for IFX therapy outcome were evaluated. Subtherapeutic IFX, i.e., concentrations below 0.6 µg/mL with the IDKmonitor ELISA, are well-known to indicate increased risk for LOR[341,342]. Thus, the relationship between IFX concentration and DissR was investigated (see **Figure 3.23B**). At earlier TDM visits, it is possible to measure high IFX concentrations, even if the patient experiences (secondary) LOR later. Since DissR was observed to be mostly timely stable, only the respectively last collected TDM serum was considered in the analysis schown in **Figure 3.23B**. With this data selection, the IFX concentration data represent a better reflection of the respective therapy outcome, since it considers possible changes of responsiveness to IFX therapy throughout the observation time. (Final) DissR tended to be lower for low IFX and additionally clustered for the different therapy outcomes. IFX-independent comparison of DissR between therapy outcomes showed significant differences, as depicted in **Figure 3.23C+D**: LOR patients had significantly lower DissR as compared to patients in remission ($p = 0.0053$ for all, $p = 0.0055$ for over-representation-corrected sera, respectively). With help of ROC analysis, a DissR cut-off indicative of undetectable IFX was determined: DissR ≤ 1.524 indicated IFX ≤ 0.6 µg/mL with 71.4 % sensitivity and 88.9 % specificity (AUC = 0.825, see **Figure 3.23E**).

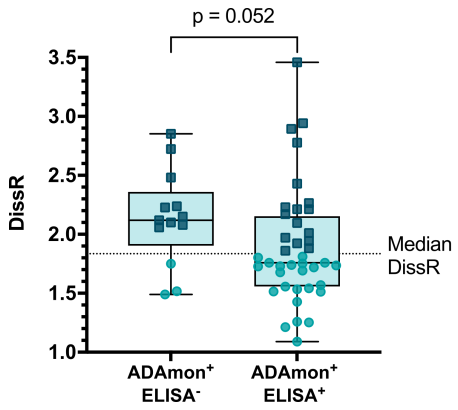

Figure 3.22.: DissR of ADAmon-positive sera grouped by ELISA result. n = 13 sera were ADAmon-only positive, while 40 sera were classified ADA-positive by both ADAmon and ELISA. Symbol color and shape indicate low (teal circles) or high DissR (dark blue squares), which are separated by the overall median DissR (1.835). Adapted from [322].

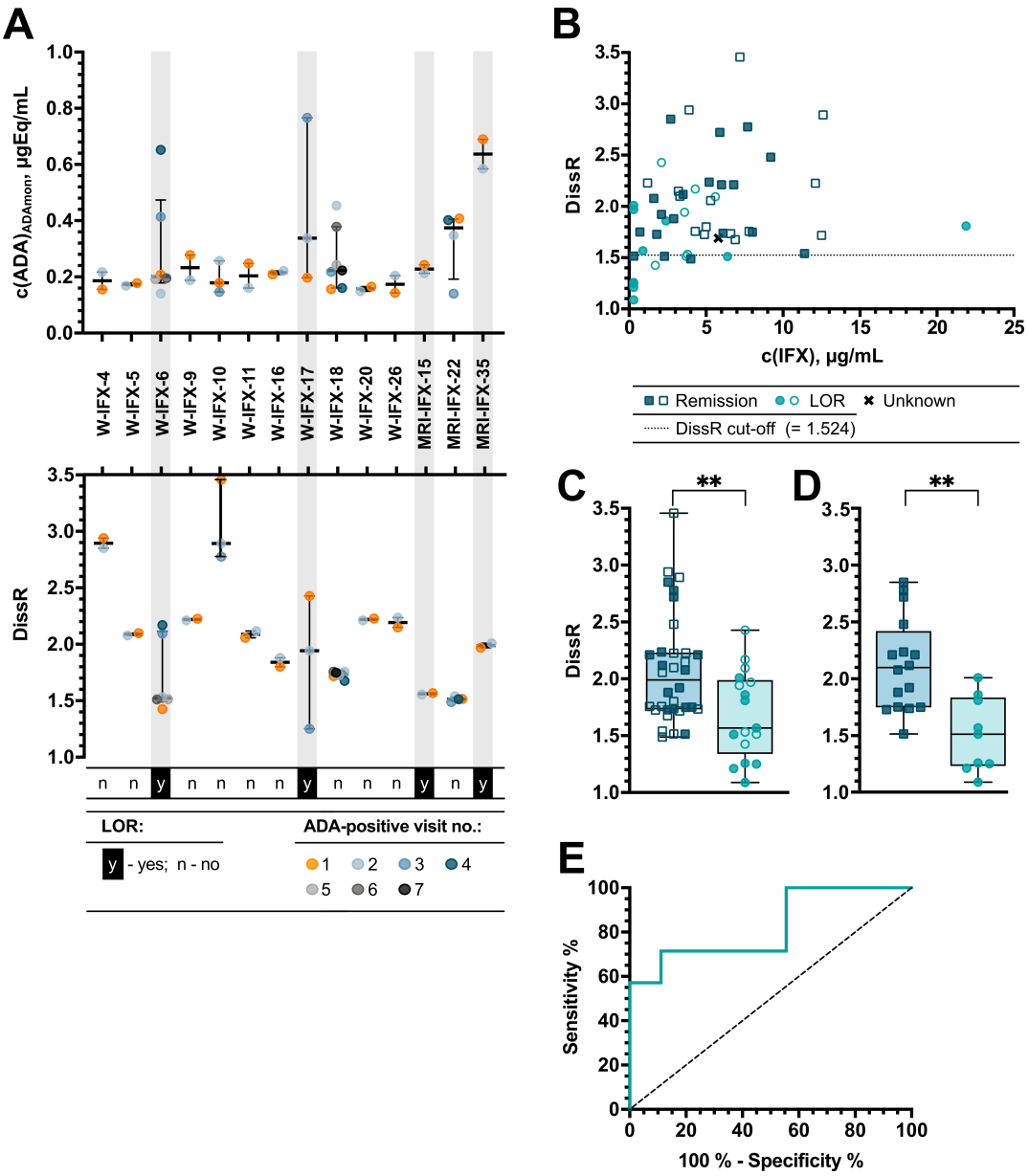

Figure 3.23.: Evaluation of the association between DissR and IFX therapy outcome. (**A**) Temporal evolution of DissR. Shown are TDM results (ADA concentrations determined by ADAmon, DissR, therapy outcome) of all patients (n = 14), which had n $\geq$ 2 ADAmon-positive sera. Symbol colors represent the number of the respective TDM visit in chronologic order. Median DissR and DissR range are indicated by black bars. (**B**) Relationship between IFX concentrations and DissR for n = 52 sera from n = 26 different patients. Here, only ELISA results for IFX were considered. The over-representation of patients with multiple available DissR results was corrected to provide a less biased analysis: To do so, only the respectively last available serum of each patient is shown as filled symbol. DissR from the serum collected at the latest available TDM visit was selected in order to obtain a better reflection of therapy outcome. Importantly, the high-IFX serum from LOR patient MRI-IFX-26 was mistakenly collected three weeks after the prior IFX infusion and is hence no true trough concentration. (**C**) DissR grouped by therapy outcome for all n = 52 sera (**, p = 0.0086). (**D**) DissR grouped by therapy outcome restricted to the n = 26 over-representation-corrected sera (**, p = 0.0014). (**E**) ROC analysis of all n = 52 sera with respect to undetectable IFX concentration (< 0.6 µg/mL). DissR cut-off at maximum Youden Index: 1.524; sensitivity: 71.4 %; specificity: 88.9 %; AUC = 0.825. Adapted from [322].

3.2.7.4. Exploiting the SPR reference channel for result plausibility evaluation

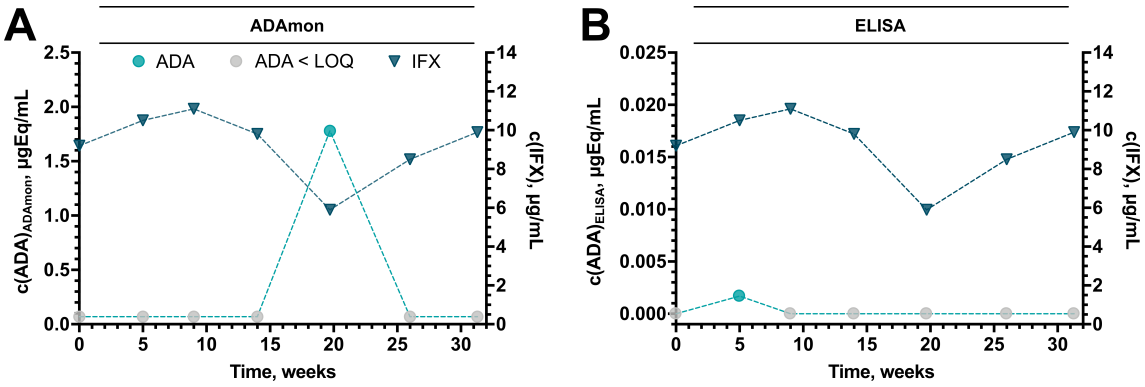

Figure 3.24.: Temporal evolution of IFX and ADA concentrations in patient W-IFX-21. (**A**) IFX concentrations determined by ELISA (dark blue squares) and ADA concentrations determined by ADAmon (circles; teal, ADA > LOQ; gray, ADA ≤ LOQ). (**B**) IFX concentrations determined by ELISA (dark blue squares) and ADA concentrations determined by ELISA (circles; teal, ADA > LOQ; gray, ADA ≤ LOQ). Adapted from [322].

The utility of the reference flow channel Fc1 in the Biacore X100 instrument is not restricted to signal referencing. As it serves to assess non-specific binding, it can be exploited to detect implausibly high unspecific binding, which may indicate that the sample material is inadequate (e.g., due to pre-analytic errors). For this means, all analytic runs were re-evaluated, during which the n = 26 ADAmon-negative and ELISA positive sera were measured (see **Figure 3.18B**). For each run, mean and SD of relative binding to Fc1 were calculated for all pulldown eluates other than the samples in question (data not shown). Two sera were classified as critically odd, as they comprised relative Fc1 binding that deviated by ≥ 3 SD from the respective run mean: For W-IFX-21b and MRI-IFX-17, the relative Fc1 binding differences from run mean were 3.07 and 3.24 SD, respectively.

The TDM data time course of patient W-IFX-21 was exploited for a preliminary validation of the Fc1-based plausibility testing strategy (see **Figure 3.24A+B**): The second serum (collected 5 weeks after the first serum) was the serum classified as odd, due to its extremely high Fc1 binding. By ELISA, this serum was ADA-positive, while in ADAmon, the excessive Fc1 binding led to an overall negative Fc2-Fc1 binding below LOQ. Importantly, ELISA does not comprise a similar sample-individual negative control as the reference channel in SPR. Thereby, inadequate sample material with excessive non-specific binding will remain unrecognized in ELISA and lead to false-positive results. The fact that antagonistic IFX and ADA levels was observed for ADAmon, but not ELISA in patient W-IFX-21, may provide first hints that the ELISA results are less plausible for this patient. Additionally, the fifth serum (collected 20 weeks after the first serum) was observed to contain high-DissR ADA (DissR = 2.721) by ADAmon, while no ADA were detected by ELISA. This result supports our observations that fast-dissociating ADA are more likely missed by ELISA.

3.3. ADA epitope mapping

ADA epitope characterization was performed with the ADAmon-derived biosensor ADAmon-EpiM, which carried IFX F(ab')$_2$ fragments on Fc2. Only ADA that bind at or close by the IFX paratope can be assessed. By this means, the ADA assessed by ADAmon-EpiM are highly likely to be of IFX-neutralizing nature, i.e., interfere with IFX function by blocking its TNF binding site. IFX F(ab')$_2$ fragments were generated with in-house-expressed IdeS protease. The donated plasmid coded for the TrxA-IdeS fusion protein, such that removal of the TrxA tag was required prior to employing IdeS for IFX digestion.

3.3.1. Yield, purity and activity of in-house-expressed IdeS

The sampling time row of IdeS expression culture showed a high level of TrxA-IdeS overexpression that was continuously increasing over 6 h until the expression culture was harvested (see **Figure 3.25A**). Even before expression induction, a band at the expected MW (nominal MW 49.4 kDa, apparent MW 40 kDa) was observed, indicating a leaky promoter. IMAC-FPLC purification of expression culture lysate SN pool was observed to have highest TrxA-IdeS content in the manually collected fractions M3 and M4 (see **Figure 3.25B+C**). To increase yield, additional fractions expected to contain TrxA-IdeS were pooled. As shown in **Figure 3.25D**, TEV protease digestion of TrxA-IdeS fusion protein was complete after 60 min. Of note, TEV protease and IdeS bands overlapped on the SDS gels due to similar MW (TEV protease apparent MW according to manufacturer: 28 kDa; untagged IdeS: 35.2 kDa). Re-purification of untagged IdeS from the TEV protease digestion batch via IMAC-FPLC yielded highest IdeS content in fractions M2 and M4, which were pooled (V $\approx$ 2.5 mL). Fraction M5 supposedly contained TEV protease-IdeS complexes that were dissociated by SDS-PAGE sample preparation and was therefore discarded (see **Figure 3.25D+E**). The protein concentration in the fraction pool was determined as $\approx$ 2.0 mg/mL by NanoDrop (IdeS molar extinction coefficient = 49390 L/(mol cm)). In view of the high protein purity observed in SDS-PAGE, it can be concluded that 5.0 mg of untagged IdeS protein were obtained from the 800 mL TrxA-IdeS expression culture.

Results of the subsequent function test with purified IdeS protease are depicted in **Figure 3.26**. As expected, IdeS exhibited high proteolytic activity towards both polyclonal IgG and IFX. The reaction was observed to be very efficient and fast, since 1 µg IdeS dilution led to complete digestion of 200 µg substrate within 15 – 30 min.

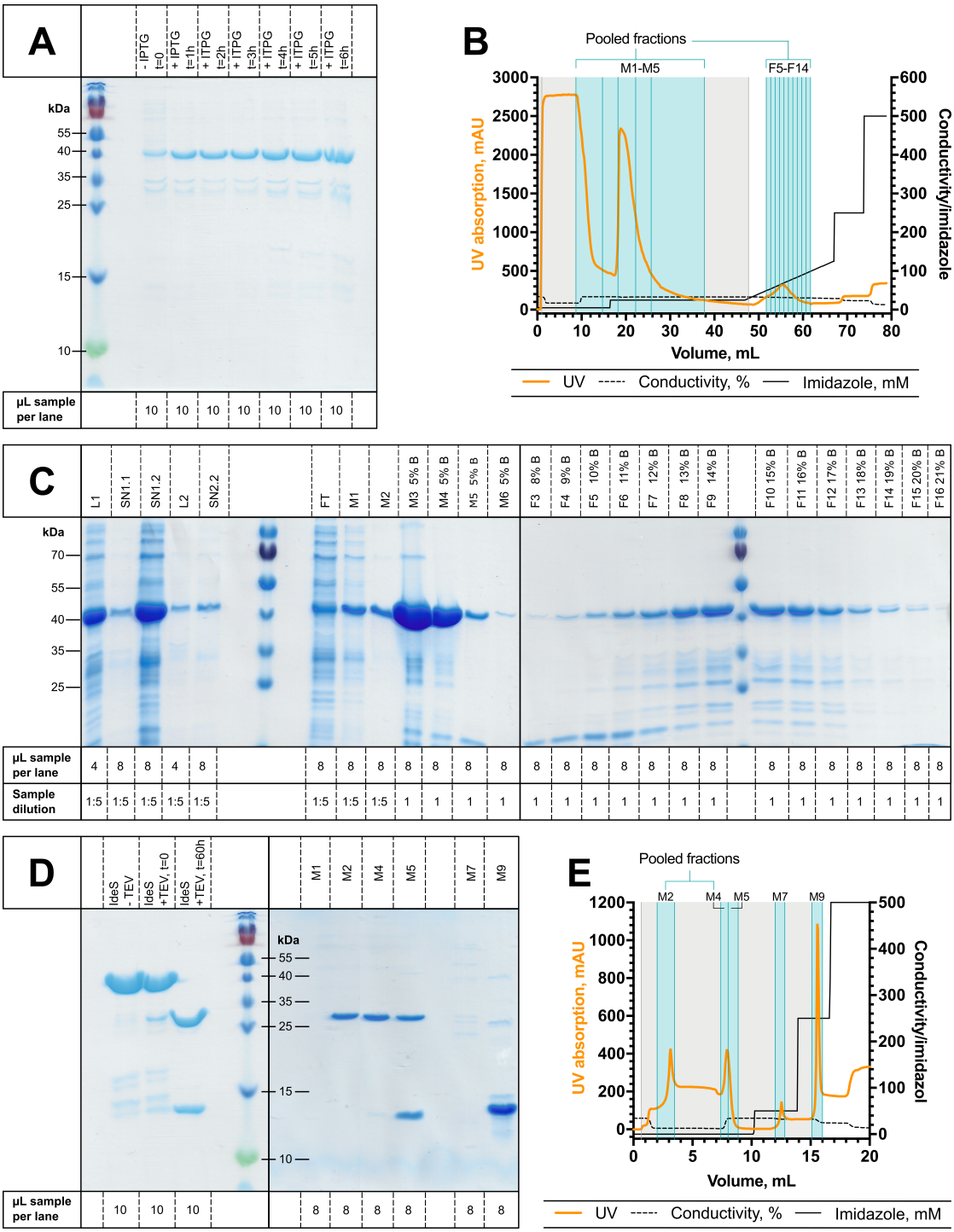

Figure 3.25.: Expression and purification of IdeS. (**A**) Test expression analysis by SDS-PAGE. (**B**) FPLC chromatogram of IdeS purification via IMAC. M fractions were collected manually, while F fractions were collected with the automated fraction collector. Gray shading marks the entire collected fractions without indication of single fractions. More relevant collected fractions are shaded in light blue with teal lines indicating single fractions. All fractions pooled for subsequent TEV protease digestion are marked by brackets. (**C**) SDS-PAGE analysis of collected FPLC fractions. B, buffer B; L, cell lysate; SN, supernatant (of pelleted lysate). (**D**) SDS-PAGE analyses of TEV protease digestion success (left) and FPLC re-purification of TEV protease-digested IdeS via IMAC. (**E**) FPLC chromatogram of IdeS re-purification via IMAC. M fractions were collected manually, while F fractions were collected with the automated fraction collector. Gray shading marks the entire collected fractions without indication of single fractions. More relevant collected fractions are shaded in light blue with teal lines indicating single fractions. All fractions pooled for subsequent TEV protease digestion are marked by brackets. All shown SDS-PAGE analyses employed reduced samples.

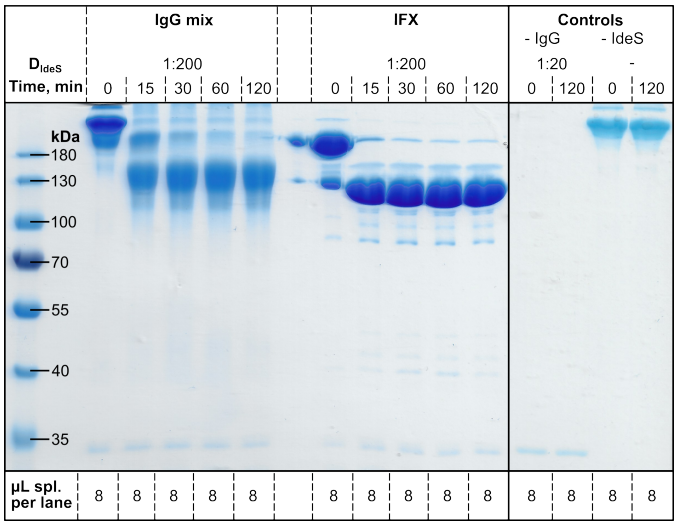

Figure 3.26.: Investigation of IdeS activity. Activity of purified IdeS was tested by sampling the digestion mix at the indicated time points after reaction start and analysis via non-reducing SDS-PAGE. Either a mix of purified IgG or IFX served as substrate (m = 200 µg). D_{IdeS}, IdeS dilution; spl., sample.

3.3.2. Generation and purification of IFX F(ab')$_2$ fragments

For preparation of the ADAmon-EpiM biosensor, 700 µg of Remicade® were digested by IdeS and the reaction batch (V = 350 µL) was purified via SEC-FPLC (see **Figure 3.27A**). SDS-PAGE analysis of SEC fractions under reducing and non-reducing conditions (see **Figure 3.27B**) showed that fractions F10 – F15 contained IFX F(ab')$_2$ fragments, while fractions F16 – F19 contained predominantly IFX Fc/2 fragments. Of note, IFX F(ab')$_2$ bands were observed at higher apparent MW than expected (observed MW: 130 – 180 kDa, expected MW: 100 kDa). Fractions F10 – F14 were pooled (V = 2.5 mL). After concentration and dialysis against PBS (V ≈ 600 µL), IFX F(ab')$_2$ concentration was determined via Bradford assay as 717 µg/mL. Considering that the IFX F(ab')$_2$ fragment comprises two thirds of the Remicade® MW, the purification yield was determined to be nearly complete (≈ 92 %).

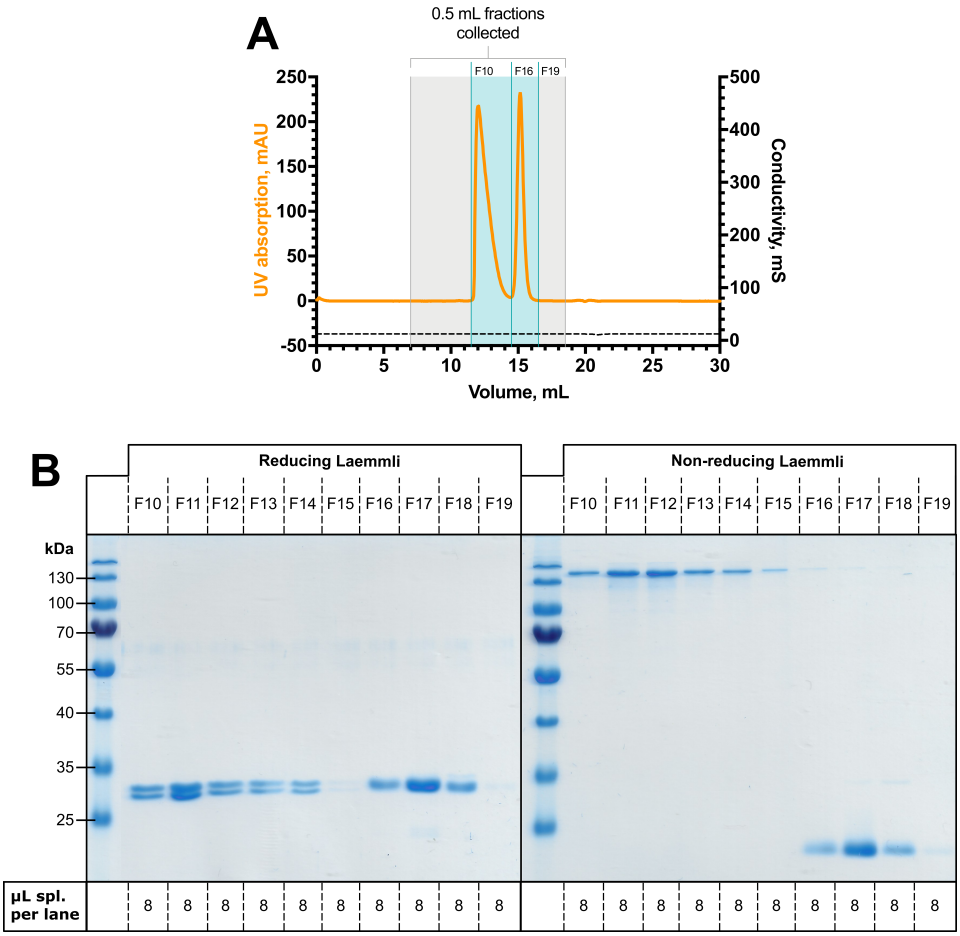

Figure 3.27.: Purification of IFX F(ab')$_2$via SEC-FPLC. (**A**) FPLC chromatogram of IFX F(ab')$_2$ purification via SEC. Gray shading marks the entire volume range, within which 0.5 mL fractions were collected. More relevant collected fractions are shaded in light blue. Teal lines marking the respective first fraction in the indicated volume range. (**B**) SDS-PAGE analysis of collected FPLC fractions. Spl., sample.

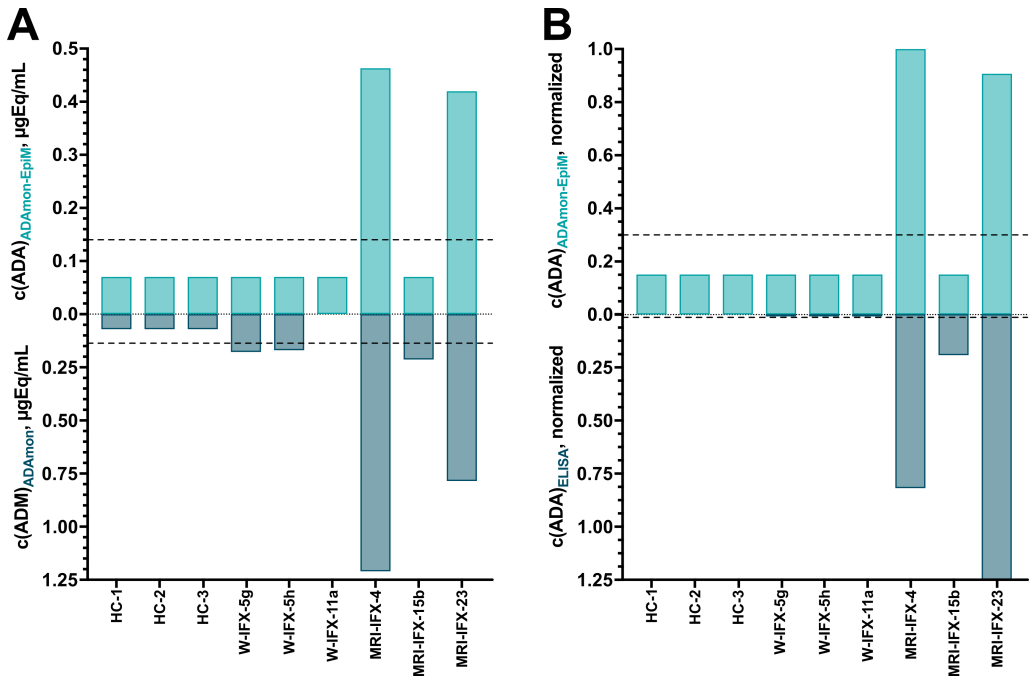

Figure 3.28.: ADAmon-EpiM validation with patient sera. (**A**) Comparison of ADAmon results with ADAmon-EpiM results for n = 9 patient sera. (**B**) Comparison of normalized ADA concentrations for ELISA and ADAmon-EpiM results for n = 9 patient sera. HC, healthy control serum. LOQ for the respective methods is marked by black dashed lines. As ADAmon-EpiM LOQ has not been determined, it was assumed to equal ADAmon LOQ.

3.3.3. ADA epitope mapping via the ADAmon-EpiM biosensor

In order to test its functionality, n = 9 patient sera were analyzed with the ADAmon-EpiM biosensor and the obtained data were compared with both ADAmon (see **Figure 3.28A**) and ELISA (see **Figure 3.28B**) results. The n = 3 healthy control sera were exclusively analyzed with the two SPR biosensors, but not ELISA, whereby no ADA were detected. n = 3 patient sera (MRI-IFX-4, MRI-IFX-15b, MRI-IFX-23) were classified as ADA-positive by both ADAmon and ELISA. n = 2 sera (W-IFX-5g, W-IFX-5h; both in remission) were ADA-positive by ADAmon-only. ADAmon-EpiM detected (presumably) neutralizing ADA in n = 2 sera (MRI-IFX-4, MRI-IFX-23), which both had to discontinue IFX due to LOR. Interestingly, sera W-IFX-5g and W-IFX-5h exhibited high DissR (2.098 and 2.079, respectively), which may explain why ELISA was negative for these samples (see **section 3.2.7.3**). W-IFX-15b, on the other hand, comprised ADA with very high IFX binding stability (DissR = 1.088) and additionally was a LOR patient.

These results could on the one hand side indicate that ADAmon-EpiM comprises worse analytic sensitivity as compared to ADAmon and/or ELISA or ADAmon-EpiM is unable to detect fast-dissociating ADA. Even though there are no obvious reasons why this should be the case, these possibilities should be considered. On the other hand, the presented results may also suggest that both neutralizing and non-neutralizing ADA may cause LOR to IFX therapy. However, a larger sample size is required to prove this hypothesis.

3.4. Diagnostic implications of temporal ADA dynamics

The following results are discussed in detail in Grasmeier et al. (2021) and the dissertation of Anna Langmann (2022)[336,343]. Therefore, only a brief summary will be provided here. Due to the notorious lack of harmonization in ADA analytics, no satisfactory consensus on the management of punctually obtained, absolute ADA concentrations exists. Therefore, we have established a strategy to interpret ADA concentration dynamics rather than single values. The results of this work are summarized in **Figure 3.29**.

In brief, 38 IBD patients on IFX maintenance therapy with a proactive TDM policy were enrolled in the study. Clinical parameters as well as IFX and ADA concentrations (determined with IDKmonitor Infliximab drug level and IDKmonitor Infliximab total ADA ELISA) were analyzed retrospectively. For a defined time period starting from the first ADA-positive TDM visit (T_0), slopes of ADA and IFX concentrations (S_{ADA} and S_{IFX}) were determined, respectively. Based on S_{ADA} and ADA status, the cohort was divided into three groups (ADA-N, ADA-↓, ADA-↑) and association with therapy outcome was evaluated (**Figure 3.29A**).

In our study format, S_{ADA} and S_{IFX} did not show antagonistic behavior (**Figure 3.29B**). S_{ADA}, but not S_{IFX} was found to be a new determinant of therapy success: As depicted in **Figure 3.29C**, ADA-↓ patients had a significantly lower risk for LOR as compared to ADA-↑ patients ($p = 0.015$). Matching survival analysis, ADA-↑ patients exhibited the highest LOR rate (60.0 %) among all groups. Another highly interesting observation was that ADA-↑ patients had predominantly persistent ADA (70.0 %), while in ADA-↓ patients, transient ADA prevailed (83.3 %).

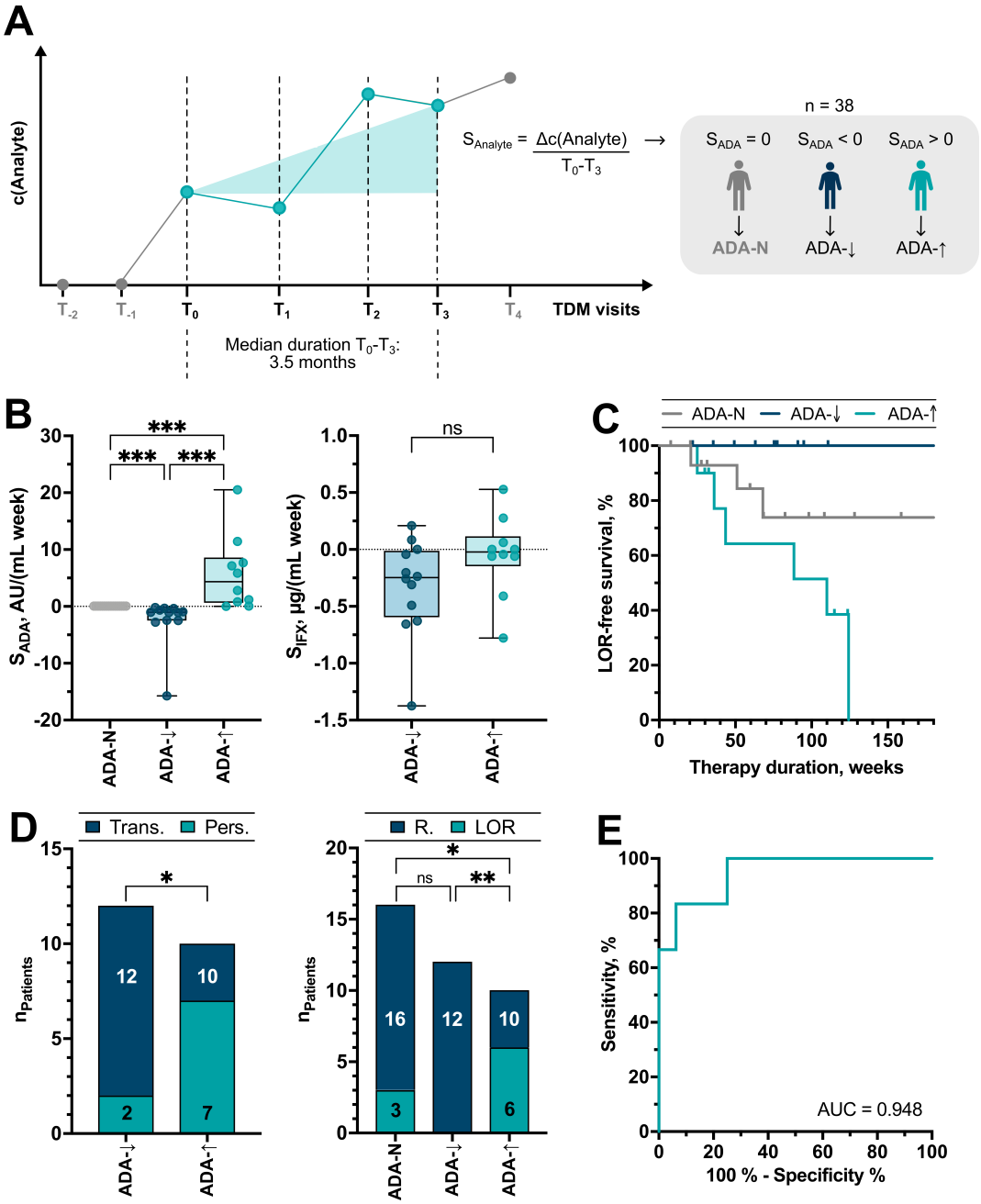

Figure 3.29.: Evaluation of diagnostic implications of (ELISA-)ADA concentration dynamics. (**A**) Schematic depiction of the analyte slope ($S_{Analyte}$) calculation principle: $S_{Analyte}$ (i.e., S_{ADA}) was determined as concentration difference between the first ADA-positive TDM visit (T_0) and the third consecutive TDM visit thereafter (T_3). The time interval T_0–T_3 had a median duration of approximately 3.5 months. Based on S_{ADA} and ADA status, the patient cohort (n = 38) was divided into three groups: ADA-negative patients (ADA-N), patients with negative S_{ADA} (ADA-↓) and patients with positive S_{ADA} (ADA-↑). (**B**) Comparison of S_{ADA} and S_{IFX} between the different S_{ADA} groups. ***, $p < 0.0001$; ns, $p = 0.144$. (**C**) Kaplan-Meier analysis for the different S_{ADA} groups with respect to LOR. LOR-free survival differed significantly between ADA-↓ and ADA-↑ ($p = 0.015$). (**D**) Comparison of ADA persistence (left) and therapy outcome (right) between the different S_{ADA} groups. *, $0.01 \leq p < 0.05$; **, $p = 0.0028$; ns, $p = 0.238$. Pers., persistent; R., remission; Trans., transient. (**E**) ROC analysis of S_{ADA} with respect to therapy outcome LOR. A S_{ADA} cut-off of approximately 2.0 AU/(mL week) was found to predict LOR with 83.3 % sensitivity and 93.8 % specificity. Adapted from [343].

3.5. Transferability of IFXmon and ADAmon assay principles to ADM

The transferability of IFXmon and ADAmon assay principles to other TNF antagonists was evaluated preliminarily by employing the respective assay protocols for the quantification of ADM and anti-ADM. Only absolutely necessary adaptations were made (e.g., other ligands), but the new assays (ADMmon and anti-ADMmon) were not optimized.

3.5.1. ADMmon biosensor assay

The preliminary validation of ADMmon assay performance is shown in **Figure 3.30**. Sensor stability evaluation showed a considerable baseline signal accumulation, in particular when starting new analytic runs (**Figure 3.30A**). ADM and msαhu binding responses remained relatively stable up to approximately 60 cycles, then msαhu binding accumulated consistently. These data indicate that the regeneration conditions may necessitate optimization.

For the determination of ADM concentrations, referenced msαhu binding response of a six-point calibration curve was utilized as calibration curve (see **Figure 3.30B**). The single calibrator concentrations were adapted to the target serum concentration window of ADM (5 – 12 µg/mL)[255]. To validate the quantitative performance of ADMmon, accuracy and precision were assessed by mini-validation with three ADM concentrations (see **Figure 3.30C**; respective ranges: 82.1 – 98.1 %, 97.6 – 99.8 %). The observed results provide first hints that – despite currently lacking further optimization – ADMmon is able to quantify ADM. The mini-validation results may, however, be improved by further optimization.

The ADMmon biosensor assay was then employed to analyze n = 45 different IBD patient sera and ADMmon results were compared with respective concentrations obtained by ELISA (see **Figure 3.31**). ADM detection was concordant in 25 (64.1 %) of n = 39 sera (for n = 6 sera, no ELISA results were available). Only ADMmon detected ADM in five sera, while ADM was exclusively detected by ELISA in nine sera. Following IFXmon, a presumable LOQ of 1.0 µg/mL was defined for ADMmon. ADMmon quantitative data were mostly inconsistent with ELISA data, both in terms of absolute concentrations and general correlation. Additionally, n = 12 samples comprised implausible binding to Fc1 (determined analogously to ADAmon; see **section 3.2.7.4**). Most of the Fc1-implausible samples were ELISA-positive, but ADMmon-negative, which may suggest that the potentially inadequate sera led to false-positive results in ELISA. Overall, validation results and patient serum analyses revealed that the ADMmon biosensor assay should be optimized further, especially in terms of regeneration. Nevertheless, it is likely that ADMmon is able to reach a similar quantitative reliability as IFXmon.

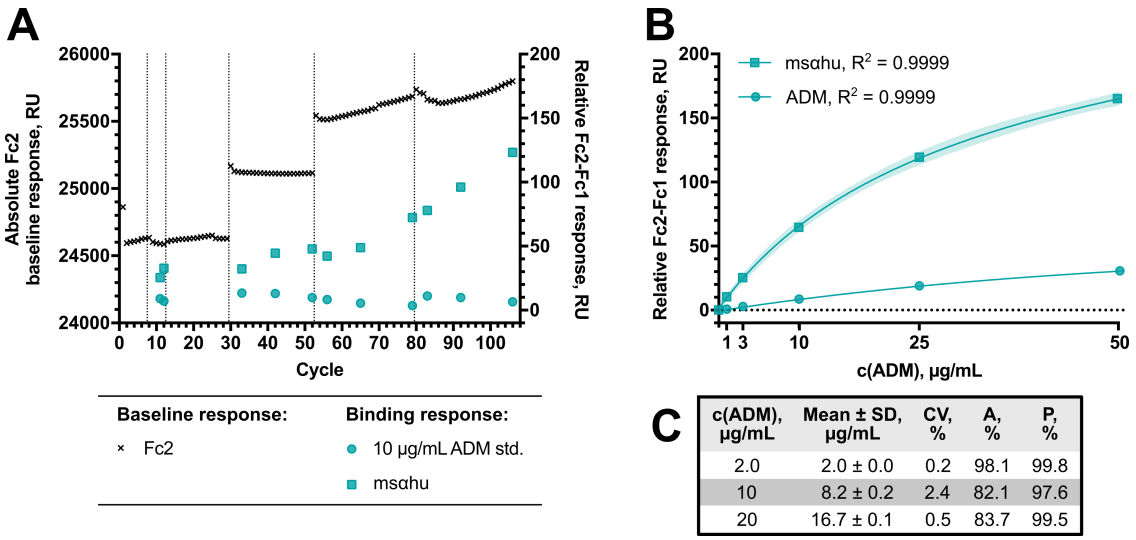

c(ADM), µg/mL	Mean ± SD, µg/mL	CV, %	A, %	P, %
2.0	2.0 ± 0.0	0.2	98.1	99.8
10	8.2 ± 0.2	2.4	82.1	97.6
20	16.7 ± 0.1	0.5	83.7	99.5

Figure 3.30.: ADMmon biosensor mini-validation. (**A**) ADMmon sensor stability. Different analytic runs are separated by dotted vertical lines. Evaluations were restricted to Fc2, as Fc2-Fc1 data were highly similar in trend. (**B**) ADMmon calibration curve with six different ADM calibrators (0, 1.0, 3.0, 10, 25, 50 µg/mL). Responses of both ADM binding and msαhu binding are shown. Curves were fit with a hyperbolic model. (**C**) Precision and accuracy mini-validation by duplicate analysis of three different ADM concentrations. A, accuracy; P, precision. Precision is given as 100 % - CV.

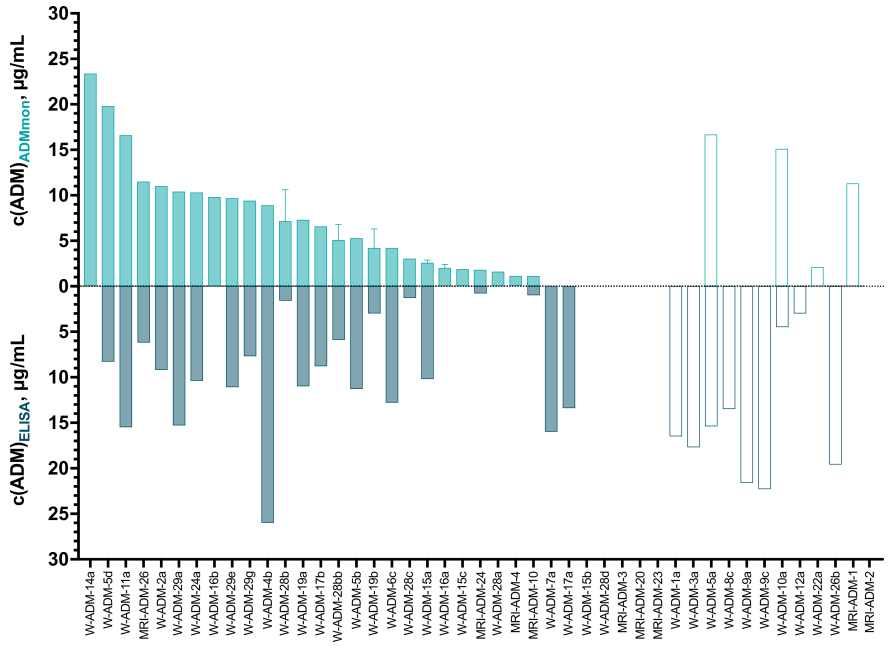

Figure 3.31.: Comparison of ADM quantification in patient sera between ADMmon and ELISA. n = 45 sera from n = 45 different IBD patients were included in the analyses. Clear bars grouped on the right plot end mark sera with implausible Fc1 binding. n = 5 sera were analyzed in duplicates and are thus shown with error bars.

3.5.2. Anti-ADMmon biosensor assay

Coupling efficiency of ADM with magnetic beads was nearly 100 % (limited only by the LOQ of the BN ProSpec® system; data not shown), like for coupling of IFX. The purity of anti-ADM pulldown eluates was evaluated analogously to ADA pulldown eluates via western blot and silver stain (see **Figure 3.32A+B**) and overall confirmed ADA pulldown data: No hSA was detected in anti-ADM pulldown eluates, but non-anti-ADM IgG bands were detected in blank serum matrix eluates and in anti-ADM-positive eluates at much higher intensity as expected for calibrator only. Conveniently, anti-ADM calibrator could be distinguished from endogenous IgG by the light chain apparent MW. As anti-ADM light chain was not visible in calibrator eluates, endogenous IgG are likely more abundant in eluates as compared to ADA. The IBD patient sera comprised an identical band pattern as (spiked) blank serum matrix in both western blot and silver stain. Just like the ADA pulldown, the presented data demonstrate that the anti-ADM pulldown procedure is suitable to significantly reduce sample matrix complexity as compared to serum.

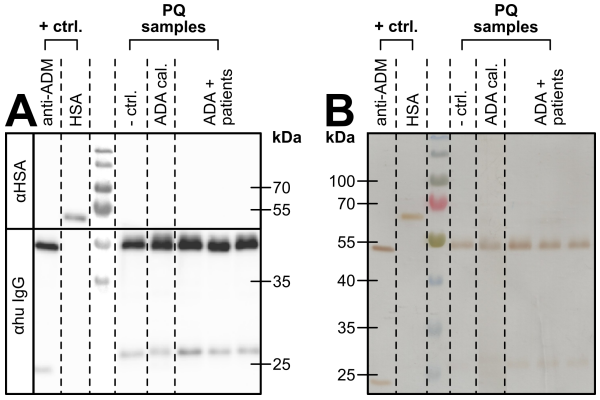

Figure 3.32.: Characterization of anti-ADM purity in pulldown eluates. (A) Western blot detection of hSA and human IgG in pulldown eluates from blank serum matrix without (- ctrl.) and with 5 µg/mL spiked anti-ADM calibrator (ADA cal.). anti-ADM and hSA positive controls (+ ctrl.) show the respective signals of 200 ng loaded protein. (B) Silver stain of anti-ADM pulldown eluates from - ctrl., ADA cal. (5 µg/mL) and three patient serum eluates (W-ADM-24a, W-ADM-28b, W-ADM-28d). Ctrl., control; αhSA, anti-hSA; αhu IgG, anti-human IgG.

The anti-ADMmon biosensor assay was preliminarily validated. Sensor stability in terms of baseline and analyte binding was observed to be excellent over at least 70 analytic cycles as depicted in **Figure 3.33A**. It can hence be concluded that the ADAmon regeneration procedure does also lead to optimal regeneration with the anti-ADMmon biosensor assay and no further optimization is necessary. A representative anti-ADMmon calibration curve is shown in **Figure 3.33B**. Surprisingly, anti-ADM calibrator at concentrations below 2.0 µg/mL was not distinguishable from blank serum matrix. This observation could be reproduced in three other analytic runs (data not shown) and suggests that revising the anti-ADM calibrator concentrations selected for calibration (which were identical to ADAmon) may be useful. The efficiency of anti-ADM pulldown was evaluated by anti-ADMmon analogously to ADAmon (see **section 3.2.1.2**, **Figure 3.33C**). Anti-ADM

pulldown efficiency was observed to be in the same range as comparable ADA pulldown efficiency results (8.6 – 17.1 %, see **Figure 3.9**). The possible proximity of the 2.0 µg/mL anti-ADM calibrator to the assay's LOQ could explain the relatively low pulldown yield result (6.3 %). For the 5.0 and 15 µg/mL anti-ADM calibrators, the determined yields (18.0 and 16.3 %, respectively) confirmed the fluorometrically determined ADA pulldown yields.

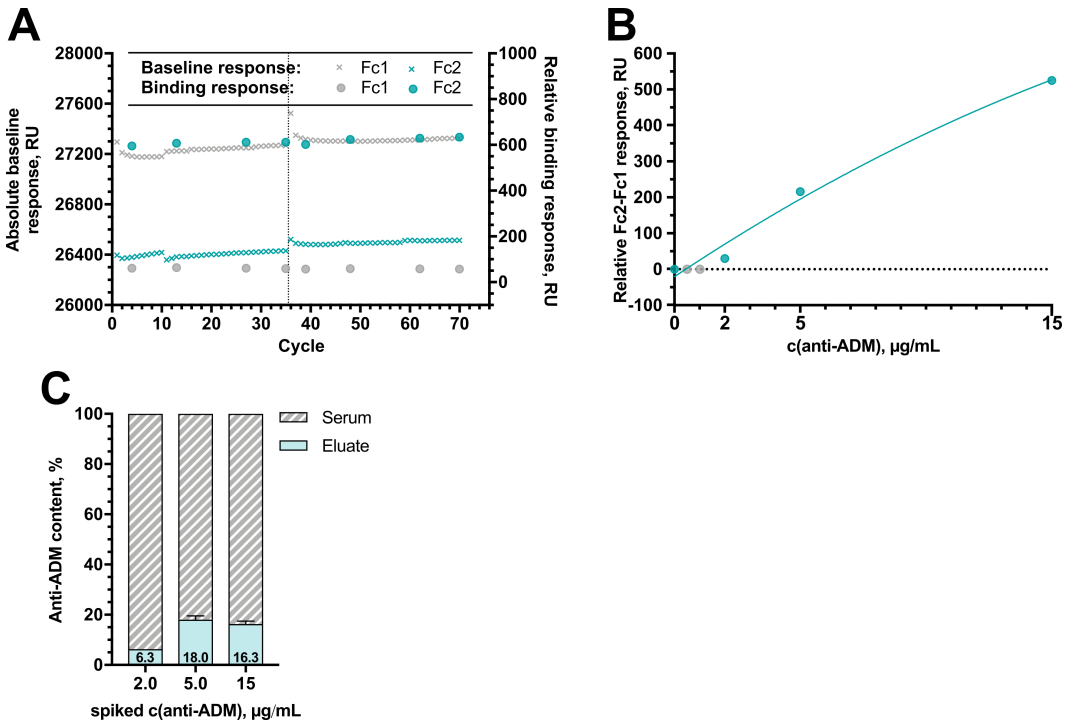

Figure 3.33.: Anti-ADMmon biosensor mini-validation. (**A**) Anti-ADMmon sensor stability. (**B**) ADMmon calibration curve with six different anti-ADM calibrators (0, 0.5, 1.0, 2.0, 5.0, 15 µg/mL). The curve was fit with a hyperbolic model excluding the two lowest non-blank calibrators, as they could not be distinguished from blank. (**C**) Pulldown efficiency evaluation by anti-ADMmon. Unlabeled anti-ADM calibrator was spiked in blank serum matrix and analyzed. Data show n = 2 replicates per concentration, recorded in two different analytic runs. In order to determine the anti-ADM content in pulldown eluates, their corresponding binding signals were normalized to the signals of 2.5 µg/mL anti-ADM standards analyzed within the same run.

The same n = 45 patient sera as previously measured by ADMmon were also analyzed by anti-ADMmon and compared with ELISA data (see **Figure 3.34A**). For n = 3 sera, no anti-ADM ELISA concentrations were available. Comparison of anti-ADM detection between anti-ADMmon and ELISA gave a method concordance of 66.7 %, which was highly similar to the analogous ADAmon analysis. n = 6 sera were anti-ADM-positive only in anti-ADMmon, while n = 8 sera were anti-ADM-positive by ELISA only. For anti-ADMmon, a presumable LOQ was defined as 1.0 or 2.0 µg/mL for each analytic run individually, depending on the resolution of low anti-ADM calibrators observed within the respective run. Matching ADAmon data, absolute anti-ADMmon concentrations were mainly discordant with ELISA results and no significant correlation was observed between the two methods. n = 3 sera exhibited implausible Fc1 binding. The evaluation of anti-

ADM DissR was especially interesting: Median observed DissR over all anti-ADMmon-positive sera (n = 16) was 1.537 (see **Figure 3.34B**)). When grouping DissR by anti-ADM detection by ELISA, anti-ADM detected by anti-ADMmon only had a significantly higher median DissR (median: 1.843) as compared to sera, which were also classified positive by ELISA (median: 1.434, p = 0.023). These results are in line with previously presented ADAmon results and provide additional support for the hypothesis that ELISA is more prone to miss fast-dissociating ADA. Additionally, DissR results were compared between subtherapeutic (< 5.0 µg/mL) and therapeutic/supratherapeutic ADM (≥ 5.0 µg/mL), as determined by ELISA (see **Figure 3.34C**). Median DissR between the groups differed significantly (1.457 vs. 1.801, p = 0.0052). Despite the small sample size, these results confirmed previous observations from ADAmon and demonstrated that low DissR is associated with reduced drug levels. Unfortunately, no therapy outcome data were available for ADM-treated patients. Nevertheless, the anti-ADMmon data provide a nice re-validation of ADAmon results and underline the diagnostic relevance of anti-drug antibody binding characteristics. Especially the anti-ADMmon results showed that the biosensor principles from ADAmon can sometimes be easily transferred to other TNF antagonists.

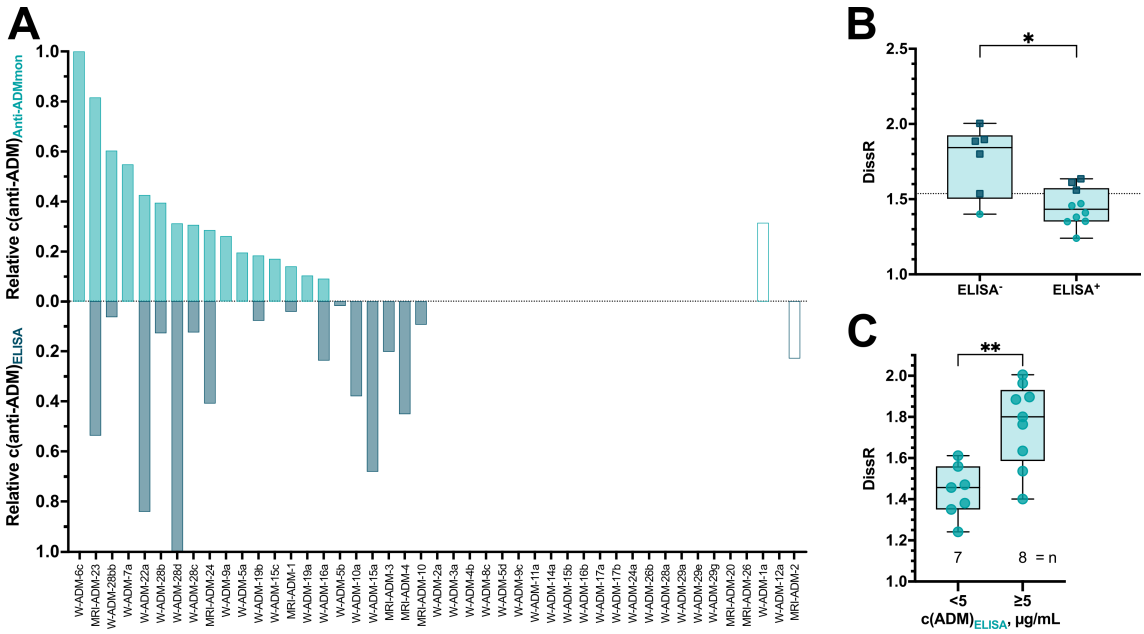

Figure 3.34.: Comparison of anti-ADM quantification in patient sera between ADMmon and ELISA. (**A**) Normalized anti-ADM quantities are shown for n = 45 sera from n = 45 different IBD patients. Clear bars grouped on the right plot end mark sera with implausible Fc1 binding. (**B**) DissR of anti-ADMmon-positive sera grouped by ELISA result. n = 6 sera were anti-ADMmon-only positive, while n = 10 sera were classified positive by both anti-ADMmon and ELISA. Symbol color and shape indicate low (teal circles) or high DissR (dark blue squares), which are separated by the overall median DissR (1.537). (**C**) Comparison of DissR between subtherapeutic (< 5 µg/mL) and therapeutic/supratherapeutic (≥ 5 µg/mL) ADM concentrations determined by ELISA. * p = 0.023; **, p = 0.0052.

4. Discussion

The aim of this dissertation was to develop SPR-based biosensor assays for the TDM of TNF antagonists and their corresponding anti-drug antibodies with the Biacore X100 system. The TNF antagonist IFX served as exemplary drug for proof-of-concept. The new biosensor assays should comprise reliable quantitative performance. Therefore, the novel assays should be validated with respect to biosensor stability, calibration, analytic sensitivity, accuracy and precision. For the ADA biosensor, drug tolerance should also be evaluated. In addition, the SPR measurements should be exploited to gain qualitative information about ADA, i.e., to characterize ADA binding stability and to estimate their IFX-neutralizing capacity. To investigate whether analytic performance and feasibility of the new SPR biosensor assays sufficed the standards for routine diagnostic application, IBD patient sera should be analyzed and compared to diagnostics-approved ELISA. In the framework of a retrospective observational patient study, methods to increase the diagnostic value of TDM results – both from the developed SPR biosensors and ELISA – should be sought. Finally, assay principle transferability to other TNF antagonists should be tested.

4.1. Evaluation of IFXmon and ADAmon biosensor quantitative assay performance with respect to diagnostic bioanalytic method requirements

4.1.1. The diagnostic utility of IFXmon as new tool for IFX monitoring

With the development and validation of IFXmon, a main aim of the present dissertation project has been completed. Validation of the optimized IFXmon biosensor assay covered biosensor stability, calibration, analytic sensitivity, accuracy and precision and, finally, method comparison with the IDKmonitor Infliximab drug level ELISA in the scope of a small patient study. It is essential to mention here that a very similar SPR method for IFX quantification in serum has been developed and validated by Beeg et al. and Thoren et al.[287,288,327]. It is therefore reasonable to compare the performance characteristics of IFXmon with their assays. Although several other groups have reported SPR methods for TNF antagonist quantification before[284,285,287–289,327,344–346], IFXmon was developed as proof-of-principle SPR assay in order to gain experience and know-how for the subsequent ADAmon development. Furthermore, IFXmon represents the first SPR-based TNF antagonist quantification assay for use with the Biacore X100 system. Other publications have reported assays for Biacore 2000[345], ProteOn XPR36 Protein Interaction Array system (Bio-Rad)[287–289,327] or custom, in-house-developed fiber optic SPR systems[284,285,289,344,346].

4.1.1.1. Evaluation of IFXmon analytic performance

The IFXmon biosensor exhibited highly stable binding over many (at least 115) cycles. This was firstly enabled by a very effective regeneration protocol, but also by additional ligand stabilization via covalent cross-linking during immobilization. To the best of my knowledge, IFXmon is the only published SPR biosensor for TNF antagonist analysis, which offers cross-linked ligands on its sensor chip surface[284,285,287–289,344–352]. Ligand cross-linking is likely not decisive for assay functionality. Nevertheless, the cross-linking procedure does neither notably increase the cost nor the duration of the IFXmon biosensor preparation. At the same time, TNF cross-linking was shown to significantly increase ligand stability without impairing biosensor functionality as compared to a non-cross-linked surface. The cross-linking thus improves cost-efficiency and biosensor lifespan for IFXmon.

Beside biosensor stability, analytic sensitivity is an important parameter of assay performance. Analytic sensitivities for several IFX quantification assays are listed in **Table 4.1**. This table reports two different sensitivity parameters: Sensitivity referring to undiluted serum, here denominated "relative sensitivity", and sensitivity referring to diluted serum, denominated "absolute sensitivity". Relative sensitivity indicates whether the assay is capable of determining IFX in patient serum at the lowest concentration that is relevant for therapeutic decision-making. To evaluate relative sensitivity, it has to be compared to the therapeutically targeted IFX trough concentration range, which is 3 – 8 µg/mL[255]. Among all assays in **Table 4.1**, IFXmon comprises the second highest LOQ. Some studies only report LOD, but have not validated LOQ. The reported LOD results by Lu et al. (2016, 2017) however strongly suggest that LOQ would be comparable to IFXmon[284,285]. Within absolute sensitivities, IFXmon LOQ is located in the middle of the observed range. The differences in analytic sensitivities are likely owed to the different technical specifications of the respectively utilized instruments and the different serum dilutions (1:10 – 1:200) resulting in differential non-specific binding background. The ELISA comprises one of the highest absolute sensitivities, as it applies the highest serum dilution (1:200) among all reported assays. As IFXmon LOQ is highly comparable to the LOQ of the diagnostics-approved ELISA, its sensitivity can be considered adequate for diagnostic application. With respect to therapeutic decision-making, the analytic sensitivity of IFXmon is certainly sufficient, as its LOQ lies well below the consensus threshold for subtherapeutic IFXmon concentration of 3 µg/mL.

All quantitative assays necessitate a calibration method that uses samples with known concentration in order to deduce the concentrations of unknown samples. For IFXmon, a hyperbolic model served for calibration. Calibration curve repeatability was excellent for IFXmon. Beeg et al. utilized a linear calibration model, but this model merely covered IFX concentrations up to 8 µg/mL[288]. As during the induction of IFX therapy, supratherapeutic IFX concentrations are often targeted, the calibration model from Beeg et al. would not be adequate for TDM during IFX induction[353]. Even a maximum

Table 4.1.: Analytic sensitivity of IFXmon and other IFX quantification assays.

Reference	Assay format	Analytic sensitivity	
		Relative*	**Absolute***
Grasmeier et al. (2023) [322]	SPR biosensor	LOQ = 0.9 µg/mL	18 ng/mL
IDKmonitor [335]	ELISA	LOQ = 0.6 µg/mL	3 ng/mL
Beeg et al. (2019) [288]	SPR biosensor	LOQ = 0.2 µg/mL	7 ng/mL
Thoren et al. (2018) [287]	SPR biosensor	LOQ = 0.5 µg/mL	50 ng/mL
Lu et al. (2017) [285]	SPR biosensor	**LOD** = 0.1 µg/mL	1 ng/mL
Lu et al. (2016) [284]	SPR biosensor	**LOD** = 0.2 µg/mL	2 ng/mL
Zeni et al. (2020) [289]	SPR biosensor	**LOD** = 3.7 µg/mL	74 ng/mL

* Relative analytic sensitivity refers to undiluted sample material and is the diagnostically relevant parameter. Absolute analytic sensitivity considers the respective dilution factor and represents a more meaningful indication of analytic capacity than relative analytic sensitivity.

calibrator concentration of 20 µg/mL, as reported for the biosensor published by Thoren et al., may require dilution of some sera from IFX induction patients. The maximum calibrator of IFX ensures interpolation coverage of all plausible trough concentrations expected in induction and maintenance therapy. Since the near-perfect assay linearity result also considered supratherapeutic IFX concentrations, no additional sample dilution is required. Thus, its broad analytic measurement range keeps the IFXmon assay procedure simple. Accuracy and precision of the IFXmon assay slightly outperformed the IDKmonitor ELISA. Comparison with accuracy and precision of the very similar SPR biosensor assays by Beeg et al. and Thoren et al. showed nearly identical accuracy and precision: IFXmon, Beeg and Thoren biosensors comprised respective mean inter-day accuracies of 97.3 %, 98.4 % and 97.6 % respectively, and respective mean inter-day precisions of 8.8 %, 8.3 % and 8.5 %. Of note, IFXmon covered a broader concentration range in these analyses. The accuracy and precision determined for the 1 µg/mL calibrator outperformed the minimum requirements for accuracy and precision at LOQ, which allow up to 25 % deviation from nominal concentration or CV, respectively [354,355]. This suggests that the LOQ of the IFXmon biosensor assay was defined sufficiently conservative. IFXmon furthermore comprised better performance for the 1 µg/mL calibrator as compared to Beeg et al, which is noticeable as Beeg reported better analytic sensitivity.

4.1.1.2. Validation of IFXmon in a real-world IBD patient study

Even though there is no official gold standard method for IFX quantification, ELISA is the most commonly employed method for IFX TDM. According to a relatively recent review by Gorovits et al. (2018), most studies publishing IFX monitoring results report that ELISA served as analytic TDM method [356]. Hence, selecting an ELISA format as reference method for comparison with IFXmon appears plausible. Method comparison regres-

sion with IBD patient sera showed high agreement between IFXmon and the IDKmonitor ELISA and suggests interchangeability, which is remarkable in view of the fundamentally different method principles. Especially for IFX concentrations below 7 µg/mL (thus covering the entire subtherapeutic and nearly the entire therapeutic range), 90.6 % of samples differed for less than 1.5 µg/mL, which is not decisive for therapy management. Even though calibrated with Remicade®, the IFX biosimilars Remsima® and Inflectra® were quantified just as reliably as Remicade® in patient sera. This finding was expected, as several studies report similar analytic performance for originator and biosimilar IFX [357–359]. Beeg et al. also report high method concordance between their SPR biosensor method and an ELISA (RIDASCREEN® IFX Monitoring, R-Biopharm) [288,327].

When the transfer of IFXmon assay principles to ADM quantification was tested after only applying a minimum of protocol changes, preliminary assay validation appeared promising. However, limited biosensor stability due to ineffective regeneration was likely responsible for the reduced method congruence with the IDKmonitor Adalimumab drug level ELISA. Nevertheless, the development of IFXmon as a proof-of-concept SPR biosensor was successful, as it comprises at least comparable performance as similar SPR biosensor methods. Method comparison regression was performed with the so far largest sample number (IFXmon: n = 84, Beeg et al.: n = 58, Thoren et al.: n = 20, Lu et al.: n = 5). Overall, the presented validation results underpin that IFXmon assay performance can keep up with the IDKmonitor ELISA and therefore likely meets diagnostic quality standards.

4.1.2. The diagnostic utility of ADAmon as new tool for drug-tolerant ADA quantification

Establishment of a SPR-based method for ADA assessment was the central aim of this dissertation project. The development of a robust method for ADA quantification was substantially complicated by several factors: First, the co-presence of IFX in patient serum hijacks ADA from detection via the biosensor, which relies on ADA binding to immobilized IFX. Second, the discrimination of ADA from other human IgG and TNF antagonist in serum is challenging due to the shared structural similarity. Therefore, no suitable enhancer step could be established, which excludes a major measure to optimize analytic sensitivity. It should be mentioned here that enhancement via a second injection with Remicade® failed (data not shown). Since SPR biosensor surfaces intended for analyte quantification comprise very high ligand density in order to maximize analytic sensitivity, all binding valencies of ADA likely interact with the surface-bound IFX and are therefore not out-competed by the injected enhancer IFX. Third, it is assumed that ADA concentrations can be highly variable, including concentrations in the low µg/mL range [360]. Fourth, the polyclonal nature of ADA, which translates to variable affinities towards IFX, frustrates absolute quantification of ADA. Therefore, ADA quantification is influenced by the affinity of the selected ADA calibrator: The closer the calibrator's affinity is to the mean affinity of the patient-individual ADA population, the more ac-

curate the quantification will be. However, no ADA calibrator fulfills this requirement for all possible patient ADA populations. Therefore, one has to keep in mind that ADA quantification in immunoassay setups always has to be viewed as semi-quantitative [361]. All of the aforementioned adversities could be overcome successfully during optimization of the ADAmon biosensor assay. The performance of ADAmon was validated with respect to ADA pulldown, biosensor stability, calibration, analytic sensitivity, accuracy and precision. After assay validation, ADAmon was employed to quantify ADA in authentic patient sera and results were compared primarily with the drug-tolerant IDKmonitor Infliximab total ADA ELISA.

4.1.2.1. ADA pulldown: The key to ADAmon assay functionality

As previously demonstrated (see **section 3.2.1.1**), application of a direct approach for ADA quantification similar to the one described by Beeg et al. was not feasible with the Biacore X100 instrument utilized in the present project [288,327]. Instead, a simple protocol for pre-analytic ADA pulldown was established as the centerpiece of the ADAmon biosensor assay. The PA step within the ADA pulldown procedure is crucial to achieve analytic drug tolerance. Even though DQ requires fewer material and hands-on time, the ADA pulldown procedure has several advantages: On one hand, ADA pulldown eluates contain timely stable total ADA, as serum IFX is removed during the pulldown procedure. In contrast, DQ samples have to be measured immediately after PA. Even more importantly, pre-analytic ADA purification yields enriched ADA and drastically reduces sample complexity, as the majority of serum proteins are depleted during the pulldown. ADA eluates consequently contain significantly less non-specific binders as compared to diluted serum, which decreases the risk for irreversible accumulation at the biosensor and therefore reduced biosensor surface wear-out.

The higher purity of ADA pulldown eluates, in contrast to IFXmon samples (1:50 diluted serum), likely explains that ADAmon biosensor chips were observed to exhibit 1.6 times longer life spans (n = 180 cycles) as compared to IFXmon biosensor chips (n = 115 cycles). Of note, the number of serum samples analyzed on one ADAmon biosensor chip was identical to IFXmon (n = 60) in the present work. The ADAmon serum sample throughput was not fully optimized in this study due to time management reasons. Since the Biacore X100 has only a low-capacity sample rack with 15 positions, a typical ADAmon analytic session with 30 cycles required repeated presence by the instrument over 11 hours in order to replace sample tubes. For the IFXmon patient study, a typical analytic run amounted for 38 cycles, as the pre-analytic sample preparation for the IFXmon assay was shorter as compared to ADAmon. Instead of increasing the number of analyzed samples per ADAmon session, the sensor was re-used the next day and new start-up cycles and a new calibration curve were recorded. Thereby, the overall required number of cycles to analyze the 60 patient sera was higher for ADAmon as compared to IFXmon. Another factor that may contribute to the high stability of the ADAmon biosensor may be ligand

cross-linking, but this hypothesis was not explicitly investigated.

Although the high purity of ADA eluates is beneficial for the ADAmon biosensor, one may ask if the ADA488 yield of approximately 16 – 21 % is sufficient. Indeed, a higher yield would have been expected. The yield of immunoprecipitation is majorly dependent on ligand:analyte affinity, processing time (especially during washing), total volume of the pulldown batch and analyte concentration[362]. The affinity of ligand:analyte binding cannot be modified, but is anyway high for ADA calibrator (monovalent K_D = 0.12 nM) and also expected to be relatively high (in the range of physiological antibody:antigen affinities) for ADA[363,364]. The processing time was kept as short as possible and in particular, the washing of beads after the pulldown incubation was minimized in repetitions and time. The total volume of the pulldown reaction was optimized to be as small as feasible. However, the utilized volume was required, since lower volumes would have led to considerable bead loss due to retention in pipette tips and unfavorable mixing in the reaction vessels during incubation (only 1.5 mL vials were compatible with the available overhead rotator). I have two main hypotheses for the observed, rather low yield: First, analyte concentration greatly impacts pulldown yield. Concentrations of spiked ADA calibrator were in the low µg/mL range or even below. For clarification, the maximum concentration employed in the ADA488 yield evaluation experiment was 5 µg/mL ADA488 in a 1:13 final dilution (corresponding to approximately 385 ng/mL or 2.5 nM). ADA (calibrator) as target analyte can therefore be justly considered low abundant. When optimizing the ADA pulldown, initially only 1 mg of IFX beads were used per reaction batch. As no ADA calibrator was detectable in pulldown eluates, the employed bead amount was increased four-fold, leading to the indicated yields. Further increase of bead amount per batch could hence likely further increase the yield, but this would exceed reasonable cost in terms of possible diagnostic applications. The second hypothesis refers to the fact that serum (also in the final dilution applied in the pulldown) is a highly complex sample matrix comparable to "overdosed" blocking agents. It is thus conceivable that ADA calibrator is partly bound – specifically or non-specifically – by other serum proteins and thereby hindered to bind to IFX, especially in combination with its low concentration. The fact that similar ADA yields were determined by fluorometry and SPR indicates that the data are correct. Despite the low pulldown yield and the theoretically error-prone, manual pulldown procedure, the ADA488 pulldown yield was observed to be reproducible and independent of ADA488 concentration over the observed concentration range (which covered most of the calibration range). Thus, the pulldown performance was accepted.

4.1.2.2. Evaluation of ADAmon analytic performance

For the IFXmon biosensor, assay calibration was performed with the same (or, in the case of IFX biosimilar analysis, a highly similar) substance as the target analyte. It is relatively straightforward to validate and compare the performances of different IFX quantification

assays, as samples of known absolute concentration can be analyzed. In contrast, when quantifying ADA, the absolute concentration cannot be known due to the aforementioned challenges in calibration. Hence, one can think of comparing ADAmon with other ADA quantification assays as searching for the best guess among all methods without knowing the true "model solution". This is important to keep in mind when discussing the analytic performance of ADAmon in comparison with other commercially available or published methods.

Like IFXmon, the ADAmon calibration curve was fit with a hyperbolic model. The SPR method by Beeg et al. utilized a linear calibration model, which might be owed to the higher IFX ligand density on their sensor chip, leading to a higher ADA concentration to reach signal saturation[288]. For ADAmon, IFX densities higher than 4500 RU were not feasible, since the inter-chip reproducibility of the ligand density decreased rapidly for higher target levels (data not shown). The ADAmon calibration curve covered all ADA concentrations observed in the later patient study, such that no re-analysis of additionally diluted samples was required.

0.14 µg/mL and 0.30 µg/mL were determined as "relative" LOD and LOQ (see definition in **section 4.1.1**) for ADAmon, respectively. When considering the mean pulldown yield of ADA calibrator 19 %, these results translate to "absolute" LOD and LOQ of 24 ng/mL and 51 ng/mL. The determined LOD and LOQ, however, are most accurate for ADA calibrator, since it is also used for calibration. For instance, patient ADA with lower mean ADA avidity as compared to ADA calibrator may comprise lower pulldown yield, resulting in higher LOD and LOQ. The absolute LOQ of IFXmon was determined as 18 ng/mL. Consequently, absolute LOQ of ADAmon was 2.8-fold higher as compared to IFXmon. Since for IFXmon, the signal enhancement factor for the 0.5 µg/mL calibrator was 10, it can be concluded from this comparison that ADAmon, in spite of lacking an enhancement step, comprises comparable analytic sensitivity. This observation can be likely attributed to the decreased non-specific binding background of the pulldown eluates. The IDKmonitor ELISA was stated to exhibit an LOQ of 10 AU/mL. Since both analytic units and the quantification principle of the ELISA method differed from IFXmon, analytic sensitivity cut-off results cannot be compared meaningfully.

Within ADAmon validation results, minimum accuracy and precision were observed for the 0.25 µg/mL ADA calibrator, which is not surprising in view of the fact that this ADA concentration is below LOQ. The accuracy of this calibrator (109.6 %) even outperformed the acceptable performance, which is defined as maximum 20 % deviation from 100 % recovery[365]. The precision (73.0 %) of the sub-LOQ calibrator was acceptable for semi-quantitative analysis below LOQ. Overall, ADAmon comprised better accuracy, but slightly lower precision than the IDKmonitor ELISA. In addition, ADAmon generally performed less reliably as compared to IFXmon. As already mentioned in the results section (see **section 3.2.5**), the lower precision can be explained by the higher manual handling effort during pre-analytic ADA pulldown. Beeg et al. report excellent accu-

racy and precision for their ADA quantification SPR biosensor (mean: 94.3 % and 2.6 %, respectively)[288]. The superiority of their data compared with ADAmon is likely based in the direct quantification method, which includes fully automated pipetting except for sample dilution[288]. The data of Beeg et al. also showcase the analytic capabilities of SPR biosensors.

Yet, ADAmon overall performance still sufficed FDA requirements for immunogenicity assays, which recommends to accept a maximum CV of 20 %[365]. ADAmon precision was comparable to the commercially available, IVD-approved RIDASCREEN® Anti-Infliximab Antibodies ELISA (R-Biopharm), which reports a mean precision of 12.2 %[366]. Since no reference ranges are established for ADA quantification and the meaningfulness of absolute ADA quantities is questionable, the precision of ADA quantification may not be significantly decisive for therapy management, as long as it fulfills the regulatory standards. In conclusion, validation of the ADAmon biosensor demonstrated that ADAmon, even though its precision is inferior to some other selected ADA quantification methods, likely suffices diagnostic standards.

4.1.2.3. Comparison of ADAmon with other ADA quantification assays: Comparing apples with oranges?

The fact that two different assays pass validation in terms of their analytic performance does not necessarily mean that the two assays generate similar results, when assessing identical samples. Therefore, it is important to also compare authentic patient material between a new diagnostic method with the gold standard method or, if such does not exist, with a diagnostics-approved assay. Method comparison was particularly interesting in the case of ADAmon, because absolute ADA quantity is unknown. ADA quantification depends on ADA calibrator affinity of the respective assay's ADA calibrator and therefore, ADA concentrations must generally be regarded as semi-quantitative[361]. By harmonization of ELISA results with ADAmon results prior to method comparison, ELISA results were set in relation to the identical ADA calibrator as ADAmon. This step thereby eliminated the contribution of calibrator affinity to the quantitative results.

Evaluation of ADA detection rates for ADAmon and the IDKmonitor ELISA allows for a cautious comparison of analytic sensitivities. In the 128 analyzed sera with both available ADAmon and ELISA results, 53 and 66 sera were above the respective LOQ. This result indicates that ELISA is more sensitive as compared to ADAmon. Taking a closer look at ELISA-only positive sera, median ADA concentration was 0.002 µgEq/mL, equivalent to 21.7 AU/mL, and therefore very close to the LOQ of ELISA (10 AU/mL; maximum result: 1026.5 AU/mL). Such low ADA concentrations constitute a diagnostic gray area. In conclusion and in line with literature, ADAmon sensitivity is likely comparable, yet slightly inferior to ELISA, but capable of detecting diagnostically relevant ADA quantities. Importantly, therapeutic decisions within the ADAmon cohort relied on ELISA TDM results. Against this background, I would like to re-evaluate the TDM history of patient

MRI-IFX-22. According to the ELISA TDM, this patient repeatedly showed undetectable or subtherapeutic IFX (in three out of the five included visits), while ADA were either negative or low (see **Appendix A**). The decision to maintain the patient on IFX was based on the low ADA profile. It is interesting that for the same patient, according to ADAmon, all but the first sera were ADA-positive. Possibly, MRI-IFX-22 was mistakenly assessed as a high-clearance case owed to false negative ELISA results.

Another factor that should be considered when comparing ADA quantitative methods is drug tolerance[302]. This project covers the first comparison of a drug-tolerant ELISA with a drug-tolerant SPR method[287,288,327]. In the study published by Beeg et al. (2021), their drug-tolerant SPR method was compared with a drug-sensitive ELISA[327]. Their finding that SPR was more sensitive than ELISA is therefore not surprising. Thoren et al. also reported a slightly higher ADA detection rate for their drug-sensitive SPR biosensor (28 %) as compared to a drug-sensitive reporter gene assay (22 %; iLite™, Euro Diagnostica)[287,367]. Reported ADA positivity rates by SPR in the present study, Beeg et al. (2021) and Thoren et al. (2018) were 41 %, 37 % and 28 %, respectively. These results nicely fit into the big picture that drug-tolerant assays lead to higher ADA detection rates[368]. Furthermore, the ADA detection rates between ADAmon and the Beeg method were highly similar, which may be carefully interpreted as comparable analytic sensitivity.

When evaluating ADA quantification in patient sera, most sera analyzed by ADAmon resulted to be in the semi-quantitative range between LOD and LOQ. Furthermore, ADA quantities did not strongly correlate with ELISA. However, comparison of absolute ADA concentration between ADAmon and ELISA showed that ELISA consistently underestimated ADA (3- to 1557-fold). This finding confirms results by Beeg et al. (2021), who observed absolute ADA quantities to be 7- to 490-fold lower for ELISA as compared to their SPR biosensor and, in addition, reported poor method correlation[288,327]. Poor method correlation and high differences in absolute concentrations have not only been described for comparison of different assay methods, but also for similar assay formats[249–251,290,361]. These discrepancies are explained by the use of different calibrators and heterogeneity of reported units (e.g., ng/mL, µgEq/mL, AU/mL, etc.)[252]. Since decades, it has been well-known among experts that research on ADA and their optimal therapeutic management is hampered by lacking harmonization and inconsistencies in assay methods as well as their reporting[251,252,356]. This does not only apply to ADA, but also to anti-ADM[252,283,369].

The transfer of ADAmon assay principles to anti-ADM quantification worked surprisingly well: In addition to the biosensor, the pulldown ligand also had to be adjusted. The whole protocol thus comprises more steps, which can potentially require optimization. Anti-ADMmon detected ADA in 38 % of all analyzed sera, while 43 % of sera were ADA-positive by ELISA. Overall, the similarity of anti-ADM results to ADAmon evaluations revalidates the ADAmon biosensor and is a flagship for the ease of SPR assay transferability.

Another benefit of the SPR biosensors is that sample-individual plausibility controls can be obtained within standard analytic runs: By also analyzing the reference channel binding of all sera, possible irregular non-specific binding can be identified. By this means, SPR can detect sera causing analytic interference (e.g., owed to pre-analytic handling errors) and thereby also the need for repeated blood sampling. In contrast, ELISA does not offer a comparable control and may report these sera as false-positives. In summary, ADAmon was shown to meet diagnostic quality standards and brings new, useful analytic functions into play.

The diagnostic value of ADAmon is, just as for any immunogenicity assessment method, its ability to identify patients at risk to develop LOR. Several studies have shown that patients with very low or undetectable IFX (< 1 µg/mL) and no ADA are likely to benefit from higher IFX exposure, whereas low-IFX patients with (high) ADA are frequently switched to an alternative drug[247,256]. ADAmon (in combination with IFXmon) can thereby be utilized as a tool for therapeutic decision-making in IFX TDM.

4.1.3. Economic and practical feasibility of IFXmon and ADAmon for routine diagnostics

Even though several SPR methods have been demonstrated to suffice bio-analytic method validation standards, they are not yet part of the method repertoire in medical laboratories[288,302,322,326–329]. Thus, establishing SPR methods in routine diagnostics faces more hurdles than, for example, setting up a new ELISA format. As routine laboratory technical staff and laboratory physicians are not familiar with the methodology, the personnel is required to take advanced training in the SPR methodology. Furthermore, the purchase of SPR instruments is expensive. However, other techniques like mass spectrometry have initially faced similar challenges and now play an important role in clinical laboratories[370,371]. Therefore, there is a possibility that SPR could also become established in laboratory medical analytics.

The cost of the developed SPR biosensors within this project are highly competitive with commercial, IVD-approved ELISA formats, as shown in **Table 4.2**. It should be mentioned that for SPR biosensors, pure material cost is indicated, while the cost of both ELISA methods is derived from kit purchasing cost and therefore includes profit margin. The material cost of IFXmon is mainly driven by sensor chip CM5, msαhu, Remicade® and TNF, whereas the cost of standard chemicals for amine coupling and buffers is marginal. For ADAmon cost calculation, Dynabeads™ M-280 Tosylactivated, sensor chip CM5 and Remicade® are most significant, as the consumption of ADA calibrator is relatively low in patient sera analyses. While IFXmon is more cost-effective than the two other ELISA methods, ADAmon cost is slightly cheaper than the RIDASCREEN®, but more expensive than the IDKmonitor ELISA. In terms of total assay duration, IFXmon and ADAmon are less time-efficient as compared to ELISA, but both SPR biosensor assays require less hands-on time than their ELISA counterparts.

Table 4.2.: Comparison of IFXmon and ADAmon economic and practical feasibility with IVD-approved ELISA.

Assay (Supplier)	Cost	Hands-on time	Total duration
IFX quantification			
IFXmon [322]	€5	30 min*	19.5 h*
IDKmonitor (Immundiagnostik) [335]	€12	60 min	3.5 h
RIDASCREEN (R-Biopharm) [372]	€23	60 min	3 h
ADA quantification			
ADAmon [322]	€23	60 min**	22 h**
IDKmonitor (Immundiagnostik) [337]	€10	1.5 h	4.5 h
RIDASCREEN (R-Biopharm) [366]	€26	1.25 h	3.5 h

Cost and durations are indicated as approximates. Cost calculation of commercially available assays is based on kit purchase, not external order analytics. * Refers to analysis of 20 sera plus necessary calibrators, blanks and standards within one analytic runs. ** Refers to analysis of 20 sera plus necessary calibrators, blanks and standards within two analytic runs.

In the present assay formats executed with Biacore X100, total assay duration of both IFXmon and ADAmon is approximately twenty-fold higher than the IVD-approved ELISA formats for the analysis of 90 samples, the equivalent of a fully loaded ELISA microtiter plate. However, multiple sensors can be combined in SPR devices with more flow cells to create high-throughput biosensor platforms capable of multiplex determination of several analytes. For example, it may be feasible to execute IFXmon and ADAmon with a Biacore 8K, which utilizes the same sensor chips as Biacore X100. Biacore 8K offers 16 flow cells in eight channels, which could be distributed into four IFXmon and four ADAmon biosensors, respectively. By this means, IFX and ADA concentrations could be obtained simultaneously, the sample throughput would be eight-fold and eight times more samples could be run on one sensor chip. Employing Biacore 8K would therefore both reduce the hands-on time and per-sample cost. The device itself is more expensive than Biacore X100, such that the presented scenario is only feasible for specialized centers with high sample throughput, which can guarantee profitable instrument load. It can be concluded that the diagnostic feasibility of IFXmon and ADAmon with Biacore X100 is restricted to low sample throughput. When employing high-throughput SPR devices capable of assay multiplexing, IFXmon and ADAmon may probably outplay ELISA in time and cost efficiency.

4.2. Quantity or quality? Investigating the therapeutic value of ADA data

Many commercial ADA monitoring tests only provide information on ADA quantity. On the contrary, ADAmon allows for both quantitative and qualitative ADA analysis. The therapeutic utility of both types of information on ADA will be evaluated in this section. Although ADA concentration monitoring has been part of routine patient care for more than two decades now, literature offers more data on the comparison of ADA detection status than on the evaluation of ADA concentrations[373]. The reason for this is the general lack of harmonization in anti-drug antibody assays and outcome measures, which complicates meta-analyses of anti-drug antibody quantification for manifold biologic drugs across different studies[262,373–375]. It is well-known that ADA concentrations are reported to be negatively correlated with IFX trough concentrations[225,239,376]. A study from Oh et al. (2017) unveiled higher ADA concentrations in patients with active as compared to quiescent disease[376], while Baert et al. (2003) found higher ADA concentrations in fistulizing CD, a particularly aggressive disease variant[239]. Furthermore, high ADA concentrations are associated with an increased risk for infusion reactions and shorter response duration to IFX therapy[239,377].

With respect to ADA quality, the data landscape is less clear. In general, the major anti-drug antibody attributes with potential clinical impact encompass precise epitopes, drug-neutralizing capacity, persistence and binding strength of anti-drug antibodies towards the drug[237,283,378,379]. It is, however, not feasible to analyze all anti-drug antibody characteristics. For instance, the analysis of anti-drug antibody epitopes has revealed that anti-TNF antagonist antibodies are mostly neutralizing[380–382], but slightly vary in their specific epitopes[383]. Even though commercial assays are available for the assessment of neutralizing ADA[279,367], the analytic discrimination of neutralizing ADA from non-neutralizing ADA becomes obsolete and has been questioned in recent literature[237,380]. For this reason, the development of ADAmon-EpiM for epitope mapping will not be further discussed here, even though its preliminary validation was successful. The main focus of the following sections will be laid on the binding stability of ADA, which was analyzed in depth in the presented dissertation project. Additionally, the therapeutic value of temporal ADA dynamics, including persistence, will be evaluated.

4.2.1. DissR as new, robust indicator of ADA dissociation velocity

Classically, inter-molecular interactions are described and characterized by the kinetic parameter K_D, which represents affinity. Standard calculation of K_D is not possible for ADAmon results owed to the polyclonal nature of anti-drug antibodies and the resulting inability to determine absolute ADA concentrations[383–387]. As explained in **section 2.3.8**, k_d is the variable utilized most commonly to describe the dissociation of binding events in literature and is independent of analyte concentration[388–390].

The Biacore X100 software is poorly suited for the kinetic analysis of ADAmon runs. Analytic runs were performed using an automated wizard program. Within this method, the dissociation phase duration was set to 60 s. However, due to system-related, unmodifiable lag times, the actual dissociation monitoring time, during which running buffer flowed over the biosensor surface, was 300 s (see **section 2.3.6**). These settings were chosen in order to minimize the duration of ADAmon cycles. The evaluation software, however, considers only the first 60 s of the dissociation phase for kinetic analyses, which is too short for reliable k_d calculation. These complications could be circumvented by re-analyzing ADAmon data with the tool Anabel, such that k_d calculation was successful. However, for ADAmon results, k_d calculation is not necessarily reasonable, which will be explained in the following.

Beside ADA, ADAmon pulldown eluates possibly contain co-purified impurities, which may influence k_d determination. It cannot be excluded that some of these impurities interfere with ADAmon analytics, e.g., by binding to the Fc part of ADA. Heterophile antibodies, for example, could be co-purified with ADA and possibly exhibit faster dissociation from ADA compared to the ADA:IFX dissociation[391]. Thereby, the observed dissociation rate would not be representative of the pure analyte's behavior. In addition, the pre-analytic sample preparation differs significantly between the few studies that report anti-drug antibody binding stability[283,288,322,327,379,392,393]. For example, Beeg et al. used 1:30 diluted serum for SPR analysis of ADA, while for ADAmon, composition and dilution of the injected samples are largely different due to the pre-analytic purification[288,327]. Likely, the same sample processed according to the protocol by Beeg et al. and by the ADAmon method will deliver different k_d results due to differential non-specific binding. Reporting k_d from ADAmon results could therefore mislead the reader that ADAmon results can be recklessly compared to other k_d data in literature, which is not the case. In order to prevent such misplaced comparisons, the new parameter DissR was introduced in this work. The concept of DissR was adopted from a comparative kinetics approach for heterogeneous analytes, which has been suggested by Cytiva[325]. Since ADAmon is conceptualized for use in diagnostic laboratories, the vivid and simple concept of DissR is beneficial in view of the fact that most medical personnel is not familiar with binding kinetic analysis[302].

We have introduced DissR as a new and reliable indicator of ADA binding stability in the so far largest study to do so[287,322,327]. Not only the total number of included sera was high, but also the number of sera available per patient was exceptional among comparable studies, which makes us the first group to report insights into the temporal dynamics of ADA binding strength and their association with therapy outcome[283,322,327,379,392,393]. As a new parameter for ADA analysis in serum, DissR required validation. The validation data in **Figure 3.15A** suggest excellent repeatability of DissR. Furthermore, DissR was observed not to be confounded by analyte concentration and patient-individual serum components. ADA calibrator had a lower DissR as compared to IBD patient ADA (see **Figure 3.15A**). This difference met our expectations and confirmed results of similar

studies, as the monoclonal ADA calibrator was generated following affinity selection, while patient-individual anti-drug antibodies are polyclonal and hence also cover lower affinities, i.e. higher dissociation velocities[327,369,383,385–387,392,394]. In conclusion, our validation experiments confirmed that DissR is robust enough for the evaluation of ADA binding stability.

4.2.2. DissR and the diagnostic significance of ADA binding properties

For the approval of therapeutic antibodies, detailed characterization of the related immunogenic response is prescribed by regulatory authorities[365,395]. Joint efforts by authorities and industry have enabled the establishment and harmonization of methods for anti-drug antibody analysis, their validation and reporting[262]. Unfortunately, the same rigor in harmonization is missing for ADA analysis in routine TDM. Hence, knowledge on binding stability of anti-drug antibodies in patients is still very limited. Additionally, binding data comparability is hampered, as explained in 4.2.1. A summary of other studies reporting binding stability of anti-drug antibodies in patients is given in **Table 4.3**.

With 54 ADAmon-positive sera included, our study exhibited the by far largest sample size to characterize ADA:IFX binding stability. Both ADA detection and ADA quantification by ADAmon were less confounded by ADA binding stability as compared to ELISA. These findings were supported by the observation that ADAmon-only positive sera had a higher median DissR than sera, in which ADA were detectable by both ADAmon and ELISA (p=0.052). Beeg et al. reported a similar method comparison with even more distinct difference ($p < 0.001$)[327]. Analogously to ADA, the results from our anti-ADMmon biosensor also confirm these findings for anti-ADM (see **Figure 3.34B**). Beeg et al. share our hypothesis that these results suggest ELISA is susceptible to missing faster-dissociating ADA, which can be explained by the extensive washing inherent to the ELISA method. One must therefore once more note that ADA concentrations should always be interpreted with caution.

Our study is the first one to evaluate the temporal evolution of ADA DissR (see **Figure 3.23**). Overall, ADA DissR was predominantly stable over time in individual patients, except for three patients: W-IFX-6, W-IFX-10 and W-IFX-17. Even though DissR in W-IFX-6 was temporarily elevated, DissR eventually decreased in all these patients over time, which indicates the development of more stable ADA:IFX binding. A similar study has been published by Joyce et al. in 2022 for anti-drug antibodies directed against PF-06480605, an anti-TNF-like ligand 1A antibody, which is a drug candidate for treatment of IBD (see **Table 4.3**)[379]. In five patients, they also observed an increase in apparent anti-drug antibody affinity, which they attributed to a maturing immunogenic response. The most dramatic drop in apparent K_D was thereby recorded within 130 days after drug application. It is possible that DissR was more stable in our cohort because only patients in IFX remission maintenance therapy were considered, meaning that the monitored ADA response was already more mature and hence more stable.

Table 4.3.: Other publications on anti-drug antibody binding stability characterization in patient samples.

Reference	Method	$n_{samples}$*	Results summary
Takacs et al. (1999) [392]	SPR	1	**Drug:** Polyethylene glycol-interferon-α2b (PEG-IFN-α2b). **Patient:** Chronic hepatitis C. **Findings:** Binding stability was evaluated by visual comparison of the dissociation phases. Patient anti-PEG-IFN-α2b antibodies were faster-dissociating as compared to the positive control (sheep polyclonal anti-PEG-IFN-α2b).
Real-Fernández (2015) [283]	SPR	3	**Drug:** ADM. **Patients:** Juvenile idiopathic arthritis. **Findings:** Whole IgG and specific anti-ADM fractions were purified by affinity chromatography from patient serum and subjected to standard kinetic analysis. K_D results indicated stronger binding for purified anti-ADM as compared to IgG fractions.
Beeg et al. (2021) [327]	SPR	22	**Drug:** IFX. **Patients:** IBD. **Findings:** Of 22 ADA-positive sera by SPR, only 14 were also positive by a drug-sensitve ELISA. SPR-only positive sera had significantly faster-dissociating ADA than sera with ADA detectable by both methods, suggesting that ELISA misses fast-dissociating ADA.
Valsecchi et al. (2021) [393]	SPR, bio-layer interferometry	1	**Drug:** Emicizumab. **Patient:** Hemophilia A (pediatric). **Findings:** Anti-emicizumab antibodies were purified from plasma. SPR kinetic analysis resulted in a K_D of 5 – 35 nM. Bio-layer interferometry resulted in a similar K_D (8.3 nM) and unveiled that anti-emicizumab antibodies were mainly directed against the drug's Fab portion.
Joyce et al. (2022) [379]	Ligand binding assay (LBA)	26	**Drug:** PF-06480605 (anti-TNF-like ligand 1A antibody) **Patients:** IBD. **Findings:** Anti-drug antibodies were affinity-enriched from serum via magnetic beads. Apparent K_D was determined using a Singulex Erenna® System. The temporal development of apparent K_D in individual patients was evaluated. K_D decreased over time, likely owed to affinity maturation. K_D was negatively correlated with anti-drug antibody quantity.

*Refers to the number of samples that were analyzed for anti-drug antibody binding stability.

Beside these insights, we have for the first time discovered an association between DissR and IFX therapy outcome. The ADAmon data indicate that low DissR, i.e., high ADA:IFX stability, is linked to LOR and undetectable IFX trough concentrations. As soon as ADA are detected, DissR may serve as a prognostic parameter to assess the patient-individual risk for LOR. It is worth to mention that patient MRI-IFX-35 in **Figure 3.23** had fast-dissociating ADA, but at a very high concentration. Since this patient later experienced LOR, this case suggests that extreme ADA concentrations may counterbalance the lower risk profile of high-DissR ADA and shows the necessity for the clinician to consider both parameters – which are accessible by the ADAmon biosensor. Based on the new insights we provide through means of the ADAmon biosensor, DissR could serve as an additional TDM parameter to facilitate the decision whether a patient with detectable ADA should continue IFX therapy. Result congruence between our ADA DissR evaluation and literature on anti-drug antibodies directed against entirely different drugs implies that part of our results may be even generalized to anti-drug antibodies beyond ADA.

4.2.3. ADA dynamics: A rewarding fresh perspective on old (ELISA) data

Obviously, accessing new qualitative information about ADA, such as their binding properties, by novel analytic methods can add value to TDM. On the other hand, developing new statistical methods to evaluate ADA quantities can also improve therapy efficacy. Our approach to gain a fresh perspective on classic ADA data was to evaluate their timely dynamics, as described in **section 3.4**. We defined the new index S_{ADA}, which indicates the slope of ADA quantity during approximately 3.5 months after first ADA detection. Some clinicians consider TDM without ADA assessment sufficient due to the supposed inverse behavior of IFX and ADA serum concentrations[396]. In our study setup, positive S_{ADA}, i.e., net rising ADA concentration, was found to be a significant risk for LOR, while IFX dynamics were not found to be associated with therapy outcome. Hence, no inverse behavior was observed – probably owed to the aggressive, proactive dosage adjustment in the cohort, which confounded the relationship between IFX and ADA concentrations. Furthermore, positive S_{ADA} was identified to be an early predictor of ADA permanence. Previous studies have reported that permanent ADA are associated with higher risk to develop high ADA concentrations and LOR as compared to transient ADA, which aligns with our results[240,254,397].

A mechanistic hypothesis for the observed significance of ADA dynamics in the first months of their appearance is that the initial immune response against IFX may be indicative of its therapeutic manageability. The time frame for S_{ADA} calculation allows for first dosage increases, if applicable, and hence already contains information about possible responsiveness to intervention. Consequently, positive S_{ADA} in spite of dose increases might be an indication that (i) the patient does not respond to the intervention and (ii) the developed ADA are permanent, which both suggest high risk of LOR. For these patients, switching to another drug may be reasonable.

In summary, S_{ADA} was found to be an easily accessible, early predictor of IFX therapy outcome. Its application in TDM could help clinicians to standardize therapeutic decision-making. We suggest that S_{ADA} above the critical cut-off should alert the gastroenterologist to closely monitor the patient and to consider therapeutic intervention. In order to ensure that ADA are detected as closely as possible to first emergence, we recommend proactive TDM in the beginning of IFX therapy. A combination of ADA dynamics, accurate clinical evaluation and other promising new TDM tools, such as population pharmacokinetic models for dashboard-driven dose adjustments, may increase the efficacy of IFX TDM[398–401].

4.3. Prospects of IFXmon and ADAmon in TDM: Can the idea hold up to real-life patient care needs?

In the previous sections, assay performance, economic feasibility and the diagnostic value of the herein developed SPR biosensors IFXmon and ADAmon have been showcased. Still, important questions remain to be answered: In view of the state of the art and emerging needs in current TDM strategies, do IFXmon and ADAmon sufficiently address the needs of patients and medical personnel? And, if so, how can the potential benefits of the developed biosensors add maximum value when integrated into daily routine laboratory analytics? First, in order to answer these questions, the topical trends and debates concerning TDM and analytic strategies for IFX treatment will be outlined. Then, IFXmon and ADAmon will be discussed in light of the current IFX TDM trends.

4.3.1. Current trends in IFX TDM

Several international expert committees have set themselves the goal of reviewing the partially controversial data situation in order to explore how TDM can be used successfully in biologic therapies. In this regards, the Int**E**rnational **C**onsortium of **T**herapeutic d**RU**ug **M**onitoring (spECTRUM), for example, has written an up-to-date and comprehensive review on developments in TDM for biologic therapies in IBD[252]. Current discussions regarding IFX TDM strategies concern (i) the benefits of proactive vs. reactive TDM, (ii) the diagnostic value of drug-tolerant ADA quantification and (iii) the therapeutic utility of more rapidly available TDM results[252]. These aspects will be complemented by an overview of (iv) additional emerging tools or strategies.

In biologic therapies, the definition of reactive TDM is restricted to the monitoring of drug and anti-drug antibodies if the disease remains active or the patient falls into relapse despite therapy[252,402]. Proactive TDM, on the contrary, describes scheduled monitoring – also when the patient displays no objective signs of active disease[252,402]. In TNF antagonist literature, most studies on proactive TDM evaluated the post-induction phase and include monitoring schemes between unique and monthly or even more fre-

quent measurements (e.g., during therapy induction)[247,343,396,403–415]. This ambiguity certainly contributes to the controversial data on the question whether proactive TDM improves patient outcome and is economically feasible. The European Crohn's and Colitis Organization (ECCO), American Gastroenterological Association (AGA) and American College of Gastroenterology (ACG) conditionally endorse reactive TDM for TNF antagonist treatment in IBD[368,416–418]. The Gastroenterological Society of Australia (GESA) suggests regular proactive TDM in cases where TDM results are likely to affect therapy decision-making[255]. However, the gastroenterology associations are very reluctant to make recommendations for or against proactive TDM given the equivocal nature of the studies[220,255,416–420]. For example, Bossuyt et al. recently published a trial, in which they compared ultra-proactive TDM via a point-of-care test with reactive TDM in IBD patients on IFX maintenance therapy[421]. Even though more dose adjustments were performed in the ultra-proactive TDM group, similar clinical outcomes were observed after one year[421]. The authors hence concluded that an ultra-proactive TDM strategy is not suitable for all patients[421]. Nonetheless, evidence is accumulating that proactive TDM can lead to improved patient outcomes, for example with respect to endoscopic remission, perianal fistula healing, treatment response durability and cost effectiveness[247,343,396,403–415]. Meta-analyses are needed to generate evidence-based guidelines, which in turn require a higher number of prospective studies as well as studies investigating the effect of proactive TDM during the induction phase[252,422].

Regardless of the TDM scheme, TDM data are influenced significantly by assay choice, as previously discussed. In this context, the diagnostic utility of drug-tolerant assays is currently discussed controversially. Drug-tolerant assays generally result in earlier ADA detection as well as higher ADA detection rates and are more likely to detect transient ADA as compared to drug-sensitive assays[248,250,255,266,368,423]. Van Stappen et al. published a post hoc analysis of the Trough Concentration Adapted Infliximab Treatment (TAXIT) trial[247,368]. Here, patients with subtherapeutic IFX and who underwent dose escalation were selected from the TAXIT cohort. One respective TDM serum was available from before and after dose escalation and from one year after optimization. These sera were retrospectively re-analyzed with an optimized drug-sensitive and an in-house developed drug-tolerant ELISA in order to compare the impacts of dose optimization on ADA. Overall, no clinical benefit for drug-tolerant ADA determination in stable clinical remission was observed. However, in 8 % of sera with ADA in the highest ADA concentration quartile according to the drug-tolerant assay, ADA were missed by the drug-sensitive assay. In the third ADA concentration quartile, ADA were not detected by the drug-sensitive ELISA in 58 % of sera. Since the presence or absence of ADA together with low IFX can direct the treating clinician to different therapy decisions, this difference should not be neglected[246]. Furthermore, both the patient selection from the TAXIT cohort for post hoc analysis and the decision for IFX optimization were based on the results of a drug-sensitive ADA assay[247,368]. Thus, the baseline for the post hoc study was likely subjected to a bias that should be kept in mind when interpreting the results. A review with

statements worth a second look was published by Mitrev et al., who stated that the ADA detected by drug-tolerant, but not drug-sensitive assays are majorly non-neutralizing [255]. Based on this assumption the authors infer that the hereby additionally detected ADA are clinically irrelevant, as they are not impairing IFX function. Atiqi et al., on the other hand, argue that this assumption is to be doubted, since low-titer ADA, as detected by drug-tolerant assays, may simply not be detectable by the lower-sensitivity neutralization assays [237]. They suggest that low-titer ADA are indeed neutralizing, but are missed by neutralization assays. Vande Casteele et al. see drug-tolerant ADA assays as a future standard method to monitor the immunogenicity of biologics, especially those with higher application frequency [250]. Prospective studies with larger cohorts and more research in general are required for significant conclusions on this topic [373]. Therefore, one should remain open to discussion regarding the clinical significance of drug-tolerant assays until more robust evidence is available.

In terms of assay performance in the TDM of biologics, not only matters the quality of the data itself, but assay duration is also becoming increasingly important. The time between blood collection and result availability is usually hours to days. Since according to guidelines, IFX TDM utilizes serum trough levels immediately before the next drug administration, therapeutic measures can often only be taken weeks after testing [220,417,419]. To investigate and address this lag time, the incorporation of faster laboratory analytics including point-of-care technologies into patient care are currently under discussion [250,252,286,424,425]. Beside assay lag times, dose optimization may demand pre-authorization from health insurance companies, which can delay therapeutic intervention. Also, attempts have been made to perform TDM at other time points within the dose cycle, e.g., at the peak level shortly after drug administration or at intermediate time points within the cycle [252,426–429]. Ungar et al. have shown that in the case of ADM, which is administered at high frequency, ADM levels were comparable at different TDM time points within a single injection cycle [427]. In the future, some new tools might aid to rationalize therapeutic decisions in biologic therapies, such as pharmacokinetic dashboards and pharmacogenomics. Based on the known association between drug clearance and therapy outcome, pharmacokinetic dashboards are employed to generate a forecast for customized, optimal drug dosing [430–432]. These integrate patient-specific clinical, biochemical and pharmacokinetic data as well as population pharmacokinetic models, which take into account important variables influencing drug metabolism [398–401,431,433]. Beside anti-drug antibodies, pharmacokinetics of biologics are known to be affected by body weight, sex, hSA and FcRn polymorphisms, to name just a few examples [252,434,435]. Pharmacogenomic data may also be integrated into dashboards, since various associations between genetic variants and the pharmacokinetics of TNF antagonists have been found [227–231]. For example, the HLA allele DQA1*05 has been identified as a risk factor for developing ADA and anti-ADM in CD patients and Billiet et al. have reported genetic variations of FcRn that are associated with TNF antagonist clearance [227,229,230]. Both pharmacokinetic dashboards as well as pharmacogenomic data may be exploited in the future to decide for example, whether a proactive

TDM strategy is feasible in individual patients. In summary, current trends suggest that in the future, therapy with TNF antagonists and other biologics will be more tailored to the individual patient. For this purpose, more complex data will be incorporated into therapeutic algorithms in order to optimally adjust patients and ensure cost-efficient drug administration.

4.3.2. Utility of IFXmon and ADAmon in real-life TDM

IFXmon and ADAmon were developed with the long-term goal of finding application in routine analytics. Accordingly, method development was aligned with new developments and trends in TNF antagonist therapeutic management and the strengths of the SPR methodology were advantageously incorporated. Our patient study results suggest that both drug tolerance and a proactive TDM strategy may be therapeutically beneficial when utilizing IFXmon and ADAmon: Regular TDM and drug-tolerant ADA assessment, especially during the induction phase and at the beginning of maintenance therapy, allow early ADA detection. As we found that DissR remained mostly stable over time and that it was significantly associated with therapy success, early availability of potentially prognostic DissR data might accelerate therapy optimization. If low-DissR ADA are detected at an early time point, it may be beneficial to optimize the dose and monitor IFX and ADA more often in spite of acceptable IFX concentrations. Especially in the low or moderate concentration range, ADA quantity alone is less meaningful, as the clinician does not known at their first emergence whether the ADA are permanent or transient. Furthermore, ADA concentration interpretation is more inconclusive. As a prognostic parameter, DissR may even be integrated into pharmacokinetic models if further studies confirm its significance. Given the promising results of our study, the clinical implications of ADA binding stability warrant further research. As a first conclusion, it can be said that our data endorse the emerging evidence for both proactive TDM and drug-tolerant ADA quantification.

By producing both quantitative and qualitative data, ADAmon aligns with the current TDM trend towards the handling of higher data complexity as it generates a higher data density as compared to ELISA, for example. When combined with IFXmon or other biosensors, as touched upon earlier (see **section 4.1.3**), the generated data density can be increased even further with almost no increase in workload. Even though the total duration of IFXmon and ADAmon analytic run sequences is relatively long (see **section 4.2**), the duration of single analyses is considerably shorter as compared to ELISA. Thus, the results of individual patients' analyses could be exported to medical reports while the analytic sequence is still ongoing. It would even be conceivable to perform TDM analyses in a point-of-care manner at care centers with laboratory infrastructure: If patient visits can be planned reliably, which more likely applies to specialized clinics, the analytic run sequence could be aligned with patient visits, such that results may be available within the duration of the appointment. However, this hypothetical strategy is more

cumbersome for ADAmon due to the pre-analytic sample processing. For this means, it would be feasible to automatize and optimize the pre-analytic procedures in order to generate a faster protocol with reduced hands-on time. While the SPR principles are likely to be very easily transferred to high-throughput instruments, especially those from Cytiva, the automation and further optimization of ADAmon pre-analytics is a more elaborate challenge, but one that should be surmountable. It can be summarized that IFXmon and ADAmon in their current form are not optimized for routine diagnostic procedures. Considering the promising results of IFXmon and ADAmon, which fit well with current trends in TNF-antagonist TDM, the effort of the still outstanding optimizations may be worthwhile. This applies not only for IFX TDM, but, given the demonstrated ease of assay transferability to ADM, also to other biologics.

4.4. Limitations of the developed SPR biosensor assays and patient studies

The present work benefited significantly from the real-world patient cohort, which was subject to an aggressive, proactive TDM strategy. Only the access to these patients allowed us to uncover the previously discussed, unparalleled associations between ADA binding properties and therapy outcome. However, it must be pointed out that the results of the present doctoral thesis project comprise some limitations, some of which have already been mentioned in other sections.

Both CD and UC patients were pooled in our evaluations to increase sample size. However, it is possible that IBD phenotype may have an impact on some of the associations examined in this project[252,436]. When interpreting the quantitative data of the herein developed biosensors, some restrictions have to be considered. The method comparison regression results between IFXmon or ADAmon with ELISA are only applicable to the specified ELISA methods by Immundiagnostik and cannot be generalized to other, not even to similar, ELISA formats. As indicated previously, especially for ADA quantification, method agreement is sometimes very poor even between ELISA[251,276,437]. Nevertheless, congruence of our method comparison findings with data from similar studies, especially the two publications from Beeg et al., imply that our results are transferable to some other ELISA formats[288,327]. However, it must be emphasized that these results should not be taken as generalizable, but that method comparability should be assessed separately for each assay. In addition, the results of the ADAmon-EpiM, ADMmon and anti-ADMmon assays should be interpreted with caution, since only preliminary verification experiments with small sample sizes were performed for these biosensors.

Not only quantitative biosensor data have to be interpreted with caution, but also all data regarding the qualitative parameter DissR. First of all, ADA pulldown eluates are by far less complex as compared to serum samples, but they do not contain ADA alone. Thus, it is possible that some patient sera contain specific impurities that potentially

confound DissR and have not been covered by our DissR validation experiments, as already indicated in **section 4.2.1**[391]. However, the suggested plausibility check via Fc1 evaluation can probably identify some of the sera at risk of falsified results through confounding nonspecific binders. Furthermore, the interpretation of DissR data regarding the outcome LOR is limited as only ten patients were available with confirmed LOR. While the LOR outcome is unambiguous, the classification of patients into the remission group is less final. It must be taken into account that remission patients may still experience treatment failure in the future, particularly because the considered duration of therapy differed between patients. We could partly circumvent the low number of LOR patients by grouping patients according to their IFX concentration, which itself is strongly correlated with therapy outcome. Nevertheless, it would be useful to evaluate a larger number of ADA-positive subjects with respect to therapy outcome[341,342]. Accordingly, our DissR data build a promising base that warrants further investigations.

Manifold studies in literature have demonstrated that diagnostically relevant analytes and even gene mutations can be analyzed with SPR, but SPR methods have not yet found their way into routine diagnostics[438–445]. Compared with ELISA, for example, SPR biosensors require more effort for their implementation in medical laboratories: Beside the expensive specialized equipment, personnel needs to be trained adequately, as typically, both medical laboratory technicians and laboratory physicians do not interface with SPR technology. The establishment of mass spectrometry in routine diagnostics, however, demonstrates that method complexity and routine application are not mutually exclusive if the method adds value[370,371]. Even though the proposed SPR biosensors IFXmon and ADAmon comprise reduced hands-on time as compared to ELISA, they are less time-efficient in their current assay formats. Multiplexing and automation are desirable outlooks of the developed biosensors to gain attractiveness for routine diagnostics. However, these processes have yet to be implemented in the future.

4.5. Conclusions

Despite decades of experience in the use of IFX for IBD treatment, ADA emergence remains a significant concern. Monitoring ADA concentrations, identifying patients at risk of developing ADA and implementing appropriate strategies to manage immunogenicity are major cornerstones for optimizing treatment outcomes in IBD patients. Our understanding of these cornerstones is still incomplete and the development of evidence-based consensus strategies for ADA management is still ongoing. On one hand, the establishment of therapeutic consensus is hampered by lack of harmonization in analytic methods, study design and reporting. On the other hand, we hypothesized that the current, predominantly quantitative, nature of ADA data by state of the art assays may be insufficient to make informed decisions.

Addressing the need for more powerful methodology, the main objective of the present

dissertation project was the development of SPR biosensor assays for measuring the exemplary TNF antagonist IFX and corresponding ADA in human serum. Through development of proof-of-concept biosensor assays, reliable and robust quantification of the analytes of interest within the respective physiologically meaningful analytic range should be demonstrated. Beside comprising comparable analytic sensitivity as ELISA, SPR biosensors offer advantages such as real-time monitoring, label-free detection, multiplexing capability, small sample volume requirement and automation potential. Especially for the more cumbersome ADA analytics, the particular advantages of the SPR methodology were exploited to generate both quantitative and qualitative data that other immunoassay methods cannot provide. By this means, it was investigated whether knowledge about ADA quality – particularly about ADA binding properties – adds diagnostic value in IFX therapy management.

The successful accomplishment of the following milestones within the present dissertation project can be reported:

1. A biosensor "IFXmon" for monitoring serum IFX concentrations was developed. A unique ligand cross-linking strategy increased the biosensor lifespan. IFXmon comprised acceptable analytic sensitivity similar to diagnostics-approved assays. IFX quantification was highly precise and accurate over the entire diagnostically relevant range. Method comparison regression with a diagnostics-approved ELISA resulted in method interchangeability, regardless whether originator or biosimilar IFX was quantified. Altogether, the present findings strongly suggest that IFXmon performance suffices diagnostic standards.

2. A biosensor "ADAmon" for ADA quantification was established, including an easy and rapid protocol for pre-analytic ADA enrichment from serum. Pre-analytic sample processing was required for the ADAmon assay due to technical specifications of the Biacore X100 instrument and interference of IFX with ADA quantification. This step yields enriched and purified ADA and is therefore beneficial in terms of assay sensitivity, instrument wear-out and subsequent ADA binding stability characterization. ADA pulldown yields were reproducible in presence of variable, high molar excess of IFX and drug tolerance was demonstrated by different methods. The ADAmon regeneration procedure enabled high sensor stability over many analytic cycles. This work covers the first method comparison of a drug-tolerant SPR assay for ADA analysis with a drug-tolerant ELISA. ADAmon performance was overall within the validation limits for diagnostic methods and comparable to ELISA, only analytic sensitivity and assay precision were slightly inferior. In line with literature, correlation of ADA quantification between ADAmon and ELISA was poor, whereby ELISA consistently reported significantly lower ADA concentrations as compared to ADAmon. Our results thus imply that ADAmon and ELISA likely assess different, ADA quality-dependent ADA populations. Additionally, a data evaluation strategy to obtain sample-individual plausibility controls was established in order to identify

sera causing analytic interference. In conclusion, ADAmon was demonstrated to meet diagnostic quality standards and to bring useful analytic features to the table.

3. With DissR, an easily accessible and robust index for ADA:IFX binding stability characterization was established, which can be retrieved from ADAmon analytic runs without any need for further experimental processing or additional sample material. After successful proof-of-principle and validation evaluations, DissR was retrospectively calculated for ADAmon-positive patients in the so far largest study to analyze ADA:IFX binding stability. Our study was the first to investigate into the temporal evolution of ADA:IFX binding stability, which uncovered that DissR may exhibit prognostic potential with respect to IFX therapy outcome. We found that high ADA:IFX binding stability was significantly correlated with future LOR and undetectable IFX concentrations in individual patients. Overall, our data on DissR provide a promising foundation for future studies to further explore its utility for personalized medicine.

4. First attempts to transfer the assay principles of IFXmon and ADAmon to ADM as another widely used TNF antagonist demonstrated that the established assay platforms can be adapted extremely fast. The anti-ADMmon biosensor in particular was able to validate the results of the ADAmon study. DissR evaluations utilizing anti-ADMmon confirmed the weakness of ELISA in assessing low-affinity anti-drug antibodies and that high anti-drug antibody binding stability is associated with low drug levels.

5. In addition to the in-house development of novel analytic techniques, a new statistical method to evaluate ADA quantities was devised. We were able to demonstrate that – especially in patients with aggressive dose intensification policies – ADA dynamics rather than punctual concentrations have predictive value with respect to LOR towards IFX therapy. Herein, S_{ADA} was defined as an easily accessible index to assess the patient-individual risk for IFX LOR.

In conclusion, the present work provides new insights on the performance and capabilities of SPR biosensor assays for IFX and ADA assessment – especially in direct comparison to ELISA, which find good agreement in recent literature. It attests that SPR can keep up with other analytic methods in terms of practical and economic feasibility. Our data suggest that ELISA methods are susceptible to missing faster-dissociating anti-drug antibodies, while SPR-based quantification is more robust against confounding by DissR. As long as the role of low-affinity ADA in IBD is unknown, it would be reasonable to employ analytic methods able to detect them in order to correctly decipher ADA pathophysiology. Our findings highlight the potential of SPR-based anti-drug antibody quantification, which could even be exploited to assess the DissR bias of other available ADA quantification methods and re-evaluate their performance and suitability. If future studies confirm our data, DissR assessment embedded into a proactive TDM strategy may facilitate and accelerate therapeutic decisions for the benefit of the patient.

Bibliography

[1] Medzhitov R. Origin and physiological roles of inflammation. *Nature*. 2008;454(7203):428–435.

[2] Takeuchi O and Akira S. Pattern recognition receptors and inflammation. *Cell*. 2010;140(6):805–820.

[3] McInnes IB and Gravallese EM. Immune-mediated inflammatory disease therapeutics: Past, present and future. *Nat Rev Immunol*. 2021;21(10):680–686.

[4] Schett G, McInnes IB and Neurath MF. Reframing immune-mediated inflammatory diseases through signature cytokine hubs. *N Engl J Med*. 2021;385(7):628–639.

[5] Baumgart DC and Carding SR. Inflammatory bowel disease: Cause and immunobiology. *Lancet*. 2007;369(9573):1627–1640.

[6] Plevris N and Lees CW. Disease monitoring in inflammatory bowel disease: Evolving principles and possibilities. *Gastroenterology*. 2022;162(5):1456–1475.e1.

[7] Baumgart DC. The diagnosis and treatment of Crohn's disease and ulcerative colitis. *Dtsch Arztebl International*. 2009;106(8):123–133.

[8] Ng SC, Shi HY, Hamidi N, Underwood FE, Tang W et al. Worldwide incidence and prevalence of inflammatory bowel disease in the 21st century: A systematic review of population-based studies. *Lancet*. 2017;390(10114):2769–2778.

[9] Mak WY, Zhao M, Ng SC and Burisch J. The epidemiology of inflammatory bowel disease: East meets west. *J Gastroenterol Hepatol*. 2020;35(3):380–389.

[10] Zhao M, Gönczi L, Lakatos PL and Burisch J. The burden of inflammatory bowel disease in Europe in 2020. *J Crohns Colitis*. 2021;15(9):1573–1587.

[11] Burisch J, Jess T, Martinato M and Lakatos PL on behalf of ECCO EpiCom. The burden of inflammatory bowel disease in Europe. *J Crohns Colitis*. 2013;7(4):322–337.

[12] van Linschoten RCA, Visser E, Niehot CD, van der Woude CJ, Hazelzet JA et al. Systematic review: Societal cost of illness of inflammatory bowel disease is increasing due to biologics and varies between continents. *Aliment Pharmacol Ther*. 2021;54(3):234–248.

[13] Frøslie KF, Jahnsen J, Moum BA and Vatn MH. Mucosal healing in inflammatory bowel disease: Results from a Norwegian population-based cohort. *Gastroenterology*. 2007;133(2):412–422.

[14] Solberg IC, Vatn MH, Høie O, Stray N, Sauar J et al. Clinical course in Crohn's disease: Results of a Norwegian population-based ten-year follow-up study. *Clin Gastroenterol Hepatol*. 2007;5(12):1430–1438.

[15] Burisch J, Katsanos KH, Christodoulou DK, Barros L, Magro F et al. Natural disease course of ulcerative colitis during the first five years of follow-up in a European population-based inception cohort—an Epi-IBD study. *J Crohns Colitis.* 2019;13(2):198–208.

[16] Burisch J, Kiudelis G, Kupcinskas L, Kievit HAL, Andersen KW et al. Natural disease course of Crohn's disease during the first 5 years after diagnosis in a European population-based inception cohort: An Epi-IBD study. *Gut.* 2019;68(3):423–433.

[17] Laass MW, Roggenbuck D and Conrad K. Diagnosis and classification of Crohn's disease. *Autoimmun Rev.* 2014;13(4-5):467–471.

[18] Annese V, Daperno M, Rutter MD, Amiot A, Bossuyt P et al. European evidence based consensus for endoscopy in inflammatory bowel disease. *J Crohns Colitis.* 2013;7(12):982–1018.

[19] Spiceland CM and Lodhia N. Endoscopy in inflammatory bowel disease: Role in diagnosis, management, and treatment. *World J Gastroenterol.* 2018;24(35):4014–4020.

[20] Wehkamp J, Götz M, Herrlinger K, Steurer W and Stange EF. Inflammatory bowel disease: Crohn's disease and ulcerative colitis. *Dtsch Arztebl International.* 2016;113(5):72–82.

[21] Peyrin-Biroulet L, Loftus EVJ, Colombel JF and Sandborn WJ. The natural history of adult Crohn's disease in population-based cohorts. *Off J Am Coll Gastroenterol.* 2010;105(2):289–297.

[22] Rubbino F, Greco L, di Cristofaro A, Gaiani F, Vetrano S et al. Journey through Crohn's disease complication: From fistula formation to future therapies. *J Clin Med.* 2021;10(23):5548.

[23] Danese S and Fiocchi C. Ulcerative colitis. *N Engl J Med.* 2011;365(18):1713–1725.

[24] Rankin GB, Watts H, Melnyk CS and Kelley ML. National cooperative Crohn's disease study: Extraintestinal manifestations and perianal complications. *Gastroenterology.* 1979;77(4, Part 2):914–920.

[25] Bernstein CN, Blanchard JF, Rawsthorne P and Yu N. The prevalence of extraintestinal diseases in inflammatory bowel disease: A population-based study. *Am J Gastroenterol.* 2001;96(4):1116–1122.

[26] Ricart E, Panaccione R, Loftus EV Jr., Tremaine WJ, Harmsen WS et al. Autoimmune disorders and extraintestinal manifestations in first-degree familial and sporadic inflammatory bowel disease: A case–control study. *Inflamm Bowel Dis.* 2004;10(3):207–214.

[27] Lakatos PL, Szamosi T and Lakatos L. Smoking in inflammatory bowel diseases: Good, bad or ugly? *World J Gastroenterol.* 2007;13(46):6134–6139.

[28] Ott C and Schölmerich J. Extraintestinal manifestations and complications in IBD. *Nat Rev Gastroenterol Hepatol.* 2013;10:585–595.

[29] Itzkowitz SH and Present DH. Consensus conference: Colorectal cancer screening and surveillance in inflammatory bowel disease. *Inflamm Bowel Dis.* 2005;11(3):314–321.

[30] Biancone L, Michetti P, Travis S, Escher JC, Moser G et al. European evidence-based consensus on the management of ulcerative colitis: Special situations. *J Crohns Colitis.* 2008;2(1):63–92.

[31] Høivik ML, Moum B, Solberg IC, Henriksen M, Cvancarova M et al. Work disability in inflammatory bowel disease patients 10 years after disease onset: Results from the IBSEN Study. *Gut.* 2013;62(3):368–375.

[32] Michael MD, Bálint A, Lovász BD, Gulácsi L, Strbák B et al. Work disability and productivity loss in patients with inflammatory bowel diseases in Hungary in the era of biologics. *Eur J Health Econ.* 2014;15(1):121–128.

[33] Cellier C, Sahmoud T, Froguel E, Adenis A, Belaiche J et al. Correlations between clinical activity, endoscopic severity, and biological parameters in colonic or ileocolonic Crohn's disease. A prospective multicentre study of 121 cases. The Groupe d'Etudes Thérapeutiques des Affections Inflammatoires Digestives. *Gut.* 1994;35(2):231–235.

[34] Jones J, Loftus EV, Panaccione R, Chen L, Peterson S et al. Relationships between disease activity and serum and fecal biomarkers in patients with Crohn's disease. *Clin Gastroenterol Hepatol.* 2008;6(11):1218–1224.

[35] Gracie DJ, Williams CJM, Sood R, Mumtaz S, Bholah HM et al. Poor correlation between clinical disease activity and mucosal inflammation, and the role of psychological comorbidity, in inflammatory bowel disease. *Am J Gastroenterol.* 2016;111(4):541–551.

[36] Norouzinia M, Chaleshi V, Alizadeh AHM and Zali MR. Biomarkers in inflammatory bowel diseases: Insight into diagnosis, prognosis and treatment. *Gastroenterol Hepatol Bed Bench.* 2017;10(3):155–167.

[37] Pineton de Chambrun G, Blanc P and Peyrin-Biroulet L. Current evidence supporting mucosal healing and deep remission as important treatment goals for inflammatory bowel disease. *Expert Rev Gastroenterol Hepatol.* 2016;10(8):915–927.

[38] Danese S, Fiorino G and Peyrin-Biroulet L. Early intervention in Crohn's disease: Towards disease modification trials. *Gut.* 2017;66(12):2179–2187.

[39] Ungaro RC, Yzet C, Bossuyt P, Baert FJ, Vanasek T et al. Deep remission at 1 year prevents progression of early Crohn's disease. *Gastroenterology.* 2020;159(1):139–147.

[40] Plevris N, Fulforth J, Lyons M, Siakavellas SI, Jenkinson PW et al. Normalization of fecal calprotectin within 12 months of diagnosis is associated with reduced risk of disease progression in patients with Crohn's disease. *Clin Gastroenterol Hepatol.* 2021;19(9):1835–1844.e6.

[41] Flynn S and Eisenstein S. Inflammatory bowel disease presentation and diagnosis. *Surg Clin North Am.* 2019;99(6):1051–1062.

[42] Daperno M, D'Haens G, Van Assche G, Baert F, Bulois P et al. Development and validation of a new, simplified endoscopic activity score for Crohn's disease: The SES-CD. *Gastrointest Endosc.* 2004;60(4):505–512.

[43] D'Haens G, Sandborn WJ, Feagan BG, Geboes K, Hanauer SB et al. A review of activity indices and efficacy end points for clinical trials of medical therapy in adults with ulcerative colitis. *Gastroenterology.* 2007;132(2):763–786.

[44] Samuel S, Bruining DH, Loftus EV, Becker B, Fletcher JG et al. Endoscopic skipping of the distal terminal ileum in Crohn's disease can lead to negative results from ileocolonoscopy. *Clin Gastroenterol Hepatol.* 2012;10(11):1253–1259.

[45] Pepys MB and Hirschfield GM. C-reactive protein: A critical update. *J Clin Invest.* 2003;111(12):1805–1812.

[46] Volanakis JE. Human C-reactive protein: Expression, structure, and function. *Mol Immunol.* 2001;38(2):189–197.

[47] Peyrin-Biroulet L, Reinisch W, Colombel JF, Mantzaris GJ, Kornbluth A et al. Clinical disease activity, C-reactive protein normalisation and mucosal healing in Crohn's disease in the SONIC trial. *Gut.* 2014;63(1):88–95.

[48] Røseth AG, Fagerhol MK, Aadland E and Schjønsby H. Assessment of the neutrophil dominating protein calprotectin in feces: A methodologic study. *Scand J Gastroenterol.* 1992;27(9):793–798.

[49] Ministro P and Martins D. Fecal biomarkers in inflammatory bowel disease: How, when and why? *Expert Rev Gastroenterol Hepatol.* 2017;11(4):317–328.

[50] Bressler B, Panaccione R, Fedorak RN and Seidman EG. Clinicians' guide to the use of fecal calprotectin to identify and monitor disease activity in inflammatory bowel disease. *Can J Gastroenterol Hepatol.* 2015;29(7):852723.

[51] Gajendran M, Loganathan P, Catinella AP and Hashash JG. A comprehensive review and update on Crohn's disease. *Dis Mon.* 2018;64(2):20–57.

[52] Wallace KL, Zheng LB, Kanazawa Y and Shih DQ. Immunopathology of inflammatory bowel disease. *World J Gastroenterol.* 2014;20(1):6–21.

[53] Graham DB and Xavier RJ. Pathway paradigms revealed from the genetics of inflammatory bowel disease. *Nature.* 2020;578(7796):527–539.

[54] Agrawal M, Allin KH, Petralia F, Colombel JF and Jess T. Multiomics to elucidate inflammatory bowel disease risk factors and pathways. *Nat Rev Gastroenterol Hepatol.* 2022;19(6):399–409.

[55] Ramos GP and Papadakis KA. Mechanisms of disease: Inflammatory bowel diseases. *Mayo Clin Proc.* 2019;94(1):155–165.

[56] Rosenstiel P, Sina C, Franke A and Schreiber S. Towards a molecular risk map—Recent advances on the etiology of inflammatory bowel disease. *Semin Immunol.* 2009;21(6):334–345.

[57] Halfvarson J. Genetics in twins with Crohn's disease: Less pronounced than previously believed? *Inflamm Bowel Dis.* 2011;17(1):6–12.

[58] Xavier RJ and Podolsky DK. Unravelling the pathogenesis of inflammatory bowel disease. *Nature.* 2007;448(7152):427–434.

[59] Jostins L, Ripke S, Weersma RK, Duerr RH, McGovern DP et al. Host–microbe interactions have shaped the genetic architecture of inflammatory bowel disease. *Nature.* 2012;491(7422):119–124.

[60] Liu JZ, van Sommeren S, Huang H, Ng SC, Alberts R et al. Association analyses identify 38 susceptibility loci for inflammatory bowel disease and highlight shared genetic risk across populations. *Nat Genet.* 2015;47(9):979–986.

[61] Ogura Y, Bonen DK, Inohara N, Nicolae DL, Chen FF et al. A frameshift mutation in NOD2 associated with susceptibility to Crohn's disease. *Nature.* 2001;411(6837):603–606.

[62] Mukherjee T, Hovingh ES, Foerster EG, Abdel-Nour M, Philpott DJ and Girardin SE. NOD1 and NOD2 in inflammation, immunity and disease. *Arch Biochem Biophys.* 2019;670:69–81.

[63] Hampe J, Franke A, Rosenstiel P, Till A, Teuber M et al. A genome-wide association scan of nonsynonymous SNPs identifies a susceptibility variant for Crohn disease in ATG16L1. *Nat Genet.* 2007;39(2):207–211.

[64] Rioux JD, Xavier RJ, Taylor KD, Silverberg MS, Goyette P et al. Genome-wide association study identifies new susceptibility loci for Crohn disease and implicates autophagy in disease pathogenesis. *Nat Genet.* 2007;39(5):596–604.

[65] McCarroll SA, Huett A, Kuballa P, Chilewski SD, Landry A et al. Deletion polymorphism upstream of IRGM associated with altered IRGM expression and Crohn's disease. *Nat Genet.* 2008;40(9):1107–1112.

[66] Bevins CL and Salzman NH. Paneth cells, antimicrobial peptides and maintenance of intestinal homeostasis. *Nat Rev Microbiol.* 2011;9(5):356–368.

[67] Deuring JJ, Fuhler GM, Konstantinov SR, Peppelenbosch MP, Kuipers EJ et al. Genomic ATG16L1 risk allele-restricted Paneth cell ER stress in quiescent Crohn's disease. *Gut.* 2014;63(7):1081–1091.

[68] Adolph TE, Tomczak MF, Niederreiter L, Ko HJ, Böck J et al. Paneth cells as a site of origin for intestinal inflammation. *Nature.* 2013;503(7475):272–276.

[69] Duerr RH, Taylor KD, Brant SR, Rioux JD, Silverberg MS et al. A genome-wide association study identifies IL23R as an inflammatory bowel disease gene. *Science.* 2006;314(5804):1461–1463.

[70] Rivas MA, Beaudoin M, Gardet A, Stevens C, Sharma Y et al. Deep resequencing of GWAS loci identifies independent rare variants associated with inflammatory bowel disease. *Nat Genet.* 2011;43(11):1066–1073.

[71] Huang H, Fang M, Jostins L, Umićević Mirkov M, Boucher G et al. Fine-mapping inflammatory bowel disease loci to single-variant resolution. *Nature.* 2017;547(7662):173–178.

[72] Fossiez F, Djossou O, Chomarat P, Flores-Romo L, Ait-Yahia S et al. T cell interleukin-17 induces stromal cells to produce proinflammatory and hematopoietic cytokines. *J Exp Med.* 1996;183(6):2593–2603.

[73] Jovanovic DV, Di Battista JA, Martel-Pelletier J, Jolicoeur FC, He Y et al. IL-17 stimulates the production and expression of proinflammatory cytokines, IL-β and TNF-α, by human macrophages. *J Immunol.* 1998;160(7):3513–3521.

[74] Awane M, Andres PG, Li DJ and Reinecker HC. NF-kappa B-inducing kinase is a common mediator of IL-17-, TNF-alpha-, and IL-1 beta-induced chemokine promoter activation in intestinal epithelial cells. *J Immunol.* 1999;162(9):5337–5344.

[75] Fujino S, Andoh A, Bamba S, Ogawa A, Hata K et al. Increased expression of interleukin 17 in inflammatory bowel disease. *Gut.* 2003;52(1):65–70.

[76] Rovedatti L, Kudo T, Biancheri P, Sarra M, Knowles CH et al. Differential regulation of interleukin 17 and interferon γ production in inflammatory bowel disease. *Gut.* 2009;58(12):1629–1636.

[77] Sugihara T, Kobori A, Imaeda H, Tsujikawa T, Amagase K et al. The increased mucosal mRNA expressions of complement C3 and interleukin-17 in inflammatory bowel disease. *Clin Exp Immunol.* 2010;160(3):386–393.

[78] Baumgart DC and Sandborn WJ. Crohn's disease. *Lancet.* 2012;380(9853):1590–1605.

[79] Ahmed I, Roy BC, Khan SA, Septer S and Umar S. Microbiome, metabolome and inflammatory bowel disease. *Microorganisms.* 2016;4(2):20.

[80] Frank DN, St. Amand AL, Feldman RA, Boedeker EC, Harpaz N and Pace NR. Molecular-phylogenetic characterization of microbial community imbalances in human inflammatory bowel diseases. *Proc Natl Acad Sci USA.* 2007;104(34):13780–13785.

[81] Willing BP, Dicksved J, Halfvarson J, Andersson AF, Lucio M et al. A pyrosequencing study in twins shows that gastrointestinal microbial profiles vary with inflammatory bowel disease phenotypes. *Gastroenterology.* 2010;139(6):1844–1854.e1.

[82] Moussata D, Goetz M, Gloeckner A, Kerner M, Campbell B et al. Confocal laser endomicroscopy is a new imaging modality for recognition of intramucosal bacteria in inflammatory bowel disease in vivo. *Gut.* 2011;60(1):26–33.

[83] Andoh A, Imaeda H, Aomatsu T, Inatomi O, Bamba S et al. Comparison of the fecal microbiota profiles between ulcerative colitis and Crohn's disease using terminal restriction fragment length polymorphism analysis. *J Gastroenterol.* 2011;46(4):479–486.

[84] Song C, Chai Z, Chen S, Zhang H, Zhang X and Zhou Y. Intestinal mucus components and secretion mechanisms: What we do and do not know. *Exp Mol Med.* 2023;55(4):681–691.

[85] Zhang YZ and Li YY. Inflammatory bowel disease: Pathogenesis. *World J Gastroenterol.* 2014;20(1):91–99.

[86] Darfeuille-Michaud A, Boudeau J, Bulois P, Neut C, Glasser AL et al. High prevalence of adherent-invasive Escherichia coli associated with ileal mucosa in Crohn's disease. *Gastroenterology.* 2004;127(2):412–421.

[87] Baumgart M, Dogan B, Rishniw M, Weitzman G, Bosworth B et al. Culture independent analysis of ileal mucosa reveals a selective increase in invasive Escherichia coli of novel phylogeny relative to depletion of Clostridiales in Crohn's disease involving the ileum. *ISME J.* 2007;1(5):403–418.

[88] Meconi S, Vercellone A, Levillain F, Payré B, Al Saati T et al. Adherent-invasive Escherichia coli isolated from Crohn's disease patients induce granulomas in vitro. *Cellular Microbiology.* 2007;9(5):1252–1261.

[89] Postler TS and Ghosh S. Understanding the holobiont: How microbial metabolites affect human health and shape the immune system. *Cell Metab.* 2017;26(1):110–130.

[90] Liu S, Zhao W, Lan P and Mou X. The microbiome in inflammatory bowel diseases: From pathogenesis to therapy. *Protein Cell*. 2021;12(5):331–345.

[91] Furusawa Y, Obata Y, Fukuda S, Endo TA, Nakato G et al. Commensal microbe-derived butyrate induces the differentiation of colonic regulatory T cells. *Nature*. 2013;504(7480):446–450.

[92] Kim MH, Kang SG, Park JH, Yanagisawa M and Kim CH. Short-chain fatty acids activate GPR41 and GPR43 on intestinal epithelial cells to promote inflammatory responses in mice. *Gastroenterology*. 2013;145(2):396–406.e10.

[93] Vernia P, Gnaedinger A, Hauck W and Breuer RI. Organic anions and the diarrhea of inflammatory bowel disease. *Dig Dis Sci*. 1988;33(11):1353–1358.

[94] Takaishi H, Matsuki T, Nakazawa A, Takada T, Kado S et al. Imbalance in intestinal microflora constitution could be involved in the pathogenesis of inflammatory bowel disease. *Int J Med Microbiol*. 2008;298(5):463–472.

[95] Lavelle A and Sokol H. Gut microbiota-derived metabolites as key actors in inflammatory bowel disease. *Nat Rev Gastroenterol Hepatol*. 2020;17(4):223–237.

[96] Zelante T, Iannitti RG, Cunha C, De Luca A, Giovannini G et al. Tryptophan catabolites from microbiota engage aryl hydrocarbon receptor and balance mucosal reactivity via interleukin-22. *Immunity*. 2013;39(2):372–385.

[97] Schirmer M, Garner A, Vlamakis H and Xavier RJ. Microbial genes and pathways in inflammatory bowel disease. *Nat Rev Microbiol*. 2019;17(8):497–511.

[98] Wlodarska M, Luo C, Kolde R, d'Hennezel E, Annand JW et al. Indoleacrylic acid produced by commensal peptostreptococcus species suppresses inflammation. *Cell Host Microbe*. 2017;22(1):25–37.e6.

[99] Cobrin GM and Abreu MT. Defects in mucosal immunity leading to Crohn's disease. *Immunol Rev*. 2005;206(1):277–295.

[100] Targan SR and Karp LC. Defects in mucosal immunity leading to ulcerative colitis. *Immunol Rev*. 2005;206(1):296–305.

[101] Di Sabatino A, Biancheri P, Rovedatti L, MacDonald TT and Corazza GR. New pathogenic paradigms in inflammatory bowel disease. *Inflamm Bowel Dis*. 2012;18(2):368–371.

[102] Britton GJ, Contijoch EJ, Mogno I, Vennaro OH, Llewellyn SR et al. Microbiotas from humans with inflammatory bowel disease alter the balance of gut Th17 and RORγt+ regulatory T cells and exacerbate colitis in mice. *Immunity*. 2019;50(1):212–224.e4.

[103] Caruso R, Lo BC and Núñez G. Host–microbiota interactions in inflammatory bowel disease. *Nat Rev Immunol.* 2020;20(7):411–426.

[104] Gassler N, Rohr C, Schneider A, Kartenbeck J, Bach A et al. Inflammatory bowel disease is associated with changes of enterocytic junctions. *Am J Physiol - Gastrointest Liver Physiol.* 2001;281(1):G216–G228.

[105] Van der Sluis M, De Koning BA, De Bruijn AC, Velcich A, Meijerink JP et al. Muc2-deficient mice spontaneously develop colitis, indicating that MUC2 is critical for colonic protection. *Gastroenterology.* 2006;131(1):117–129.

[106] Fritz T, Niederreiter L, Adolph T, Blumberg RS and Kaser A. Crohn's disease: NOD2, autophagy and ER stress converge. *Gut.* 2011;60(11):1580–1588.

[107] Hou JK, El-Serag H and Thirumurthi S. Distribution and manifestations of inflammatory bowel disease in Asians, Hispanics, and African Americans: A systematic review. *Am J Gastroenterol.* 2009;104(8):2100–2109.

[108] Hou JK, Abraham B and El-Serag H. Dietary intake and risk of developing inflammatory bowel disease: A systematic review of the literature. *Am J Gastroenterol.* 2011;106(4):563–673.

[109] Zhang P, Jain P, Tsao C, Wu K and Jiang S. Proactively reducing anti-drug antibodies via immunomodulatory bioconjugation. *Angew Chem Int Ed.* 2019;58(8):2433–2436.

[110] Cosnes J. Tobacco and IBD: Relevance in the understanding of disease mechanisms and clinical practice. *Best Pract Res Clin Gastroenterol.* 2004;18(3):481–496.

[111] Birrenbach T and Böcker U. Inflammatory bowel disease and smoking: A review of epidemiology, pathophysiology, and therapeutic implications. *Inflamm Bowel Dis.* 2004;10(6):848–859.

[112] Cornish JA, Tan E, Simillis C, Clark SK, Teare J and Tekkis PP. The risk of oral contraceptives in the etiology of inflammatory bowel disease: A meta-analysis. *Am J Gastroenterol.* 2008;103(9):2394–2400.

[113] Rodríguez LAG, Ruigómez A and Panés J. Acute gastroenteritis is followed by an increased risk of inflammatory bowel disease. *Gastroenterology.* 2006;130(6):1588–1594.

[114] Nash P, Kerschbaumer A, Dörner T, Dougados M, Fleischmann RM et al. Points to consider for the treatment of immune-mediated inflammatory diseases with Janus kinase inhibitors: A consensus statement. *Ann Rheum Dis.* 2021;80(1):71–87.

[115] Cai Z, Wang S and Li J. Treatment of inflammatory bowel disease: A comprehensive review. *Front Med.* 2021;8:765474.

[116] Punchard NA, Greenfield SM and Thompson RPH. Mechanism of action of 5-aminosalicylic acid. *Mediators Inflamm.* 1992;1(3):480976.

[117] Bruscoli S, Febo M, Riccardi C and Migliorati G. Glucocorticoid therapy in inflammatory bowel disease: Mechanisms and clinical practice. *Front Immunol.* 2021;12:691480.

[118] Baumgart DC and Le Berre C. Newer biologic and small-molecule therapies for inflammatory bowel disease. *N Engl J Med.* 2021;385(14):1302–1315.

[119] Melsheimer R, Geldhof A, Apaolaza I and Schaible T. Remicade® (infliximab): 20 years of contributions to science and medicine. *Biologics.* 2019;13:139–178.

[120] Amiot A, Bouguen G, Bonnaud G, Bouhnik Y, Hagege H et al. Clinical guidelines for the management of inflammatory bowel disease: Update of a French national consensus. *Dig Liver Dis.* 2021;53(1):35–43.

[121] Kandavel P, Eder SJ and Adler J. Reduced systemic corticosteroid use among pediatric patients with inflammatory bowel disease in a large learning health system. *J Pediatr Gastroenterol Nutr.* 2021;73(3):345–351.

[122] Claßen M, de Laffolie J, Claßen M, Schnell A, Sohrabi K and Hoerning A. Significant advantages for first line treatment with TNF-alpha inhibitors in pediatric patients with inflammatory bowel disease – Data from the multicenter CEDATA-GPGE registry study. *Front Pediatr.* 2022;10:903677.

[123] Jongsma MME, Aardoom MA, Cozijnsen MA, van Pieterson M, de Meij T et al. First-line treatment with infliximab versus conventional treatment in children with newly diagnosed moderate-to-severe Crohn's disease: An open-label multicentre randomised controlled trial. *Gut.* 2022;71(1):34–42.

[124] Wang K, Zhang H, Kugathasan S, Annese V, Bradfield JP et al. Diverse genome-wide association studies associate the IL12/IL23 pathway with Crohn disease. *Am J Hum Genet.* 2009;84(3):399–405.

[125] Almradi A, Hanzel J, Sedano R, Parker CE, Feagan BG et al. Clinical trials of IL-12/IL-23 inhibitors in inflammatory bowel disease. *BioDrugs.* 2020;34(6):713–721.

[126] Bachmann M, Kukkurainen S, Hytönen VP and Wehrle-Haller B. Cell adhesion by integrins. *Physiol Rev.* 2019;99(4):1655–1699.

[127] Danese S, Semeraro S, Marini M, Roberto I, Armuzzi A et al. Adhesion molecules in inflammatory bowel disease: Therapeutic implications for gut inflammation. *Dig Liver Dis.* 2005;37(11):811–818.

[128] Feagan BG, Rutgeerts P, Sands BE, Hanauer S, Colombel JF et al. Vedolizumab as induction and maintenance therapy for ulcerative colitis. *N Engl J Med.* 2013;369(8):699–710.

[129] Sandborn WJ, Feagan BG, Rutgeerts P, Hanauer S, Colombel JF et al. Vedolizumab as induction and maintenance therapy for Crohn's disease. *N Engl J Med.* 2013;369(8):711–721.

[130] Wyant T, Fedyk E and Abhyankar B. An overview of the mechanism of action of the monoclonal antibody vedolizumab. *J Crohns Colitis.* 2016;10(12):1437–1444.

[131] O'Shea JJ, Schwartz DM, Villarino AV, Gadina M, McInnes IB and Laurence A. The JAK-STAT pathway: Impact on human disease and therapeutic intervention. *Annu Rev Med.* 2015;66(1):311–328.

[132] Dudek P, Fabisiak A, Zatorski H, Malecka-Wojciesko E and Talar-Wojnarowska R. Efficacy, safety and future perspectives of JAK inhibitors in the IBD treatment. *J Clin Med.* 2021;10(23):5660.

[133] Carswell EA, Old LJ, Kassel RL, Green S, Fiore N and Williamson B. An endotoxin-induced serum factor that causes necrosis of tumors. *Proc Natl Acad Sci USA.* 1975;72(9):3666–3670.

[134] Aggarwal BB, Gupta SC and Kim JH. Historical perspectives on tumor necrosis factor and its superfamily: 25 years later, a golden journey. *Blood.* 2012;119(3):651–665.

[135] Köhler G and Milstein C. Continuous cultures of fused cells secreting antibody of predefined specificity. *Nature.* 1975;256(5517):495–497.

[136] Boulianne GL, Hozumi N and Shulman MJ. Production of functional chimaeric mouse/human antibody. *Nature.* 1984;312(5995):643–646.

[137] Morrison SL, Johnson MJ, Herzenberg LA and Oi VT. Chimeric human antibody molecules: Mouse antigen-binding domains with human constant region domains. *Proc Natl Acad Sci USA.* 1984;81(21):6851–6855.

[138] Morrison SL. Genetically engineered (chimeric) antibodies. *Hosp Pract.* 1989;24(10):65–80.

[139] Beutler B, Milsark IW and Cerami AC. Passive immunization against cachectin/tumor necrosis factor protects mice from lethal effect of endotoxin. *Science.* 1985;229(4716):869–871.

[140] Tracey KJ, Fong Y, Hesse DG, Manogue KR, Lee AT et al. Anti-cachectin/TNF monoclonal antibodies prevent septic shock during lethal bacteraemia. *Nature.* 1987;330(6149):662–664.

[141] Knight DM, Trinh H, Le J, Siegel S, Shealy D et al. Construction and initial characterization of a mouse-human chimeric anti-TNF antibody. *Mol Immunol.* 1993;30(16):1443–1453.

[142] Clark MA, Plank LD, Connolly AB, Streat SJ, Hill AA et al. Effect of a chimeric antibody to tumor necrosis factor-alpha on cytokine and physiologic responses in patients with severe sepsis - A randomized, clinical trial. *Crit Care Med.* 1998;26(10):1650–1659.

[143] Braegger C, Nicholls S, Murch S, MacDonald T and Stephens S. Tumour necrosis factor alpha in stool as a marker of intestinal inflammation. *The Lancet.* 1992;339(8785):89–91.

[144] Murch SH, Braegger CP, Walker-Smith JA and MacDonald TT. Location of tumour necrosis factor alpha by immunohistochemistry in chronic inflammatory bowel disease. *Gut.* 1993;34(12):1705–1709.

[145] Nielsen OH, Brynskov J and Bendtzen K. Circulating and mucosal concentrations of tumour necrosis factor and inhibitor(s) in chronic inflammatory bowel disease. *Dan Med Bull.* 1993;40(2):247–249.

[146] Reinecker HC, Steffen M, Witthoeft T, Pflueger I, Schreiber S et al. Enhanced secretion of tumour necrosis factor-alpha, IL-6, and IL-1β by isolated lamina propria monouclear cells from patients with ulcerative colitis and Crohn's disease. *Clin Exp Immunol.* 1993;94(1):174–181.

[147] Breese EJ, Michie CA, Nicholls SW, Murch SH, Williams CB et al. Tumor necrosis factor α-producing cells in the intestinal mucosa of children with inflammatory bowel disease. *Gastroenterology.* 1994;106(6):1455–1466.

[148] Hopkins SJ and Meager A. Cytokines in synovial fluid: II. The presence of tumour necrosis factor and interferon. *Clin Exp Immunol.* 1988;73(1):88–92.

[149] Saxne T, Palladino Jr MA, Heinegãrd D, Talal N and Wollheim FA. Detection of tumor necrosis factor α but not tumor necrosis factor β in rheumatoid arthritis synovial fluid and serum. *Arthritis Rheum.* 1988;31(8):1041–1045.

[150] Derkx B, Taminiau J, Radema S, Stronkhorst A, Wortel C et al. Tumour-necrosis-factor antibody treatment in Crohn's disease. *Lancet.* 1993;342(8864):173–174.

[151] Elliott M, Maini R, Feldmann M, Long-Fox A, Charles P et al. Repeated therapy with monoclonal antibody to tumour necrosis factor α (cA2) in patients with rheumatoid arthritis. *Lancet.* 1994;344(8930):1125–1127.

[152] van Dullemen HM, van Deventer SJ, Hommes DW, Bijl HA, Jansen J et al. Treatment of Crohn's disease with anti-tumor necrosis factor chimeric monoclonal antibody (cA2). *Gastroenterology.* 1995;109(1):129–135.

[153] Targan SR, Hanauer SB, van Deventer SJ, Mayer L, Present DH et al. A short-term study of chimeric monoclonal antibody cA2 to tumor necrosis factor-α for Crohn's disease. *N Engl J Med.* 1997;337(15):1029–1036.

[154] Maini RN, Breedveld FC, Kalden JR, Smolen JS, Davis D et al. Therapeutic efficacy of multiple intravenous infusions of anti-tumor necrosis factor α monoclonal antibody combined with low-dose weekly methotrexate in rheumatoid arthritis. *Arthritis Rheum.* 1998;41(9):1552–1563.

[155] Rutgeerts P, D'Haens G, Targan S, Vasiliauskas E, Hanauer SB et al. Efficacy and safety of retreatment with anti-tumor necrosis factor antibody (infliximab) to maintain remission in Crohn's disease. *Gastroenterology.* 1999;117(4):761–769.

[156] Rutgeerts P, Feagan BG, Lichtenstein GR, Mayer LF, Schreiber S et al. Comparison of scheduled and episodic treatment strategies of infliximab in Crohn's disease. *Gastroenterology.* 2004;126(2):402–413.

[157] Rutgeerts P, Diamond RH, Bala M, Olson A, Lichtenstein GR et al. Scheduled maintenance treatment with infliximab is superior to episodic treatment for the healing of mucosal ulceration associated with Crohn's disease. *Gastrointest Endosc.* 2006;63(3):433–442.

[158] Food and Drug Administration. FDA-Approved Drugs: Remicade [Internet]. Food and Drug Administration [cited 2023 Jul 9]. Available from: `https://www.accessdata.fda.gov/scripts/cder/daf/index.cfm?event=overview.process&ApplNo=103772`.

[159] European Medicines Agency. Medicines: Remicade [Internet]. European Medicines Agency [cited 2023 Jul 9]. Available from: `https://www.ema.europa.eu/en/medicines/human/EPAR/remicade`.

[160] Peyrin-Biroulet L, Sandborn W, Sands BE, Reinisch W, Bemelman W et al. Selecting therapeutic targets in inflammatory bowel disease (STRIDE): Determining therapeutic goals for treat-to-target. *Am J Gastroenterol.* 2015;110(9):1324–1338.

[161] Turner D, Ricciuto A, Lewis A, D'Amico F, Dhaliwal J et al. STRIDE-II: An update on the selecting therapeutic targets in inflammatory bowel disease (STRIDE) initiative of the international organization for the study of IBD (IOIBD): Determining therapeutic goals for treat-to-target strategies in IBD. *Gastroenterology.* 2021;160(5):1570–1583.

[162] Food and Drug Administration. FDA-Approved Drugs: Enbrel [Internet]. Food and Drug Administration [cited 2023 Jul 9]. Available from: `https://www.accessdata.fda.gov/scripts/cder/daf/index.cfm?event=overview.process&ApplNo=103795`.

[163] Swissmedic. Neuzulassungen: Cimzia, Pulver und Lösungsmittel (Certolizumab pegol) [Internet]. Swissmedic [cited 2023 Sep 17]. Available from: `https://www.swissmedic.ch/swissmedic/de/home/humanarzneimittel/authorisations/new-medicines/cimzia_--pulver-und-loesungsmittel--certolizumab-pegol-.html`.

[164] Food and Drug Administration. FDA-Approved Drugs: Cimzia [Internet]. Food and Drug Administration [cited 2023 Jul 9]. Available from: https://www.accessdata.fda.gov/scripts/cder/daf/index.cfm?event=overview.process&ApplNo=125160.

[165] European Medicines Agency. Medicines (search for "active substance" = "certolizumab") [Internet]. European Medicines Agency [cited 2023 Jul 9]. Available from: https://www.ema.europa.eu/en/medicines/search_api_aggregation_ema_active_substance_and_inn_common_name/certolizumab%20pegol?search_api_views_fulltext=tnf%20blocker.

[166] Food and Drug Administration. FDA-Approved Drugs: Humira [Internet]. Food and Drug Administration [cited 2023 Jul 9]. Available from: https://www.accessdata.fda.gov/scripts/cder/daf/index.cfm?event=overview.process&ApplNo=125057.

[167] Food and Drug Administration. Purple Book database of licensed biological products (search for "proprietary name" = "Humira") [Internet]. Food and Drug Administration [cited 2023 Sep 17]. Available from: https://purplebooksearch.fda.gov/patent-list.

[168] Food and Drug Administration. FDA-Approved Drugs: Simponi Aria [Internet]. Food and Drug Administration [cited 2023 Jul 9]. Available from: https://www.accessdata.fda.gov/scripts/cder/daf/index.cfm?event=overview.process&ApplNo=125433.

[169] Derbyshire M and Shina S. Patent expiry dates for biologicals: 2018 update. *GaBI J.* 2019;8(1):24–31.

[170] Urquhart L. Top companies and drugs by sales in 2022. *Nat Rev Drug Discov.* 2023;22:260.

[171] Breese EJ and MacDonald TT. TNF alpha secreting cells in normal and diseased human intestine. *Adv Exp Med Biol.* 1995;371B:821–824.

[172] Ślebioda TJ and Kmieć Z. Tumour necrosis factor superfamily members in the pathogenesis of inflammatory bowel disease. *Mediators Inflamm.* 2014;2014:325129.

[173] Monaco C, Nanchahal J, Taylor P and Feldmann M. Anti-TNF therapy: Past, present and future. *Int. Immunol.* 2015;27(1):55–62.

[174] Kriegler M, Perez C, DeFay K, Albert I and Lu S. A novel form of TNF/cachectin is a cell surface cytotoxic transmembrane protein: Ramifications for the complex physiology of TNF. *Cell.* 1988;53(1):45–53.

[175] Issuree PDA, Maretzky T, McIlwain DR, Monette S, Qing X et al. iRHOM2 is a critical pathogenic mediator of inflammatory arthritis. *J Clin Invest.* 2013;123(2):928–932.

[176] European Medicines Agency. Medicines (search for "active substance" = "infliximab") [Internet]. European Medicines Agency [cited 2022 Sep 23]. Available from: https://www.ema.europa.eu/en/medicines/search_api_aggregation_ema_active_substance_and_inn_common_name/infliximab.

[177] European Medicines Agency. Medicines (search for "active substance" = "etanercept") [Internet]. European Medicines Agency [cited 2023 Jul 9]. Available from: https://www.ema.europa.eu/en/medicines/search_api_aggregation_ema_active_substance_and_inn_common_name/etanercept?search_api_views_fulltext=tnf%20blocker.

[178] European Medicines Agency. Medicines (search for "active substance" = "adalimumab") [Internet]. European Medicines Agency [cited 2023 Jul 9]. Available from: https://www.ema.europa.eu/en/medicines/search_api_aggregation_ema_active_substance_and_inn_common_name/adalimumab?search_api_views_fulltext=tnf%20blocker.

[179] European Medicines Agency. Medicines (search for "active substance" = "golimumab") [Internet]. European Medicines Agency [cited 2023 Jul 9]. Available from: https://www.ema.europa.eu/en/medicines/search_api_aggregation_ema_active_substance_and_inn_common_name/golimumab?search_api_views_fulltext=tnf%20blocker.

[180] Food and Drug Administration. FDA-Approved Drugs: Simponi [Internet]. Food and Drug Administration [cited 2023 Jul 9]. Available from: https://www.accessdata.fda.gov/scripts/cder/daf/index.cfm?event=overview.process&ApplNo=125289.

[181] Food and Drug Administration. Biosimilar product information [Internet]. Food and Drug Administration [cited 2022 Sep 23]. Available from: https://www.fda.gov/drugs/biosimilars/biosimilar-product-information.

[182] Brockhaus M, Schoenfeld HJ, Schlaeger EJ, Hunziker W, Lesslauer W and Loetscher H. Identification of two types of tumor necrosis factor receptors on human cell lines by monoclonal antibodies. *Proc Natl Acad Sci USA*. 1990;87(8):3127–3131.

[183] Dembic Z, Loetscher H, Gubler U, Pan YCE, Lahm HW et al. Two human TNF receptors have similar extracellular, but distinct intracellular, domain sequences. *Cytokine*. 1990;2(4):231–237.

[184] Loetscher H, Pan YCE, Lahm HW, Gentz R, Brockhaus M et al. Molecular cloning and expression of the human 55 kd tumor necrosis factor receptor. *Cell*. 1990;61(2):351–359.

[185] Kalliolias GD and Ivashkiv LB. TNF biology, pathogenic mechanisms and emerging therapeutic strategies. *Nat Rev Rheumatol*. 2016;12(1):49–62.

[186] Grell M, Douni E, Wajant H, Löhden M, Clauss M et al. The transmembrane form of tumor necrosis factor is the prime activating ligand of the 80 kDa tumor necrosis factor receptor. *Cell*. 1995;83(5):793–802.

[187] Tartaglia LA, Ayres T, Wong GH and Goeddel DV. A novel domain within the 55 kd TNF receptor signals cell death. *Cell*. 1993;74(5):845–853.

[188] Hsu H, Xiong J and Goeddel DV. The TNF receptor 1-associated protein TRADD signals cell death and NF-κB activation. *Cell*. 1995;81(4):495–504.

[189] Micheau O and Tschopp J. Induction of TNF receptor I-mediated apoptosis via two sequential signaling complexes. *Cell*. 2003;114(2):181–190.

[190] Hsu H, Huang J, Shu HB, Baichwal V and Goeddel DV. TNF-dependent recruitment of the protein kinase RIP to the TNF receptor-1 signaling complex. *Immunity*. 1996;4(4):387–396.

[191] Ting AT, Pimentel-Muiños FX and Seed B. RIP mediates tumor necrosis factor receptor 1 activation of NF-kappaB but not Fas/APO-1-initiated apoptosis. *EMBO J.* 1996;15(22):6189–6196.

[192] Haas TL, Emmerich CH, Gerlach B, Schmukle AC, Cordier SM et al. Recruitment of the linear ubiquitin chain assembly complex stabilizes the TNF-R1 signaling complex and is required for TNF-mediated gene induction. *Mol Cell*. 2009;36(5):831–844.

[193] Tokunaga F, Sakata Si, Saeki Y, Satomi Y, Kirisako T et al. Involvement of linear polyubiquitylation of NEMO in NF-κB activation. *Nat Cell Biol*. 2009;11(2):123–132.

[194] Brenner D, Blaser H and Mak TW. Regulation of tumour necrosis factor signalling: Live or let die. *Nat Rev Immunol*. 2015;15(6):362–374.

[195] Wang C, Deng L, Hong M, Akkaraju GR, Inoue Ji and Chen ZJ. TAK1 is a ubiquitin-dependent kinase of MKK and IKK. *Nature*. 2001;412(6844):346–351.

[196] Wu J, Huang Z, Ren J, Zhang Z, He P et al. Mlkl knockout mice demonstrate the indispensable role of Mlkl in necroptosis. *Cell Res*. 2013;23(8):994–1006.

[197] Murphy JM, Czabotar PE, Hildebrand JM, Lucet IS, Zhang JG et al. The pseudokinase MLKL mediates necroptosis via a molecular switch mechanism. *Immunity*. 2013;39(3):443–453.

[198] Bertheloot D, Latz E and Franklin BS. Necroptosis, pyroptosis and apoptosis: An intricate game of cell death. *Cell Mol Immunol*. 2021;18(5):1106–1121.

[199] Rothe M, Sarma V, Dixit VM and Goeddel DV. TRAF2-mediated activation of NF-κB by TNF receptor 2 and CD40. *Science*. 1995;269(5229):1424–1427.

[200] van Loo G and Bertrand MJM. Death by TNF: A road to inflammation. *Nat Rev Immunol.* 2023;23(5):289–303.

[201] Günther C, Neumann H, Neurath MF and Becker C. Apoptosis, necrosis and necroptosis: Cell death regulation in the intestinal epithelium. *Gut.* 2013;62(7):1062–1071.

[202] Van den Brande JM, Braat H, van den Brink GR, Versteeg HH, Bauer CA et al. Infliximab but not etanercept induces apoptosis in lamina propria T-lymphocytes from patients with Crohn's disease. *Gastroenterology.* 2003;124(7):1774–1785.

[203] Atreya R, Zimmer M, Bartsch B, Waldner MJ, Atreya I et al. Antibodies against tumor necrosis factor (TNF) induce T-cell apoptosis in patients with inflammatory bowel diseases via TNF receptor 2 and intestinal CD14+ macrophages. *Gastroenterology.* 2011;141(6):2026–2038.

[204] Vos ACW, Wildenberg ME, Duijvestein M, Verhaar AP, van den Brink GR and Hommes DW. Anti–tumor necrosis factor-α antibodies induce regulatory macrophages in an Fc region-dependent manner. *Gastroenterology.* 2011;140(1):221–230.e3.

[205] Vos ACW, Wildenberg ME, Arijs I, Duijvestein M, Verhaar AP et al. Regulatory macrophages induced by infliximab are involved in healing in vivo and in vitro. *Inflamm Bowel Dis.* 2012;18(3):401–408.

[206] McRae BL, Levin AD, Wildenberg ME, Koelink PJ, Bousquet P et al. Fc Receptor-mediated effector function contributes to the therapeutic response of anti-TNF monoclonal antibodies in a mouse model of inflammatory bowel disease. *J Crohns Colitis.* 2016;10(1):69–76.

[207] Levin AD, Wildenberg ME and van den Brink GR. Mechanism of action of anti-TNF therapy in inflammatory bowel disease. *J Crohns Colitis.* 2016;10(8):989–997.

[208] Dostert C, Grusdat M, Letellier E and Brenner D. The TNF family of ligands and receptors: Communication modules in the immune system and beyond. *Physiol Rev.* 2019;99(1):115–160.

[209] Di Sabatino A, Ciccocioppo R, Luinetti O, Ricevuti L, Morera R et al. Increased enterocyte apoptosis in inflamed areas of Crohn's disease. *Dis Colon Rectum.* 2003;46(11):1498–1507.

[210] Zeissig S, Bojarski C, Buergel N, Mankertz J, Zeitz M et al. Downregulation of epithelial apoptosis and barrier repair in active Crohn's disease by tumour necrosis factor α antibody treatment. *Gut.* 2004;53(9):1295–1302.

[211] Woznicki JA, Saini N, Flood P, Rajaram S, Lee CM et al. TNF-α synergises with IFN-γ to induce caspase-8-JAK1/2-STAT1-dependent death of intestinal epithelial cells. *Cell Death Dis.* 2021;12(10):864.

[212] Holtmann MH, Douni E, Schütz M, Zeller G, Mudter J et al. Tumor necrosis factor-receptor 2 is up-regulated on lamina propria T cells in Crohn's disease and promotes experimental colitis in vivo. *Eur J Immunol.* 2002;32(11):3142–3151.

[213] Perrier C, de Hertogh G, Cremer J, Vermeire S, Rutgeerts P et al. Neutralization of membrane TNF, but not soluble TNF, is crucial for the treatment of experimental colitis. *Inflamm Bowel Dis.* 2013;19(2):246–253.

[214] Sandborn WJ, Hanauer SB, Katz S, Safdi M, Wolf DG et al. Etanercept for active Crohn's disease: A randomized, double-blind, placebo-controlled trial. *Gastroenterology.* 2001;121(5):1088–1094.

[215] Shivaji UN, Sharratt CL, Thomas T, Smith SCL, Iacucci M et al. Review article: Managing the adverse events caused by anti-TNF therapy in inflammatory bowel disease. *Aliment Pharmacol Ther.* 2019;49(6):664–680.

[216] Ovacik M and Lin K. Tutorial on monoclonal antibody pharmacokinetics and its considerations in early development. *Clin Transl Sci.* 2018;11(6):540–552.

[217] Panaccione R and Ghosh S. Optimal use of biologics in the management of Crohn's disease. *Therap Adv Gastroenterol.* 2010;3(3):179–189.

[218] de Silva PSA, Nguyen DD, Sauk J, Korzenik J, Yajnik V and Ananthakrishnan AN. Long-term outcome of a third anti-TNF monoclonal antibody after the failure of two prior anti-TNFs in inflammatory bowel disease. *Aliment Pharmacol Ther.* 2012;36(5):459–466.

[219] Park SC and Jeen YT. Current and emerging biologics for ulcerative colitis. *Gut Liver.* 2015;9(1):18–27.

[220] Vande Casteele N, Herfarth H, Katz J, Falck-Ytter Y and Singh S. American Gastroenterological Association institute technical review on the role of therapeutic drug monitoring in the management of inflammatory bowel diseases. *Gastroenterology.* 2017;153(3):835–857.e6.

[221] Hindryckx P, Novak G, Vande Casteele N, Khanna R, Laukens D et al. Incidence, prevention and management of anti-drug antibodies against therapeutic antibodies in inflammatory bowel disease: A practical overview. *Drugs.* 2017;77(4):363–377.

[222] Vermeire S, Gils A, Accossato P, Lula S and Marren A. Immunogenicity of biologics in inflammatory bowel disease. *Therap Adv Gastroenterol.* 2018;11:1756283X17750355.

[223] Vaisman-Mentesh A, Gutierrez-Gonzalez M, DeKosky BJ and Wine Y. The molecular nechanisms that underlie the immune biology of anti-drug antibody formation following treatment with monoclonal antibodies. *Front Immunol.* 2020;11:1951.

[224] Segal S, Tzehoval E and Feldman M. Immunological tolerance: High-dose antigen-induced suppressor cells from tolerant animals inactivate antigen-presenting macrophages. *Proc Natl Acad Sci USA*. 1979;76(5):2405–2409.

[225] Vermeire S, Noman M, Assche GV, Baert F, D'Haens G and Rutgeerts P. Effectiveness of concomitant immunosuppressive therapy in suppressing the formation of antibodies to infliximab in Crohn's disease. *Gut*. 2007;56(9):1226.

[226] Baert F, Kondragunta V, Lockton S, Casteele NV, Hauenstein S et al. Antibodies to adalimumab are associated with future inflammation in Crohn's patients receiving maintenance adalimumab therapy: A post hoc analysis of the Karmiris trial. *Gut*. 2016;65(7):1126–1131.

[227] Billiet T, Dreesen E, Cleynen I, Wollants WJ, Ferrante M et al. A genetic variation in the neonatal Fc-receptor affects anti-TNF drug concentrations in inflammatory bowel disease. *Am J Gastroenterol*. 2016;111(10):1438–1445.

[228] Romero-Cara P, Torres-Moreno D, Pedregosa J, Vílchez JA, García-Simón MS et al. A FCGR3A polymorphism predicts anti-drug antibodies in chronic inflammatory bowel disease patients treated with anti-TNF. *Int J Med Sci*. 2018;15(1):10–15.

[229] Sazonovs A, Kennedy NA, Moutsianas L, Heap GA, Rice DL et al. HLA-DQA1*05 carriage associated with development of anti-drug antibodies to infliximab and adalimumab in patients with Crohn's disease. *Gastroenterology*. 2020;158(1):189–199.

[230] Wilson A, Peel C, Wang Q, Pananos AD and Kim RB. HLADQA1*05 genotype predicts anti-drug antibody formation and loss of response during infliximab therapy for inflammatory bowel disease. *Aliment Pharmacol Ther*. 2020;51(3):356–363.

[231] Salvador-Martín S, Pujol-Muncunill G, Bossacoma F, Navas-López VM, Gallego-Fernández C et al. Pharmacogenetics of trough serum anti-TNF levels in paediatric inflammatory bowel disease. *Br J Clin Pharmacol*. 2021;87(2):447–457.

[232] Bartelds GM, Wijbrandts CA, Nurmohamed MT, Wolbink GJ, de Vries N et al. Anti-adalimumab antibodies in rheumatoid arthritis patients are associated with interleukin-10 gene polymorphisms. *Arthritis Rheum*. 2009;60(8):2541–2542.

[233] Dirks NL and Meibohm B. Population pharmacokinetics of therapeutic monoclonal antibodies. *Clin Pharmacokinet*. 2010;49(10):633–659.

[234] Gill KL, Machavaram KK, Rose RH and Chetty M. Potential sources of intersubject variability in monoclonal antibody pharmacokinetics. *Clin Pharmacokinet*. 2016;55(7):789–805.

[235] Pratesi S, Nencini F, Grosso F, Dies L, Bormioli S et al. T cell response to infliximab in exposed patients: A longitudinal analysis. *Front Immunol*. 2019;9:3113.

[236] Quistrebert J, Hässler S, Bachelet D, Mbogning C, Musters A et al. Incidence and risk factors for adalimumab and infliximab anti-drug antibodies in rheumatoid arthritis: A European retrospective multicohort analysis. *Semin Arthritis Rheum.* 2019;48(6):967–975.

[237] Atiqi S, Hooijberg F, Loeff FC, Rispens T and Wolbink GJ. Immunogenicity of TNF-inhibitors. *Front Immunol.* 2020;11:312.

[238] van Schie KA, Kruithof S, Ooijevaar-de Heer P, Derksen NI, van de Bovenkamp FS et al. Restricted immune activation and internalisation of anti-idiotype complexes between drug and antidrug antibodies. *Ann Rheum Dis.* 2018;77(10):1471–1479.

[239] Baert F, Noman M, Vermeire S, Van Assche G, D' Haens G et al. Influence of immunogenicity on the long-term efficacy of infliximab in Crohn's disease. *N Engl J Med.* 2003;348(7):601–608.

[240] Vande Casteele N, Gils A, Singh S, Ohrmund L, Hauenstein S et al. Antibody response to infliximab and its impact on pharmacokinetics can be transient. *Am J Gastroenterol.* 2013;108(6):962–971.

[241] O'Meara S, Nanda KS and Moss AC. Antibodies to infliximab and risk of infusion reactions in patients with inflammatory bowel disease: A systematic review and meta-analysis. *Inflamm Bowel Dis.* 2014;20(1):1–6.

[242] Doessegger L and Banholzer ML. Clinical development methodology for infusion-related reactions with monoclonal antibodies. *Clin Transl Immunol.* 2015;4(7):e39.

[243] van Schie KA, Heer POD, Kruithof S, Plasencia C, Jurado T et al. Infusion reactions during infliximab treatment are not associated with IgE anti-infliximab antibodies. *Ann Rheum Dis.* 2017;76(7):1285–1288.

[244] Papamichael K, Cheifetz AS, Melmed GY, Irving PM, Vande Casteele N et al. Appropriate therapeutic drug monitoring of biologic agents for patients with inflammatory bowel diseases. *Clin Gastroenterol Hepatol.* 2019;17(9):1655–1668.e3.

[245] Kennedy NA, Heap GA, Green HD, Hamilton B, Bewshea C et al. Predictors of anti-TNF treatment failure in anti-TNF-naive patients with active luminal Crohn's disease: A prospective, multicentre, cohort study. *Lancet Gastroenterol Hepatol.* 2019;4(5):341–353.

[246] Ma C, Battat R, Jairath V and Vande Casteele N. Advances in therapeutic drug monitoring for small-molecule and biologic therapies in inflammatory bowel disease. *Curr Treatm Opt Gastroenterol.* 2019;17(1):127–145.

[247] Vande Casteele N, Ferrante M, Assche GV, Ballet V, Compernolle G et al. Trough concentrations of infliximab guide dosing for patients with inflammatory bowel disease. *Gastroenterology.* 2015;148(7):1320–1329.e3.

[248] Cheifetz AS, Abreu MT, Afif W, Cross RK, Dubinsky MC et al. A comprehensive literature review and expert consensus statement on therapeutic drug monitoring of biologics in inflammatory bowel disease. *Am J Gastroenterol.* 2021;116(10):2014–2025.

[249] Lázár-Molnár E and Delgado JC. Immunogenicity assessment of tumor necrosis factor antagonists in the clinical laboratory. *Clin Chem.* 2016;62(9):1186–1198.

[250] Vande Casteele N. Assays for measurement of TNF antagonists in practice. *Frontline Gastroenterol.* 2017;8(4):236–242.

[251] Imbrechts M, Van Stappen T, Compernolle G, Tops S and Gils A. Anti-infliximab antibodies: How to compare old and new data? *J Pharm Biomed Anal.* 2020;177:112842.

[252] Papamichael K, Afif W, Drobne D, Dubinsky MC, Ferrante M et al. Therapeutic drug monitoring of biologics in inflammatory bowel disease: Unmet needs and future perspectives. *Lancet Gastroenterol Hepatol.* 2022;7(2):171–185.

[253] Ungar B, Chowers Y, Yavzori M, Picard O, Fudim E et al. The temporal evolution of antidrug antibodies in patients with inflammatory bowel disease treated with infliximab. *Gut.* 2014;63(8):1258–1264.

[254] Roblin X, Marotte H, Leclerc M, Del Tedesco E, Phelip J et al. Combination of C-reactive protein, infliximab trough levels, and stable but not transient antibodies to infliximab are associated with loss of response to infliximab in inflammatory bowel disease. *J Crohns Colitis.* 2015;9(7):525–531.

[255] Mitrev N, Vande Casteele N, Seow CH, Andrews JM, Connor SJ et al. IBD Sydney Organisation and the Australian Inflammatory Bowel Diseases Consensus Working Group. Review article: Consensus statements on therapeutic drug monitoring of anti-tumour necrosis factor therapy in inflammatory bowel diseases. *Aliment Pharmacol Ther.* 2017;46(11-12):1037–1053.

[256] Steenholdt C, Brynskov J, Thomsen OØ, Munck LK, Fallingborg J et al. Individualised therapy is more cost-effective than dose intensification in patients with Crohn's disease who lose response to anti-TNF treatment: A randomised, controlled trial. *Gut.* 2014;63(6):919–927.

[257] Kelly OB, Donnell SO, Stempak JM, Steinhart AH and Silverberg MS. Therapeutic drug monitoring to guide infliximab dose adjustment is associated with better endoscopic outcomes than clinical decision making alone in active inflammatory bowel disease. *Inflamm Bowel Dis.* 2017;23(7):1202–1209.

[258] Guidi L, Pugliese D, Tonucci TP, Berrino A, Tolusso B et al. Therapeutic drug monitoring is more cost-effective than a clinically based approach in the banagement

of loss of response to infliximab in inflammatory bowel disease: An observational multicentre study. *J Crohns Colitis*. 2018;12(9):1079–1088.

[259] Steenholdt C, Bendtzen K, Brynskov J, Thomsen OØ and Ainsworth MA. Clinical implications of measuring drug and anti-drug antibodies by different assays when optimizing infliximab treatment failure in Crohn's disease: Post hoc analysis of a randomized controlled trial. *Am J Gastroenterol*. 2014;109(7):1055–1064.

[260] Vande Casteele N and Gils A. Pharmacokinetics of anti-TNF monoclonal antibodies in inflammatory bowel disease: Adding value to current practice. *J Clin Pharmacol*. 2015;55(S3):S39–S50.

[261] Kalden JR and Schulze-Koops H. Immunogenicity and loss of response to TNF inhibitors: Implications for rheumatoid arthritis treatment. *Nat Rev Rheumatol*. 2017;13(12):707–718.

[262] Myler H, Pedras-Vasconcelos J, Phillips K, Hottenstein CS, Chamberlain P et al. Anti-drug antibody validation testing and reporting harmonization. *The AAPS Journal*. 2021;24:4.

[263] Patton A, Mullenix MC, Swanson SJ and Koren E. An acid dissociation bridging ELISA for detection of antibodies directed against therapeutic proteins in the presence of antigen. *J Immunol Methods*. 2005;304(1-2):189–195.

[264] Wang SL, Ohrmund L, Hauenstein S, Salbato J, Reddy R et al. Development and validation of a homogeneous mobility shift assay for the measurement of infliximab and antibodies-to-infliximab levels in patient serum. *J Immunol Methods*. 2012;382(1):177–188.

[265] Van Stappen T, Brouwers E, Vermeire S and Gils A. Validation of a sample pretreatment protocol to convert a drug-sensitive into a drug-tolerant anti-infliximab antibody immunoassay. *Drug Test Anal*. 2017;9(2):243–247.

[266] Kharlamova N, Hermanrud C, Dunn N, Ryner M, Hambardzumyan K et al. Drug tolerant anti-drug antibody assay for infliximab treatment in clinical practice identifies positive cases earlier. *Front Immunol*. 2020;11:1365.

[267] Kricka LJ. Application of bioluminescence and chemiluminescence in biomedical sciences. In: *Methods in Enzymology*. Vol. 305. Academic Press; 2000. p. 333-345.

[268] Kricka L. Clinical applications of chemiluminescence. *Anal Chim Acta*. 2003;500(1-2):279–286.

[269] Wang C, Wu J, Zong C, Xu J and Ju HX. Chemiluminescent immunoassay and its applications. *Chin J Anal Chem*. 2012;40(1):3–10.

[270] Wu Y, Liu X, Chen Y, Woods R, Lee N et al. An electrochemiluminescence (ECL)-based assay for the specific detection of anti-drug antibodies of the IgE isotype. *J Pharm Biomed Anal.* 2013;86:73–81.

[271] Kim JS, Kim SH, Kwon B and Hong S. Comparison of immunogenicity test methods used in clinical studies of infliximab and its biosimilar (CT-P13). *Exp Rev Clin Immunol.* 2015;11(sup1):33–41.

[272] Boute N, Lowe P, Berger S, Malissard M, Robert A and Tesar M. NanoLuc luciferase – A multifunctional tool for high throughput antibody screening. *Front Pharmacol.* 2016;7:27.

[273] Nath N, Flemming R, Godat B and Urh M. Development of NanoLuc bridging immunoassay for detection of anti-drug antibodies. *J Immunol Methods.* 2017;450:17–26.

[274] Berger AE, Gleizes A, Waeckel L, Roblin X, Krzysiek R et al. Validation study of a new random-access chemiluminescence immunoassay analyzer i-TRACK10® to monitor infliximab and adalimumab serum trough levels and anti-drug antibodies. *Int J Mol Sci.* 2022;23(17):9561.

[275] Qi H and Zhang C. Electrogenerated chemiluminescence biosensing. *Anal Chem.* 2020;92(1):524–534.

[276] Afonso J, Lopes S, Gonçalves R, Caldeira P, Lago P et al. Detection of anti-infliximab antibodies is impacted by antibody titer, infliximab level and IgG4 antibodies: A systematic comparison of three different assays. *Therap Adv Gastroenterol.* 2016;9(6):781–794.

[277] Ainsworth MA, Bendtzen K and Brynskov J. Tumor necrosis factor-alpha binding capacity and anti-infliximab antibodies measured by fluid-phase radioimmunoassays as predictors of clinical efficacy of infliximab in Crohn's disease. *Am J Gastroenterol.* 2008;103(4):944–948.

[278] van Schouwenburg PA, Bartelds GM, Hart MH, Aarden L, Wolbink GJ and Wouters D. A novel method for the detection of antibodies to adalimumab in the presence of drug reveals "hidden" immunogenicity in rheumatoid arthritis patients. *J Immunol Methods.* 2010;362(1-2):82–88.

[279] Lallemand C, Kavrochorianou N, Steenholdt C, Bendtzen K, Ainsworth MA et al. Reporter gene assay for the quantification of the activity and neutralizing antibody response to TNFα antagonists. *Journal of Immunological Methods.* 2011;373(1):229–239.

[280] Gils A, Vande Casteele N, Poppe R, Van de Wouwer M, Compernolle G et al. Development of a universal anti-adalimumab antibody standard for interlaboratory harmonization. *Ther Drug Monit.* 2014;36(5):669–673.

[281] Pan J, Small T, Qin D, Li S, Wang L et al. Comparison of the NIDS® rapid assay with ELISA methods in immunogenicity testing of two biotherapeutics. *J Pharmacol Toxicol Methods.* 2011;63(2):150–159.

[282] Corstjens PLAM, Fidder HH, Wiesmeijer KC, de Dood CJ, Rispens T et al. A rapid assay for on-site monitoring of infliximab trough levels: A feasibility study. *Anal Bioanal Chem.* 2013;405(23):7367–7375.

[283] Real-Fernández F, Cimaz R, Rossi G, Simonini G, Giani T et al. Surface plasmon resonance-based methodology for anti-adalimumab antibody identification and kinetic characterization. *Anal Bioanal Chem.* 2015;407(24):7477–7485.

[284] Lu J, Van Stappen T, Spasic D, Delport F, Vermeire S et al. Fiber optic-SPR platform for fast and sensitive infliximab detection in serum of inflammatory bowel disease patients. *Biosens Bioelectron.* 2016;79:173–179.

[285] Lu J, Spasic D, Delport F, Van Stappen T, Detrez I et al. Immunoassay for detection of infliximab in whole blood using a fiber-optic surface plasmon resonance biosensor. *Anal Chem.* 2017;89(6):3664–3671.

[286] Verstockt B, Moors G, Bian S, Van Stappen T, Van Assche G et al. Influence of early adalimumab serum levels on immunogenicity and long-term outcome of anti-TNF naive Crohn's disease patients: The usefulness of rapid testing. *Aliment Pharmacol Ther.* 2018;48(7):731–739.

[287] Thoren KL, Pasi B, Delgado JC, Wu AHB and Lynch KL. Quantitation of infliximab and detection of antidrug antibodies in serum by use of surface plasmon resonance. *J Appl Lab Med.* 2018;2(5):725–736.

[288] Beeg M, Nobili A, Orsini B, Rogai F, Gilardi D et al. A surface plasmon resonance-based assay to measure serum concentrations of therapeutic antibodies and anti-drug antibodies. *Sci Rep.* 2019;9(1):2064.

[289] Zeni L, Perri C, Cennamo N, Arcadio F, D'Agostino G et al. A portable optical-fibre-based surface plasmon resonance biosensor for the detection of therapeutic antibodies in human serum. *Sci Rep.* 2020;10(1):11154.

[290] Gils A, Van Stappen T, Dreesen E, Storme R, Vermeire S and Declerck PJ. Harmonization of infliximab and anti-infliximab assays facilitates the comparison between originators and biosimilars in clinical samples. *Inflamm Bowel Dis.* 2016;22(4):969–975.

[291] Homola J, Yee SS and Gauglitz G. Surface plasmon resonance sensors: Review. *Sens Actuators B Chem.* 1999;54(1-2):3–15.

[292] Perumal V and Hashim U. Advances in biosensors: Principle, architecture and applications. *J Appl Biomed.* 2014;12(1):1–15.

[293] Erb EM, Chen X, Allen S, Roberts CJ, Tendler SJ et al. Characterization of the surfaces generated by liposome binding to the modified dextran matrix of a surface plasmon resonance sensor chip. *Anal Biochem.* 2000;280(1):29–35.

[294] Rich RL, Hoth LR, Geoghegan KF, Brown TA, LeMotte PK et al. Kinetic analysis of estrogen receptor/ligand interactions. *Proc Natl Acad Sci USA.* 2002;99(13):8562–8567.

[295] Teh HF, Peh WYX, Su X and Thomsen JS. Characterization of protein-DNA interactions using surface plasmon resonance spectroscopy with various assay schemes. *Biochemistry.* 2007;46(8):2127–2135.

[296] Madeira A, Vikeved E, Nilsson A, Sjögren B, Andrén PE and Svenningsson P. Identification of protein-protein interactions by surface plasmon resonance followed by mass spectrometry. *Curr Protoc Protein Sci.* 2011;65(1):19.21.1–19.21.9.

[297] Liu L. Efficient hit and lead compound evaluation strategy based on off-rate screening by surface plasmon resonance. *J Med Chem.* 2014;57(7):2843–2844.

[298] Del Vecchio K, Stahelin RV. Using surface plasmon resonance to quantitatively assess lipid-protein interactions. In: Waugh MG, editor. *Lipid Signaling Protocols.* Vol. 1376. New York: Humana Press; 2016. p. 141-153.

[299] Stevenson CEM. Analysis of protein-DNA interactions using surface plasmon resonance and a ReDCaT chip. In: Lawson DM, Daviter T, Johnson CM, McLaughlin SH, Williams MA, editors. *Protein-Ligand Interactions: Methods and Applications.* Vol. 2263. New York: Springer US; 2021. p. 369-379.

[300] Dobrovodský D and Di Primo C. Do conformational changes contribute to the surface plasmon resonance signal? *Biosens Bioelectron.* 2023;232:115296.

[301] Nguyen HH, Park J, Kang S and Kim M. Surface plasmon resonance: A versatile technique for biosensor applications. *Sensors.* 2015;15(5):10481–10510.

[302] Masson JF. Surface plasmon resonance clinical biosensors for medical diagnostics. *ACS Sens.* 2017;2(1):16–30.

[303] Wood RW. On a remarkable case of uneven distribution of light in a diffraction grating spectrum. *Proc Phys Soc.* 1902;18(1):269.

[304] Maystre D. Theory of Wood's anomalies. In: Enoch S and Bonod N, editors. *Plasmonics: From Basics to Advanced Topics.* Springer Series in Optical Sciences, vol. 167. Berlin, Heidelberg: Springer Berlin, Heidelberg; 2012. p. 39-83.

[305] Fano U. The theory of anomalous diffraction gratings and of quasi-stationary waves on metallic surfaces (Sommerfeld's waves). *J Opt Soc Am.* 1941;31(3):213–222.

[306] Ritchie RH. Plasma losses by fast electrons in thin films. *Phys Rev.* 1957;106(5):874–881.

[307] Bohm D and Pines D. A collective description of electron interactions. I. Magnetic interactions. *Phys Rev.* 1951;82(5):625–634.

[308] Pines D and Bohm D. A collective description of electron interactions: II. Collective vs individual particle aspects of the interactions. *Phys Rev.* 1952;85(2):338–353.

[309] Bohm D and Pines D. A collective description of electron interactions: III. Coulomb interactions in a degenerate electron gas. *Phys Rev.* 1953;92(3):609–625.

[310] Otto A. Excitation of nonradiative surface plasma waves in silver by the method of frustrated total reflection. *Z Phys A Hadrons Nucl.* 1968;216(4):398–410.

[311] Kretschmann E and Raether H. Notizen: Radiative decay of non radiative surface plasmons excited by light. *Z Naturforsch A.* 1968;23(12):2135–2136.

[312] Kretschmann E. Die Bestimmung optischer Konstanten von Metallen durch Anregung von Oberflächenplasmaschwingungen. *Z Phys A Hadrons Nucl.* 1971;241(4):313–324.

[313] Cullen D, Brown R and Lowe C. Detection of immuno-complex formation via surface plasmon resonance on gold-coated diffraction gratings. *Biosensors.* 1987;3(4):211–225.

[314] Flanagan MT and Pantell RH. Surface plasmon resonance and immunosensors. *Electron Lett.* 1984;20(23):968–970.

[315] Löfås S and Johnsson B. A novel hydrogel matrix on gold surfaces in surface plasmon resonance sensors for fast and efficient covalent immobilization of ligands. *J Chem Soc Chem Commun.* 1990;21:1526–1528.

[316] Jönsson U, Fägerstam L, Ivarsson B, Johnsson B, Karlsson R et al. Real-time biospecific interaction analysis using surface plasmon resonance and a sensor chip technology. *BioTechniques.* 1991;11(5):620–627.

[317] Liedberg B, Nylander C and Lunström I. Surface plasmon resonance for gas detection and biosensing. *Sens Actuators.* 1983;4:299–304.

[318] Liedberg B, Lundström I and Stenberg E. Principles of biosensing with an extended coupling matrix and surface plasmon resonance. *Sens Actuators B Chem.* 1993;11(1):63–72.

[319] Liedberg B, Nylander C and Lundström I. Biosensing with surface plasmon resonance — how it all started. *Biosens Bioelectron.* 1995;10(8):i–ix.

[320] Jönsson U and Malmqvist M. Real time biospecific interaction analysis. The integration of surface plasmon resonance detection, general biospecific interface chemistry and microfluidics into one analytical system. *Adv Biosensors.* 1992;2:291–336.

[321] Place JF, Sutherland RM and Dähne C. Opto-electronic immunosensors: A review of optical immunoassay at continuous surfaces. *Biosensors.* 1985;1(4):321–353.

[322] Grasmeier MK, Weber S, Treiber M, Thaler MA and Luppa PB. Surface plasmon resonance assays for the therapeutic drug monitoring of infliximab indicate clinical relevance of anti-infliximab antibody binding properties. *Clin Chem Lab Med.* 2023;61(7):1255–1265.

[323] Miyazaki SM, Shimizu FM, Ferreira M. 6 - Surface plasmon resonance (SPR) for sensors and biosensors. In: Da Róz AL, Ferreira M, de Lima Leite F, Oliveira ON, editors. *Nanocharacterization Techniques.* William Andrew Publishing; 2017. p. 183-200.

[324] Löfås S, Malmqvist M, Rönnberg I, Stenberg E, Liedberg B and Lundström I. Bioanalysis with surface plasmon resonance. *Sensors and Actuators B: Chemical.* 1991;5(1):79–84.

[325] GE Healthcare Life Sciences. *Biacore X100 Assay Handbook.* Uppsala: 2012.

[326] Pawula M, Altintas Z and Tothill IE. SPR detection of cardiac troponin T for acute myocardial infarction. *Talanta.* 2016;146:823–830.

[327] Beeg M, Burti C, Allocati E, Ciafardini C, Banzi R et al. Surface plasmon resonance unveils important pitfalls of enzyme-linked immunoassay for the detection of anti-infliximab antibodies in patients' sera. *Sci Rep.* 2021;11(1):14976.

[328] Abid SA, Ahmed Muneer A, Al-Kadmy IM, Sattar AA, Beshbishy AM et al. Biosensors as a future diagnostic approach for COVID-19. *Life Sciences.* 2021;273:119117.

[329] Das CM, Kong KV and Yong KT. Diagnostic plasmonic sensors: Opportunities and challenges. *Chem Commun.* 2022;58(69):9573–9585.

[330] von Pawel-Rammingen U, Johansson BP and Björck L. IdeS, a novel streptococcal cysteine proteinase with unique specificity for immunoglobulin G. *EMBO J.* 2002;21(7):1607–1615.

[331] Bogomolovas J, Simon B, Sattler M and Stier G. Screening of fusion partners for high yield expression and purification of bioactive viscotoxins. *Protein Expr Purif.* 2009;64(1):16–23.

[332] Poiesi C, Albertini A, Ghielmi S, Cassani G and Corti A. Kinetic analysis of TNF-α oligomer-monomer transition by surface plasmon resonance and immunochemical methods. *Cytokine.* 1993;5(6):539–545.

[333] Kumar G. Principle and method of silver staining of proteins separated by sodium dodecyl sulfate–polyacrylamide gel electrophoresis. In: Kurien BT and Scofield RH, editors. *Protein Gel Detection and Imaging: Methods and Protocols*. New York: Springer New York; 2018. p. 231-236.

[334] Armbruster DA and Pry T. Limit of blank, limit of detection and limit of quantitation. *Clin Biochem Rev*. 2008;29 Suppl 1(Suppl 1):S49–S52.

[335] Immundiagnostik AG. IDKmonitor Infliximab drug level ELISA: Instruction manual [Internet]. Immundiagnostik AG [cited 2022 Sep 23]. Available from: `https://www.immundiagnostik.com/de/testkits/k-9655`.

[336] Langmann AF. *Bestimmung von Infliximab Und Anti-Infliximab-Antikörpern Im Rahmen Des Therapeutischen Drug- Und Immunogenitäts-Monitoring Bei Chronisch Entzündlichen Darmerkrankungen*. [doctoral thesis]. Munich: Technische Universität München; 2022.

[337] Immundiagnostik AG. IDKmonitor Infliximab total ADA ELISA: Instruction manual [Internet]. Immundiagnostik AG [cited 2022 Sep 23]. Available from: `https://www.immundiagnostik.com/de/testkits/k-9654`.

[338] Strand V, Gonçalves J, Hickling TP, Jones HE, Marshall L and Isaacs JD. Immunogenicity of biosimilars for rheumatic diseases, plaque psoriasis, and inflammatory bowel disease: A review from clinical trials and regulatory documents. *BioDrugs*. 2020;34(1):27–37.

[339] Yanai H, Lichtenstein L, Assa A, Mazor Y, Weiss B et al. Levels of drug and antidrug antibodies are associated with outcome of interventions after loss of response to infliximab or adalimumab. *Clin Gastroenterol Hepatol*. 2015;13(3):522–530.

[340] Tun GSZ, Robinson K, Marshall L, Wright A, Thompson L et al. The effect of infliximab dose escalation in inflammatory bowel disease patients with antibodies to infliximab. *Eur J Gastroenterol Hepatol*. 2022;34(3):295–301.

[341] Vande Casteele N, Feagan BG, Gils A, Vermeire S, Khanna R et al. Therapeutic drug monitoring in inflammatory bowel disease: Current state and future perspectives. *Curr Gastroenterol Rep*. 2014;16(4):378.

[342] Brandse JF, van den Brink GR, Wildenberg ME, van der Kleij D, Rispens T et al. Loss of infliximab into feces is associated with lack of response to therapy in patients with severe ulcerative colitis. *Gastroenterology*. 2015;149(2):350–355.e2.

[343] Grasmeier MK, Langmann AF, Langmann P, Treiber M, Thaler MA and Luppa PB. Dynamics of serum concentrations of antibodies to infliximab: A new approach for predicting secondary loss of response in inflammatory bowel diseases. *Therap Adv Gastroenterol*. 2021;14:17562848211037849.

[344] Bian S, Lu J, Delport F, Vermeire S, Spasic D et al. Development and validation of an optical biosensor for rapid monitoring of adalimumab in serum of patients with Crohn's disease. *Drug Test Anal.* 2018;10(3):592–596.

[345] Bustos RH, Zapata C, Esteban E, García JC, Jáuregui E and Jaimes D. Label-free quantification of anti-TNF-α in patients treated with adalimumab using an optical biosensor. *Sensors.* 2018;18(3):691.

[346] Qu JH, Ordutowski H, Van Tricht C, Verbruggen R, Barcenas Gallardo A et al. Point-of-care therapeutic drug monitoring of adalimumab by integrating a FO-SPR biosensor in a self-powered microfluidic cartridge. *Biosens Bioelectron.* 2022;206:114125.

[347] Kang SE, Park JK, Yoo HJ, Kang HS, Park YW et al. Efficacy of novel bispecific antibody targeting TNF-α/CXCL10 in the treatment of experimental arthritis. *Transl Res.* 2021;232:75–87.

[348] Kaymakcalan Z, Sakorafas P, Bose S, Scesney S, Xiong L et al. Comparisons of affinities, avidities, and complement activation of adalimumab, infliximab, and etanercept in binding to soluble and membrane tumor necrosis factor. *Clin Immunol.* 2009;131(2):308–316.

[349] Ogura T, Tanaka Y and Toyoda H. Whole cell-based surface plasmon resonance measurement to assess binding of anti-TNF agents to transmembrane target. *Anal Biochem.* 2016;508:73–77.

[350] Schreiber S, Yamamoto K, Muniz R and Iwura T. Physicochemical analysis and biological characterization of FKB327 as a biosimilar to adalimumab. *Pharmacol Res Perspect.* 2020;8(3):e00604.

[351] Shealy DJ, Cai A, Staquet K, Baker A, Lacy ER et al. Characterization of golimumab, a human monoclonal antibody specific for human tumor necrosis factor α. *MAbs.* 2010;2(4):428–439.

[352] Velayudhan J, Chen YF, Rohrbach A, Pastula C, Maher G et al. Demonstration of functional similarity of proposed biosimilar ABP 501 to adalimumab. *BioDrugs.* 2016;30(4):339–351.

[353] Sparrow MP, Papamichael K, Ward MG, Riviere P, Laharie D et al. Therapeutic drug monitoring of biologics during induction to prevent primary non-response. *J Crohns Colitis.* 2020;14(4):542–556.

[354] International Council for Harmonisation of Technical Requirements for Registration of Pharmaceuticals for Human Use. ICH guideline M10 on bioanalytical method validation - Step 5 [Internet]. International Council for Harmonisation of Technical Requirements for Registration of Pharmaceuticals for Human Use; 2023 [cited 2023 Mar 3]. Available from:

https://www.ema.europa.eu/en/documents/scientific-guideline/ich-guideline-m10-bioanalytical-method-validation-step-5_en.pdf.

[355] European Medicines Agency. Guideline on bioanalytical method validation (EMEA/CHMP/EWP/192217/2009 Rev. 1 Corr. 2) [Internet]. European Medicines Agency; 2015 [cited 2023 Mar 3]. Available from: https://www.ema.europa.eu/en/documents/scientific-guideline/guideline-bioanalytical-method-validation_en.pdf.

[356] Gorovits B, Baltrukonis DJ, Bhattacharya I, Birchler MA, Finco D et al. Immunoassay methods used in clinical studies for the detection of anti-drug antibodies to adalimumab and infliximab. *Clin Exp Immunol.* 2018;192(3):348–365.

[357] Afonso J, de Sousa HT, Rosa I, Carvalho J, Dias CC and Magro F. Therapeutic drug monitoring of CT-P13: A comparison of four different immunoassays. *Therap Adv Gastroenterol.* 2017;10(9):661–671.

[358] Magro F, Rocha C, Vieira AI, Sousa HT, Rosa I et al. The performance of Remicade®-optimized quantification assays in the assessment of Flixabi® levels. *Therap Adv Gastroenterol.* 2018;11:1756284818796956.

[359] Neveu B, Kunst A, Prosser C and Robitaille R. An in vitro comparison of four different immunoassays for the monitoring of infliximab biosimilars drug levels. *Clin Biochem.* 2020;78:58–62.

[360] Vaisman-Mentesh A, Rosenstein S, Yavzori M, Dror Y, Fudim E et al. Molecular landscape of anti-drug antibodies reveals the mechanism of the immune response following treatment with TNFα antagonists. *Front Immunol.* 2019;10:2921.

[361] Luo YR, Chakraborty I, Lazar-Molnar E, Wu AHB and Lynch KL. Development of label-free immunoassays as novel solutions for the measurement of monoclonal antibody drugs and antidrug antibodies. *Clin Chem.* 2020;66(10):1319–1328.

[362] Bonifacino JS, Dell'Angelica EC and Springer TA. Immunoprecipitation. *Curr Protoc Immunol.* 2001;41(1):8.3.1–8.3.28.

[363] Eisen HN and Siskind GW. Variations in affinities of antibodies during the immune response. *Biochemistry.* 1964;3(7):996–1008.

[364] Desikan R, Antia R and Dixit NM. Physical 'strength' of the multi-protein chain connecting immune cells: Does the weakest link limit antibody affinity maturation? *BioEssays.* 2021;43(4):2000159.

[365] Food and Drug Administration. Immunogenicity testing of therapeutic protein products - Developing and validation assays for anti-drug antibody detection. Guidance for Industry [Internet]. Food and Drug Administration; 2019 [cited 2023 May 12]. Available from: Availablefrom:https://www.fda.gov/media/119788/download.

[366] R-Biopharm AG. RIDASCREEN Anti-IFX Antibodies ELISA: Instruction manual [Internet]. R-Biopharm AG [cited 2023 Mar 22]. Available from: https://clinical.r-biopharm.com/wp-content/uploads/2016/03/g09042_ridascreen-anti-ifx-antibodies_2019-11-05_de.pdf.

[367] Pavlov IY, Carper J, Lázár-Molnár E and Delgado JC. Clinical laboratory application of a reporter-gene assay for measurement of functional activity and neutralizing antibody response to infliximab. *Clin Chim Acta.* 2016;453:147–153.

[368] Van Stappen T, Vande Casteele N, Van Assche G, Ferrante M, Vermeire S and Gils A. Clinical relevance of detecting anti-infliximab antibodies with a drug-tolerant assay: Post hoc analysis of the TAXIT trial. *Gut.* 2018;67(5):818–826.

[369] Bio-Rad Antibodies. Infliximab antibody AbD20436_hIgG1 [Internet]. Bio-Rad Antibodies [cited 2023 May 11]. Available from: https://www.bio-rad-antibodies.com/monoclonal/infliximab-antibody-abd20436-higg1-hca233.html.

[370] Vogeser M and Seger C. A decade of HPLC–MS/MS in the routine clinical laboratory – Goals for further developments. *Clin Biochem.* 2008;41(9):649–662.

[371] Jannetto PJ and Fitzgerald RL. Effective use of mass spectrometry in the clinical laboratory. *Clin Chem.* 2016;62(1):92–98.

[372] R-Biopharm AG. RIDASCREEN Infliximab Monitoring ELISA: Instruction manual [Internet]. R-Biopharm [cited 2023 Mar 22]. Available from: https://clinical.r-biopharm.com/wp-content/uploads/2015/01/g09041_ridascreen-ifx-monitoring_2019-11-14_en.pdf.

[373] Bots SJ, Parker CE, Brandse JF, Löwenberg M, Feagan BG et al. Anti-drug antibody formation against biologic agents in inflammatory bowel disease: A systematic review and meta-analysis. *BioDrugs.* 2021;35(6):715–733.

[374] Nanda KS, Cheifetz AS and Moss AC. Impact of antibodies to infliximab on clinical outcomes and serum infliximab levels in patients with inflammatory bowel disease (IBD): A meta-analysis. *Am J Gastroenterol.* 2013;108(1):40–47.

[375] Ma C, Hanzel J, Panaccione R, Sandborn WJ, D'Haens GR et al. CORE-IBD: A multidisciplinary international consensus initiative to develop a core outcome set for randomized controlled trials in inflammatory bowel disease. *Gastroenterology.* 2022;163(4):950–964.

[376] Oh EH, Ko DH, Seo H, Chang K, Kim GU et al. Clinical correlations of infliximab trough levels and antibodies to infliximab in South Korean patients with Crohn's disease. *World J Gastroenterol.* 2017;23(8):1489–1496.

[377] Farrell RJ, Alsahli M, Jeen YT, Falchuk KR, Peppercorn MA and Michetti P. Intravenous hydrocortisone premedication reduces antibodies to infliximab in Crohn's disease: A randomized controlled trial. *Gastroenterology.* 2003;124(4):917–924.

[378] Tatarewicz SM, Mytych DT, Manning MS, Swanson SJ, Moxness MS and Chirmule N. Strategic characterization of anti-drug antibody responses for the assessment of clinical relevance and impact. *Bioanalysis.* 2014;6(11):1509–1523.

[379] Joyce A, Shea C, You Z, Gorovits B and Lepsy C. Determination of anti-drug antibody affinity in clinical study samples provides a tool for evaluation of immune response maturation. *AAPS J.* 2022;24(6):114.

[380] van Schie KA, Hart MH, de Groot ER, Kruithof S, Aarden LA et al. The antibody response against human and chimeric anti-TNF therapeutic antibodies primarily targets the TNF binding region. *Ann Rheum Dis.* 2015;74(1):311–314.

[381] van Schie KA, Kruithof S, van Schouwenburg PA, Vennegoor A, Killestein J et al. Neutralizing capacity of monoclonal and polyclonal anti-natalizumab antibodies: The immune response to antibody therapeutics preferentially targets the antigen-binding site. *J Allergy Clin Immunol.* 2017;139(3):1035–1037.e6.

[382] van Schouwenburg PA, van de Stadt LA, de Jong RN, van Buren EEL, Kruithof S et al. Adalimumab elicits a restricted anti-idiotypic antibody response in autoimmune patients resulting in functional neutralisation. *Ann Rheum Dis.* 2013;72(1):104–109.

[383] van Schouwenburg PA, Kruithof S, Votsmeier C, van Schie KA, Hart MH et al. Functional analysis of the anti-adalimumab response using patient-derived monoclonal antibodies. *J Biol Chem.* 2014;289(50):34482–34488.

[384] Ständer S, R. Grauslund L, Scarselli M, Norais N and Rand K. Epitope mapping of polyclonal antibodies by hydrogen–deuterium exchange mass spectrometry (HDX-MS). *Anal Chem.* 2021;93(34):11669–11678.

[385] Aniol-Nielsen C, Toft-Hansen H, Dahlbäck M, Nielsen CH and Solberg H. Calibration–free concentration analysis for quantification of anti-drug specific antibodies in polyclonal positive control antibodies and in clinical samples. *J Immunol Methods.* 2021;497:113002.

[386] Lenders M, Scharnetzki D, Heidari A, Di Iorio D, Wegner SV and Brand E. Generation and characterization of a polyclonal human reference antibody to measure anti-drug antibody titers in patients with fabry disease. *Int J Mol Sci.* 2021;22(5):2680.

[387] Schick AJ, Lundin V, Low J, Peng K, Vandlen R and Wecksler AT. Epitope mapping of anti-drug antibodies to a clinical candidate bispecific antibody. *mAbs.* 2022;14(1):2028337.

[388] Mason DW and Williams AF. The kinetics of antibody binding to membrane antigens in solution and at the cell surface. *Biochem J.* 1980;187(1):1–20.

[389] Olson WC, Spitznagel TM and Yarmush ML. Dissociation kinetics of antigen-antibody interactions: Studies on a panel of anti-albumin monoclonal antibodies. *Mol Immunol.* 1989;26(2):129–136.

[390] O'Shannessy DJ, Brigham-Burke M, Soneson KK, Hensley P and Brooks I. Determination of rate and equilibrium binding constants for macromolecular interactions using surface plasmon resonance: Use of nonlinear least squares analysis methods. *Anal Biochem.* 1993;212:457–468.

[391] Levinson SS and Miller JJ. Towards a better understanding of heterophile (and the like) antibody interference with modern immunoassays. *Clin Chim Acta.* 2002;325(1):1–15.

[392] Takacs MA, Jacobs SJ, Bordens RM and Swanson SJ. Detection and characterization of antibodies to PEG-IFN-alpha2b using surface plasmon resonance. *J Interferon Cytokine Res.* 1999;19(7):781–789.

[393] Valsecchi C, Gobbi M, Beeg M, Adams T, Castaman G et al. Characterization of the neutralizing anti-emicizumab antibody in a patient with hemophilia A and inhibitor. *J Thromb Haemost.* 2021;19(3):711–718.

[394] Knappik A, Ge L, Honegger A, Pack P, Fischer M et al. Fully synthetic human combinatorial antibody libraries (HuCAL) based on modular consensus frameworks and CDRs randomized with trinucleotides. *J Mol Biol.* 2000;296(1):57–86.

[395] *The United States Pharmacopeia. National Formulary.* Issue 2. Rockville (MD): United States Pharmacopeial Convention; 2023. <1106> Immunogenicity assays - design and validation of immunogenicity assays to detect anti-drug antibodies.

[396] Papamichael K, Vajravelu RK, Vaughn BP, Osterman MT and Cheifetz AS. Proactive infliximab monitoring following reactive testing is associated with better clinical outcomes than reactive testing alone in patients with inflammatory bowel disease. *J Crohns Colitis.* 2018;12(7):804–810.

[397] Steenholdt C, Al-khalaf M, Brynskov J, Bendtzen K, Thomsen Oleϕ and Ainsworth MA. Clinical implications of variations in anti-infliximab antibody levels in patients with inflammatory bowel disease. *Inflamm Bowel Dis.* 2012;18(12):2209–2217.

[398] Dubinsky MC, Phan BL, Singh N, Rabizadeh S and Mould DR. Pharmacokinetic dashboard-recommended dosing Is different than standard of care dosing in infliximab-treated pediatric IBD patients. *AAPS J.* 2017;19(1):215–222.

[399] Eser A, Primas C, Reinisch S, Vogelsang H, Novacek G et al. Prediction of individual serum infliximab concentrations in inflammatory bowel disease by a Bayesian dashboard system. *J Clin Pharmacol.* 2018;58(6):790–802.

[400] Strik AS, Löwenberg M, Mould DR, Berends SE, Ponsioen CI et al. Efficacy of dashboard driven dosing of infliximab in inflammatory bowel disease patients; a randomized controlled trial. *Scand J Gastroenterol.* 2021;56(2):145–154.

[401] Dave MB, Dherai AJ, Desai DC, Mould DR and Ashavaid TF. Optimization of infliximab therapy in inflammatory bowel disease using a dashboard approach—an Indian experience. *Eur J Clin Pharmacol.* 2021;77(1):55–62.

[402] Shmais M, Regueiro M and Hashash JG. Proactive versus reactive therapeutic drug monitoring: Why, when, and how? *Inflamm Intest Dis.* 2021;7(1):50–58.

[403] Vaughn BP, Martinez-Vazquez M, Patwardhan VR, Moss AC, Sandborn WJ and Cheifetz AS. Proactive therapeutic concentration monitoring of infliximab may improve outcomes for patients with inflammatory bowel disease: Results from a pilot observational study. *Inflamm Bowel Dis.* 2014;20(11):1996–2003.

[404] Cornillie F, Hanauer SB, Diamond RH, Wang J, Tang KL et al. Postinduction serum infliximab trough level and decrease of C-reactive protein level are associated with durable sustained response to infliximab: A retrospective analysis of the ACCENT I trial. *Gut.* 2014;63(11):1721–1727.

[405] Davidov Y, Ungar B, Bar-Yoseph H, Carter D, Haj-Natour O et al. Association of induction infliximab levels with clinical response in perianal Crohn's disease. *J Crohns Colitis.* 2017;11(5):549–555.

[406] Papamichael K, Chachu KA, Vajravelu RK, Vaughn BP, Ni J et al. Improved Long-term outcomes of patients with inflammatory bowel disease receiving proactive compared with reactive monitoring of serum concentrations of infliximab. *Clin Gastroenterol Hepatol.* 2017;15(10):1580–1588.e3.

[407] Papamichael K, Juncadella A, Wong D, Rakowsky S, Sattler LA et al. Proactive therapeutic drug monitoring of adalimumab is associated with better long-term outcomes compared with standard of care in patients with inflammatory bowel disease. *J Crohns Colitis.* 2019;13(8):976–981.

[408] Assa A, Matar M, Turner D, Broide E, Weiss B et al. Proactive monitoring of adalimumab trough concentration associated with increased clinical remission in children with Crohn's disease compared with reactive monitoring. *Gastroenterology.* 2019;157(4):985–996.e2.

[409] Dreesen E, Baert F, Laharie D, Bossuyt P, Bouhnik Y et al. Monitoring a combination of calprotectin and infliximab identifies patients with mucosal healing of Crohn's disease. *Clin Gastroenterol Hepatol.* 2020;18(3):637–646.e11.

[410] Negoescu DM, Enns EA, Swanhorst B, Baumgartner B, Campbell JP et al. Proactive vs reactive therapeutic drug monitoring of infliximab in Crohn's disease: A cost-effectiveness analysis in a simulated cohort. *Inflamm Bowel Dis.* 2020;26(1):103–111.

[411] Sánchez-Hernández JG, Rebollo N, Martin-Suarez A, Calvo MV and Muñoz F. A 3-year prospective study of a multidisciplinary early proactive therapeutic drug monitoring programme of infliximab treatments in inflammatory bowel disease. *Br J Clin Pharmacol.* 2020;86(6):1165–1175.

[412] Syed N, Tolaymat M, Brown SA, Sivasailam B and Cross RK. Proactive drug monitoring is associated with higher persistence to infliximab and adalimumab treatment and lower healthcare utilization compared with reactive and clinical monitoring. *Crohns Colitis 360.* 2020;2(3):otaa050.

[413] Lyles JL, Mulgund AA, Bauman LE, Su W, Fei L et al. Effect of a practice-wide anti-TNF proactive therapeutic drug monitoring program on outcomes in pediatric patients with inflammatory bowel disease. *Inflamm Bowel Dis.* 2021;27(4):482–492.

[414] Syversen SW, Jørgensen KK, Goll GL, Brun MK, Sandanger Ø et al. Effect of therapeutic drug monitoring vs standard therapy during maintenance infliximab therapy on disease control in patients with immune-mediated inflammatory diseases: A randomized clinical trial. *JAMA.* 2021;326(23):2375–2384.

[415] Liefferinckx C, Bottieau J, Toubeau JF, Thomas D, Rahier JF et al. Collecting new peak and intermediate infliximab levels to predict remission in inflammatory bowel diseases. *Inflamm Bowel Dis.* 2022;28(2):208–217.

[416] Gomollón F, Dignass A, Annese V, Tilg H, Van Assche G et al. 3rd European evidence-based consensus on the diagnosis and management of Crohn's disease 2016: Part 1: Diagnosis and medical management. *J Crohns Colitis.* 2017;11(1):3–25.

[417] Feuerstein JD, Nguyen GC, Kupfer SS, Falck-Ytter Y, Singh S et al. American Gastroenterological Association institute guideline on therapeutic drug monitoring in inflammatory bowel disease. *Gastroenterology.* 2017;153(3):827–834.

[418] Lichtenstein GR, Loftus EV, Isaacs KL, Regueiro MD, Gerson LB and Sands BE. ACG clinical guideline: Management of Crohn's disease in adults. *Am J Gastroenterol.* 2018;113(4):481–517.

[419] Torres J, Bonovas S, Doherty G, Kucharzik T, Gisbert JP et al. ECCO guidelines on therapeutics in Crohn's disease: Medical treatment. *J Crohns Colitis.* 2020;14(1):4–22.

[420] Steinhart AH, Panaccione R, Targownik L, Bressler B, Khanna R et al. Clinical practice guideline for the medical management of perianal fistulizing Crohn's disease: The Toronto consensus. *Inflam Bowel Dis.* 2019;25(1):1–13.

[421] Bossuyt P, Pouillon L, Claeys S, D'Haens S, Hoefkens E et al. Ultra-proactive therapeutic drug monitoring of infliximab based on point of care testing in inflammatory bowel disease: Results of a pragmatic trial. *J Crohns Colitis.* 2022;16(2):199–206.

[422] Papamichael K, Casteele NV, Ferrante M, Gils A and Cheifetz AS. Therapeutic drug monitoring during induction of anti–tumor necrosis factor therapy in inflammatory bowel disease: Defining a therapeutic drug window. *Inflamm Bowel Dis.* 2017;23(9):1510–1515.

[423] Grossberg LB, Cheifetz AS and Papamichael K. Therapeutic drug monitoring of biologics in Crohn's disease. *Gastroenterol Clin North Am.* 2022;51(2):299–317.

[424] Van Stappen T, Bollen L, Casteele NV, Papamichael K, Van Assche G et al. Rapid test for infliximab drug concentration allows immediate dose adaptation. *Clin Transl Gastroenterol.* 2016;7(12):e206.

[425] Irving PM and Gecse KB. Optimizing therapies using therapeutic drug monitoring: Current strategies and future perspectives. *Gastroenterology.* 2022;162(5):1512–1524.

[426] Stein R, Lee D, Leonard MB, Thayu M, Denson LA et al. Serum infliximab, antidrug antibodies, and tumor necrosis factor predict sustained response in pediatric Crohn's disease. *Inflamm Bowel Dis.* 2016;22(6):1370–1377.

[427] Ungar B, Engel T, Yablecovitch D, Lahat A, Lang A et al. Prospective observational evaluation of time-dependency of adalimumab immunogenicity and drug concentrations: The POETIC Study. *Am J Gastroenterol.* 2018;113(6):890–898.

[428] Lega S, Phan BL, Rosenthal CJ, Gordon J, Haddad N et al. Proactively optimized infliximab monotherapy is as effective as combination therapy in IBD. *Inflamm Bowel Dis.* 2019;25(1):134–141.

[429] Hanžel J, Zdovc J, Kurent T, Sever N, Javornik K et al. Peak concentrations of ustekinumab after intravenous induction therapy identify patients with Crohn's disease likely to achieve endoscopic and biochemical remission. *Clin Gastroenterol Hepatol.* 2021;19(1):111–118.e10.

[430] Kevans D, Murthy S, Mould DR and Silverberg MS. Accelerated clearance of infliximab is associated with treatment failure in patients with corticosteroid-refractory acute ulcerative colitis. *J Crohns Colitis.* 2018;12(6):662–669.

[431] Vande Casteele N, Jeyarajah J, Jairath V, Feagan BG and Sandborn WJ. Infliximab exposure-response relationship and thresholds associated with endoscopic healing in patients with ulcerative colitis. *Clin Gastroenterol Hepatol.* 2019;17(9):1814–1821.e1.

[432] Battat R, Hemperly A, Truong S, Whitmire N, Boland BS et al. Baseline clearance of infliximab is associated with requirement for colectomy in patients with acute severe ulcerative colitis. *Clin Gastroenterol Hepatol.* 2021;19(3):511–518.e6.

[433] Ogasawara K and Alexander GC. Use of population pharmacokinetic analyses among FDA-approved biologics. *Clin Pharmacol Drug Dev.* 2019;8(7):914–921.

[434] Dreesen E, Berends S, Laharie D, D'Haens G, Vermeire S et al. Modelling of the relationship between infliximab exposure, faecal calprotectin and endoscopic remission in patients with Crohn's disease. *Br J Clin Pharmacol.* 2021;87:106–118.

[435] Lefevre PLC, Shackelton LM and Vande Casteele N. Factors influencing drug disposition of monoclonal antibodies in inflammatory bowel disease: Implications for personalized medicine. *BioDrugs.* 2019;33(5):453–468.

[436] Vermeire S, Dreesen E, Papamichael K and Dubinsky MC. How, when, and for whom should we perform therapeutic drug monitoring? *Clin Gastroenterol Hepatol.* 2020;18(6):1291–1299.

[437] West TA, Sam M and Toong C. Comparison of three commercially available ELISA assays for anti-infliximab antibodies. *Pathology (Phila.).* 2021;53(4):508–514.

[438] Fu E, Chinowsky T, Nelson K, Johnston K, Edwards T et al. SPR imaging-based salivary diagnostics system for the detection of small molecule analytes. *Ann N Y Acad Sci.* 2007;1098(1):335–344.

[439] Mariani S and Minunni M. Surface plasmon resonance applications in clinical analysis. *Anal Bioanal Chem.* 2014;406(9):2303–2323.

[440] Wang W, Mai Z, Chen Y, Wang J, Li L et al. A label-free fiber optic SPR biosensor for specific detection of C-reactive protein. *Sci Rep.* 2017;7(1):16904.

[441] Aray A, Chiavaioli F, Arjmand M, Trono C, Tombelli S et al. SPR-based plastic optical fibre biosensor for the detection of C-reactive protein in serum. *J Biophotonics.* 2016;9(10):1077–1084.

[442] Omar NAS, Fen YW, Abdullah J, Mustapha Kamil Y, Daniyal WMEMM et al. Sensitive detection of dengue virus type 2 E-proteins signals using self-assembled monolayers/reduced graphene oxide-PAMAM dendrimer thin film-SPR optical sensor. *Sci Rep.* 2020;10(1):2374.

[443] Shang J, Ye G, Shi K, Wan Y, Luo C et al. Structural basis of receptor recognition by SARS-CoV-2. *Nature.* 2020;581(7807):221–224.

[444] Sierpe R, Kogan MJ and Bollo S. Label-free oligonucleotide-based SPR biosensor for the detection of the gene mutation causing prothrombin-related thrombophilia. *Sensors.* 2020;20(21):6240.

[445] Kim HM, Jeong DH, Lee HY, Park JH and Lee SK. Design and validation of fiber optic localized surface plasmon resonance sensor for thyroglobulin immunoassay with high sensitivity and rapid detection. *Sci Rep.* 2021;11(1):15985.

Appendices

A. Patient cohort

IFXmon and ADAmon patient cohort

n_{sera}	$n_{patients}$	Analyses
84	15	IFXmon
129	44	ADAmon
54	14	IFXmon & ADAmon
159	**45**	**Total**

				ELISA			SPR				
n_{serum}	$n_{patient}$	$ID_{patient}$	ID_{visit}	IFX, µg/mL	ADA, AU/mL	ADA, µgEq/mL	IFX, µg/mL	ADA, µgEq/mL	DissR	Therapy outcome*	Visit date
1	1	W-IFX-1	a	1.9	<LOQ	<LOQ	3.1	<LOD	NA		10.05.19
2	1	W-IFX-1	b	5.6	<LOQ	<LOQ	NA	<LOD	NA		19.06.19
3	1	W-IFX-1	c	2.8	11.5	0.0001	5.3	<LOD	NA	R	11.09.19
4	1	W-IFX-1	d	2.7	<LOQ	<LOQ	2.5	<LOD	NA		24.10.19
5	1	W-IFX-1	e	4.6	<LOQ	<LOQ	4.9	<LOD	NA		04.12.19
6	1	W-IFX-1	f	4.5	<LOQ	<LOQ	3.9	<LOD	NA		19.02.20
7	2	W-IFX-2	a	<LOQ	<LOQ	<LOQ	<LOD	NA	NA		09.05.20
8	2	W-IFX-2	b	19.4	<LOQ	<LOQ	17.9	NA	NA		23.05.19
9	2	W-IFX-2	c	14.7	<LOQ	<LOQ	14.6	NA	NA		20.06.19
10	2	W-IFX-2	d	9.2	<LOQ	<LOQ	11.8	NA	NA		19.07.19
11	2	W-IFX-2	e	8.7	<LOQ	<LOQ	9.4	NA	NA	R	22.08.19
12	2	W-IFX-2	f	6.8	<LOQ	<LOQ	7.0	<LOD	NA		30.10.19
13	2	W-IFX-2	g	6.2	<LOQ	<LOQ	6.7	NA	NA		04.12.19
14	2	W-IFX-2	h	4.7	<LOQ	<LOQ	5.3	NA	NA		16.01.20
15	2	W-IFX-2	i	2.1	<LOQ	<LOQ	3.0	NA	NA		05.03.20
16	3	W-IFX-3	a	5.8	<LOQ	<LOQ	6.7	NA	NA		26.06.19
17	3	W-IFX-3	b	5.0	<LOQ	<LOQ	6.5	NA	NA		07.08.19
18	3	W-IFX-3	c	5.7	<LOQ	<LOQ	4.7	NA	NA	R	18.09.19
19	3	W-IFX-3	d	5.0	<LOQ	<LOQ	5.8	NA	NA		30.10.19
20	3	W-IFX-3	f	4.8	<LOQ	<LOQ	5.9	<LOD	NA		15.01.20
21	3	W-IFX-3	g	3.5	<LOQ	<LOQ	4.5	NA	NA		03.03.20
22	4	W-IFX-4	a	5.0	34.9	0.0045	5.7	<LOD	NA		27.05.19
23	4	W-IFX-4	b	4.9	48.7	0.0072	4.1	NA	NA		03.07.19
24	4	W-IFX-4	c	3.9	20.1	0.0017	4.0	0.155	2.941		13.08.19
25	4	W-IFX-4	cc	8.3	<LOQ	<LOQ	NA	<LOD	NA	R	25.09.19
26	4	W-IFX-4	d	3.1	15.1	0.0007	2.7	<LOD	NA		08.11.19
27	4	W-IFX-4	e	3.3	15.3	0.0007	4.3	<LOD	NA		20.12.19
28	4	W-IFX-4	f	2.7	<LOQ	<LOQ	NA	0.217	2.850		29.01.20
29	4	W-IFX-4	g	3.6	<LOQ	<LOQ	NA	<LOD	NA		10.03.20
30	5	W-IFX-5	a	2.9	<LOQ	<LOQ	NA	<LOD	NA		22.05.19
31	5	W-IFX-5	b	4.3	11.5	0.0001	NA	<LOD	NA		05.07.19
32	5	W-IFX-5	c	5.1	<LOQ	<LOQ	NA	<LOD	NA		15.08.19
33	5	W-IFX-5	d	<LOQ	55.0	0.0085	NA	<LOD	NA	R	27.09.19
34	5	W-IFX-5	e	3.5	<LOQ	<LOQ	NA	<LOD	NA		13.11.19
35	5	W-IFX-5	f	5.2	<LOQ	<LOQ	NA	<LOD	NA		23.12.19
36	5	W-IFX-5	g	3.3	<LOQ	<LOQ	NA	0.178	2.098		05.02.20
37	5	W-IFX-5	h	1.6	<LOQ	<LOQ	NA	0.169	2.079		10.03.20
38	6	W-IFX-6	a	5.0	159.6	0.0305	5.1	<LOD	NA		22.05.19
39	6	W-IFX-6	b	1.7	205.4	0.0410	2.7	0.208	1.426		05.07.19
40	6	W-IFX-6	c	3.8	164.4	0.0316	NA	0.140	1.532		13.08.19
41	6	W-IFX-6	d	5.6	156.6	0.0298	3.9	0.414	2.095	LOR	11.09.19
42	6	W-IFX-6	dd	4.3	213.9	0.0430	NA	0.652	2.169		14.10.19
43	6	W-IFX-6	e	3.7	287.8	0.0615	6.3	0.192	1.514		20.11.19
44	6	W-IFX-6	f	6.4	216.2	0.0436	6.6	0.195	1.512		18.12.19
45	6	W-IFX-6	g	3.9	173.5	0.0336	6.2	NA	NA		17.01.20
46	7	W-IFX-8	a	3.4	<LOQ	<LOQ	NA	<LOD	NA		10.05.19
47	7	W-IFX-8	b	4.8	10.4	0.0001	NA	<LOD	NA		17.06.19
48	7	W-IFX-8	c	4.5	<LOQ	<LOQ	NA	<LOD	NA		17.07.19
49	7	W-IFX-8	d	9.3	<LOQ	<LOQ	NA	<LOD	NA		14.08.19
50	7	W-IFX-8	e	11.6	10.7	0.0001	NA	<LOD	NA	LOR	11.09.19
51	7	W-IFX-8	f	8.7	<LOQ	<LOQ	NA	<LOD	NA		14.11.19
52	7	W-IFX-8	g	2.5	<LOQ	<LOQ	NA	<LOD	NA		18.01.20
53	7	W-IFX-8	h	2.5	<LOQ	<LOQ	NA	<LOD	NA		31.01.20
54	7	W-IFX-8	i	5.6	<LOQ	<LOQ	NA	<LOD	NA		04.03.20

				ELISA			SPR				
n_{serum}	$n_{patient}$	$ID_{patient}$	ID_{visit}	IFX, µg/mL	ADA, AU/mL	ADA, µgEq/mL	IFX, µg/mL	ADA, µgEq/mL	DissR	Therapy outcome*	Visit date
55	8	W-IFX-9	a	7.8	17.9	0.0012	8.2	<LOD	NA		16.05.20
56	8	W-IFX-9	b	12.1	<LOQ	<LOQ	11.2	0.278	2.226		19.06.19
57	8	W-IFX-9	c	7.1	36.4	0.0048	6.4	<LOD	NA		22.07.19
58	8	W-IFX-9	d	8.7	42.4	0.0060	7.6	<LOD	NA	R	30.08.19
59	8	W-IFX-9	dd	6.8	26.9	0.0030	NA	0.188	2.212		10.10.19
60	8	W-IFX-9	e	14.6	12.3	0.0002	14.9	<LOD	NA		09.01.20
61	8	W-IFX-9	f	16.1	11.8	0.0001	18.8	<LOD	NA		07.02.20
62	8	W-IFX-9	g	12.8	<LOQ	<LOQ	14.5	<LOD	NA		09.03.20
63	9	W-IFX-10	a	7.2	39.9	0.0055	8.4	0.179	3.458		17.06.19
64	9	W-IFX-10	b	8.8	47.6	0.0070	9.5	<LOD	NA		25.07.19
65	9	W-IFX-10	c	12.6	35.2	0.0046	14.1	0.257	2.892	R	28.08.19
66	9	W-IFX-10	d	6.4	123.6	0.0226	6.7	<LOD	NA		15.10.19
67	9	W-IFX-10	e	5.2	87.9	0.0151	7.3	<LOD	NA		04.12.19
68	9	W-IFX-10	f	7.7	99.4	0.0175	8.5	0.146	2.776		16.01.20
69	10	W-IFX-11	a	6.5	<LOQ	<LOQ	7.2	NA	NA		10.05.19
70	10	W-IFX-11	b	5.3	<LOQ	<LOQ	6.7	0.248	2.058		17.06.19
71	10	W-IFX-11	c	3.5	<LOQ	<LOQ	3.6	0.160	2.117		25.07.19
72	10	W-IFX-11	d	3.2	<LOQ	<LOQ	4.0	NA	NA		29.08.19
73	10	W-IFX-11	f	6.0	<LOQ	<LOQ	5.3	NA	NA	R	30.10.19
74	10	W-IFX-11	g	8.9	<LOQ	<LOQ	8.0	NA	NA		29.11.19
75	10	W-IFX-11	h	3.9	<LOQ	<LOQ	4.3	NA	NA		09.01.20
76	10	W-IFX-11	i	9.5	<LOQ	<LOQ	8.7	NA	NA		07.02.20
77	10	W-IFX-11	j	6.7	<LOQ	<LOQ	5.9	NA	NA		11.03.20
78	11	W-IFX-12	b	6.6	<LOQ	<LOQ	NA	<LOD	NA	R	26.07.19
79	12	W-IFX-15	a	<LOQ	729.6	0.2282	<LOD	NA	NA	LOR	31.07.19
80	12	W-IFX-15	b	<LOQ	1026.5	0.5060	<LOD	20.168	1.088		15.08.19
81	13	W-IFX-16	a	<LOQ	<LOQ	<LOQ	NA	<LOD	NA		01.08.19
82	13	W-IFX-16	b	26.0	<LOQ	<LOQ	NA	<LOD	NA		13.08.19
83	13	W-IFX-16	c	13.6	<LOQ	<LOQ	NA	<LOD	NA	R	11.09.19
84	13	W-IFX-16	e	5.0	59.7	0.0094	NA	0.209	1.800		04.12.19
85	13	W-IFX-16	f	2.9	117.7	0.0214	NA	0.221	1.881		15.01.20
86	14	W-IFX-17	a	<LOQ	<LOQ	<LOQ	<LOD	<LOD	NA		01.08.19
87	14	W-IFX-17	b	8.8	18.6	0.0014	7.2	<LOD	NA		14.08.19
88	14	W-IFX-17	c	2.0	<LOQ	<LOQ	2.0	<LOD	NA	LOR	12.09.19
89	14	W-IFX-17	d	2.1	29.7	0.0035	1.8	0.197	2.428		16.10.19
90	14	W-IFX-17	e	3.6	164.0	0.0315	2.8	0.338	1.942		13.11.20
91	14	W-IFX-17	f	<LOQ	540.0	0.1411	<LOD	0.766	1.251		23.01.20
92	15	W-IFX-18	a	12.5	11.1	0.0001	11.7	0.156	1.717		10.05.19
93	15	W-IFX-18	b	7.8	14.0	0.0005	7.0	0.454	1.758		20.06.19
94	15	W-IFX-18	c	6.6	25.8	0.0027	6.2	0.218	1.734		02.08.19
95	15	W-IFX-18	cc	6.9	24.1	0.0024	NA	0.160	1.675	R	12.09.19
96	15	W-IFX-18	d	4.9	16.8	0.0010	4.8	0.242	1.726		04.11.19
97	15	W-IFX-18	e	4.3	22.1	0.0020	5.4	0.379	1.758		23.12.19
98	15	W-IFX-18	f	8.0	<LOQ	<LOQ	8.5	0.223	1.748		24.01.20
99	15	W-IFX-18	g	5.8	<LOQ	<LOQ	6.4	<LOD	NA		09.03.20
100	16	W-IFX-20	a	0.8	17.5	0.0012	NA	<LOD	NA		17.06.19
101	16	W-IFX-20	b	1.2	22.1	0.0020	NA	<LOD	NA		13.08.19
102	16	W-IFX-20	c	1.2	21.0	0.0018	NA	0.165	2.229	R	02.10.19
103	16	W-IFX-20	d	6.0	13.4	0.0004	NA	0.149	2.211		05.11.19
104	16	W-IFX-20	e	1.5	<LOQ	<LOQ	NA	<LOD	NA		15.01.20
105	17	W-IFX-21	a	9.2	<LOQ	<LOQ	NA	<LOD	NA		15.05.19
106	17	W-IFX-21	b	10.5	20.6	0.0017	NA	<LOD	NA		19.06.19
107	17	W-IFX-21	c	11.1	<LOQ	<LOQ	NA	<LOD	NA		17.07.19
108	17	W-IFX-21	d	9.8	<LOQ	<LOQ	NA	<LOD	NA	R	21.08.19
109	17	W-IFX-21	e	5.9	<LOQ	<LOQ	NA	1.780	2.721		30.09.19
110	17	W-IFX-21	f	8.5	<LOQ	<LOQ	NA	<LOD	NA		13.11.19
111	17	W-IFX-21	g	9.9	<LOQ	<LOQ	NA	<LOD	NA		20.12.19
112	18	W-IFX-22	b	9.5	<LOQ	<LOQ	14.0	NA	NA		06.12.19
113	18	W-IFX-22	c	13.1	<LOQ	<LOQ	10.7	NA	NA	R	13.01.20
114	18	W-IFX-22	d	10.4	<LOQ	<LOQ	6.4	NA	NA		20.02.20
115	19	W-IFX-23	b	19.2	<LOQ	<LOQ	20.2	<LOD	NA		11.11.19
116	19	W-IFX-23	c	15.6	<LOQ	<LOQ	18.2	<LOD	NA		10.12.19
117	19	W-IFX-23	d	12.8	<LOQ	<LOQ	16.3	<LOD	NA	R	09.01.20
118	19	W-IFX-23	e	15.4	<LOQ	<LOQ	17.6	<LOD	NA		05.02.20
119	19	W-IFX-23	f	17.5	23.7	0.0023	17.1	<LOD	NA		03.03.20

n_{serum}	$n_{patient}$	$ID_{patient}$	ID_{visit}	ELISA			SPR			Therapy outcome*	Visit date
				IFX, µg/mL	ADA, AU/mL	ADA, µgEq/mL	IFX, µg/mL	ADA, µgEq/mL	DissR		
120	20	W-IFX-25	a	<LOQ	<LOQ	<LOQ	<LOD	<LOD	NA		08.01.20
121	20	W-IFX-25	b	10.7	<LOQ	<LOQ	11.1	NA	NA	R	07.02.20
122	20	W-IFX-25	c	9.2	<LOQ	<LOQ	10.1	0.201	2.480		05.03.20
123	20	W-IFX-25	d	8.3	<LOQ	<LOQ	8.9	NA	NA		04.03.20
124	21	W-IFX-26	a	3.2	<LOQ	<LOQ	3.3	0.143	2.149		17.05.19
125	21	W-IFX-26	b	3.2	<LOQ	<LOQ	3.1	NA	NA	R	11.07.19
126	21	W-IFX-26	c	5.2	<LOQ	<LOQ	4.5	0.205	2.236		02.09.19
127	21	W-IFX-26	d	4.8	<LOQ	<LOQ	4.6	NA	NA		23.12.19
128	22	MRI-IFX-1	c	2.7	84.5	0.0144	NA	<LOD	NA	?	11.12.20
129	23	MRI-IFX-4	a	<LOQ	394.2	0.0915	NA	1.672	1.257	LOR	25.02.19
130	24	MRI-IFX-14	b	6.1	24.1	0.0024	NA	<LOD	NA	?	21.08.20
131	25	MRI-IFX-15	a	NA	92.1	0.0160	NA	0.243	1.555	LOR	16.12.16
132	25	MRI-IFX-15	b	0.9	92.8	0.0161	NA	0.213	1.567		10.02.17
133	26	MRI-IFX-17	a	1.6	95.8	0.0168	NA	<LOD	NA	?	07.04.17
134	27	MRI-IFX-18	a	NA	76.6	0.0128	NA	0.783	2.263	?	08.06.18
135	28	MRI-IFX-19	a	2.4	202.4	0.0403	NA	2.091	1.860	LOR	14.10.16
136	29	MRI-IFX-22	a	<LOQ	<LOQ	<LOQ	NA	<LOD	NA		03.12.19
137	29	MRI-IFX-22	c	<LOQ	<LOQ	<LOQ	NA	0.408	1.515		05.03.20
138	29	MRI-IFX-22	d	11.4	22.2	0.0021	NA	0.348	1.541	R	26.06.20
139	29	MRI-IFX-22	f	4.0	<LOQ	<LOQ	NA	0.140	1.488		19.03.21
140	29	MRI-IFX-22	g	2.3	NA	NA	NA	0.402	1.513		07.01.22
141	30	MRI-IFX-23	a	<LOQ	602.2	0.1662	NA	0.785	1.212	LOR	30.12.19
142	31	MRI-IFX-25	a	21.9	17.2	0.0011	NA	0.226	1.809	LOR	18.08.16
143	32	MRI-IFX-26	a	11.9	21.3	0.0019	NA	<LOD	NA	?	22.05.20
144	33	MRI-IFX-27	a	2.1	39.3	0.0054	NA	0.144	1.922	R	28.08.20
145	34	MRI-IFX-28	a	3.1	<LOQ	<LOQ	NA	<LOD	NA	?	17.09.20
146	35	MRI-IFX-29	a	5.8	30.9	0.0037	NA	0.181	1.690	?	04.12.20
147	36	MRI-IFX-30	a	1.5	<LOQ	<LOQ	NA	<LOD	NA	?	05.03.21
148	36	MRI-IFX-30	b	9.6	<LOQ	<LOQ	NA	<LOD	NA		06.08.21
149	37	MRI-IFX-31	a	5.1	<LOQ	<LOQ	NA	<LOD	NA	?	14.05.21
150	38	MRI-IFX-32	a	1.2	<LOQ	<LOQ	NA	<LOD	NA	?	28.07.21
151	39	MRI-IFX-35	a	<LOQ	<10.0	<LOQ	NA	<LOD	NA		05.11.21
152	39	MRI-IFX-35	b	<LOQ	339.6	0.0756	NA	0.690	1.969	LOR	14.04.22
153	39	MRI-IFX-35	c	<LOQ	226.7	0.0461	NA	0.585	2.009		10.06.22
154	40	MRI-IFX-36	a	3.3	<LOQ	<LOQ	NA	<LOD	NA	?	03.12.21
155	41	MRI-IFX-40	a	1.8	103.1	0.0183	NA	0.276	1.729	R	14.04.22
156	42	MRI-IFX-42	a	6.1	40.7	0.0056	NA	0.464	1.738	R	29.04.22
157	43	MRI-IFX-44	a	1.9	<LOQ	<LOQ	NA	<LOD	NA	?	27.05.22
158	44	MRI-IFX-45	a	5.1	<LOQ	<LOQ	NA	<LOD	NA	?	27.05.22
159	45	MRI-IFX-46	a	0.7	20.2	0.0017	NA	0.224	1.752	R	03.06.22
		LOQ (ELISA) or LOD (SPR):		<0.6	<10.0	<0.0001	<0.6	<0.14			

* **Therapy outcome:**
LOR, loss of response;
R, remission;
?, unknown.

ADMmon and anti-ADMmon patient cohort

n_{sera}	$n_{patients}$	Analyses
45	31	ADMmon
45	31	Anti-ADMmon
45	31	ADMmon & anti-ADMmon
45	**31**	**Total**

				ELISA		SPR			
n_{serum}	$n_{patient}$	$ID_{patient}$	ID_{visit}	ADM, µg/mL	Anti-ADM, AU/mL	ADM, µg/mL	Anti-ADM, µgEq/mL	DissR	Visit date
1	1	W-ADM-1	a	16.5	<LOQ	<LOQ	4.355	1.537	24.06.19
2	2	W-ADM-2	a	9.2	<LOQ	11.0	<LOQ	1.764	26.06.19
3	3	W-ADM-3	a	17.7	<LOQ	<LOQ	<LOQ	1.781	27.06.19
4	4	W-ADM-4	b	26.0	<LOQ	8.9	<LOQ	1.773	25.11.19
5	5	W-ADM-5	a	15.4	<LOQ	16.7	2.714	2.005	23.05.19
6	5	W-ADM-5	b	11.3	11.7	5.3	<LOQ	2.074	17.07.19
7	5	W-ADM-5	d	8.3	<LOQ	19.8	<LOQ	1.964	04.12.19
8	6	W-ADM-6	c	12.8	<LOQ	4.2	13.831	1.801	08.01.20
9	7	W-ADM-7	a	16.0	<LOQ	<LOQ	7.590	1.897	14.08.19
10	8	W-ADM-8	c	13.5	<LOQ	<LOQ	<LOQ	1.937	14.11.19
11	9	W-ADM-9	a	21.6	<LOQ	<LOQ	3.614	1.885	17.06.19
12	9	W-ADM-9	c	22.3	<LOQ	<LOQ	<LOQ	2.008	14.11.19
13	10	W-ADM-10	a	4.5	231.3	15.1	<LOQ	1.711	30.10.19
14	11	W-ADM-11	a	15.5	<LOQ	23.4	<LOQ	2.068	01.11.19
15	12	W-ADM-12	a	3.0	<LOQ	<LOQ	<LOQ	2.565	22.05.19
16	13	W-ADM-14	a	<LOQ	<LOQ	16.6	<LOQ	2.326	09.07.19
17	14	W-ADM-15	a	10.2	414.0	2.6	<LOQ	1.774	22.07.19
18	14	W-ADM-15	b	NA	NA	<LOQ	<LOQ	1.969	11.09.19
19	14	W-ADM-15	c	NA	NA	1.9	2.362	1.622	09.10.19
20	15	W-ADM-16	a	<LOQ	143.8	2.0	1.276	1.381	07.08.19
21	15	W-ADM-16	b	<LOQ	<LOQ	9.8	<LOQ	1.619	27.09.19
22	16	W-ADM-17	a	13.4	<LOQ	<LOQ	<LOQ	1.896	27.05.19
23	16	W-ADM-17	b	8.8	<LOQ	6.6	<LOQ	1.962	22.07.19
24	17	W-ADM-19	a	11.0	<LOQ	7.3	1.451	1.401	10.12.19
25	17	W-ADM-19	b	3.0	47.3	4.2	2.558	1.457	24.02.20
26	18	W-ADM-22	a	<LOQ	511.3	2.1	5.889	1.350	12.12.19
27	19	W-ADM-24	a	10.4	<LOQ	10.3	0.282	1.694	21.01.20
28	20	W-ADM-26	b	19.6	<LOQ	<LOQ	<LOQ	2.084	24.02.20
29	21	W-ADM-28	a	13.1	10.0	1.6	<LOQ	1.819	28.06.19
30	21	W-ADM-28	b	5.9	78.1	7.2	5.467	1.635	10.07.19
31	21	W-ADM-28	bb	1.6	39.0	5.1	8.352	1.471	05.08.19
32	21	W-ADM-28	c	1.3	75.9	3.0	4.253	1.612	26.08.19
33	21	W-ADM-28	d	<LOQ	607.9	<LOQ	4.335	1.241	18.11.19
34	22	W-ADM-29	a	15.3	<LOQ	10.4	<LOQ	2.129	17.05.19
35	22	W-ADM-29	e	11.1	<LOQ	9.7	<LOQ	1.798	17.09.19
36	22	W-ADM-29	g	7.7	<LOQ	9.4	<LOQ	1.814	13.01.20
37	23	MRI-ADM-1	a	NA	25.5	11.3	1.947	1.410	31.08.18
38	24	MRI-ADM-2	a	<LOQ	139.5	<LOQ	<LOQ	1.962	24.08.16
39	25	MRI-ADM-3	a	<LOQ	123.01	<LOQ	<LOQ	2.345	18.12.15
40	26	MRI-ADM-4	a	<LOQ	274.1	1.1	<LOQ	2.033	12.04.18
41	27	MRI-ADM-10	a	1.0	57.1	1.1	<LOQ	2.572	10.08.16
42	28	MRI-ADM-20	a	NA	46.4	<LOQ	0.679	1.707	06.03.20
43	29	MRI-ADM-23	a	NA	326.4	<LOQ	11.281	1.353	06.03.22
44	30	MRI-ADM-24	a	0.8	248.7	1.8	3.959	1.560	18.03.22
45	31	MRI-ADM-26	a	6.2	<LOQ	11.5	<LOQ	2.346	19.08.22
			LOQ:	<0.6	<10.0	<1.0	<1.0 or 2.0		

B. Sequence data

DNA and protein sequences

bp DNA **pET_1b_TrxA_IdeS (6617 bp)** TrxA IdeS

```
1 TGGCGAATGGGACGCGCCCTGTAGCGGCGCATTAAGCGCGGCGGGTGTGGTGGTTACGCGCAGCGTGACCGCTACACTTGCCAGCGCCCTAGCGCCCGCT
101 CCTTTCGCTTTCTTCCCTTCCTTTCTCGCCACGTTCGCCGGCTTTCCCCGTCAAGCTCTAAATCGGGGGCTCCCTTTAGGGTTCCGATTTAGTGCTTTAC
201 GGCACCTCGACCCCAAAAAACTTGATTAGGGTGATGGTTCACGTAGTGGGCCATCGCCCTGATAGACGGTTTTTCGCCCTTTGACGTTGGAGTCCACGTT
301 CTTTAATAGTGGACTCTTGTTCCAAACTGGAACAACACTCAACCCTATCTCGGTCTATTCTTTTGATTTATAAGGGATTTTGCCGATTTCGGCCTATTGG
401 TTAAAAAATGAGCTGATTTAACAAAAATTTAACGCGAATTTTAACAAAATATTAACGTTTACAATTTCAGGTGGCACTTTTCGGGGAAATGTGCGCGGAA
501 CCCCTATTTGTTTATTTTTCTAAATACATTCAAATATGTATCCGCTCATGAATTAATTCTTAGAAAAACTCATCGAGCATCAAATGAAACTGCAATTTAT
601 TCATATCAGGATTATCAATACCATATTTTTGAAAAAGCCGTTTCTGTAATGAAGGAGAAAACTCACCGAGGCAGTTCCATAGGATGGCAAGATCCTGGTA
701 TCGGTCTGCGATTCCGACTCGTCCAACATCAATACAACCTATTAATTTCCCCTCGTCAAAAATAAGGTTATCAAGTGAGAAATCACCATGAGTGACGACT
801 GAATCCGGTGAGAATGGCAAAAGTTTATGCATTTCTTTCCAGACTTGTTCAACAGGCCAGCCATTACGCTCGTCATCAAAATCACTCGCATCAACCAAAC
901 CGTTATTCATTCGTGATTGCGCCTGAGCGAGACGAAATACGCGATCGCTGTTAAAAGGACAATTACAAACAGGAATCGAATGCAACCGGCGCAGGAACAC
1001 TGCCAGCGCATCAACAATATTTTCACCTGAATCAGGATATTCTTCTAATACCTGGAATGCTGTTTTCCCGGGGATCGCAGTGGTGAGTAACCATGCATCA
1101 TCAGGAGTACGGATAAAATGCTTGATGGTCGGAAGAGGCATAAATTCCGTCAGCCAGTTTAGTCTGACCATCTCATCTGTAACATCATTGGCAACGCTAC
1201 CTTTGCCATGTTTCAGAAACAACTCTGGCGCATCGGGCTTCCCATACAATCGATAGATTGTCGCACCTGATTGCCCGACATTATCGCGAGCCCATTTATA
1301 CCCATATAAATCAGCATCCATGTTGGAATTTAATCGCGGCCTAGAGCAAGACGTTTCCCGTTGAATATGGCTCATAACACCCCTTGTATTACTGTTTATG
1401 TAAGCAGACAGTTTTATTGTTCATGACCAAAATCCCTTAACGTGAGTTTTCGTTCCACTGAGCGTCAGACCCCGTAGAAAAGATCAAAGGATCTTCTTGA
1501 GATCCTTTTTTTCTGCGCGTAATCTGCTGCTTGCAAACAAAAAAACCACCGCTACCAGCGGTGGTTTGTTTGCCGGATCAAGAGCTACCAACTCTTTTTC
1601 CGAAGGTAACTGGCTTCAGCAGAGCGCAGATACCAAATACTGTCCTTCTAGTGTAGCCGTAGTTAGGCCACCACTTCAAGAACTCTGTAGCACCGCCTAC
1701 ATACCTCGCTCTGCTAATCCTGTTACCAGTGGCTGCTGCCAGTGGCGATAAGTCGTGTCTTACCGGGTTGGACTCAAGACGATAGTTACCGGATAAGGCG
1801 CAGCGGTCGGGCTGAACGGGGGGTTCGTGCACACAGCCCAGCTTGGAGCGAACGACCTACACCGAACTGAGATACCTACAGCGTGAGCTATGAGAAAGCG
1901 CCACGCTTCCCGAAGGGAGAAAGGCGGACAGGTATCCGGTAAGCGGCAGGGTCGGAACAGGAGAGCGCACGAGGGAGCTTCCAGGGGGAAACGCCTGGTA
2001 TCTTTATAGTCCTGTCGGGTTTCGCCACCTCTGACTTGAGCGTCGATTTTTGTGATGCTCGTCAGGGGGGCGGAGCCTATGGAAAAACGCCAGCAACGCG
2101 GCCTTTTTACGGTTCCTGGCCTTTTGCTGGCCTTTTGCTCACATGTTCTTTCCTGCGTTATCCCCTGATTCTGTGGATAACCGTATTACCGCCTTTGAGT
2201 GAGCTGATACCGCTCGCCGCAGCCGAACGACCGAGCGCAGCGAGTCAGTGAGCGAGGAAGCGGAAGAGCGCCTGATGCGGTATTTTCTCCTTACGCATCT
2301 GTGCGGTATTTCACACCGCATATATGGTGCACTCTCAGTACAATCTGCTCTGATGCCGCATAGTTAAGCCAGTATACACTCCGCTATCGCTACGTGACTG
2401 GGTCATGGCTGCGCCCCGACACCCGCCAACACCCGCTGACGCGCCCTGACGGGCTTGTCTGCTCCCGGCATCCGCTTACAGACAAGCTGTGACCGTCTCC
2501 GGGAGCTGCATGTGTCAGAGGTTTTCACCGTCATCACCGAAACGCGCGAGGCAGCTGCGGTAAAGCTCATCAGCGTGGTCGTGAAGCGATTCACAGATGT
2601 CTGCCTGTTCATCCGCGTCCAGCTCGTTGAGTTTCTCCAGAAGCGTTAATGTCTGGCTTCTGATAAAGCGGGCCATGTTAAGGGCGGTTTTTTCCTGTTT
2701 GGTCACTGATGCCTCCGTGTAAGGGGGATTTCTGTTCATGGGGGTAATGATACCGATGAAACGAGAGAGGATGCTCACGATACGGGTTACTGATGATGAA
2801 CATGCCCGGTTACTGGAACGTTGTGAGGGTAAACAACTGGCGGTATGGATGCGGCGGGACCAGAGAAAAATCACTCAGGGTCAATGCCAGCGCTTCGTTA
2901 ATACAGATGTAGGTGTTCCACAGGGTAGCCAGCAGCATCCTGCGATGCAGATCCGGAACATAATGGTGCAGGGCGCTGACTTCCGCGTTTCCAGACTTTA
3001 CGAAACACGGAAACCGAAGACCATTCATGTTGTTGCTCAGGTCGCAGACGTTTTGCAGCAGCAGTCGCTTCACGTTCGCTCGCGTATCGGTGATTCATTC
3101 TGCTAACCAGTAAGGCAACCCCGCCAGCCTAGCCGGGTCCTCAACGACAGGAGCACGATCATGCGCACCCGTGGGGCCGCCATGCCGGCGATAATGGCCT
3201 GCTTCTCGCCGAAAGGTTTGGTGGCGGGACCAGTGACGAAGGCTTGAGCGAGGGCGTGCAAGATTCCGAATACCGCAAGCGACAGGCCGATCATCGTCGC
3301 GCTCCAGCGAAAGCGGTCCTCGCCGAAAATGACCCAGAGCGCTGCCGGCACCTGTCCTACGAGTTGCATGATAAAGAAGACAGTCATAAGTGCGGCGACG
3401 ATAGTCATGCCCCGCGCCCACCGGAAGGAGCTGACTGGGTTGAAGGCTCTCAAGGGCATCGGTCGAGATCCCGGTGCCTAATGAGTGAGCTAACTTACAT
3501 TAATTGCGTTGCGCTCACTGCCCGCTTTCCAGTCGGGAAACCTGTCGTGCCAGCTGCATTAATGAATCGGCCAACGCGCGGGGAGAGGCGGTTTGCGTAT
3601 TGGGCGCCAGGGTGGTTTTTCTTTTCACCAGTGAGACGGGCAACAGCTGATTGCCCTTCACCGCCTGGCCCTGAGAGAGTTGCAGCAAGCGGTCCACGCT
3701 GGTTTGCCCCAGCAGGCGAAAATCCTGTTTGATGGTGGTTAACGGCGGGATATAACATGAGCTGTCTTCGGTATCGTCGTATCCCACTACCGAGATATCC
3801 GCACCAACGCGCAGCCCGGACTCGGTAATGGCGCGCATTGCGCCCAGCGCCATCTGATCGTTGGCAACCAGCATCGCAGTGGGAACGATGCCCTCATTCA
3901 GCATTTGCATGGTTTGTTGAAAACCGGACATGGCACTCCAGTCGCCTTCCCGTTCCGCTATCGGCTGAATTTGATTGCGAGTGAGATATTTATGCCAGCC
4001 AGCCAGACGCAGACGCGCCGAGACAGAACTTAATGGGCCCGCTAACAGCGCGATTTGCTGGTGACCCAATGCGACCAGATGCTCCACGCCCAGTCGCGTA
4101 CCGTCTTCATGGGAGAAAATAATACTGTTGATGGGTGTCTGGTCAGAGACATCAAGAAATAACGCCGGAACATTAGTGCAGGCAGCTTCCACAGCAATGG
4201 CATCCTGGTCATCCAGCGGATAGTTAATGATCAGCCCACTGACGCGTTGCGCGAGAAGATTGTGCACCGCCGCTTTACAGGCTTCGACGCCGCTTCGTTC
4301 TACCATCGACACCACCACGCTGGCACCCAGTTGATCGGCGCGAGATTTAATCGCCGCGACAATTTGCGACGGCGCGTGCAGGGCCAGACTGGAGGTGGCA
4401 ACGCCAATCAGCAACGACTGTTTGCCCGCCAGTTGTTGTGCCACGCGGTTGGGAATGTAATTCAGCTCCGCCATCGCCGCTTCCACTTTTTCCCGCGTTT
4501 TCGCAGAAACGTGGCTGGCCTGGTTCACCACGCGGGAAACGGTCTGATAAGAGACACCGGCATACTCTGCGACATCGTATAACGTTACTGGTTTCACATT
4601 CACCACCCTGAATTGACTCTCTTCCGGGCGCTATCATGCCATACCGCGAAAGGTTTTGCGCCATTCGATGGTGTCCGGGATCTCGACGCTCTCCCTTATG
4701 CGACTCCTGCATTAGGAAGCAGCCCAGTAGTAGGTTGAGGCCGTTGAGCACCGCCGCCGCAAGGAATGGTGCATGCAAGGAGATGGCGCCCAACAGTCCC
4801 CCGGCCACGGGGCCTGCCACCATACCCACGCCGAAACAAGCGCTCATGAGCCCGAAGTGGCGAGCCCGATCTTCCCCATCGGTGATGTCGGCGATATAGG
4901 CGCCAGCAACCGCACCTGTGGCGCCGGTGATGCCGGCCACGATGCGTCCGGCGTAGAGGATCGAGATCTCGATCCCGCGAAATTAATACGACTCACTATA
5001 GGGGAATTGTGAGCGGATAACAATTCCCCTCTAGAAATAATTTTGTTTAACTTTAAGAAGGAGATATACCATGAGCGATAAAATTATTCACCTGACTGAC
5101 GACAGTTTTGACACGGATGTACTCAAAGCGGACGGGGCGATCCTCGTCGATTTCTGGGCAGAGTGGTGCGGTCCGTGCAAAATGATCGCCCCGATTCTGG
5201 ATGAAATCGCTGACGAATATCAGGGCAAACTGACCGTTGCAAAACTGAACATCGATCAAAACCCTGGCACTGCGCCGAAATATGGCATCCGTGGTATCCC
5301 GACTCTGCTGCTGTTCAAAAACGGTGAAGTGGCGGCAACCAAAGTGGGTGCACTGTCTAAAGGTCAGTTGAAAGAGTTCCTCGACGCTAACCTGGCCGGA
5401 TCTGGCAGTGGTTCTGGTCATCACCATCACCATCACTCCGCGGGTAGCGAGAATCTTTATTTTCAGGGCGCCATGGATAGTTTTTCTGCTAATCAAGAGA
5501 TTAGATATTCGGAAGTAACACCTTATCACGTTACTTCCGTTTGGACCAAAGGAGTTACTCCTCCAGCAAACTTCACTCAAGGTGAAGATGTTTTTCACGC
5601 TCCTTATGTTGCTAACCAAGGATGGTATGATATTACCAAAACATTCAATGGAAAAGACGATCTTCTTTGCGGGGCTGCCACAGCAGGGAATATGCTTCAC
5701 TGGTGGTTCGATCAAAACAAAGACCAAATTAAACGTTATTTGGAAGAGCATCCAGAAAAGCAAAAAATAAACTTCAATGGCGAACAGATGTTTGACGTAA
5801 AAGAAGCTATCGACACTAAAAACCACCAGCTAGATAGTAAATTATTTGAATATTTTAAAGAAAAAGCTTTCCCTTATCTATCTACTAAACACCTAGGAGT
5901 TTTCCCTGATCATGTAATTGATATGTTCATTAACGGCTACCGCCTTAGTCTAACTAACCACGGTCCAACGCCAGTAAAAGAAGGTAGTAAAGATCCCCGA
6001 GGTGGTATTTTTGACGCCGTATTTACAAGAGGTGATCAAAGTAAGCTATTGACAAGTCGTCATGATTTTAAAGAAAAAAATCTCAAAGAAATCAGTGATC
6101 TCATTAAGAAAGAGTTAACCGAAGGCAAGGCTCTAGGCCTATCACACACCTACGCTAACGTACGCATCAACCATGTTATAAACCTGTGGGGAGCTGACTT
6201 TGATTCTAACGGGAACCTTAAAGCTATTTATGTAACAGACTCTGATAGTAATGCATCTATTGGTATGAAGAAATACTTTGTTGGTGTTAATTCCGCTGGA
```

bp DNA **pET_1b_TrxA_IdeS (6617 bp)** TrxA IdeS [continued]

```
6301 AAAGTAGCTATTTCTGCTAAAGAAATAAAAGAAGATAATATTGGTGCTCAAGTACTAGGGTTATTTACACTTTCAACAGGGCAAGATAGTTGGAATCAGA
6401 CCAATTAAGGTACCGGATCCGAATTCGAGCTCCGTCGACAAGCTTGCGGCCGCACTCGAGCACCACCACCACCACCACTGAGATCCGGCTGCTAACAAAG
6501 CCCGAAAGGAAGCTGAGTTGGCTGCTGCCACCGCTGAGCAATAACTAGCATAACCCCTTGGGGCCTCTAAACGGGTCTTGAGGGGTTTTTTGCTGAAAGG
6601 AGGAACTATATCCGGAT
```

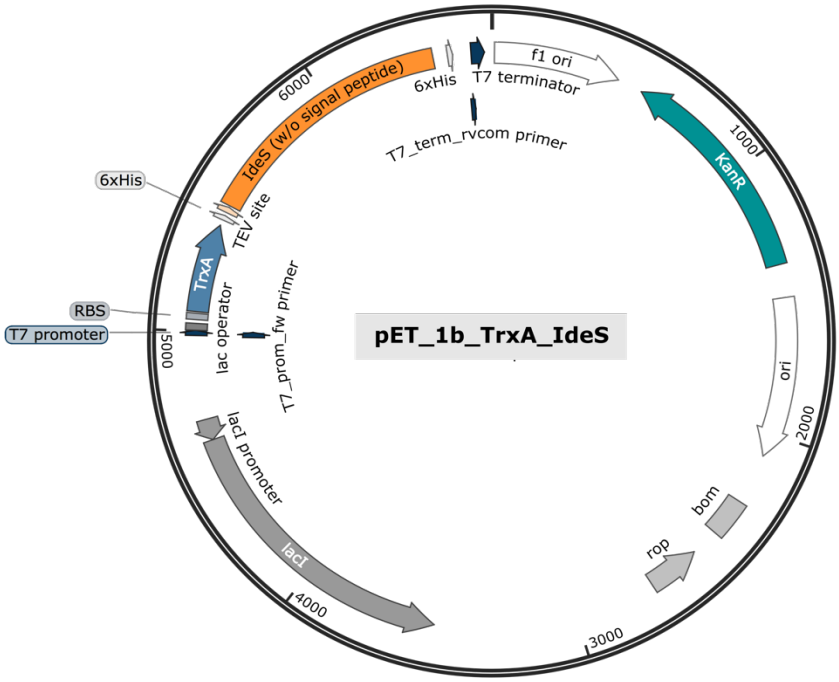

This plasmid was obtained as a kind gift from Professor Ulrich von Pawel-Rammingen.
References details are indicated in the Materials and methods chapter.

aa Protein **TrxA-IdeS (445 aa)** TrxA IdeS

```
1   MSDKIIHLTDDSFDTDVLKADGAILVDFWAEWCGPCKMIAPILDEIADEYQGKLTVAKLNIDQNPGTAPKYGIRGIPTLLLFKNGEVAATKVGALSKGQL
101 KEFLDANLAGSGSGSGHHHHHHSAGSENLYFQGAMDSFSANQEIRYSEVTPYHVTSVWTKGVTPPANFTQGEDVFHAPYVANQGWYDITKTFNGKDDLLC
201 GAATAGNMLHWWFDQNKDQIKRYLEEHPEKQKINFNGEQMFDVKEAIDTKNHQLDSKLFEYFKEKAFPYLSTKHLGVFPDHVIDMFINGYRLSLTNHGPT
301 PVKEGSKDPRGGIFDAVFTRGDQSKLLTSRHDFKEKNLKEISDLIKKELTEGKALGLSHTYANVRINHVINLWGADFDSNGNLKAIYVTDSDSNASIGMK
401 KYFVGVNSAGKVAISAKEIKEDNIGAQVLGLFTLSTGQDSWNQTN*
```

C. List of publications

Journal contributions

2. Grasmeier MK*, Weber S, Treiber M, Thaler MA and Luppa PB. Surface plasmon resonance assays for the therapeutic drug monitoring of infliximab indicate clinical relevance of anti-infliximab antibody binding properties. *Clin Chem Lab Med.* 2023;61(7):1255–1265.

1. Grasmeier MK*, Langmann AF*, Langmann P, Treiber M, Thaler MA and Luppa PB. Dynamics of serum concentrations of antibodies to infliximab: A new approach for predicting secondary loss of response in inflammatory bowel diseases. *Therap Adv Gastroenterol.* 2021;14:17562848211037849.

*First author(s)

Poster presentations

5. Quantity or quality? Deciphering the diagnostic relevance of anti-drug antibody analysis by surface plasmon resonance. **DGKL Jahrestagung 2022** (Mannheim, DE).

4. Drug-tolerant quantification of pre-purified anti-infliximab antibodies in patient serum by use of a surface plasmon resonance biosensor. **EuroMedLab 2021** (Munich, DE).

3. Anti-Infliximab Antibody Dynamics as a New Predictor of Loss of Response to Infliximab. **2021 AACC Annual Scientific Meeting + Clinical Lab Expo** (Atlanta, US – online participation).

2. Biosensor-based monitoring of TNF antagonists and anti-drug antibodies for patient-tailored therapy of inflammatory autoimmune disease. **MGC Science Day 2019, Klinikum rechts der Isar der Technischen Universität München** (Munich, DE).

1. Biosensor-based monitoring of TNF antagonists and anti-drug antibodies for patient-tailored therapy of inflammatory autoimmune disease. **DGKL-Jahrestagung 2019** (Magdeburg, DE).

D. Eidesstattliche Erklärung

Ich, Melina Katharina Grasmeier, erkläre an Eides statt, dass ich die bei der promotionsführenden Einrichtung TUM School of Natural Sciences der TUM zur Promotionsprüfung vorgelegte Arbeit mit dem Titel:

Biosensor-based monitoring of TNF antagonists and anti-drug antibodies in inflammatory bowel disease

unter der Anleitung und Betreuung durch:

Herrn Prof. Dr. Martin Elsner und **Herrn Prof. Dr. Peter B. Luppa**

ohne sonstige Hilfe erstellt und bei der Abfassung nur die gemäß § 7 Abs. 6 und 7 angegebenen Hilfsmittel benutzt habe.

- ☑ Ich habe keine Organisation eingeschaltet, die gegen Entgelt Betreuer*innen für die Anfertigung von Dissertationen sucht, oder die mir obliegenden Pflichten hinsichtlich der Prüfungsleistungen für mich ganz oder teilweise erledigt.
- ☑ Ich habe die Dissertation in dieser oder ähnlicher Form in keinem anderen Prüfungsverfahren als Prüfungsleistung vorgelegt.
- ☑ Teile der Dissertation wurden in Fachzeitschriften (siehe Liste der Vorveröffentlichungen) veröffentlicht.
- ☑ Ich habe den angestrebten Doktorgrad noch nicht erworben und bin nicht in einem früheren Promotionsverfahren für den angestrebten Doktorgrad endgültig gescheitert.
- ☐ Ich habe bereits am _____ bei der promotionsführenden Einrichtung _____ der Hochschule _____ unter Vorlage einer Dissertation mit dem Thema _____ die Zulassung zur Promotion beantragt mit dem Ergebnis: _____
- ☑ Ich habe keine Kenntnis über ein strafrechtliches Ermittlungsverfahren in Bezug auf wissenschaftsbezogene Straftaten gegen mich oder eine rechtskräftige strafrechtliche Verurteilung mit Wissenschaftsbezug.

Die öffentlich zugängliche Promotionsordnung sowie die Richtlinien zur Sicherung guter wissenschaftlicher Praxis und für den Umgang mit wissenschaftlichem Fehlverhalten der TUM sind mir bekannt, insbesondere habe ich die Bedeutung von § 27 PromO (Nichtigkeit der Promotion) und § 28 PromO (Entzug des Doktorgrades) zur Kenntnis genommen. Ich bin mir der Konsequenzen einer falschen Eidesstattlichen Erklärung bewusst.

Mit der Aufnahme meiner personenbezogenen Daten in die Alumni-Datei bei der TUM bin ich

☑ einverstanden.

☐ nicht einverstanden.

Egling, den 16. Dezember 2023

Melina K. Grasmeier